AD A108725

AFWAL-TR-80-3143

LEVEL II

VORTEX FLOW CORRELATION

DTIC
SELECTED
DEC 18 1981
E

JANUARY 1981

"riginal ...
plates: ... riuctions
ions will b ... black and
white"

TECHNICAL REPORT AFWAL-TR-80-3143
FINAL REPORT FOR PERIOD MAY 1980 - OCTOBER 1980

405228

81 18   02 9

NOTICE

When Government drawings, specifications, or other data are used for any purpose other than in connection with a definitely related Government procurement operation, the United States Government thereby incurs no responsibility nor any obligation whatsoever; and the fact that the government may have formulated, furnished, or in any way supplied the said drawings, specifications, or other data, is not to be regarded by implication or otherwise as in any manner licensing the holder or any other person or corporation, or conveying any rights or permission to manufacture use, or sell any patented invention that may in any way be related thereto.

This report has been reviewed by the Office of Public Affairs (ASD/PA) and is releasable to the National Technical Information Service (NTIS). At NTIS, it will be available to the general public, including foreign nations.

This technical report has been reviewed and is approved for publication.
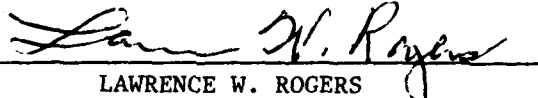
LAWRENCE W. ROGERS
Project Engineer

LOWELL C. KEEL, Major, USAF
Chief, Aerodynamics & Airframe Branch
Aeromechanics Division

FOR THE COMMANDER

PETER J. BUTKEWICZ
Colonel, USAF
Chief, Aeromechanics Division

"If your address has changed, if you wish to be removed from our mailing list, or if the addressee is no longer employed by your organization please notify AFWAL/FIMM W-PAFB, OH 45433 to help us maintain a current mailing list".

Copies of this report should not be returned unless return is required by security considerations, contractual obligations, or notice on a specific document.

DISCLAIMER NOTICE

THIS DOCUMENT IS BEST QUALITY PRACTICABLE. THE COPY FURNISHED TO DTIC CONTAINED A SIGNIFICANT NUMBER OF PAGES WHICH DO NOT REPRODUCE LEGIBLY.

REPORT DOCUMENTATION PAGE	READ INSTRUCTIONS BEFORE COMPLETING FORM	
1. REPORT NUMBER AFWAL-TR-80-3143	2. GOVT ACCESSION NO. AD-A108725	3. RECIPIENT'S CATALOG NUMBER
4. TITLE (and Subtitle) VORTEX FLOW CORRELATION		5. TYPE OF REPORT & PERIOD COVERED Final Report May–October 1980
		6. PERFORMING ORG. REPORT NUMBER NOR-80-152
7. AUTHOR(s) Gary E. Erickson		8. CONTRACT OR GRANT NUMBER(s) F33615-80-C-3024
9. PERFORMING ORGANIZATION NAME AND ADDRESS Northrop Corporation, Aircraft Division 3901 W. Broadway Hawthorne, California 90250		10. PROGRAM ELEMENT, PROJECT, TASK AREA & WORK UNIT NUMBERS Project 2307
11. CONTROLLING OFFICE NAME AND ADDRESS Flight Dynamics Laboratory (AFWAL/FIMM) Air Force Wright Aeronautical Laboratories (AFSC) Wright-Patterson AFB, Ohio 45433		12. REPORT DATE January 1981
		13. NUMBER OF PAGES 332
14. MONITORING AGENCY NAME & ADDRESS(if different from Controlling Office)		15. SECURITY CLASS. (of this report) Unclassified
		15a. DECLASSIFICATION DOWNGRADING SCHEDULE

16. DISTRIBUTION STATEMENT (of this Report)

Approved for public release;
distribution unlimited.

17. DISTRIBUTION STATEMENT (of the abstract entered in Block 20, if different from Report)

18. SUPPLEMENTARY NOTES

19. KEY WORDS (Continue on reverse side if necessary and identify by block number)

Water Tunnels; Vortex Flows; Flow Simulations; Slender Wings and Bodies;
Vortex Breakdown; Vortex Asymmetry; Vorticity; Boundary Layers; Reynolds
Number; Steady and Unsteady Flows; Adverse Pressure Gradient; Wing-LEX
and Wing-Canard Geometries; Missiles.

20. ABSTRACT (Continue on reverse side if necessary and identify by block number)

Key parameters have been identified which permit correlation of vortex
flow simulations in a water tunnel with wind tunnel and flight data.
Vortex generation, vortex sheet and core location, and vortex strength
on thin slender wings are accurately represented in a water tunnel due
to the insensitivity of separation point location to changes in Reynolds
number. The fact that theoretical methods which ignore viscous effects
can reasonably predict vortex flow aerodynamics is one indication of the

DD FORM 1473 1 JAN 73   EDITION OF 1 NOV 65 IS OBSOLETE

20. (continued)

Reynolds number insensitivity of these flow phenomena. For wings and bodies where separation point varies with Reynolds number, the fundamental vortex structure is similar regardless of Reynolds number value since vortices at a distance from the generating surfaces are embedded in essentially irrotational flow. External pressure gradient is an important parameter affecting vortex stability and, although there is yet no theoretical verification that this parameter is the dominant one, vortex burst at higher angles of attack for a given configuration occurs at comparable positions in water tunnels as in wind tunnels and flight. A water tunnel is a powerful diagnostic tool capable of providing high-quality flow visualization of complex fluid flows and insight into the phenomenological aspects of vortex generation, interactions between multiple vortices and aerodynamic surfaces and vortex burst.

Foreword

This report, entitled "Vortex Flow Correlation," is the documentation of a study aimed at determining the utility and the limitations of hydrodynamic testing in aerodynamic research and development. The emphasis is on establishing levels of confidence in the correlation of high and low Reynolds number vortex flow phenomena in specific flow situations.

Accession For	
NTIS GRA&I	☒
DTIC TAB	☐
Unannounced	☐
Justification	
By	
Distribution/	
Availability Codes	
Dist	Avail and/or Special
A	

VORTEX FLOW CORRELATION

TABLE OF CONTENTS

LIST OF ILLUSTRATIONS

LIST OF ILLUSTRATIONS (Continued)

ix

LIST OF ILLUSTRATIONS (Continued)

LIST OF ILLUSTRATIONS (Continued)

LIST OF ILLUSTRATIONS (Continued)

LIST OF ILLUSTRATIONS (Continued)

xv

LIST OF ILLUSTRATIONS (Continued)

LIST OF ILLUSTRATIONS (Continued)

LIST OF ILLUSTRATIONS (Concluded)

LIST OF TABLES

SECTION 1

INTRODUCTION

A comprehensive program has been conducted with the objective of identification of the key parameters permitting correlation of water tunnel data with wind tunnel and flight test results. This was accomplished by reviewing the applications of water tunnels to hydrodynamic and aerodynamic problems with emphasis on the simulation of separation-induced vortex flows. The pertinent governing equations of motion for the various vortex flow regimes were investigated in order to isolate key parameters affecting vortex flow behavior. Subsequently, several vortex flow situations amenable to proper simulation in a water tunnel were identified. An approach and preliminary plan for water tunnel studies of a specific vortex flow problem relevant to a current Air Force technology program have been outlined.

SECTION 2

PROGRAM OBJECTIVES AND APPROACH

The objective of this program was identification of key parameters which will permit correlation of water tunnel data with wind tunnel and flight test results.

The program consisted of three major tasks, as follows:

TASK I — Literature Survey of Water Tunnel Applications.

TASK II — Identification of Key Parameters Permitting Correlation of Water Tunnel Results with Wind Tunnel and Flight Data.

TASK III — Identification of Water Tunnel Applications to Vortex Flows.

Hydrodynamic test facilities have been utilized extensively in the past to study the flow about hydrodynamic and aerodynamic shapes. The advent of highly maneuverable aircraft and missile configurations has resulted in a resurgence in the usage of water tunnels to investigate the separated flow characteristics in the high-angle-of-attack regime. TASK I was devoted to a literature survey to determine the exact role that water tunnels have played in technology development. This includes a review of flow simulation studies using water tunnels, results from which provided insight into the utility of a water tunnel for vortex flow studies.

Dynamic flow similarity of two geometrically similar bodies requires the equivalency of certain dimensionless parameters which reflect the relative importance of viscous, inertial, gravitational, and elastic forces. For the special, albeit complex, case of separation-induced vortex flows, much experimental and theoretical data exist which indicate that certain classes of vortex flows exhibited by aircraft and missile configurations can be simulated in a vivid, rapid, and inexpensive manner in a water tunnel., TASK II encompassed a coupling of Northrop's broad experimental water tunnel, wind tunnel, and flight test data base (which includes many excellent correlations) with a theoretical approach, whereby simplifications to the Navier-Stokes equations of motion appropriate to the specific regimes comprising a vortex flow are analyzed. The integration of theoretical and experimental vortex flow studies provide guidelines pertaining to the correlation of water tunnel data to wind tunnel and flight results for appropriate vortex flow problems. Northrop's experience in water tunnel testing was used to evaluate the relative importance of each key parameter derived from the governing equations.

The key parameters identified in the theoretical approach in TASK II were used in TASK III to identify many vortex flow problems of relevance to configurations of present and future designs which lend themselves to water tunnel testing. Northrop's water tunnel data base of most aircraft in the present U.S. inventory and several foreign aircraft configurations formed a solid basis for the accomplishment of this task.

The ongoing Forward Swept Wing (FSW) Technology Program conducted jointly by DARPA/AFWAL exemplifies the increased research activity related to this long-dormant concept. Northrop water tunnel studies have suggested that conventional

3

vortex lift concepts may be ineffective due to the flow charac-
teristics peculiar to forward sweep. Application of these
high-energy rotational flows to enhance subsonic/transonic
maneuver capability is desirable and, consequently, a specific
vortex flow problem for study in a water tunnel featuring
the FSW concept was outlined in TASK III.

SECTION 3

TASK I - LITERATURE SURVEY OF WATER TUNNEL APPLICATIONS

3.1   WATER TUNNEL APPLICATIONS

Historically, hydrodynamic test facilities have been used in naval research. Water towing tanks, water channels, and water tunnels have been employed to investigate the resistance of surface ships and submersibles and cavitation phenomena on rudders, propellers, and hydrofoils. References 1-6 provide representative results from such studies. Water tunnels are to be distinguished from water channels and water tanks in that the latter two have a free surface primarily for testing of partially submerged objects for marine applications which require gravity forces (Froude number) to be accounted for. References 7 and 8 provide excellent reviews of hydrodynamic tunnel applications to numerous flow situations. Studies in water include: boundary layer transition, unsteady turbulent boundary layers, turbulent wakes, cascade flow, unsteady effects on oscillating cylinders and airfoils, parachute drag, high-speed trains, and ground cushion vehicles (see References 9-16). Further applications of water tunnels, tanks, and channels, as revealed by the literature survey, include: rotor ground effects, jets exhausting into a cross-flow, convective plumes, bottom topography effects on rotating flows, simulation of the fluid mechanics of aortic valves (internal flow models), velocity and temperature fluctuation measurements, acoustic water tunnel studies, holographic investigation of boundary layers, and effects of flexible and compliant walls (see References 17-25).

The advent of first-generation supersonic transport configurations stimulated extensive use of water tunnels in gaining an understanding of complex three-dimensional flow fields. Utilization of vortex-induced lift derived from controlled leading-edge separation stimulated many studies of slender wings under static and dynamic flow conditions (References 26 and 27). Theoretical models of the vortex flows shed from a slender delta wing and of the inner core itself were developed and, to augment these pursuits, water tunnels (essentially cylindrical tubes) with diverging test sections and swirl vane arrangements were used in an attempt to provide explanations of the development and breakdown of axisymmetrical vortex cores (References 28 and 29).

Impressive results have been obtained in a water tunnel from studies of slender wings and forebodies (Reference 30). Flow studies, typically in a water tow tank, have also been made of subsonic transport aircraft which pose a flight safety hazard stemming from the interaction of the highly-persistent wing tip vortices with trailing aircraft (Reference 31).

A significant finding from the literature survey is that relatively few water tunnel facilities have been utilized in the investigation of the complex vortex flow interactions of advanced fighter and missile configurations. Studies made at Northrop Corporation in the United States, ONERA (Office National d'Etudes et de Recherches Aerospatiales) in France, NAE (National Aeronautical Establishment) in Canada, NEAR (Nielsen Engineering and Research) in the United States, NPL (National Physical Laboratory) in England, and others have shown the utility of water tunnels in the investigation of wing and body vortex flows and vortex interactions, canard-wing arrangements, engine inlet and exhaust effects, gun gas ingestion, in-flight refueling probes, deflected flaps, radome strakes, etc. using high-fidelity scale models of fighter

6

aircraft and generic fighter-type configurations (see References 32-35 for example). Tactical missile and missile-like arrangements have been tested in many of the facilities above and also at BAC (British Aerospace Company) in England and VKI (Von Karman Institute) in Belgium but, in general, a lack of data, relative to slender wing results, is evident from the literature survey.

The study of flow control by means of high-velocity jets was pioneered by ONERA and, more recently, studied by Northrop on existing aircraft configurations (References 36-37). Tests have also been made of multiple-jet VSTOL configurations in ground effect, for example, a VSTOL fighter model featuring vectorable 2-D nozzles and forward lift jet arrangement (Reference 38).

Water tunnels are in widespread use throughout the world for a multiplicity of aerodynamic and hydrodynamic flow applications. TABLE I lists many of the existing water tunnels, many of which are currently in use, the location of each facility, and typical flow phenomena studies for which the facility is utilized. The purpose of this table is to point out the capability which exists for the study of complex vortex flows and flowfield interactions.

Figure 1 presents sketches and photographs of several, but by no means all, water tunnel facilities which are in use today. In terms of diversity of flow phenomena to which a water tunnel has been applied and quality and variety of flow visualization techniques, the ONERA Hydraulic Analogy Laboratory is unsurpassed. Typical vortex flow results obtained in the ONERA 22 x 22-cm water tunnel, a vertical tunnel functioning by gravity discharge which has been in operation since 1952, are shown in Figure 2 (from Reference 7). Special note should be made of the excellent agreement between water tunnel

7

22 CM X 22 CM WATER
TUNNEL FOR TESTS
WITH A FLOW
VELOCITY > 0
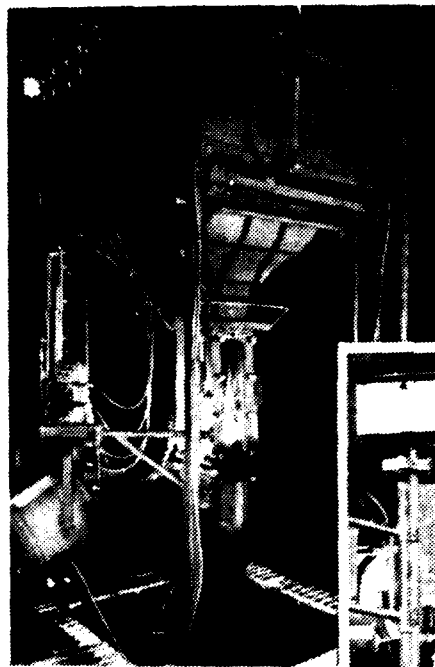
HYDRAULIC TANK
FOR STATIC TESTS
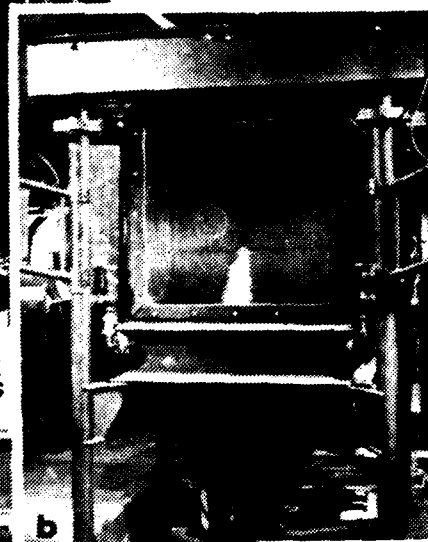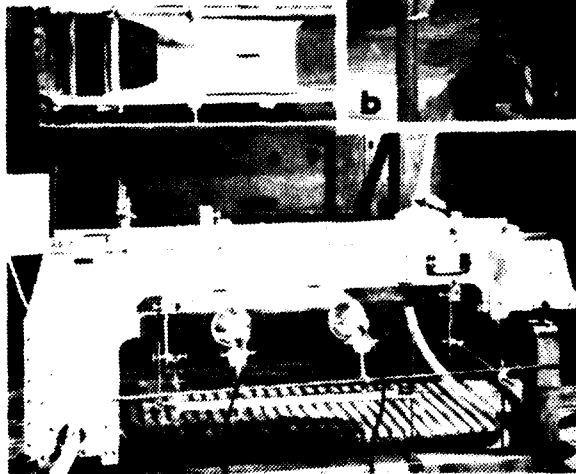
FREE-SURFACE DUCT
FOR THE HYDRAULIC
ANALOGY OF SUPER-
SONIC PHENOMENA
($\gamma = 2$)

(a) ONERA HYDRAULIC ANALOGY LABORATORY (REFERENCE 7)

FIGURE 1. WATER TUNNEL FACILITIES THROUGHOUT THE WORLD
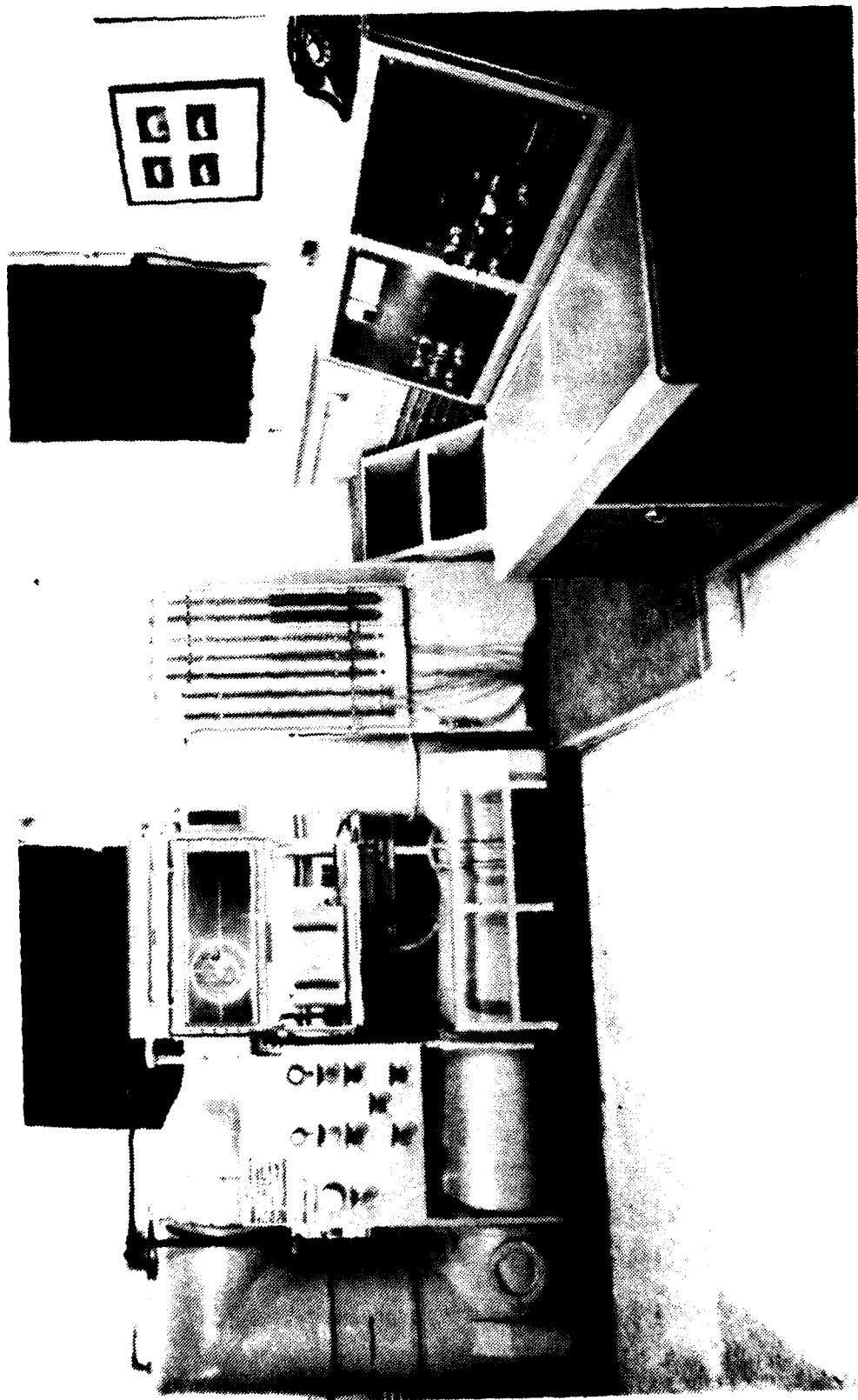
(b) NATIONAL AERONAUTICAL ESTABLISHMENT (NAE) 10 X 13-INCH WATER TUNNEL (REFERENCE 8)

FIGURE 1. CONTINUED
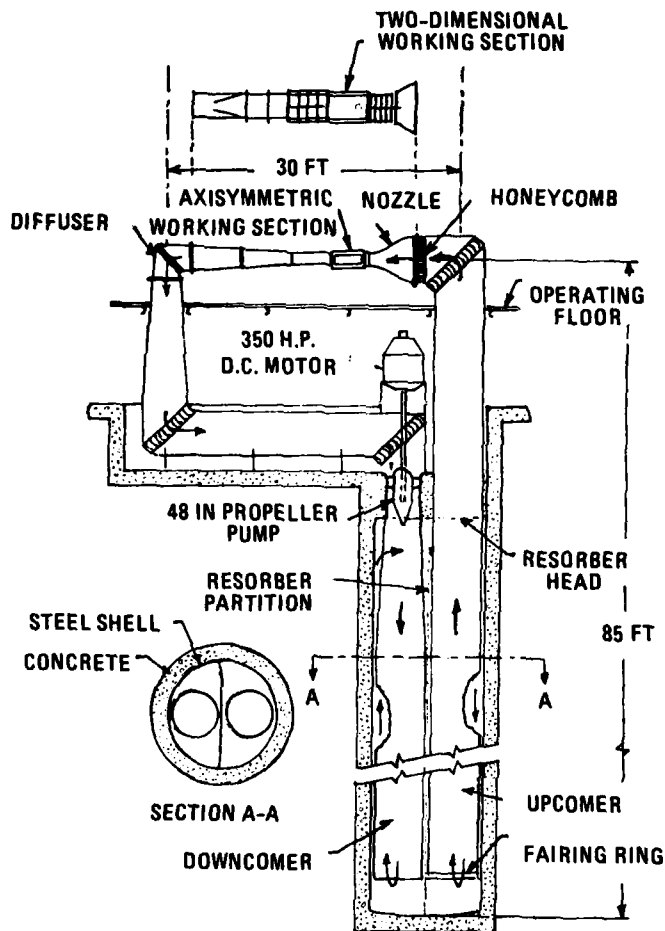
(c) CAL TECH HIGH SPEED WATER TUNNEL (HSWT).
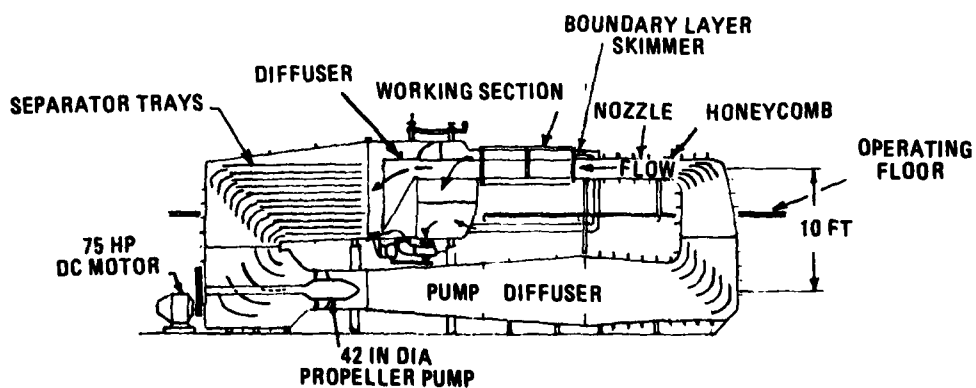
(d) CAL TECH FREE SURFACE WATER TUNNEL (FSWT).

FIGURE 1. CONTINUED

10

STORAGE TANKS

TUNNEL DRIVE MOTOR

CAMERA CANOPY

TEST SECTION

FIBERGLASS CONTRACTION

GAS EXTRACTION & PRESSURIZATION DOME

PUMP & FILTER (HIDDEN)

PROPELLER SECTION

CAMERA SUPPORT POST

PRESSURE CONTROLS

HONEYCOMB & SCREEN SECTION
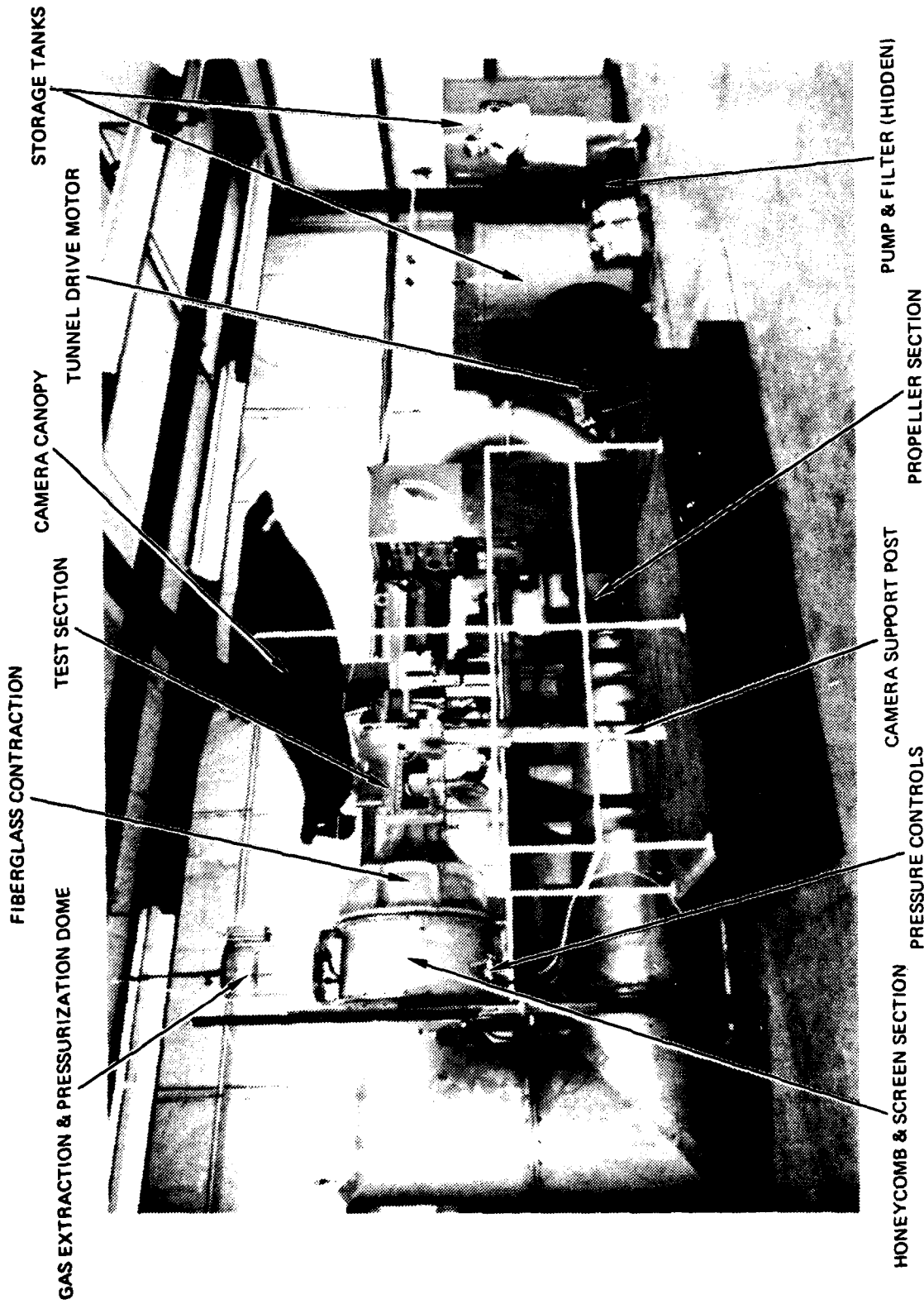
(e) AEROMECHANICS LABORATORY (AVRADCOM) 0.2 METER X 0.3 METER WATER TUNNEL.

FIGURE 1. CONTINUED

11

CORNER VANES FITTER

DYE TANKS

SUPPLY THROUGH TUNNEL WALL TO MODEL

ELECTRIC MOTOR AND CONTROL EQUIPMENT

WORKING SECTION

FIXED PITCH IMPELLER

INPUT VALVE

BOTTOM DRAIN

TOP DRAIN
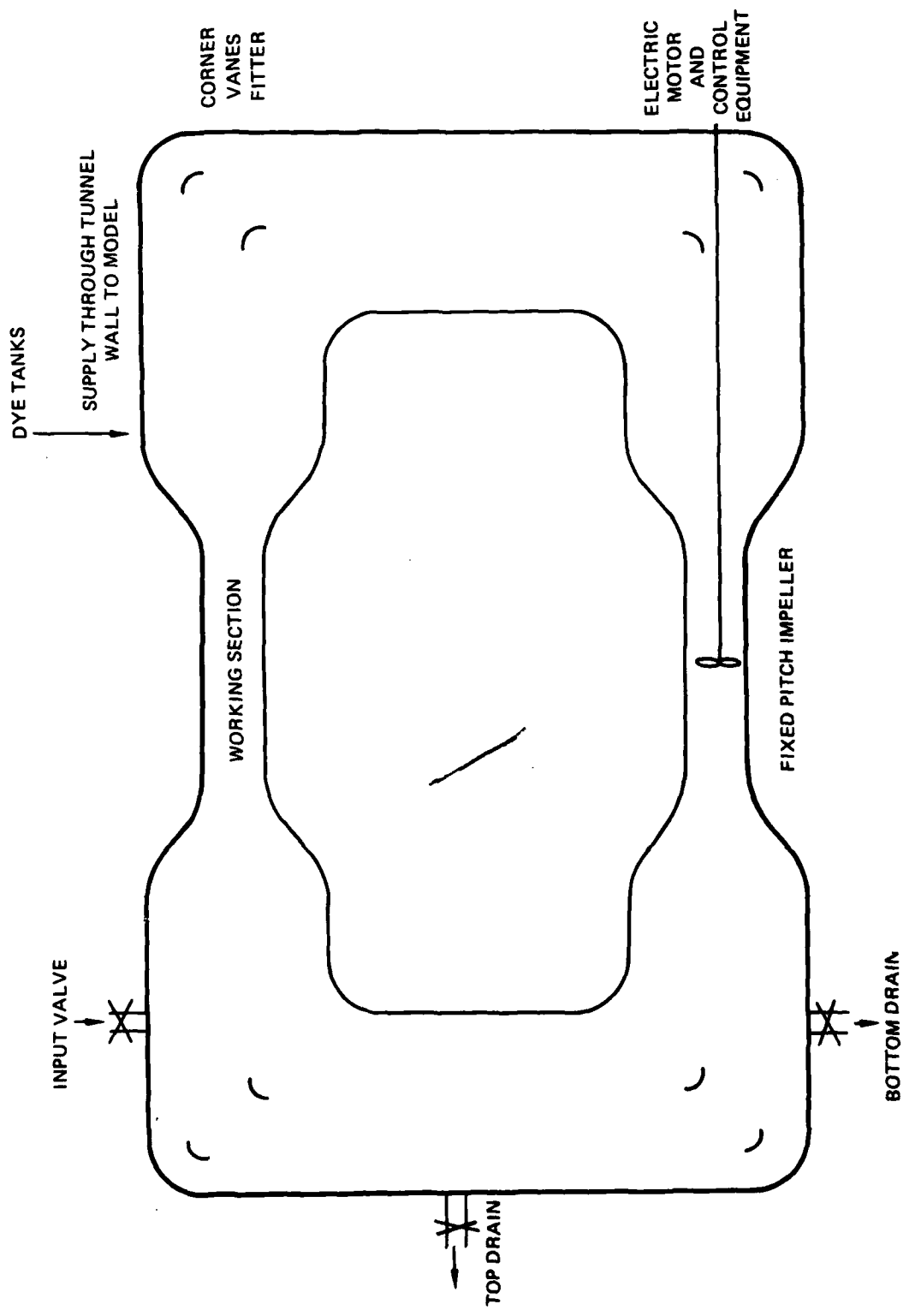
(F) BRITISH AEROSPACE DYNAMICS GROUP 18 X 18-INCH WATER TUNNEL (REFERENCE 11)

FIGURE 1. CONTINUED
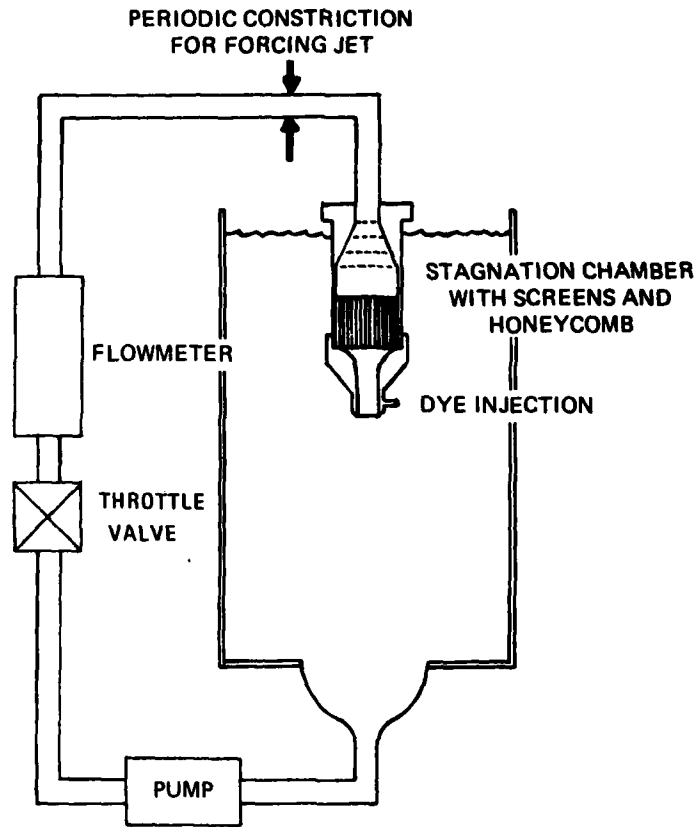
(g) UNIVERSITY OF SO. CALIF. WATER-JET FACILITY.
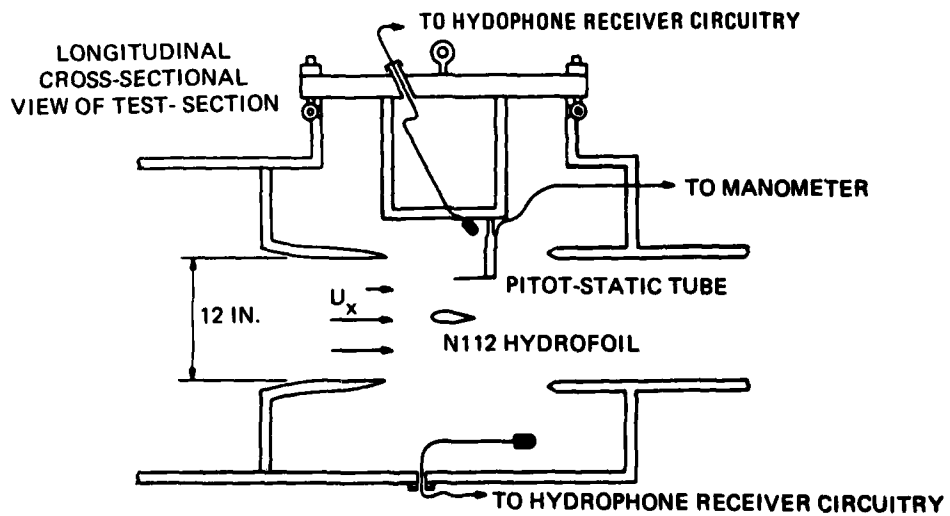
(h) DTNSRDC 12-INCH VARIABLE PRESSURE WATER TUNNEL

FIGURE 1. CONTINUED.

13

AP = ANEMOMETER PROBE,
C = CHILLER,
DI = DYE INJECTOR,
H = HONEYCOMB,
M = MODEL,
OPV = ORIFICE PLATE VALVE,
R = RESERVOIR,
S = SUMP,
SC = SCREENS,
WS = WORKING SECTION
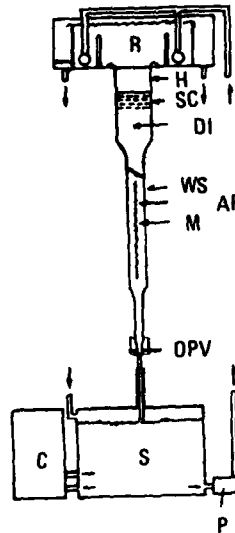
(i) University of Calif. — Santa Barbara 10-cm Diameter Water Tunnel.
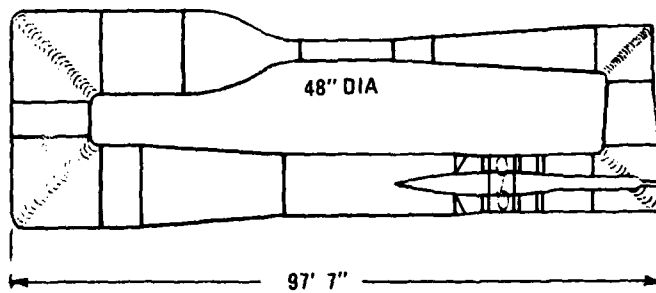
(j) Pennsylvania State University 48-in. Water Tunnel.

FIGURE 1. CONTINUED.
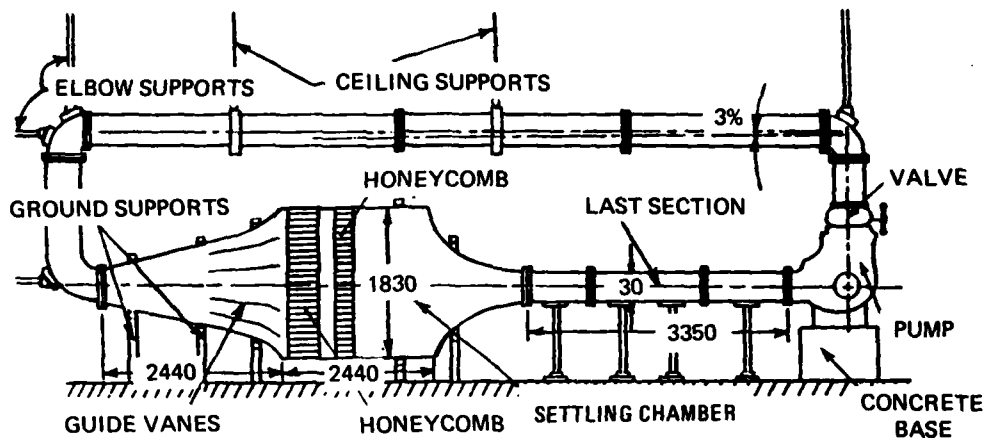
(K) VIRGINIA POLYTECHNIC AND STATE UNIVERSITY WATER TUNNEL (UNITS IN CM.)
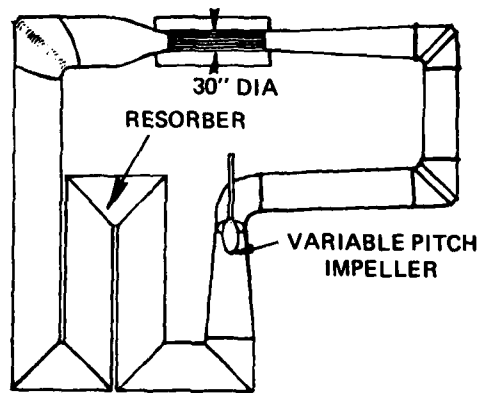
(I) ARL 30-INCH WATER TUNNEL

FIGURE 1. CONTINUED

80-00246
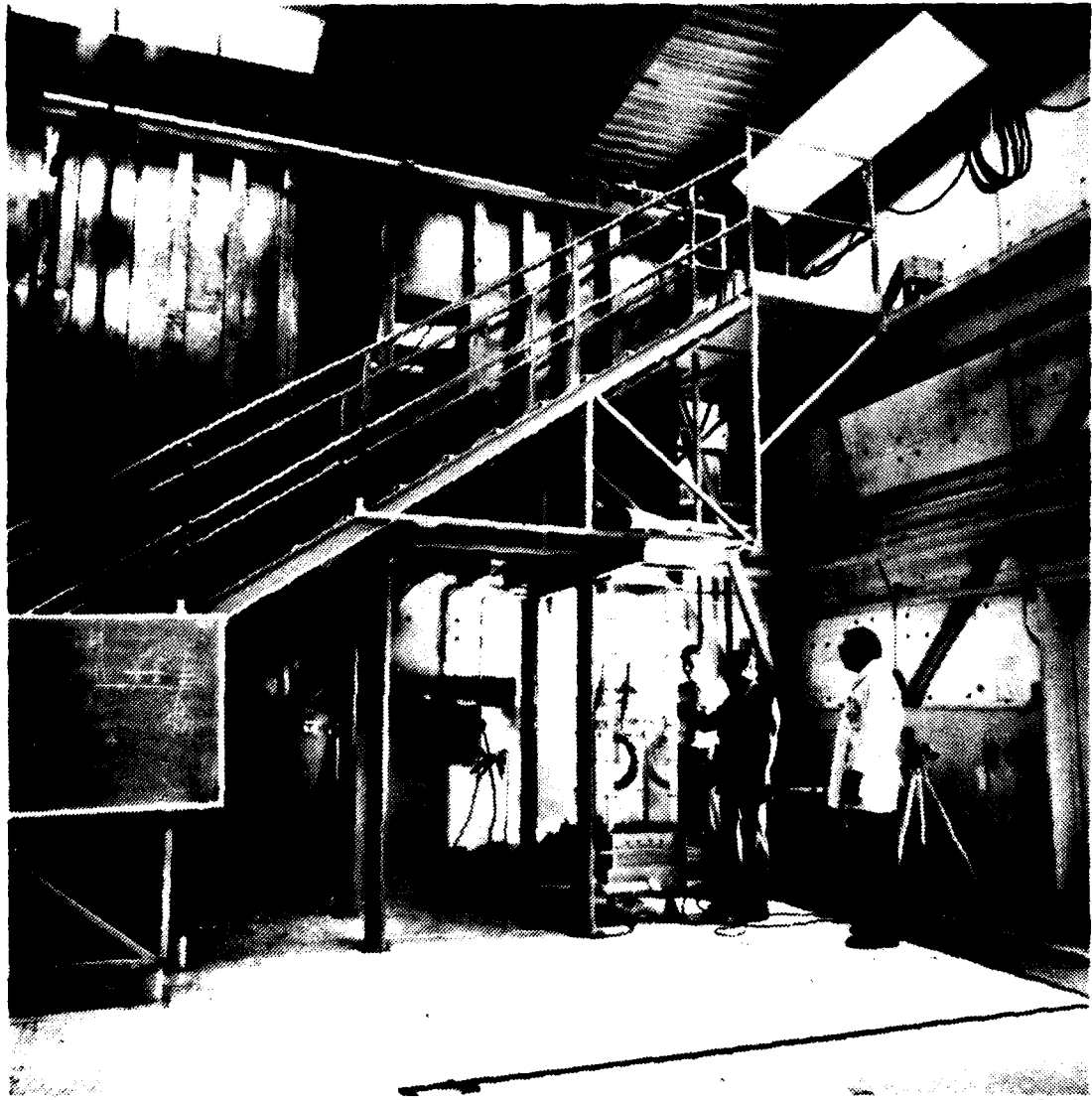
(m) NORTHROP 0.41 X 0.61-METER (16 X 24-INCH) DIAGNOSTIC WATER TUNNEL FACILITY (DWTF).

FIGURE 1. CONTINUED

REMOTELY CONTROLLED DYE PROBE

HOISTING CABLES

TEST SECTION 0.41 × 0.61 × 1.83

PERFORATED PLATE

HONEYCOMB FLOW STRAIGHTENERS AND FOAM

CORRUGATED PIPE SECTION

0.305 PIPE

PUMP

VALVE

WATER LEVEL

DIRECTION OF FLOW

PERFORATED PLATE

1.83

4.72

SIDE VIEW
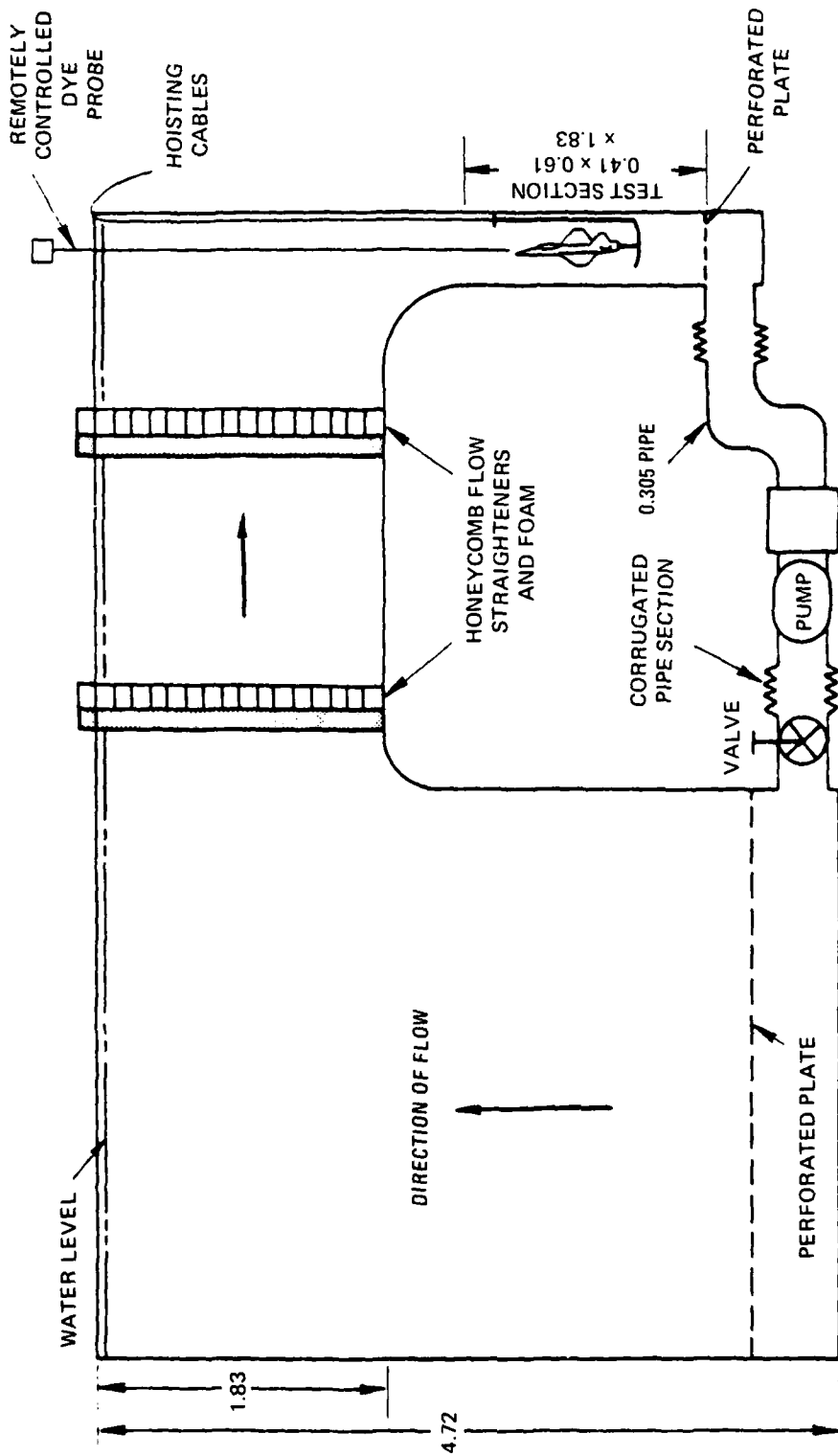
(n) SCHEMATIC OF THE NORTHROP DIAGNOSTIC WATER TUNNEL FACILITY
(ALL DIMENSIONS IN METERS)

FIGURE 1. CONCLUDED.

17

(a) AND (b) 1/140-SCALE "CONCORDE" AT 12 DEGREES ANGLE OF ATTACK AND 10 DEGREES OF SIDESLIP; $Re = 2 \times 10^4$.

(d) AND (f) 1/72-SCALE DOUGLAS F-5D AIRCRAFT AT 15 DEGREES ANGLE OF ATTACK AND ZERO SIDESLIP.

(c) AND (e) FLIGHT TESTS OF THE DOUGLAS F-5D AIRCRAFT

FIGURE 2. TYPICAL VORTEX FLOW RESULTS FROM THE ONERA 22 X 22-CM WATER TUNNEL (FROM REFERENCE 7)

(g)

(g) FLOW ABOUT A CONCORDE
MODEL WITH VERTICAL
DESCENDING MOTION
ABOVE THE GROUND
SIMULATED BY A MOVING BELT.

(h) KARMAN VORTICES DOWN-
STREAM OF A PLATE AT ZERO
INCIDENCE.

(i) PHENOMENON OF VORTEX
BREAKDOWN IN THE PRE-
SENCE OF AN ADVERSE
PRESSURE GRADIENT.

(j) VORTICES PRODUCED BY
ROTOR BLADES OF A HELI-
COPTER IN TRANSLATION.

(k) UNSTEADY SEPARATION
ABOVE A WING OSCILLATING
IN PITCH
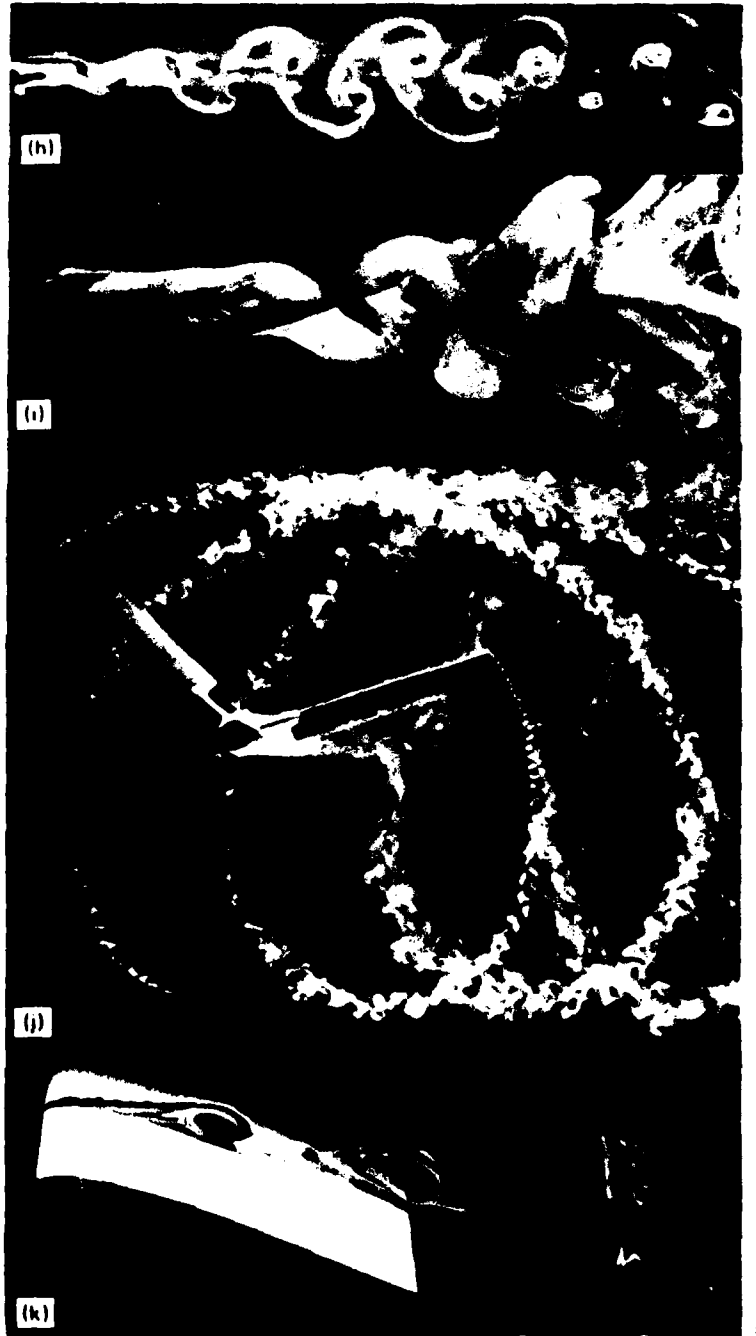
FIGURE 2. CONCLUDED

and flight test results. (Note: A new 40 x 40-cm water tunnel is presently under construction at ONERA.)

The High Speed Water Tunnel (HSWT) at the California Institute of Technology is unique in that flow velocities up to 100 ft/sec and pressures from 100 psig to the vapor pressure of water can be attained. Furthermore, a three-component strain-gage balance, a dynamic balance and oscillator, and a laser doppler velocimeter (LDV)are available for use in this facility. Cavitation separation is one of many flow phenomena which has been studied at Cal Tech in both the HSWT and Free Surface Water Tunnel (FSWT), typical results being shown in Figure 3 (from Reference 39). An outstanding example of a water tunnel simulating at very small scale a large-scale flow phenomenon occurring in nature is the vortical wake shed on the lee-side of an island, as depicted in a NASA aerial photograph which was very well-represented in small-scale water tunnel tests at the California Institute of Technology (Reference 40).

The National Aeronautical Establishment (NAE) in Ottawa, Canada has utilized a water tunnel to visualize a variety of fluid flow phenomena. Representative results are shown in Figures 4 and 5 (from Reference 8). More recently, a missile-type configuration undergoing oscillatory motions has been studied as a means of understanding complex vortical motions in unsteady flow (Reference 41).

The Northrop Diagnostic Water Tunnel Facility (DWTF) evolved from an earlier pilot water tunnel with 6x6-inch vertical test section. This small experimental facility demonstrated the utility of a hydrodynamic test facility in visualizing concentrated vortical motions. Typical results from this tunnel are shown in Figure 6. The Northrop DWTF is a closed-return tunnel used for high-quality flow visualization of complex three-dimensional flow fields. It has been used almost exclusively in the study of fighter aircraft vortex
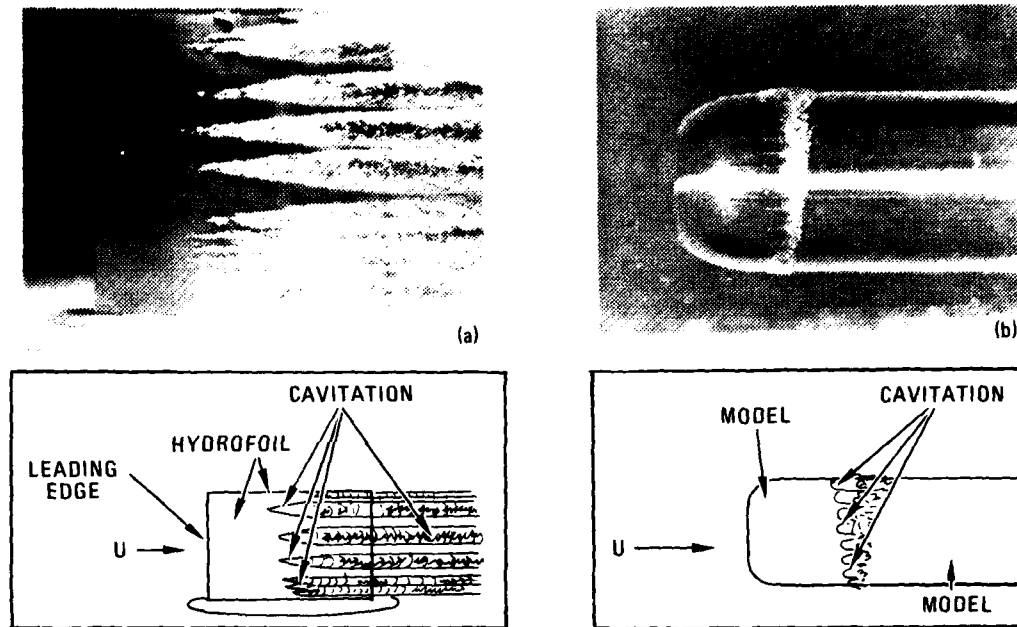
PHOTOGRAPHS ILLUSTRATING THE STRIKING DIFFERENCE IN THE PHYSICAL AP-
PEARANCE OF CAVITATION IN TWO DIFFERENT TYPES OF CAVITATION SEPARATION.
CAVITATION (a) ON A BI-CONVEX HYDROFOIL, SHOWING NUCLEATE SEPARATION
(U = 51 FTS^{-1}, σ = 0.11); (b) ON THE SWEDISH HEADFORM, SHOWING VISCOUS LAMI-
NAR SEPARATION (U = 40 FTS^{-1}, σ = 0.424; BY COURTESY OF ACOSTA).
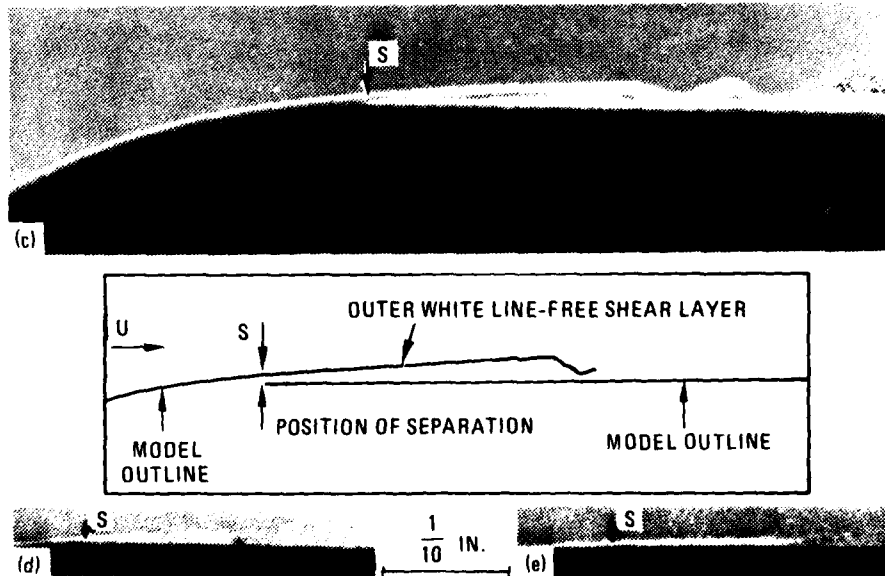
SILHOUETTE SCHLIEREN PHOTOGRAPHS, SHOWING LAMINAR SEPARATION UNDER
NON-CAVITATING CONDITIONS. (c) 2 IN. HEMISPHERICAL NOSE MOUNTED IN THE
FSWT (R $\sim$ 10^5). SOME DETAILS OF THE REATTACHMENT MECHANISM ARE ALSO
OBSERVED. FLOW FROM LEFT TO RIGHT. ACTUAL LENGTH OF SEPARATED REGION
$\sim$ 0.25 IN. (d) HEMISPHERICAL NOSE MOUNTED IN THE HSWT (R = 6.04 X 10^5). (e)
SWEDISH HEADFORM MOUNTED IN THE HSWT (R = 4.39 X 10^5). SCALE SHOWN FOR
(d), (e).

**FIGURE 3. TYPICAL RESULTS FROM THE CALIFORNIA INSTITUTE OF TECHNOLOGY
WATER TUNNEL FACILITIES (FROM REF 39)**

21
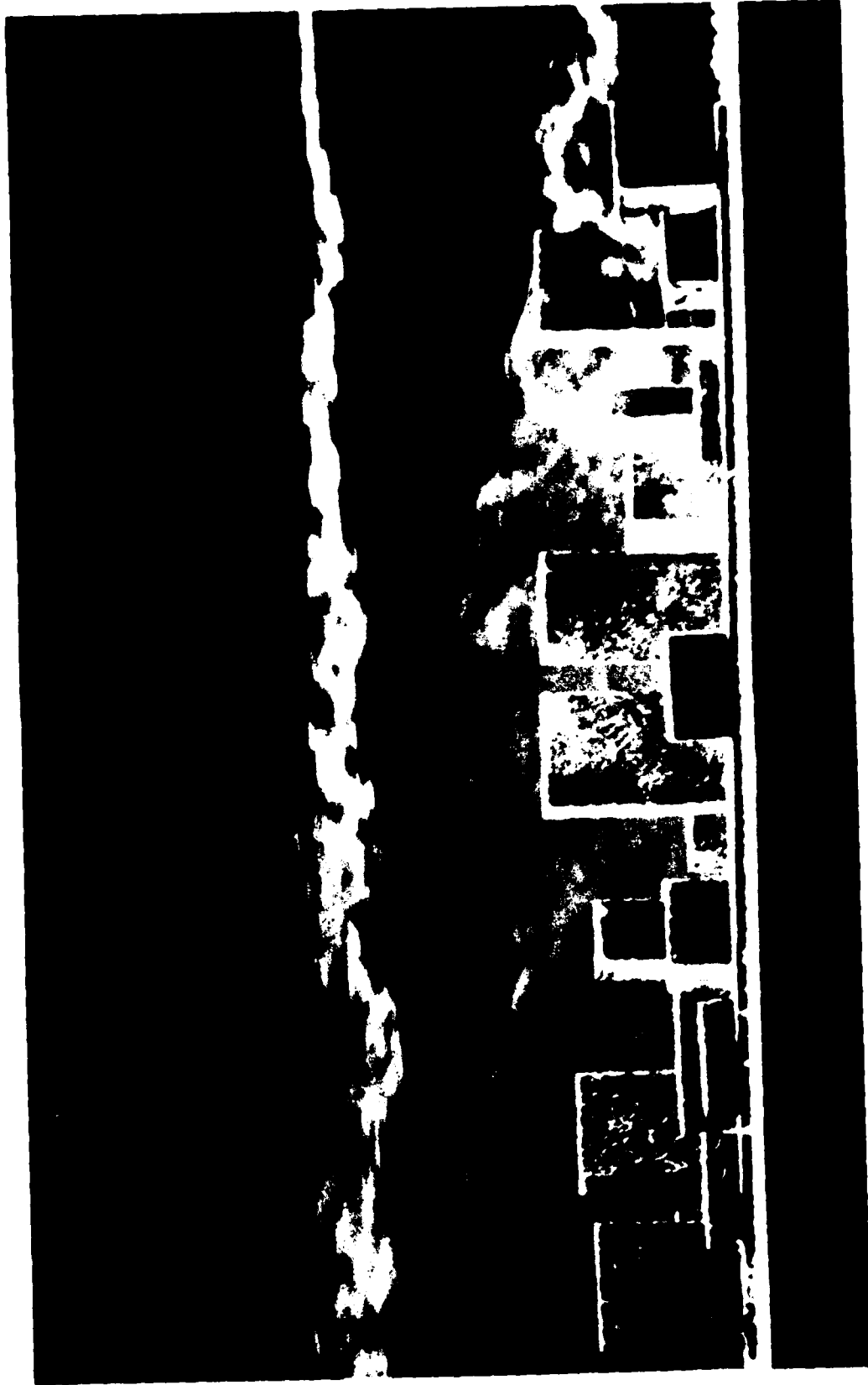
FIGURE 4. WATER TUNNEL SIMULATION OF GROUND WIND OVER CITY IN THE NAE FACILITY (REFERENCE 8)
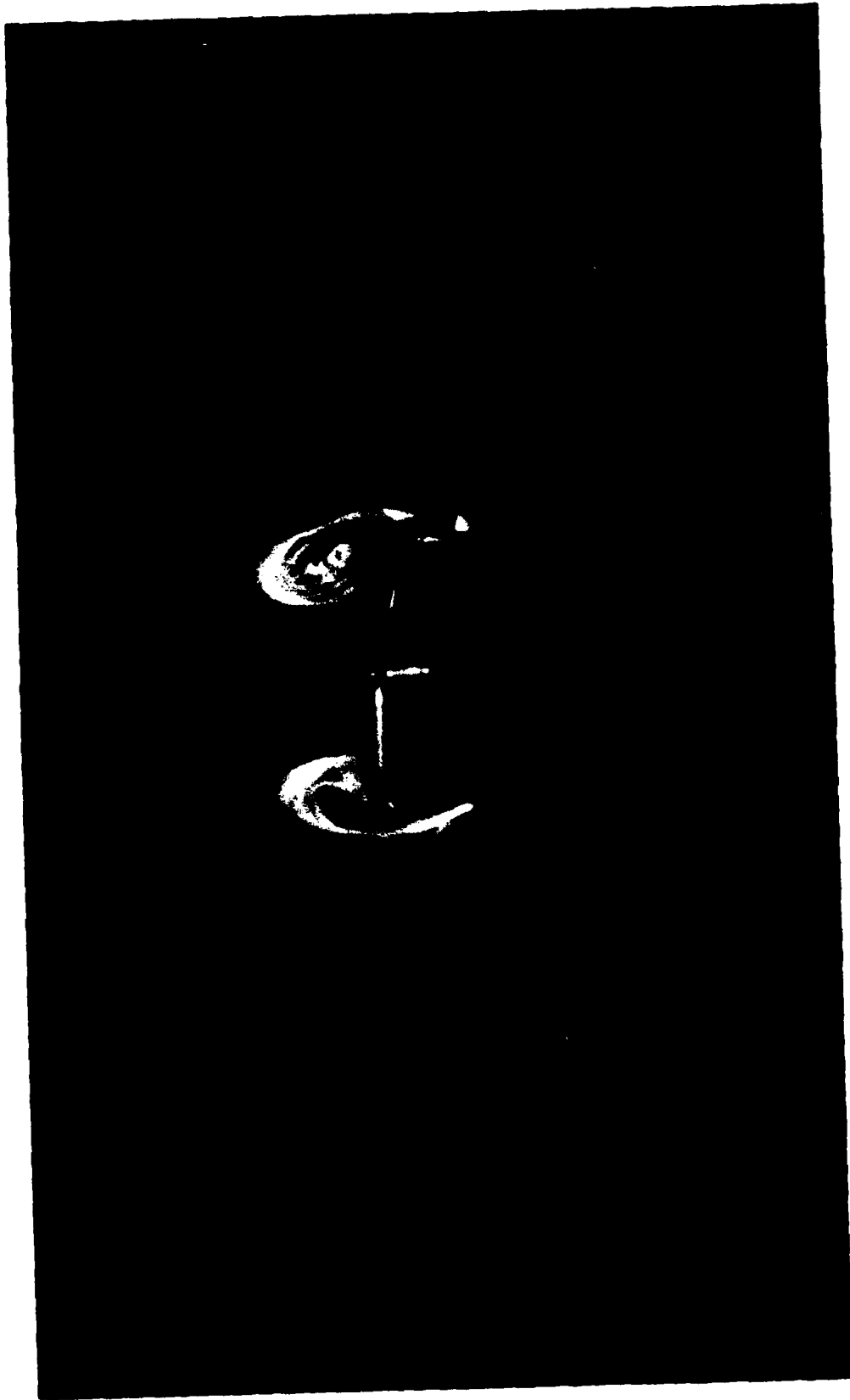
(a) VORTEX PAIR SHED FROM A LIFTING FUSELAGE

FIGURE 5 TYPICAL RESULTS FROM THE NAE WATER TUNNEL (FROM REFERENCE 8)
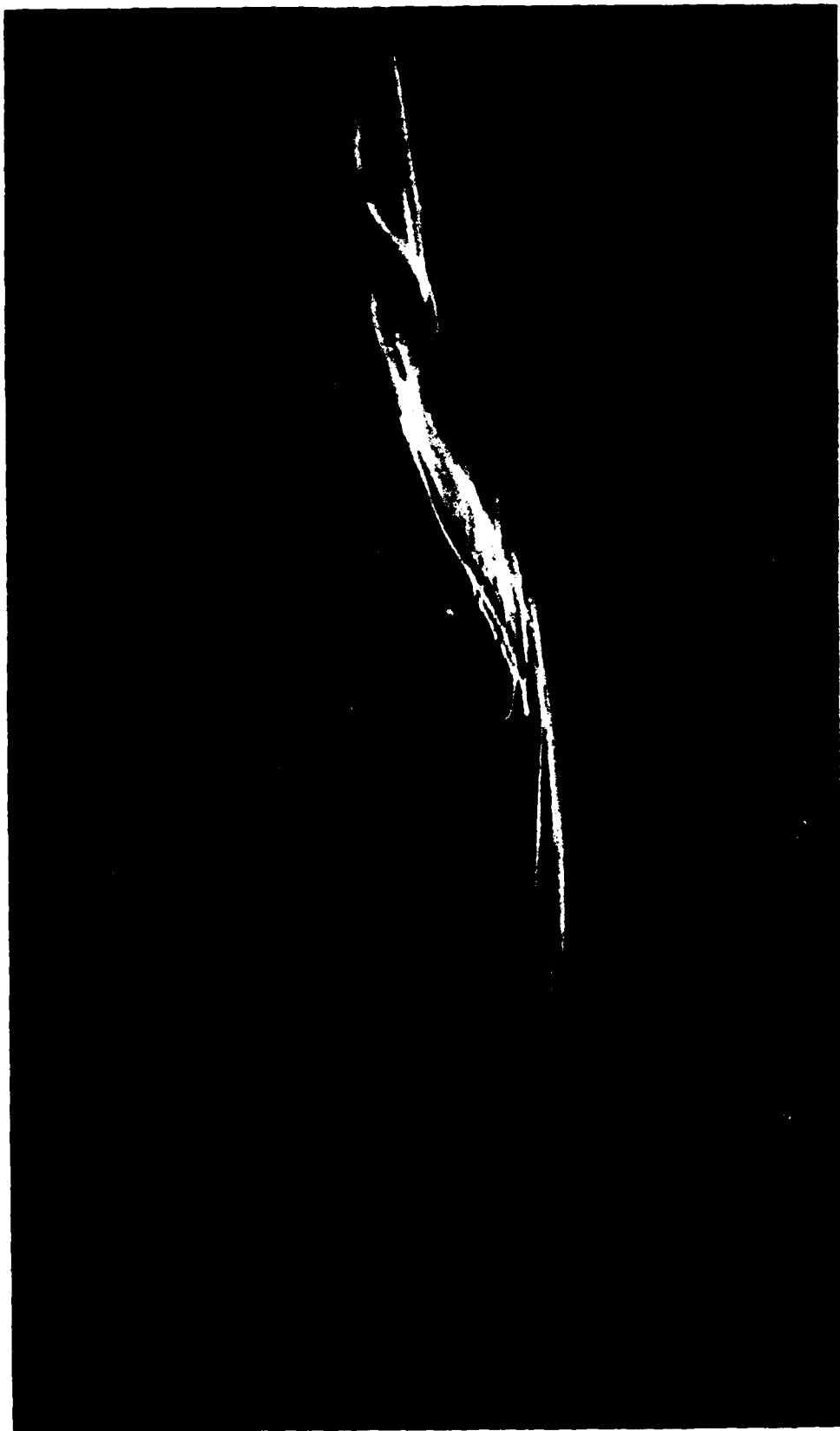
(b) FLOW ABOUT A TRANSPORT AIRCRAFT MODEL WITH UPSWEPT REAR FUSELAGE

FIGURE 5. CONCLUDED

WATER TUNNEL
DEVELOPMENT
AND
APPLICATION
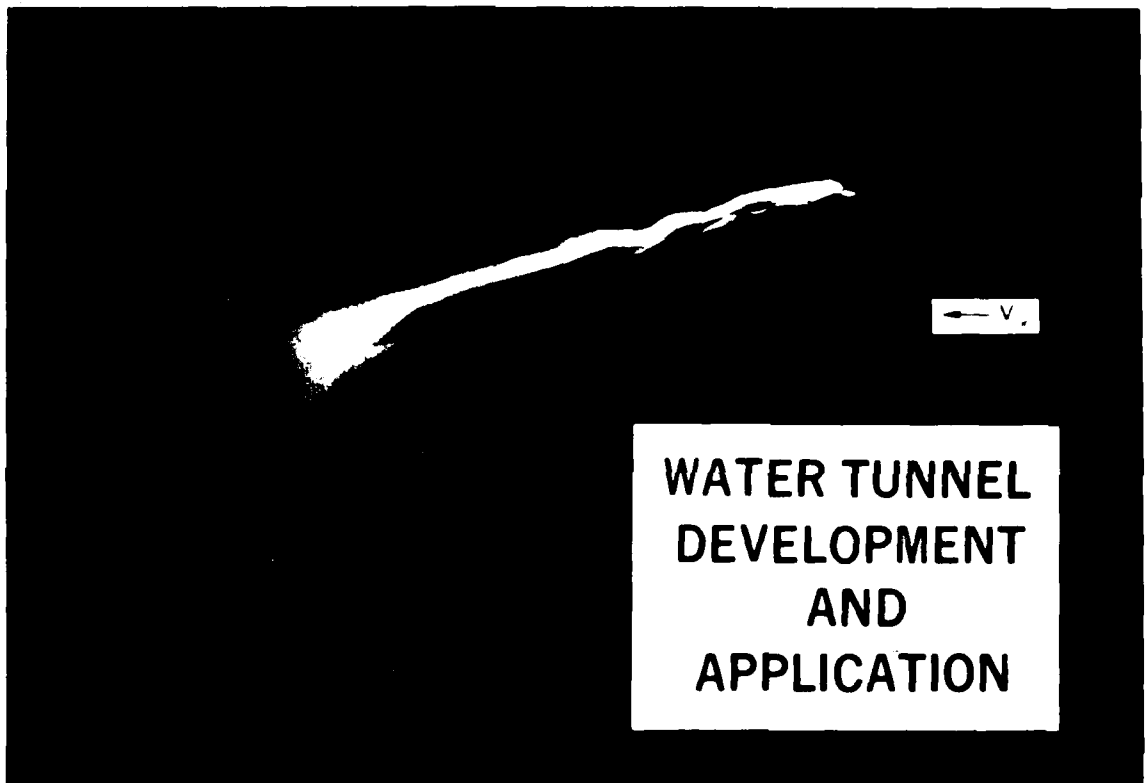
(a) YF 17 MODEL MOUNTED IN TEST SECTION - SIDE VIEW

FIGURE 6. TYPICAL RESULTS FROM THE NORTHROP 6 X 6 INCH PILOT WATER TUNNEL

FIGURE 6. CONCLUDED

flows and vortex interactions at high angles of attack. Models of virtually all the fighter aircraft in the present U.S. inventory and several foreign aircraft configurations have been studied. Representative results are shown in Figure 7. The tunnel is nominally operated at a test section velocity of 0.25 feet per second which corresponds to a Reynolds number of approximately $3(10^4)$ per foot. Figure 1 shows the layout of the water tunnel. The test section is 16 inches by 24 inches by 6 feet long and is oriented in the vertical direction. The model is accessed through the top of the tunnel by means of cables connected to the model support system.

The model support system consists of a sting and yaw arc arrangement which is capable of pitch angles from -10° to 70°, concurrent with a sideslip angle range of -20° to 20°. The pitch angle can be manually adjusted from the side of the test section while the sideslip angle is preset prior to model installation.

Dye injection into the flow field is accomplished through a remotely-controlled dye probe and through dye tubes internally- or externally-mounted to the test models. Inlet flows and exhaust jets can be simulated in the water tunnel through the use of water flow meters that can accurately provide a suction or blowing rate.

An automated pitch, roll, and yaw mechanism has been developed in preparation for in-depth studies of vortex flows in oscillatory motions. A single degree-of-freedom (roll) sting is available which has been used in the past for wing rock studies (Reference 42).

3.2   WATER TUNNEL FLOW VISUALIZATION TECHNIQUES

The techniques for flow visualization of vortex flow phenomena in a water tunnel can be divided into the use of

FORE BODY VORTEX

LEX VORTEX
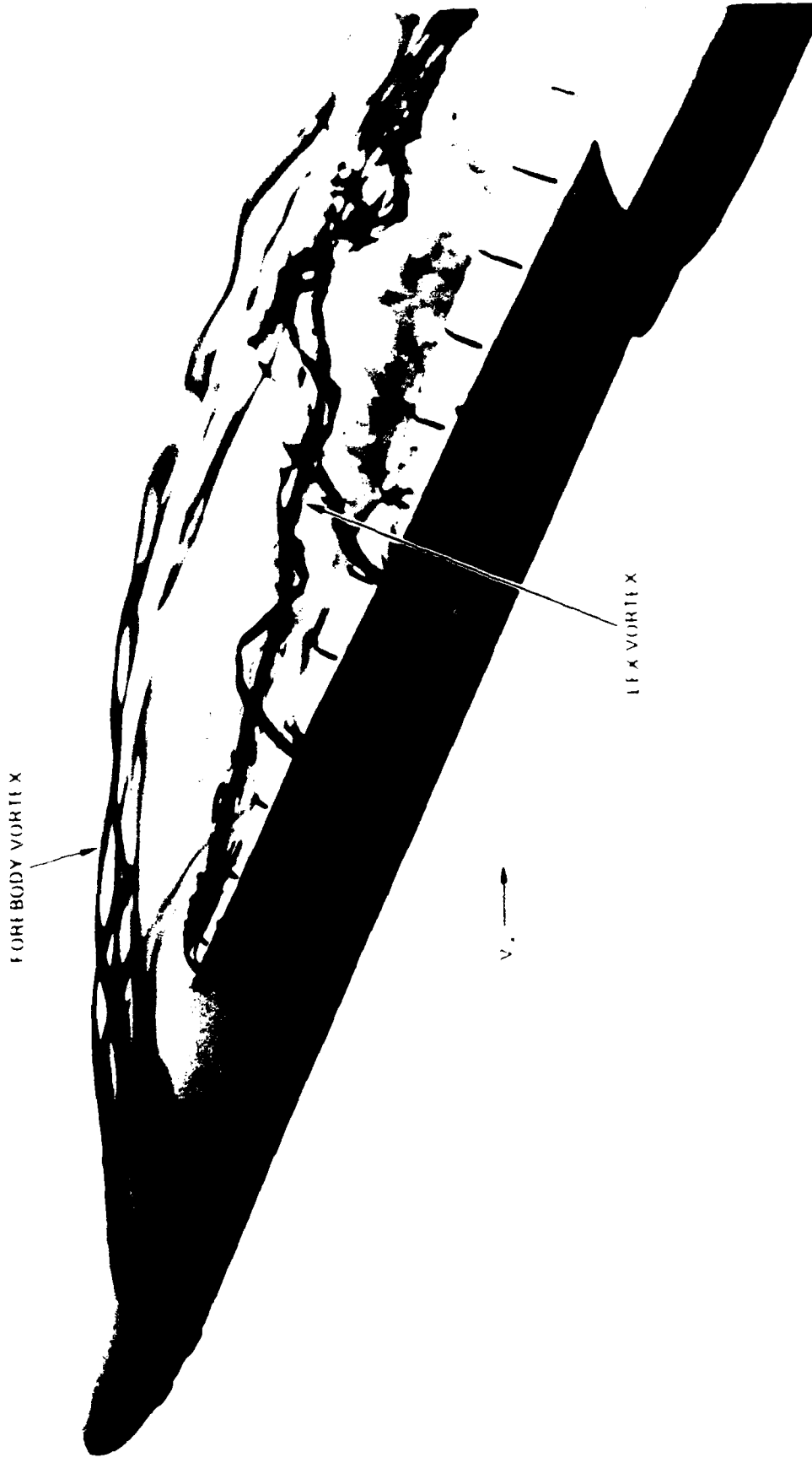
(a) NORTHROP F-18L MODEL MOUNTED IN TEST SECTION

FIGURE 7   TYPICAL RESULTS FROM THE NORTHROP DIAGNOSTIC WATER TUNNEL FACILITY

FOREBODY VORTICES

(b) NORTHROP F-5F MODEL MOUNTED IN TEST SECTION

FIGURE 7. CONTINUED

SPIRAL CORE BREAKDOWN

LEX VORTEX CORE

(C) 0.5-SCALE WATER TUNNEL MODEL OF NASA GENERAL RESEARCH CONFIGURATION DEPICTING SPIRAL VORTEX CORE BREAKDOWN PHENOMENON

FIGURE 7. CONCLUDED

suspended particles and the injection of colored dyes. An aluminum powder in suspension in the water and illuminated by an intense light source will reflect sufficient light for good photographic results as discussed in Reference 8. The aluminum particles have been found to remain in solution better than most materials. The use of particles has the disadvantage in that they uniformly cover the entire flow field and so cannot be used in select locations. The high concentration of the particles in the water makes it necessary to flush and clean the tunnel at the conclusion of the tests. In place of solid particles, air or hydrogen bubbles can be used for flow visualization which eliminates any contamination of the tunnel water. The diameter of the air bubbles must be kept small to reduce their buoyancy and so allow them to follow the local flow motions. Hydrogen gas can be produced by electrolysis of water at a cathode. Passing an electric current through a wire can generate a sheet of hydrogen bubbles along the whole length of the wire. The entire model or any exposed metal parts of the model can also be used as a cathode to generate the bubbles. (Reference 43 provides an excellent review of this technique.)

Cavitation has also been used to visualize vortex core trajectories (see Reference 44). Cavitation can be induced in the vortex cores by varying the test section static pressure. The parameter used to characterize this phenomenon is the cavitation inception coefficient defined by

$$\sigma = 2(p_\infty - p_v)/\rho V_\infty{}^2 \qquad \text{Equation 1}$$

Since the vortex cores are the lowest pressure points in the flow, visible cavitation bubbles occur there when the local pressure is approximately equal to the vapor pressure of water, p_v, which is a known function of water temperature (see Reference 45 for a complete discussion of cavitating flows). Provided controlled cavitation occurs, where the vapor

bubble diameters remain small, the bubbles will tend to follow streamlines more closely and, in the limit, the technique is analogous to the hydrogen bubble method. Due to the difficulty of controlling cavitation, however, the vapor bubbles may become quite large. The introduction of significant volume into the vortex core regions under conditions of large-scale cavitation is expected to distort the flow and, in general, have a large effect on the core behavior.

To study local details of flows, such as the structure of a vortex, dye can be injected at selected locations. The dye is injected into the external flow through ports distributed along the body of the model or through a remotely actuated dye probe. One type of dye that has been used is fluorescent under ultraviolet light. Because only the dye is fluorescent, this method reduces reflections and shadows on the model. The fluorescent dye will dominate the main flow and the tunnel has to be drained frequently. The dyes that have been used extensively at Northrop are food dyes that are available in a variety of colors. Contamination of the main flow is not a problem, as the color can be bleached out by the addition of chlorine.

Another technique for flow visualization uses a dilute suspension of bentonite in the tunnel. The bentonite has the property of streaming double refraction. When the flow around the model is illuminated with polarized light, the shear patterns, and so the vortex flow patterns, in the water become visible (Reference 46). The bentonite particles themselves are microscropic and remain in suspension in the tunnel. This technique was developed for use in the Cal Tech water tunnel. (For an updated description of these facilities, an excellent review is provided in Reference 47.)

TABLE I - WATER TUNNEL FACILITIES

COMPANY/UNIVERSITY	LOCATION	APPLICATIONS
Northrop 16 x 24-inch Test Section: V_∞ = .25 fps; Re_c = 30,000 (typical)	Hawthorne, California	Slender Wing & Forebody Vortex Shedding; Fighter Aircraft Vortex Flow Interactions: Flow Control by Cross Jet; Nozzle Plume and Engine Inlet Studies; Slender Wing Rock Phenomena; Multiple-Jet VSTOL in Ground Effect; Cruciform Missile Configurations; Forward Swept Wing (FSW) Concepts.
ONERA Water Tunnel: 22 x 22-cm Test Section; $V_{\infty max}$ = 20 cm/s; Re_c = 20,000 (typical) Water Tank: Static Tests Thin Tank: 2-D Highly- Viscous Flows "Supersonic" Tank: (free surface) hydraulic analogy	Chatillon-Sous-Bagneux, France	Vortex Flows; Spinning/Oscillating Models; Air Intake & Engine Exhaust Studies; 2- & 3-D Flows; Jets; Ground Effects; Unsteady Flows; Flow within Turbomachinery.

TABLE I - WATER TUNNEL FACILITIES (Continued)

COMPANY/UNIVERSITY	LOCATION	APPLICATIONS
National Aeronautical Establishment (NAE) 10 x 13-in. Test Section; $V_\infty = 0.2 - 10$ ft/s Re = $1.3 \times 10^4 - 6.5 \times 10^5$ (per foot)	Ottawa, Canada	Boundary Layer Separation; Flow Through Lifting Propeller; Internal Flows; Jets; Ground Effects; Ground Cushion Vehicle; Delta Wing Vortices; Body Vortices.
California Institute of Technology HSWT: 35.6-cm diameter; $V_{\infty max} = 100$ fps; pressures from 100 psig to vapor pressure of water; force measurement capability FSWT: 50.8-cm x 76.2 cm; $V_{\infty max} = 25$ fps	Pasadena, California	Flapped Hydrofoil Studies; Sound Transmission; Spin-Stabilized Projectile Trajectories; Chemically-Reacting Turbulent Shear Layers; Leading-Edge Flutter of Super-cavitating Airfoils; Cavitating Cascade Flows; Trailing Vortices Behind Lifting Hydrofoils; Delta Wing Leading Edge Vortices; Forebody Vortices.
Von Karman Inst. for Fluid Dynamics (VKI) 15 x 15-cm. Test Section; $V_\infty = 0.21$ m/s; $Re_d = 4200$	Rhode-Saint-Genese, Belgium	Rotor Performance; Vortex Flows on Missile with Wing-Strake; Delta Wing Vortices.

TABLE I - WATER TUNNEL FACILITIES (Continued)

COMPANY/UNIVERSITY	LOCATION	APPLICATIONS
Virginia Polytechnic Inst. and State University (VPI-SU) 25 x 30-cm. Test Section, $V_{\infty max}$ = 2.5 m/s; Re_c = 70,000	Blacksburg, Va.	Transient and Oscillatory Separating Laminar Flows.
Penn. State University 48-inch diameter Test Section; $V_{\infty max}$ = 83 fps	University Park, Pa.	Boundary Layer Transition, Cavitation Flows, Eddy Structures in Viscous Sublayer, Horizontal Buoyancy Effects; Rotor Performance; Propeller Time-Dependent Forces Due to Non-Uniform Flow, Hydrofoil Studies.
NASA Ames (AVRADCOM) 0.2 x 0.3-meter Test Section; $V_{\infty max}$ = 6 m/s; Re_c = 21,000	Moffett Field, Ca.	Dynamic Stall of Airfoils, Vortex Interactions in Multiple Vortex Wakes, Unsteady Turbulent Boundary Layers; General Fuselage Shapes, Wing Tip Vortex Minimization.
U.S. Air Force Wright Aeronautical Laboratory 6 x 6-inch Test Section; V_∞ = 0.35 fps; Re_c = 15,000	Dayton, Ohio	Body Vortices; Nozzle Plumes; Forward Swept Wings.

35

TABLE I - WATER TUNNEL FACILITIES (Continued)

COMPANY/UNIVERSITY	LOCATION	APPLICATIONS
California University 30-cm-diameter Test Section; $V_{x_{max}}$ = 30 cm/s; Re_l = 1.6 x 10³	Santa Barbara, Ca.	Vortex Flows; Laser Doppler Anemometer Development; Biological Studies
British Aerospace Dynamics Group 45.7 x 45.7-cm. Test Section; $V_{x_{max}}$ = 3 m/s	Warton, England	Body Vortex Interactions with Wing Panels on a Missile Configuration.
University of Iowa 30 x 36-in. Test Section (Hydraulic Flume); Re_l = 8.0 x 10⁴	Iowa City, Iowa	Flow Separation on a Spheroid at Incidence
Aeronautical Research Labs (ARL) 25 x 25-cm. Test Section; V_x = 7.4 cm/s; Re_l = 9800	Melbourne, Australia	Vortex Breakdown Over Wings with Highly- Swept Leading Edges.
University of So. Calif. Water-Jet Facility V_{exit} = 1.4 m/s; Re_{max} = 40,000	Los Angeles, Ca.	Geometry of Large-Scale Structures in Turbulent Mixing Layers

36

TABLE I - WATER TUNNEL FACILITIES (Continued)

COMPANY/UNIVERSITY	LOCATION	APPLICATIONS
Admiralty Research Lab (ARL) 30-inch diameter Test Section; $V_{x_{max}} = 60$ fps	England	(Not in use at present time)
National Physical Lab (NPL) 13 x 10-inch Test Section; $V_x = 5$-8 fps; $Re_c = 50,000$	Teddington, England	Vortex Shedding from Slender Cones; Leading-Edge Vortices on Delta Wings (Static; Pitching).
University of Southampton 13 x 10-inch Test Section; $V_{x_{max}} = 20$ fps; $Re_c = 30,000$ (Note: This tunnel is a copy of the NPL tunnel.)	Southampton, England	Leading-Edge Vortex Flows; Cavitation Damage.
Nielsen Engineering and Research (NEAR) 36 x 56-cm Test Section; $V_{x_{max}} = 6$ m/sec; $Re_c = 1.5 \times 10^5$; Force Measurement Capability	Mountain View, Ca.	Body Vortex Formation on Missiles and Fighter Aircraft.

TABLE I - WATER TUNNEL FACILITIES (Continued)

COMPANY/UNIVERSITY	LOCATION	APPLICATIONS
DTNSRDC 12-inch Variable Pressure (Open-Jet Type); 36-inch Variable Pressure (Open-Jet Type); Force Measurement Capability; $v_{x_{max}} = 60$ fps; $Re_\ell = 5.6 \times 10^5$	Bethesda, Maryland	Propeller - Nozzle Performance; Grid Turbulence; Body Vortex Formation; Unsteady Cavitation on Oscillating Hydrofoils
United Aircraft Corp.	E. Hartford, Conn.	Cascade Flows: Helicopter Rotor Wake Patterns.
TRG, Inc.	Melville, N.Y.	Flow-Induced Noise.
Oceanics, Inc. (Water Channel)	Plainview, N.Y.	Rotor Model Tests with Highly Deflected Wakes; Ground Effects; Helicopter Rotor Flow Patterns; Propeller-Induced Unsteady Forces on Rudder.
Rochester Applied Science Associates, Inc.	Rochester, N.Y.	Hydrofoil Loading and Cavitation
Institut de Saint-Cyr	France	Cavitation Flows
University of Manchester	Manchester, England	(Not in use at present time)
AVA	Germany	Cavitation Phenomena
SOGREAH	France	Cavitation Phenomena

38

TABLE I - WATER TUNNEL FACILITIES (Continued)

COMPANY/UNIVERSITY	LOCATION	APPLICATIONS
CEA	France	Flows in Heat Exchanger
Institute of Bucharest	Bulgaria	Viscous Flows
NASA Langley Research Center (Tow Tank)	Hampton, Virginia	Trailing Vortices
University of Kyushu (Tow Tank)	Kyushu, Japan	Trailing Vortices
Douglas Aircraft (Tow Tank)	Huntington Beach, Ca.	Trailing Vortices
U.S. Naval Postgraduate School	Monterey, California	Fluid Force on Oscillating Cylindens Forces on Roughened Cylinders in Harmonic Flow; Vortex Flows in Tubes.
Dornier GmbH	Friedrichshafen, W. Germany	Wing Tip Effects on Airfoil Design for General Aviation Aircraft.
California University	Los Angeles, Ca.	Tracer - Particle Generator for use in Holographic Flow Visualization; Motion of Near-Neutrally Buoyant Tracers in Vortical Flows.
Stuggart University	Stuttgart, W. Germany	Fluid Motion Downstream of 2-D Tollmien-Schlicting Waves.

TABLE I - WATER TUNNEL FACILITIES (Continued)

COMPANY/UNIVERSITY	LOCATION	APPLICATIONS
Princeton University (Water Channel)	Trenton, N.J.	Instability and Transition in Axisymmetric Wakes of Slender Bodies of Revolution.
Case Western Reserve University	Cleveland, Ohio	Stability of Heated Laminar Boundary Layers.
Purdue University	Lafayette, Ind.	Turbulent Boundary Layers.
California University	San Diego, Ca.	Turbulence in Stratified Flow and Ocean Physics.
Technische Physische Dieust	Netherlands	Holographic Investigation of Boundary Cavitation Phenomena.
California University	La Jolla, Ca.	Turbulent Velocity and Temperature Fluctuations in Wake of Sphere; Chemical Reaction Product Fluctuations in Reacting and Nonreacting Turbulent Wake of Sphere.
Swedish State Shipbuilding	Göteborg, Sweden	Cavitation Flows.
Tennesse University Space Institute	Tullahoma, Tenn.	Inlet Vortex Systems.
Michigan University	Ann Arbor, Michigan	Cavitation Nuclei Spectra Measurements.
Bristol University	Bristol, England	Decay of Trailing Vortices.

TABLE I - WATER TUNNEL FACILITIES (Continued)

COMPANY/UNIVERSITY	LOCATION	APPLICATIONS
Max Plank Inst. fuer Stroemungsforschung	Goettingen, W. Germany	Interaction Between Turbulent Boundary Layers and Compliant Walls.
Boeing Scientific Research Labs	Seattle, Washington	2-D Tests of Pitching Airfoils.
Lockheed-Georgia (Water Channel)	Marietta, Georgia	Boundary Layer Studies.
General Dynamics	San Diego, California	Turbulent Film Boiling Tests of Heated Flat Plate.
Notre Dame University	South Bend, Ind.	Boundary Layer Characteristics.
(Undetermined) (See Reference 184)	U.S.S.R.	Cavitating Wings; Vortex Flows (Delta Wings); Rotor in Ground Effect; Cavitating Flows; Unsteady Flow Past Plane Cascades; Fuselage Nose Vortices; Jet in a Cross-Flow
USAF Aero-Propulsion Lab	WPAFB, Ohio	Swirl Effects on Ramjet Dump Combuster; Fuselage Nose Vortices; Nozzle Plumes.
National Aerospace Lab	Tokyo, Japan	Cavitating Inducer Instabilities; Flow Separation in a Divergent Channel.

41

TABLE I - WATER TUNNEL FACILITIES (Continued)

COMPANY/UNIVERSITY	LOCATION	APPLICATIONS
MIT	Cambridge, Mass.	Hydrodynamic Forces and Moments on a Submerged Body of Revolution; Propellers; Rudders.
Messerschmitt-Beolkow-Blohm GmbH	Ottobrun, W. Germany	Wing-Strake Vortex Flows.
Atmospheric Environment Service	Ontario, Canada	Convective Plumes.
DFVLR	Freiburg, W. Germany	Boundary Layers; Ground Effects; Wakes; Unsteady Flows; Wing-Strake Vortices
University of Alabama	Huntsville, Ala.	Unsteady Pressures and Forces on Submerged Bodies.
Delaware University	Newark, Del.	Bottom Topography Effects on Rotating Flows.
Montreal University	Montreal, Canada	Plane Jet in Crossflow with Vortex Shedding Control.
Johns Hopkins University	Baltimore, Md.	Fluid Material Line Growth in Grid-Generated Isotropic Turbulent Flow; Stratified Flows.

TABLE I - WATER TUNNEL FACILITIES (Concluded)

COMPANY/UNIVERSITY	LOCATION	APPLICATIONS
Oxford University	Oxford, England	Fluid Mechanics of Aortic Valves; Cavitation.
Tohoku University	Sendai, Japan	Surface Pressures on Hydrofoil Profiles in Cascade.
Tokyo University	Tokyo, Japan	Torsional Stall Futter of an Airfoil.
Aix-Marseille Universite	Marseille, France	Aerodynamics of Porous Sheets.
Akademiia Nauk Ukrainskoi SSR	Kiev, Ukrainian SSR	Hydro-Gas Ramjet Engine Model Aerodynamic Damping of Trubomachine Blade Virbrations; Cavitation; Turbulent Boundary Layers.
SIGMA Research Institute	Olomouc, Czechoslovakia	Cavitation Erosion Resistance.

43

SECTION 4

TASK II - IDENTIFICATION OF KEY PARAMETERS PERMITTING CORRE-
LATION OF WATER TUNNEL RESULTS WITH WIND TUNNEL
AND FLIGHT DATA

4.1   INTRODUCTION

A remarkable feature of vortices shed from aircraft and
missile configurations at high angles of attack is the simi-
larity under particular external conditions of vortex flow
behavior in sub-scale and full-scale tests. Water tunnel test
facilities have shown great utility in the study of these
complex fluid-mechanics phenomena.

The flow phenomena which must be simulated in order to
ensure correlation of water tunnel, wind tunnel, and flight
tests results are:

    (1) Vortex Generation
    (2) Vortex Sheet and Core Location
    (3) Vortex Core Breakdown (or Burst)

A discussion of vorticity in fluid flows is now pre-
sented, followed by discussions of vortex flow fluid mechanics
involving vortex development, interactions, and breakdown on
slender wings and slender bodies up to high angles of attack.

4.2   VORTICITY IN FLUID FLOWS

This paragraph is intended to provide a brief discussion
of the concept of vorticity and the development of fluid

44

flows. As will be discussed subsequently, vortex sheet and core locations and the aerodynamic loading on slender wings can be reasonably predicted by theoretical methods which assume "infinite" Reynolds numbers, that is, viscous forces are ignored. However, the vortex sheet which originates from the wing leading edge consists of distributed vorticity which is generated in the viscous flow near the wing surface. Vorticity is related to the angular momentum of the fluid. In boundary layers, where viscous effects are significant, large velocity gradients are produced and vorticity is generated. Boundary layer fluid mechanics can be adequately expressed in terms of momentum changes due to convection, viscous diffusion, and pressure gradient effects. In order to properly locate the boundary layer in the flow as a whole, however, vorticity must be considered.

A solid boundary such as a wing or body can be regarded as a distributed source of vorticity. The vorticity generated at the surface is carried away from the surface by diffusion and convection. This determines the entire flow, whose development, in turn, controls the production of vorticity. For attached flow, vorticity is shed at the wing trailing edge into the trailing vortex system and, for bodies, into the body wake.

When the Reynolds number is very small (less than 1), corresponding to Stokes flow or creep flow, convection of vorticity is very slow compared even with diffusion over distances of the order of a characteristic length (ℓ). For Reynolds numbers between 1 to 10, convection of vorticity near the body leads to formation of a separation line which moves forward from the rear as Reynolds number increases. The flow has a separation bubble and a steady laminar wake, provided the Reynolds number remains below a critical value at which the wake becomes unstable. At Reynolds numbers at or above this critical Reynolds number, the vorticity undergoes a

redistribution mode which builds up to large oscillations in the wakes of cylindrical bodies. This mode is of a general type leading to the familiar von Karman vortex street or staggered parallel rows of vortices. (Note: Water tank studies by Prandtl (Reference 48) show quite lucidly this flow phenomenon, as illustrated in Figure 8 (from Reference 48).) When the vorticity close to the cylinder is fluctuating between large positive and negative values, substantial fluctuating forces on the cylinder are experienced.

For three-dimensional bluff bodies (a sphere, for example), the critical Reynolds number values are higher because there is no mode of vorticity redistribution in the wake that has the very marked instability of rows of staggered vortices. The dominant mode is often a spiral vortex.

4.3   SLENDER WING LEADING-EDGE VORTEX FLOW SIMULATION

The following paragraphs present detailed discussions of the following flow phenomena: (1) vortex generation; (2) vortex sheet and core location; and (3) vortex core breakdown. Theoretical approaches are presented which are augmented by experimental studies in order that key flow parameters affecting vortex behavior may be identified.

4.3.1 Vortex Generation

Bodies with salient edges often have a fixed line of separation at the edge. The flow up to the edge is accelerating, but the flow around it would involve retardations that would separate any boundary layer. On thin, sharp-edged wings, the boundary layer on the lower surface cannot negotiate the very large pressure gradients at the leading edge and, consequently, a fixed line of separation exists and a sheet of distributed vorticity is shed at the leading edge. For slender

46
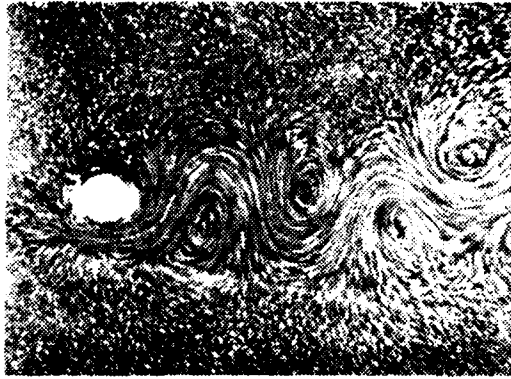
FIGURE 8. VON KARMAN VORTEX STREET; $RE_D = 250$ (REFERENCE 48)
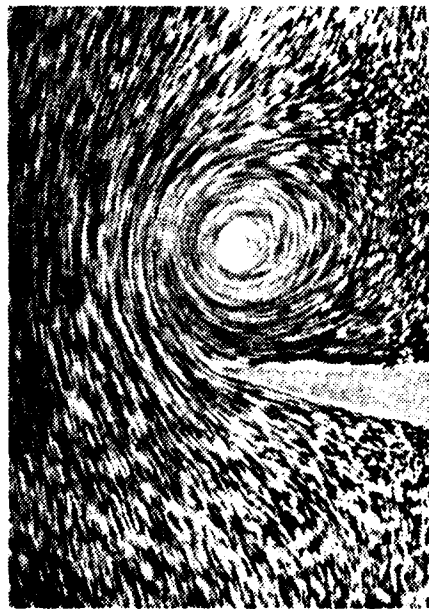
(WATER CHANNEL — REF 48)
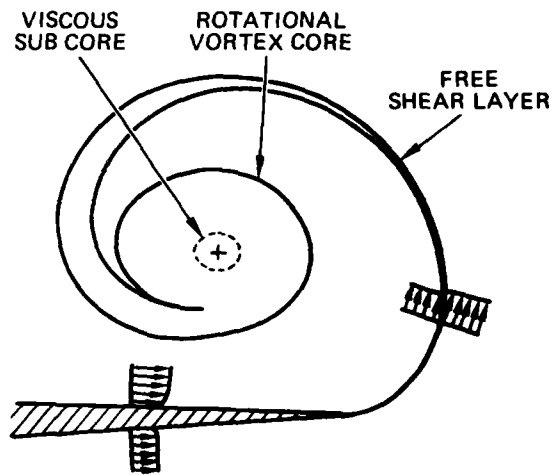
FIGURE 9. VORTEX SHEET ROLL-UP ON A THIN SLENDER WING

wings, the vortex sheets roll up into the classical leading-edge spiral vortices with concentrated cores as sketched in Figure 9. Separation occurs at a sharp leading edge whether the lower surface boundary layer is laminar or turbulent (unless, of course, the Reynolds number is so low as to result in a Stokes flow phenomenon). Since this condition is satisfied in a water tunnel, wind tunnel, and in flight, vortex generation on thin, sharp-edged slender wings is accurately represented in a hydrodynamic test facility.

In Reference 49 calculations on a delta wing at low angles of attack show that the leading-edge vortex sheet contains about 60 percent of the total shed vorticity and the strength of the reversed vorticity in the trailing edge vortex sheet is approximately one-half this. The remainder goes into the horseshoe vortices as described in Reference 50. Flow studies in a water tunnel (Reference 51) indicate that the origin at the wing of a concentrated trailing vortex lies in the region where the secondary vortex reaches the trailing edge of the wing and its rotation has the same sense as the secondary vortex as sketched in Figure 10 (from Reference 51) and Figure 11. The concentrated trailing vortex and the secondary vortex are two separate vortices, however. The counterrotating trailing vortex leads to a very heterogeneous downwash field behind the wing. Reference 52 has indicated that this might be the reason for the relatively high induced drag of slender wings.

At high angles of attack, Reference 49 shows the flow pattern on a delta wing to be dominated by the leading-edge separations and that there is no reason to suppose significant amounts of trailing vorticity are generated between the attachment lines (about 1 percent of the total vorticity). Calculations indicate the reversed trailing vorticity in the trailing vortex sheet has about 15 percent of the strength of the vorticity contained in the leading-edge vortex sheet.

48

V_∞
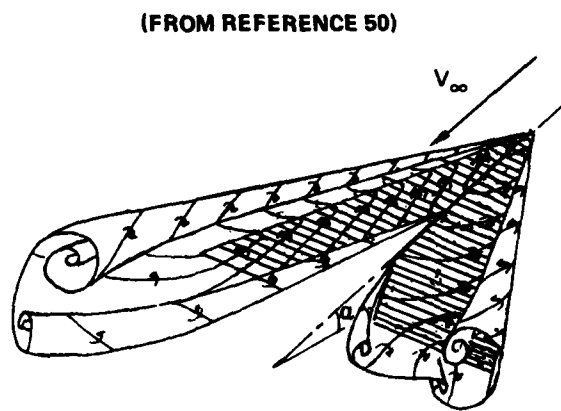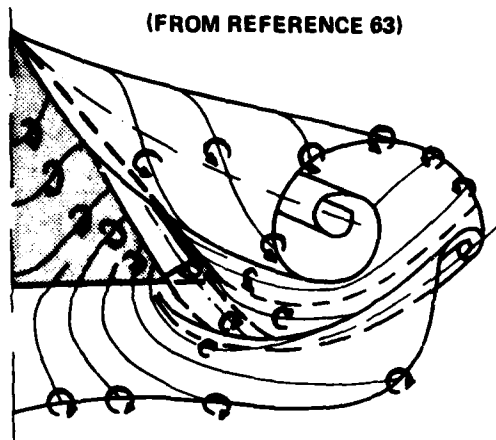
FIGURE 10. VORTEX FORMATION BEHIND SLENDER WINGS (SCHEMATIC)

α

V_∞

LEADING EDGE
FREE VORTEX SHEET

TRAILING EDGE
FREE VORTEX SHEET

y

A ← B ←

x

A ← B ←

VORTEX CORE   (VORTEX SHEET)

z

$q_n = 0$
$\Delta p = 0$

$q_n = 0$

SECTION A-A (WING)

z

$q_n = 0$

$\Delta p = 0$

y

SECTION B-B (WAKE)
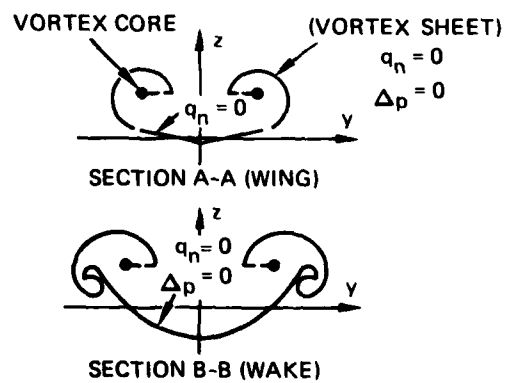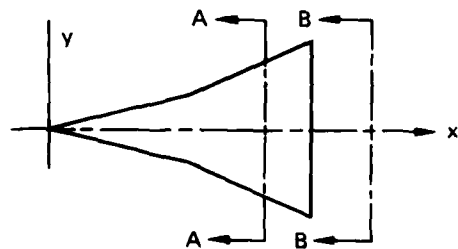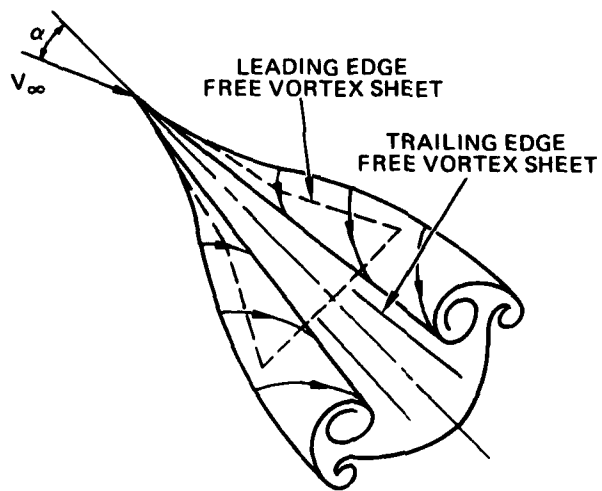
FIGURE 11. FLOW PAST A SLENDER WING WITH LEADING-EDGE VORTEX FLOW

A water tunnel is useful in visualizing the reversed trailing vorticity by injecting air or dye on the surface almost at the trailing edge. The trailing vorticity rolls up into a core which is at first inclined upwards and outwards by the induced velocity field and then turns back to form a spiral around the leading-edge vortex. The horseshoe vortices between the upper surface attachment lines cannot be visualized because of their very low strength.

The effect of trailing edge geometry may be quite significant, as sketched in Figure 10 (from Reference 50). The essential difference between the two vortex patterns depicted in this figure is in the ratios of the strengths of the leading-edge and trailing-edge vortices. Of significance to water tunnel simulation is that a considerable interaction can occur between the leading- and trailing-edge vortical flows. This has been observed in Northrop water tunnel studies and is also documented in ONERA studies in Reference 53.

4.3.2 Vortex Sheet and Core Location

Three-dimensional regions of separation in laminar and turbulent boundary layers exist in many diverse fashions on lifting aerodynamic configurations immersed in flows from subsonic to hypersonic speeds (see Reference 54). A common characteristic in all speed regimes (provided the leading-edge is subsonic), however, is that the three-dimensional boundary layer detaches from the surface along a swept separation line and, in many cases, rolls up into a vortical motion. The scale of the vortical flow relative to the undisturbed boundary layer thickness depends on the configuration, its attitude to the free-stream, and the significance of compressibility. Of foremost interest to this report is the incompressible flow about slender wings (and bodies) at angle of attack where the

50

<u>size of the vortical flow is many times greater than the undisturbed boundary layer thickness</u>.

Dynamic Similarity

Consider the requirements for dynamic similarity of two fluid motions. The Navier-Stokes equations describing fluid motion in dimensionless form may be written:

$$(\bar{q}\nabla)\bar{q} = -(p_\infty/\rho U_\infty^2)\,\nabla p \;+\; Re\nabla^2\bar{q} \qquad\qquad \text{Equation 2}$$

where $Re = U_\infty \ell/\nu$ is the Reynolds number. From this, it is seen that for two motions to be dynamically similar, the Reynolds number must assume the same value for both motions.

In practice, water behaves as a sensibly incompressible medium because, although the speed of sound is little more than 4 times that in air, the velocities are much less and the Mach numbers correspondingly low. The density (ρ), kinematic viscosity (μ), and dynamic viscosity (ν) of water are approximately 800, 60, and 0.080 times those of air. A given Reynolds number may be obtained in water with a model roughly one-third the linear size (ℓ) at one-quarter the free-stream speed (U_∞). The model load, however, is proportional to $\rho \ell^2 U_\infty^2$ and would be nearly 5 times that in air at the same Reynolds number.

A water tunnel is, however, generally operated at Reynolds numbers well below those of wind tunnels and flight. For example, Reynolds numbers in a water tunnel are typically of order 10^3 to 10^4, whereas in wind tunnels and in flight, 10^5 to 10^6 and 10^7 to 10^8, respectively. For the test results of a water tunnel to truly represent the real situation, the fluid motion under consideration must be of the kind which is insensitive to changes in Reynolds number within the above ranges. At the very least, <u>the fundamental structure of the flow must be similar, regardless of Reynolds number</u>.

51

Regions of a Vortex Flow

The flow phenomenon characterized by free vortex sheets emerging from the leading edges of slender wings, which roll up into two vortex cores of concentrated vorticity can, in general, be divided into three regions:

(1) The inviscid flow outside the surface boundary layer, vortex sheet (free shear layer) and vortex core

(2) The boundary layer flow near the wing

(3) The vorticity flow inside the vortex sheet and vortex core.

Each regime has its own specific characteristics.

An excellent review of theoretical methods to predict vortex sheet and core locations and the nonlinear vortex-induced loads on slender wings in steady flow is provided in Reference 55. Special note is made, however, of four relatively recent nonconical flow methods which are: (1) the leading-edge suction analogy - Polhamus (Reference 56); (2) the quasi-vortex-lattice method - Mehrotra (Reference 57); (3) the free-vortex-sheet method - Boeing (Reference 58); and (4) the nonlinear lifting surface theory - Northrop (Reference 59). The methods are called non-conical because each satisfies the trailing-edge Kutta condition. The methods differ in approach and to the degree to which they predict the surface load distributions. Each method, however, pertains to the inviscid flow regime (1). Surface boundary layer and vortex sheet and core viscous effects are not taken into account. The fact that computational methods ignoring viscous effects are capable of predicting the aerodynamics of vortical flows with reasonable accuracy is one indication of the Reynolds number insensitivity

of such flows. Some pertinent differences between each of the methods are listed below. For a more complete description of the first three methods listed above, a review is given in Reference 60.

1. The suction analogy is always coupled with a potential-flow solution and is useful for estimating the over-all forces and moments at small computer cost. However, it does not provide details of the surface load distribution.

2. The quasi-vortex-lattice potential flow method of Lan (Ref. 61) has been extended by Mehrotra (Ref. 57) to include vortex-flow effects. This is done by modeling with discrete trailing-vortex filaments, in a manner similar to Mook and Maddox (Ref. 62), the shape, position and influence of the shed vortex sheet for both complete or partial-span leading-edge separation. Furthermore, the leading-edge boundary condition is exactly satisfied.

3. The free-vortex-sheet method of Boeing models the wing surface and free sheet with doublet panels that have biquadratic strength. Thickness effects may be modeled with source panels that have bilinear strength. The free sheet, whose shape and position must be determined by iteration, is kinematically coupled to a fixed (fed) sheet that approximately represents vortex core effects. The entire set of doublet strengths is also determined simultaneously during the iteration process.

4. The Northrop non-linear lifting surface theory has not been previously documented, hence, an overview of this approach is warranted. The new approach to this problem adopts a vortex sheet representation for the leading-edge vortex flow instead of discrete

53

vortex lines. Because the vortex sheet leaves
the leading-edge smoothly, the Kutta condition is
better satisfied there. This sheet, after leaving
the leading-edge, tends to roll inward, to form a
spirally-shaped cone. Mathematically, it would be
very difficult to analyze the roll-up process
completely into a vortex core. Therefore, in this
approach, the spiral sheet calculation is terminated
prior to completion of the roll up process and the
cut-off portion of the sheet is represented by a
discrete vortex core of varying strength along
its length. The increased strength is the result of
feeding by the original vortex sheet. Such a
representation is illustrated in Figure 11. As far
as the trailing vortex sheet is concerned, the
discrete representation is still retained. The
vortex lines of constant strength emerge from the
edges of adjoining elements of the wing. This
assumption is consistent with the vorticity model
used on the wing as well as on the leading-edge
vortex sheet. Since the trailing-edge wake vorti-
city does not have the close interference with the
wing as does the leading-edge vortex sheet, this
vortex line approach is considered quite adequate
for the present purpose. The vorticity model is
given in Figure 12, which uses a piecewise linear
vorticity distribution along the chordwise rays,
corresponding to a doublet distribution of parabolic
nature. Across the span, the equivalent doublet
distribution is constant.

The method features an iterative procedure. This is
necessary because the shapes of the vortex sheets
are not known a priori. The calculation starts with
an assumed shape which can be quite simple, as is
demonstrated in Figure 13. Based on this shape,

54

UNWRAPPED FREE
VORTEX SHEET

V-LINE

t

s

t

s

SURFACE ELEMENT

OBLIQUE COORDINATE
SYSTEM

t

γ_t

γ

θ

s

γ_s

NORMAL COMPONENT
OF VORTICITY
WHEN $\gamma_s = 0$

t

γ_t

$\gamma_{n'}$

s

VORTICITY DISTRIBUTION
ALONG S-LINE

$\gamma_{n'}$

s
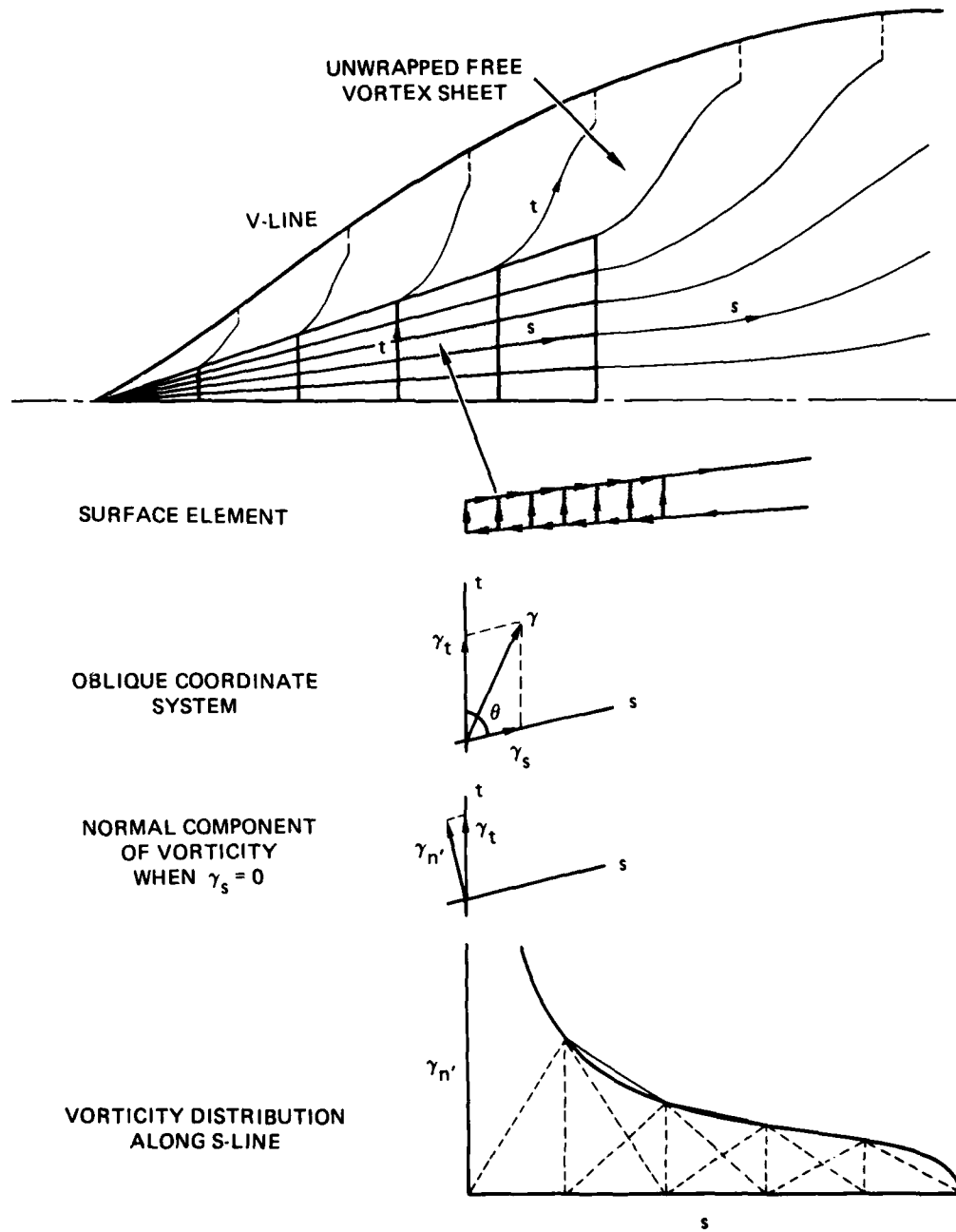
FIGURE 12. SURFACE VORTICITY MODEL FOR THE WING WITH LEADING
EDGE VORTEX FLOW

INITIAL SHAPES
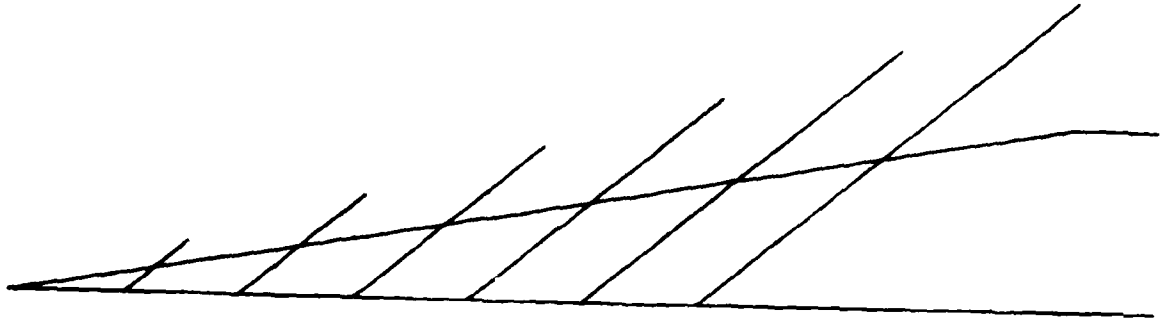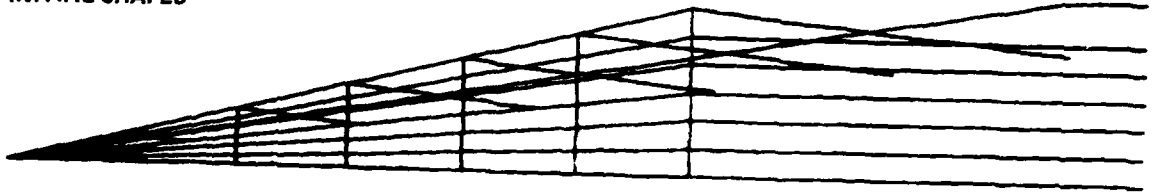
CONVERGED SOLUTION
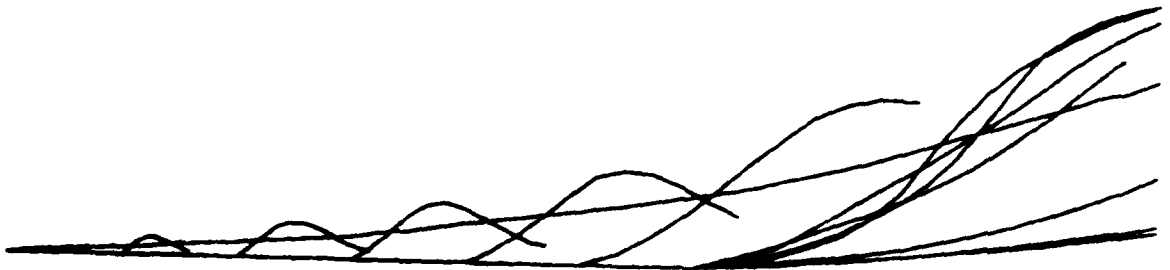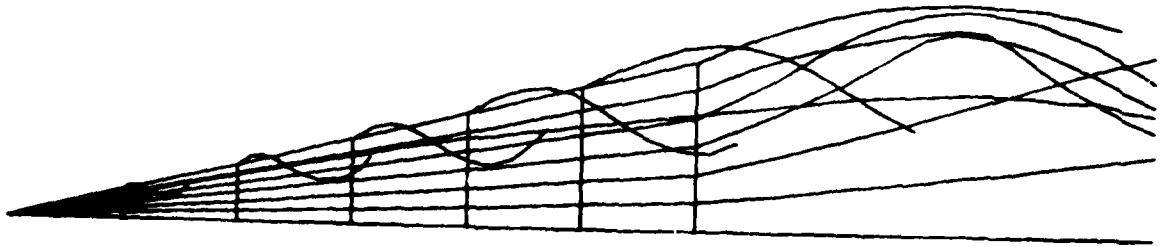
FIGURE 13. THE SHAPES OF THE LEADING-EDGE AND TRAILING-EDGE
VORTEX SHEETS AND POSITION OF THE VORTEX CORE AS DETERMINED
BY THE NONLINEAR LIFTING SURFACE THEORY FOR A DELTA WING OF
ASPECT RATIO 1 AT 20 DEGREES ANGLE OF ATTACK

the vortex strength is calculated on the wing. In turn, the shape of the leading and trailing vortex sheets are determined by calculating the velocities and making the vortex lines parallel to the local streamline. The velocity is also calculated on the vortex core. However, the core position is not determined by the calculated velocity alone. It is determined in part to locate at the center of the leading-edge vortex sheet and, in addition, to be coincident with the velocity vector. These two steps are repeated until the shape of the vortex sheet is invariant.

The Nonlinear Lifting Surface Theory program has been run for a delta wing of aspect ratio 1 at 20 degrees angle of attack. The initial vortex sheet and core shapes are very simple, as plotted in Figure 13. The final converged results are also shown in the same graph. As described above, the leading edge vortex lines depicted in the figure are the local vortex lines on a leading edge vortex sheet, while the trailing edge vortex lines and vortex core are discrete. The spiral shape is obvious. Inside the wake, the leading-edge vortex sheet and the trailing-edge vortex sheet roll up into two distinct vortex formations rotating in opposite sense to each other. This is in agreement with observations in Reference 63. The calculated loading distributions are plotted in Figure 14, which shows typical distributions at four chordwise stations $X/C_r = 0.3$, 0.5, 0.7 and 0.9, C_r being the root chord. The numerical results are compared with test data (Ref. 63) and the agreement is satisfactory. The analysis overestimates the loading on the outer span beyond the vortex core position. This is is to be expected since there is a secondary counter-rotating vortex arising out of viscous separation in this region which has not been included in the theory. The agreement deteriorates toward the apex due to the inadequate determination of the vortex core position in this region. The

57
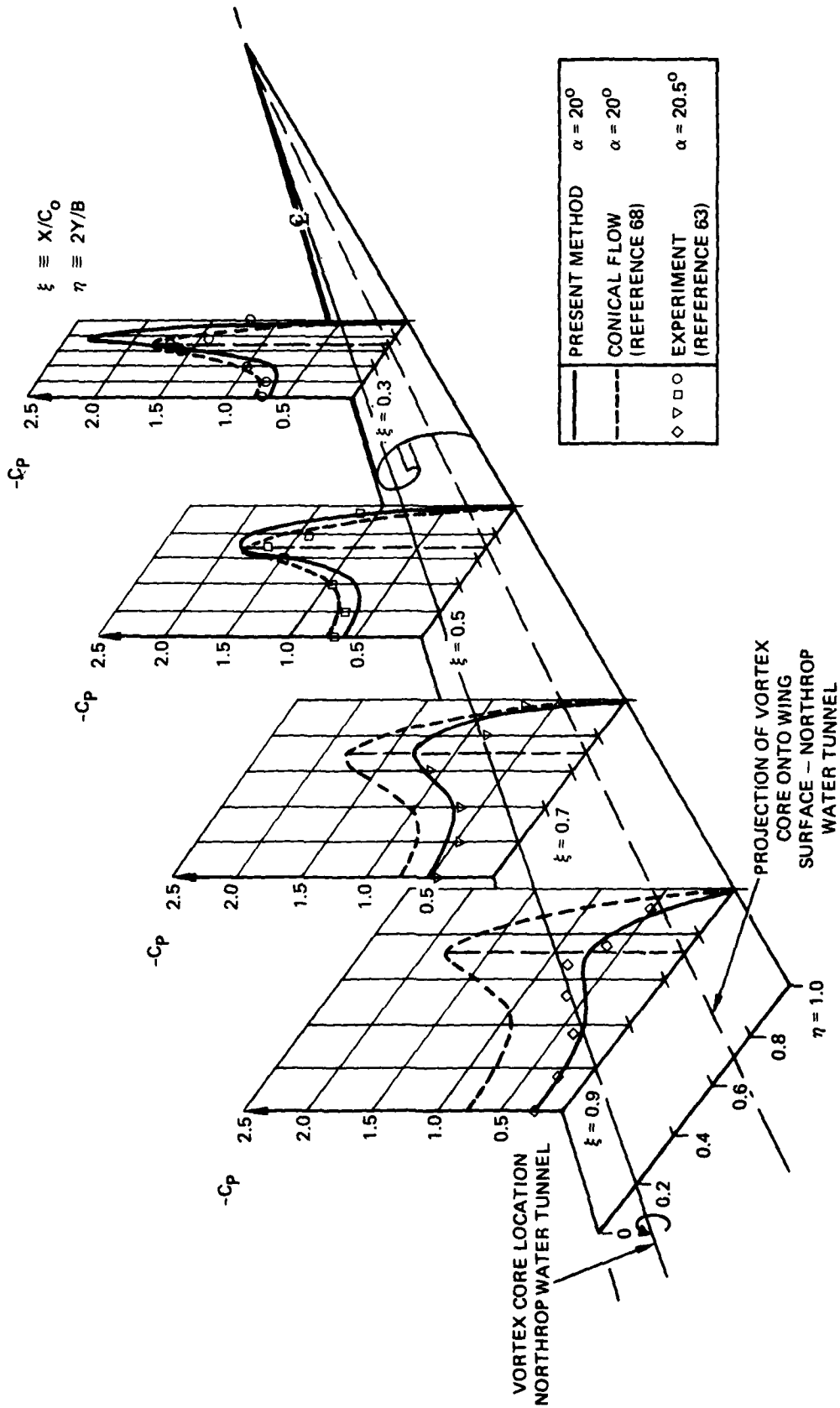
FIGURE 14. LOADING DISTRIBUTIONS OF A DELTA WING OF ASPECT RATIO 1 AT 20 DEGREES ANGLE OF ATTACK (NORTHROP WATER TUNNEL VORTEX CORE LOCATION ALSO SHOWN FOR REFERENCE).

total theoretical lift coefficient C_L in this case is 0.785, compared with test data of 0.625 (Ref. 63) and 0.71 (Ref. 64). The total pitching moment coefficient about the aerodynamic center is -0.132 compared with test data of -0.110 (Ref. 64). The fact that theoretical methods which neglect viscous effects can reasonably predict vortex flow aerodynamics is one indication of the Reynolds number insensitivity of these flow phenomena. This, in turn, lends credence to data obtained on thin, slender wings in a low Reynolds number water tunnel facility.

Inviscid Flow Regime

The inviscid flow regime (1) is governed by the potential flow equation (Laplace Equation):

$$\nabla^2 \phi = 0 \qquad \qquad \text{Equation 3}$$

subject to the boundary conditions:

$q_n = 0$ at the outer edge of the wing boundary layer
and
$q_n = 0 \qquad \Delta p = 0$ on the vortex sheet.

In the above, as shown previously in Figure 11, ϕ is the perturbation potential, q_n is the normal velocity, and Δp the pressure differential across the vortex sheet. From this set of equations alone, excluding the viscous regions (2) and (3) from consideration, it is possible to determine the location of the vortex sheet and vortex core and, hence, the lift characteristics of the wing. Since the vortex sheet originates from the wing leading edge, its strength is essentially independent of Reynolds number and, consequently, one expects the water tunnel to be capable of simulating the position of the vortex sheet and vortex core as well as the lift, should the water tunnel have a force measurement capability.

Indeed, experimental results support this reasoning. Reference 65 has indicated that force and moment measurements made in the Cal Tech HSWT on slender wings are in good agreement with results obtained in air. Northrop water tunnel measurements of the location of the vortex centerline, which is depicted in the flow visualization photograph in Figure 15, are in good agreement with theoretical results from the Northrop Nonlinear Lifting Surface Theory as shown in Figures 14 and 16; with the theoretical method in Reference 66 depicted in Figure 17; and with water tunnel and wind tunnel measurements from Reference 26 as presented in Figures 18 and 19. The inadequacies of the early theoretical methods developed in References 67 and 68 in predicting lateral positions of the vortex core are evident in the latter two figures. Good agreement is obtained, however, between water tunnel vortex core lateral location and the theoretical suction peak determined from the Boeing free-vortex-sheet method (see Reference 69) as presented in Figure 20. Smoke and water vapor flow visualization results obtained in wind tunnels in References 70 and 71, respectively, are seen to agree well with water tunnel studies of similar planforms as shown in Figures 21 and 22. Even on yawed slender wings, excellent correlation is achieved between low-Reynolds-number vortex core locations obtained in water with core positions obtained in wind tunnel flow visualization and experimental and theoretical pressure distributions from References 71 through 73 (see Figures 23 to 25). The reduction in leeward suction peak is due to reduced vortex strength and an upward displacement of the vortex core as can be seen in the water tunnel photograph in Figure 26. At extreme values of sideslip at which the leeward wing leading edge is effectively a "trailing edge" the flow situation depicted in the water tunnel photographs in Figure 27 is in agreement with the theoretical flow streamlines from Reference 52 and experimental surface pressure distributions from Reference 71.

LEADING EDGE VORTICES
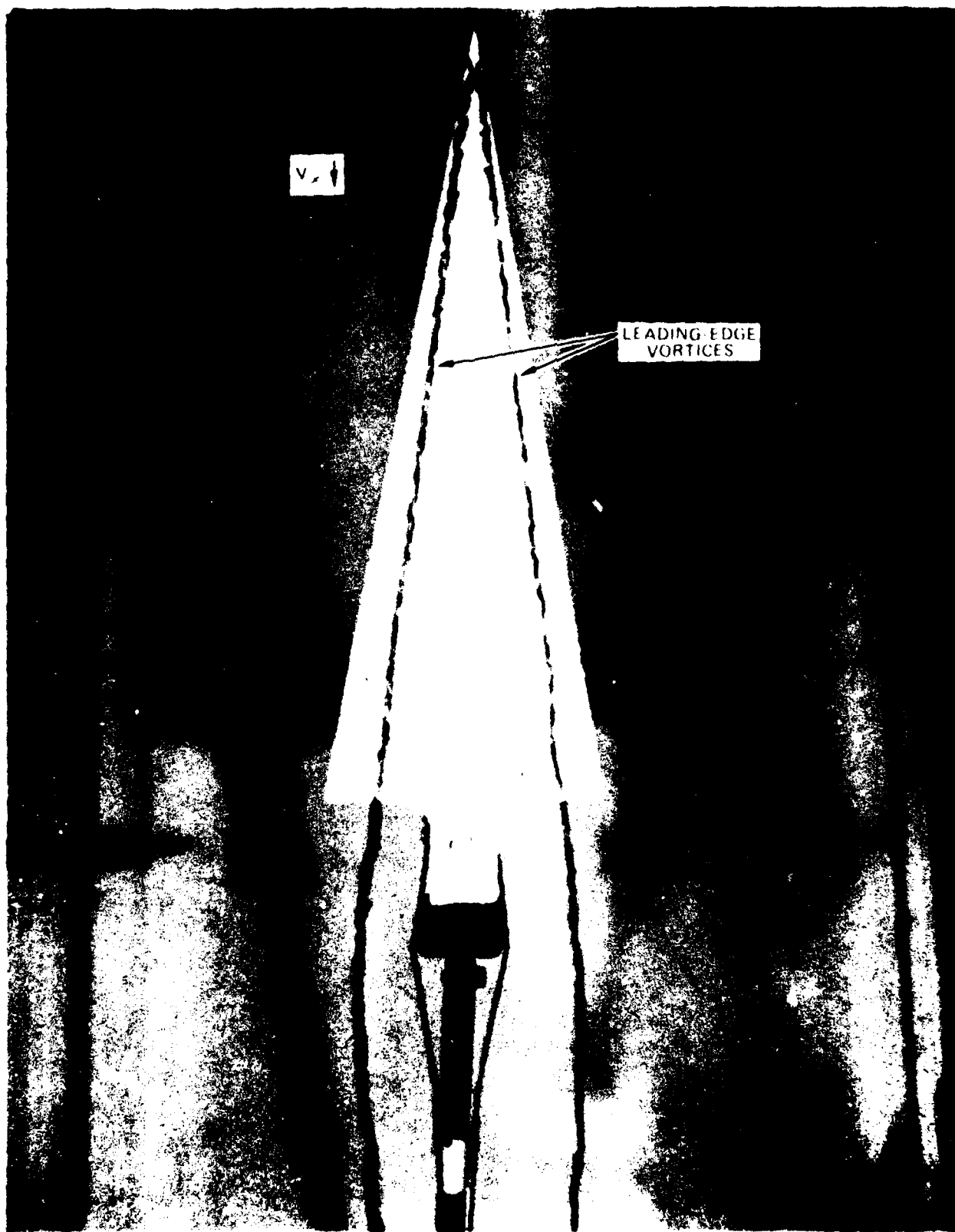
(a) PLANVIEW

FIGURE 15. VORTEX CORE TRAJECTORY OVER A SLENDER WING
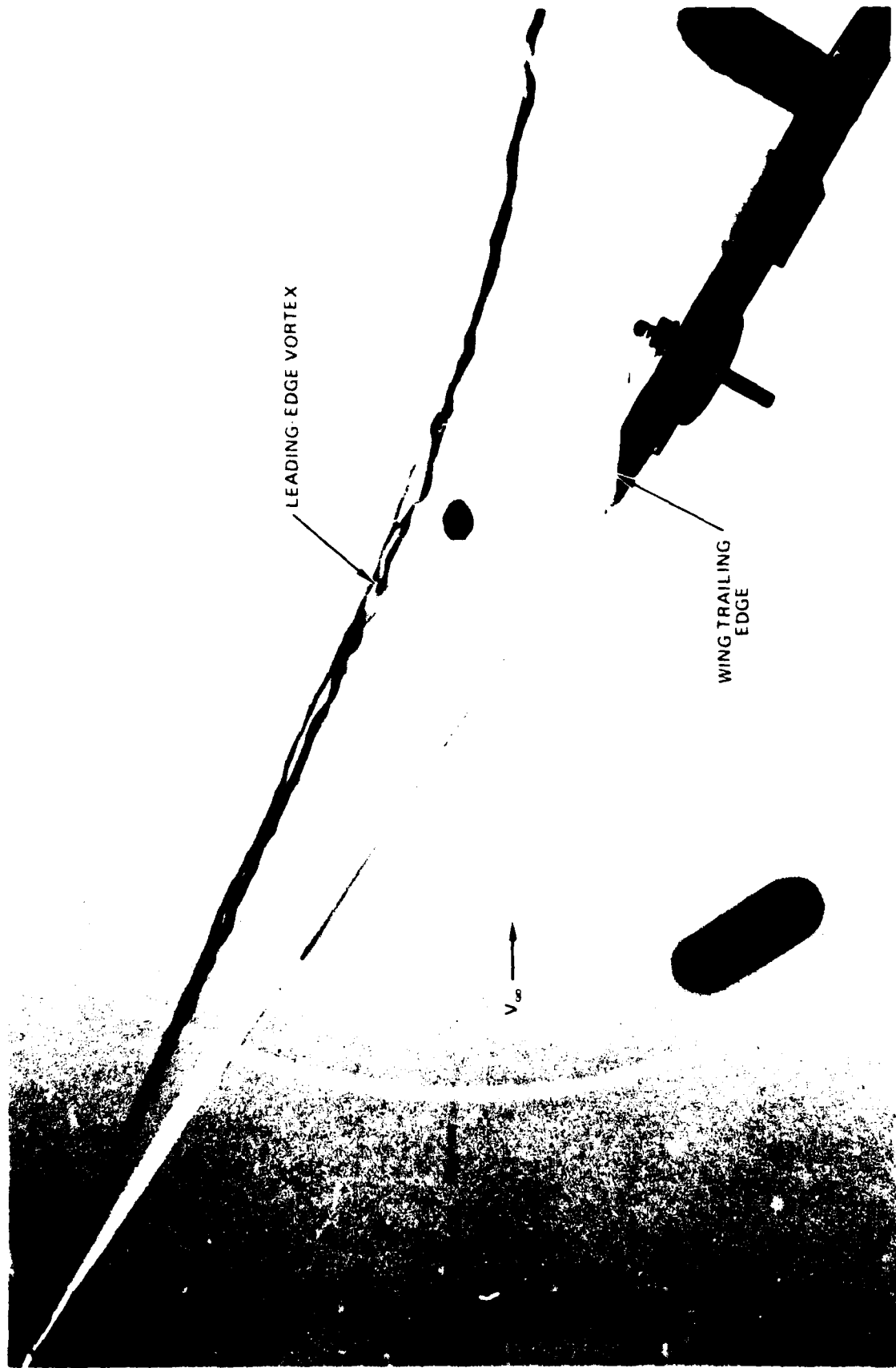
LEADING-EDGE VORTEX

WING TRAILING EDGE

(b) SIDEVIEW

FIGURE 15. CONCLUDED

X = LONGITUDINAL DISTANCE ALONG CHORD

C_O = WING CENTERLINE CHORD
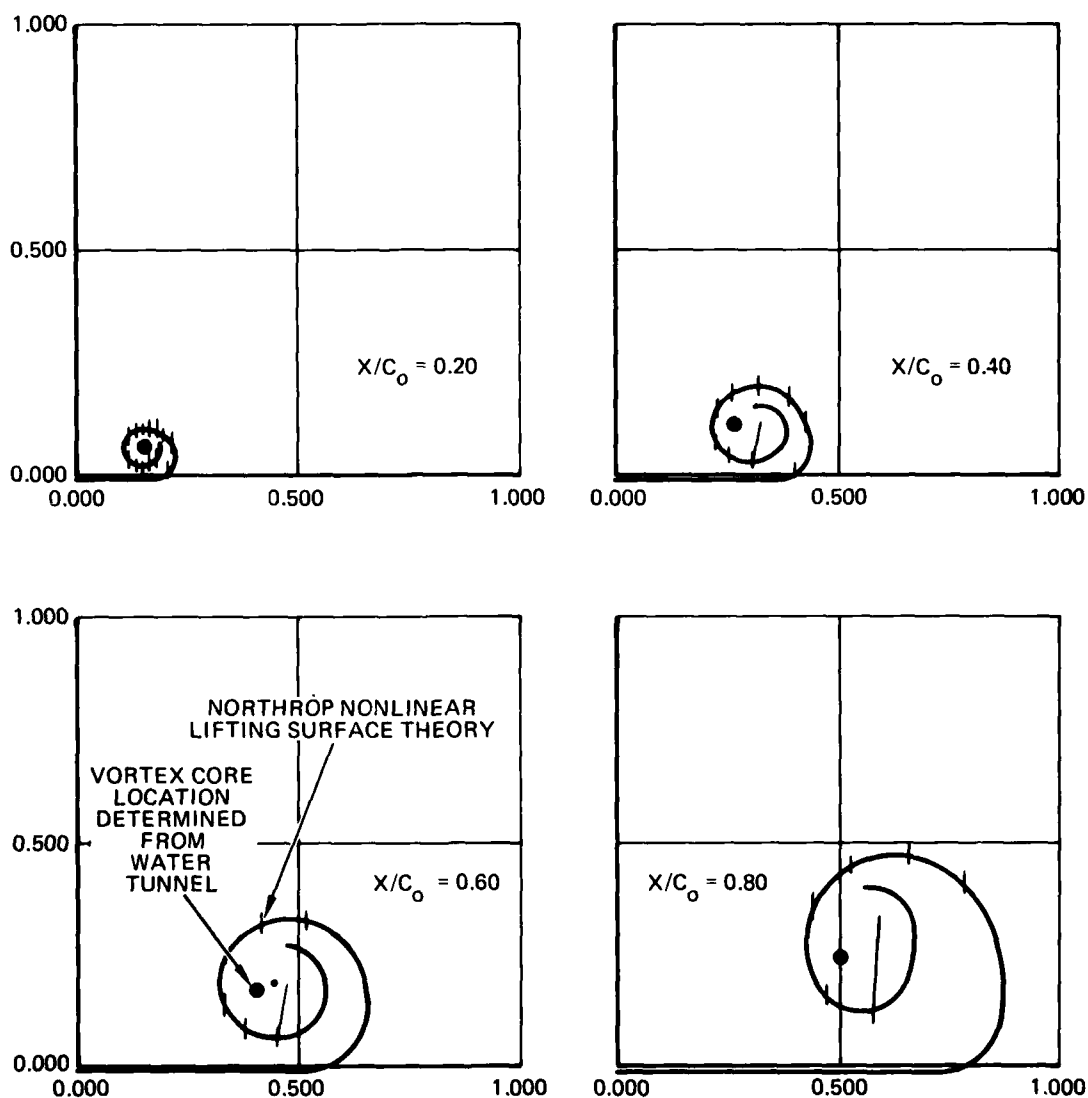
FIGURE 16. VORTEX SHEET AND CORE LOCATIONS ON A DELTA WING OF
ASPECT RATIO 1 AT 20 DEGREES ANGLE OF ATTACK.

63
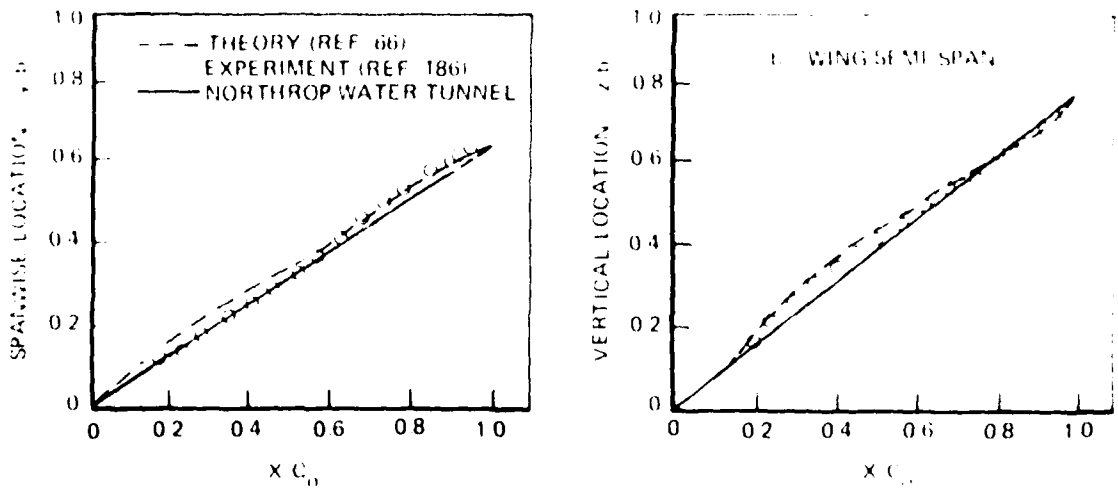
(a) SPANWISE AND VERTICAL LOCATIONS OF VORTEX CORE
ON A DELTA WING OF ASPECT RATIO 1 AT 14 DEGREES
ANGLE OF ATTACK.
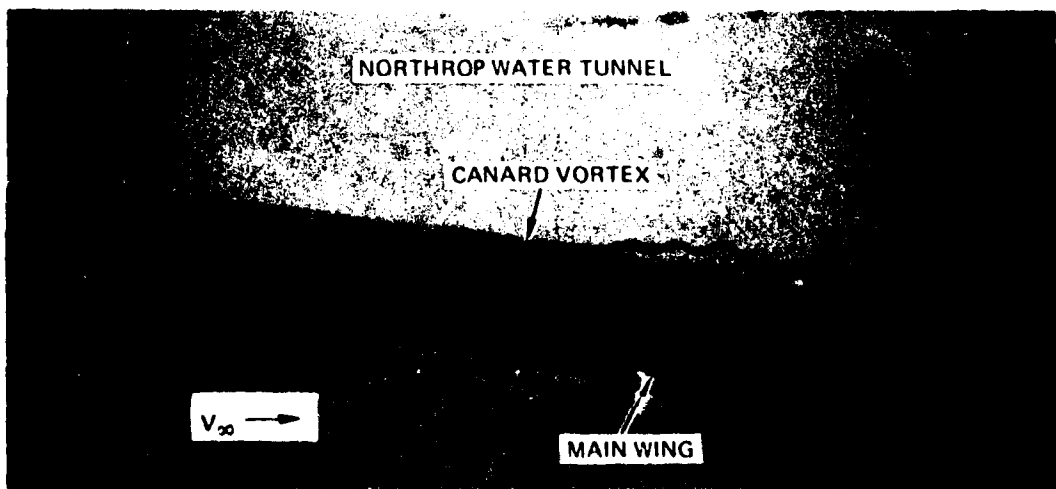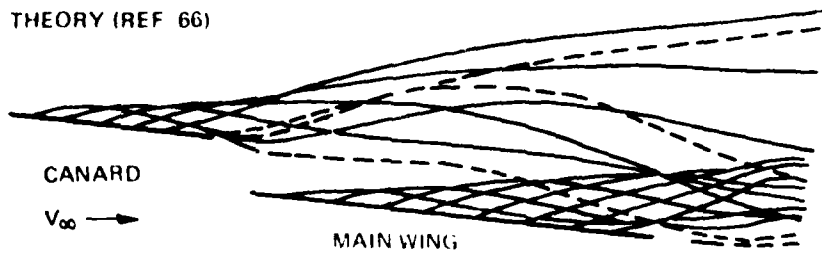
(b) WAKE-SHAPE AND CORE LOCATION ON A CANARD-WING
AT 15 DEGREES ANGLE OF ATTACK

FIGURE 17. VORTEX CORE LOCATIONS ON WING ALONE AND
CANARD WING ARRANGEMENTS — THEORY AND EXPERIMENT
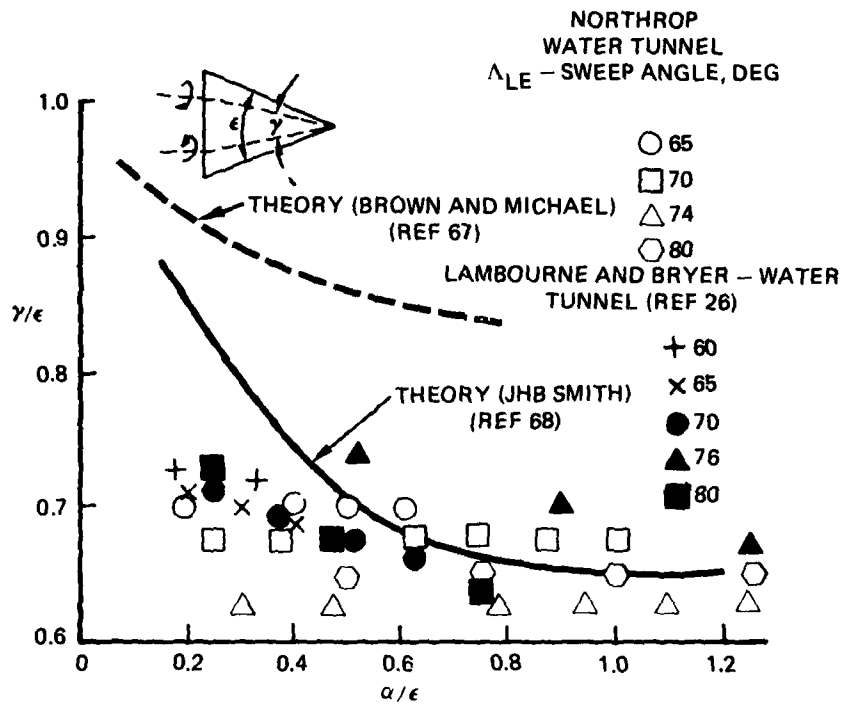
FIGURE 18. VORTEX CORE TRAJECTORIES
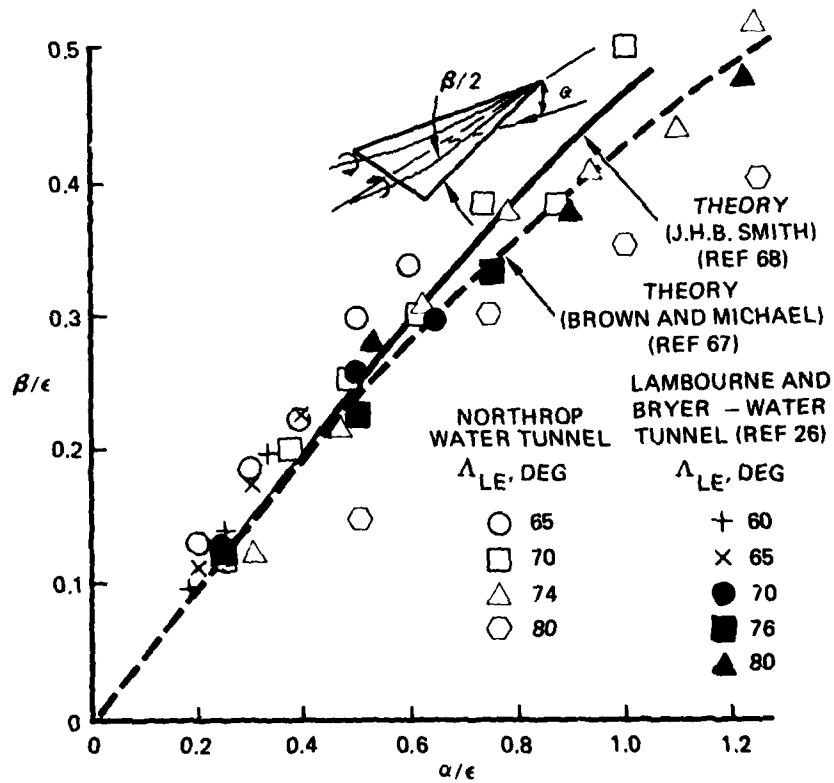
FIGURE 19. VORTEX CORE TRAJECTORIES
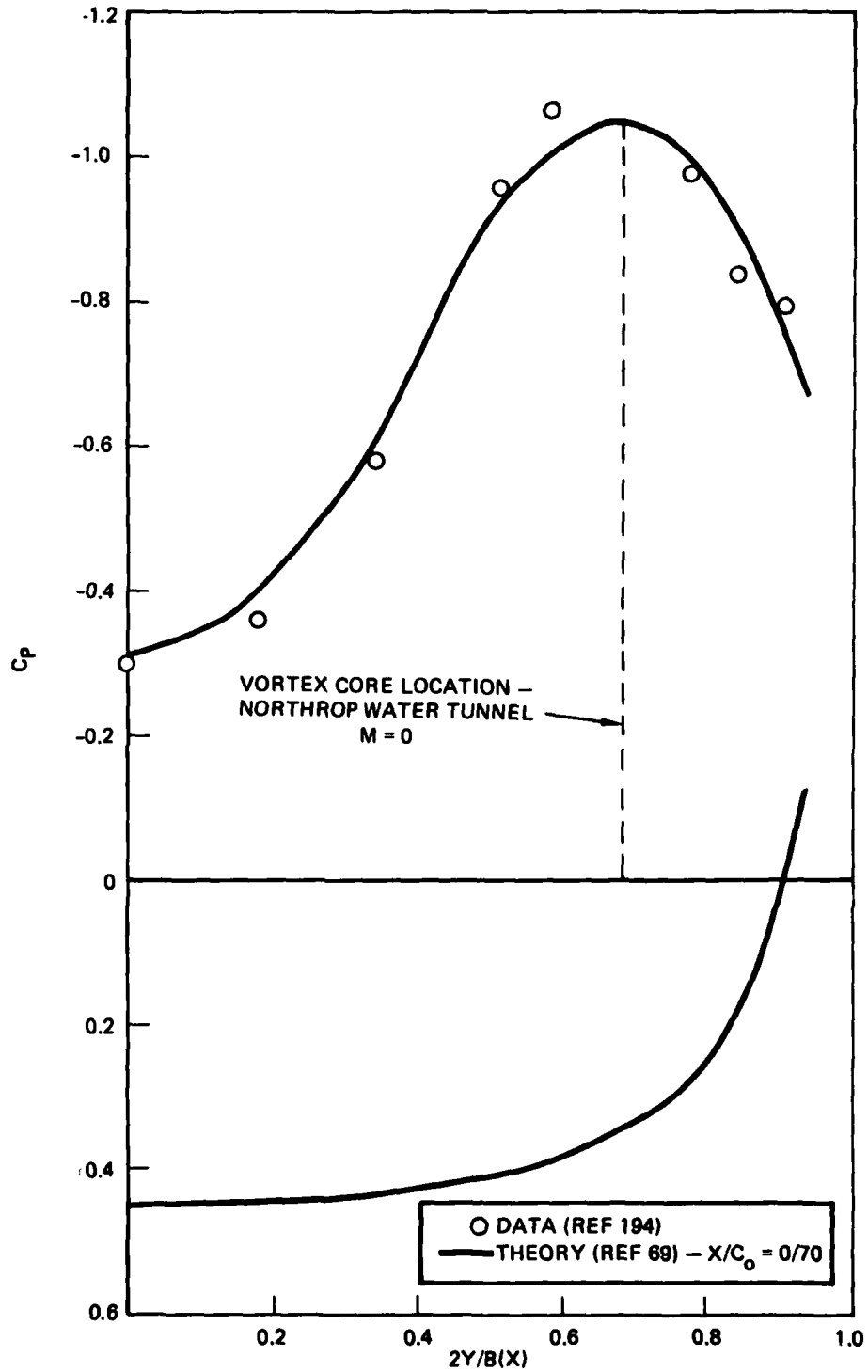
FIGURE 20. COMPARISON OF WATER TUNNEL VORTEX CORE LATERAL
POSITION WITH THEORETICAL SUCTION PEAK FOR AN ASPECT RATIO
0.52 DELTA WING AT 30 DEGREES ANGLE OF ATTACK (THEORY AND
EXPERIMENT FROM REFS 69 AND 194 AT M = 0.70)
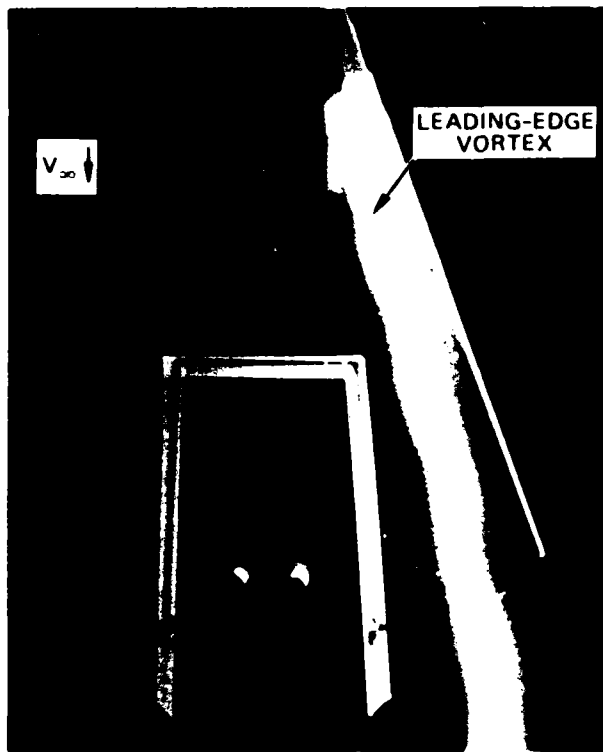
NORTHROP WIND TUNNEL
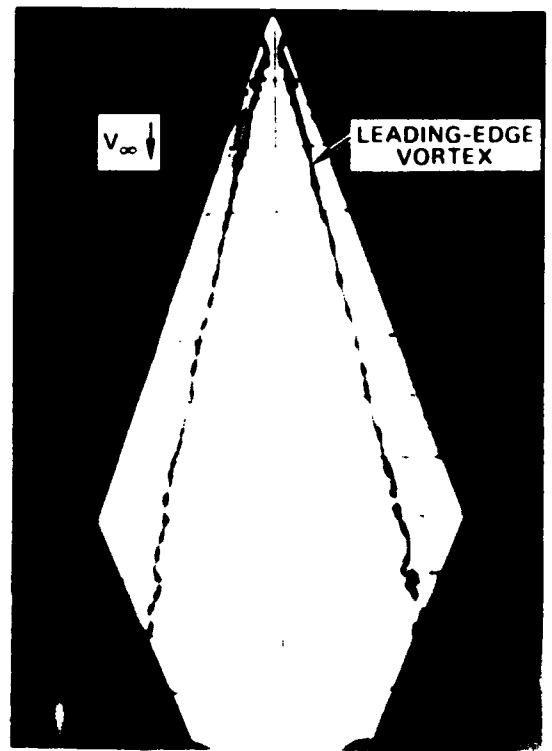
WATER TUNNEL

FIGURE 21. WIND TUNNEL AND WATER TUNNEL VORTEX PATHS ON DIAMOND PLANFORMS AT 20 DEGREES ANGLE OF ATTACK
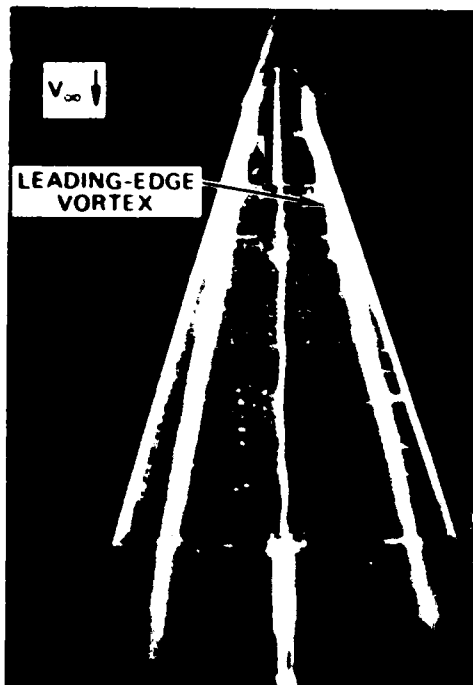
WIND TUNNEL (REF. 71)
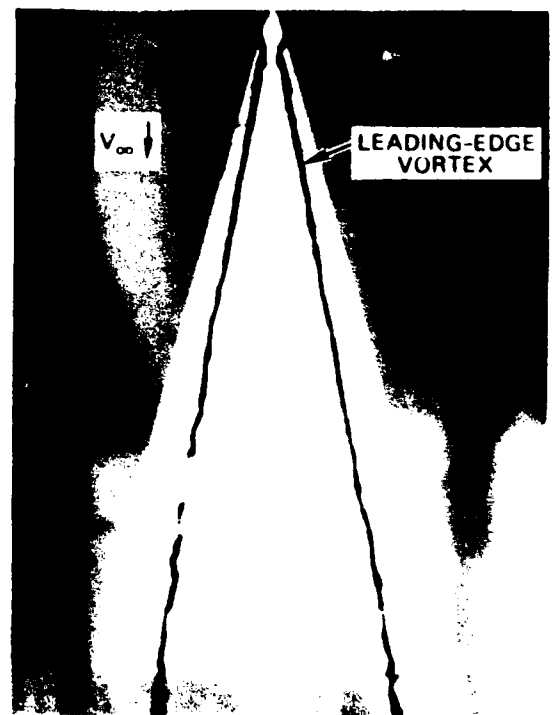
WATER TUNNEL

FIGURE 22. WIND TUNNEL AND WATER TUNNEL VORTEX PATHS ON A 74-DEGREE DELTA PLANFORM AT 20 DEGREES ANGLE OF ATTACK

Labels visible in figure:
- LEEWARD VORTEX
- WINDWARD VORTEX
- V
- LEEWARD VORTEX
- WINDWARD VORTEX
- V
- INCREASED ANGLE OF ATTACK
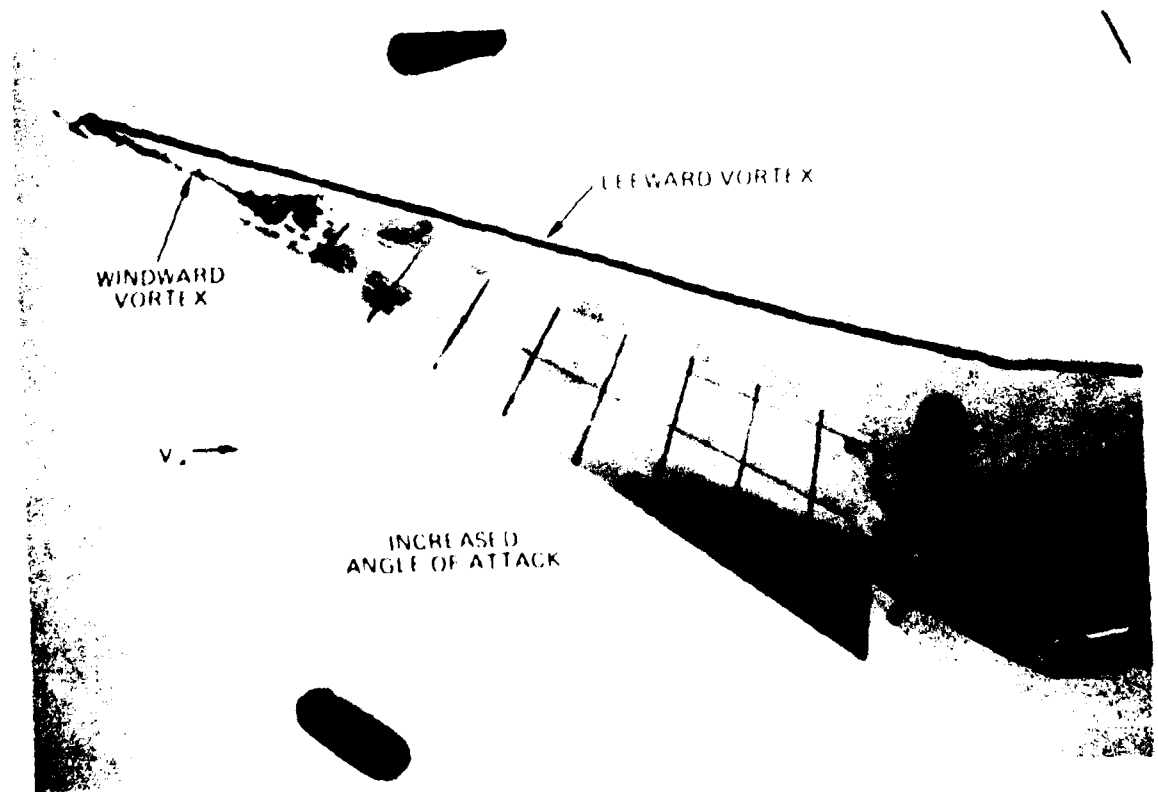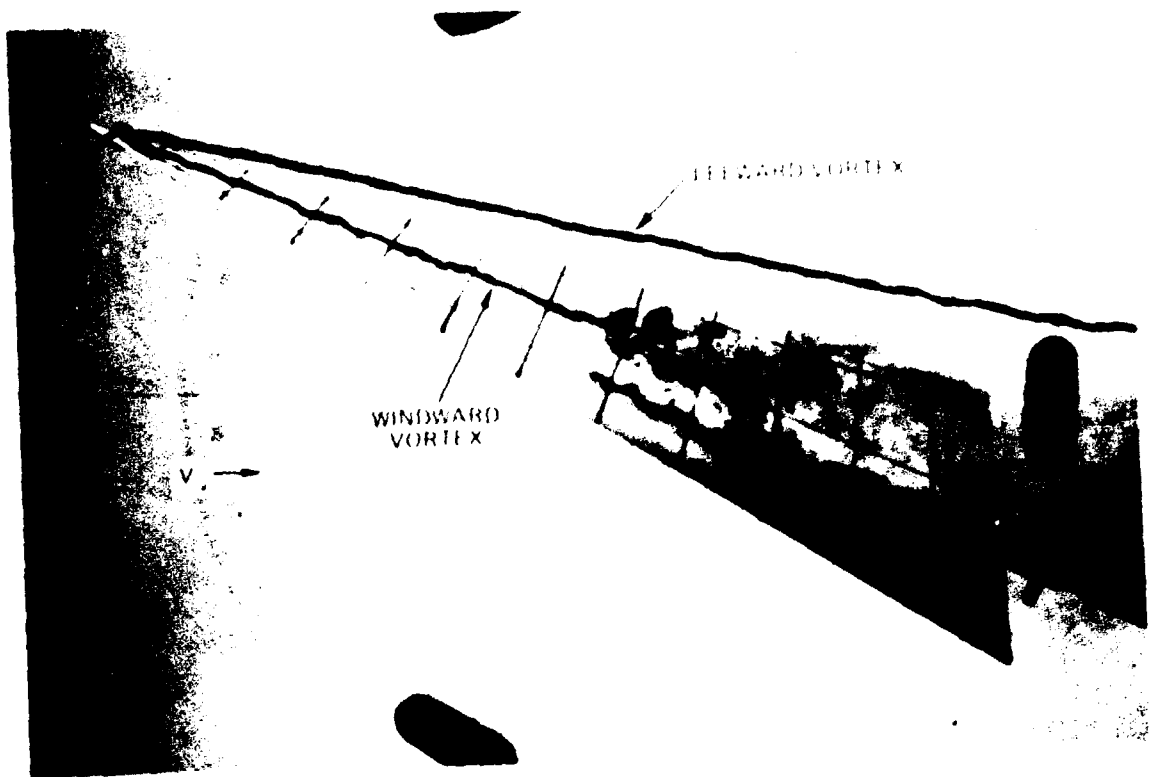
FIGURE 23. YAWED DELTA WING VORTEX CORE PATHS (NORTHROP WATER TUNNEL)
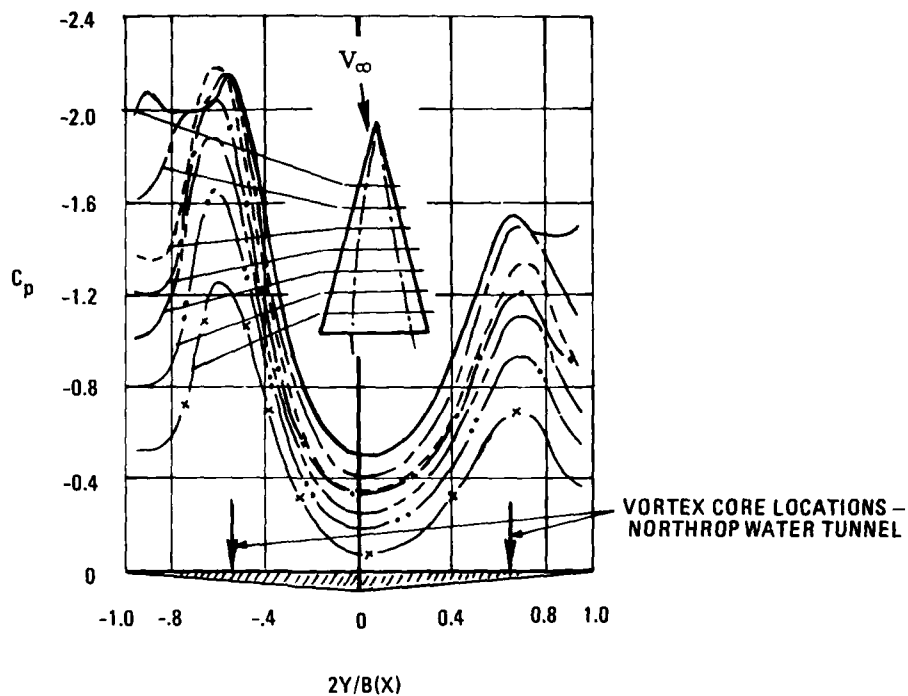
(a) EXPERIMENTAL PRESSURE DISTRIBUTIONS ON A YAWED DELTA
WING OF ASPECT RATIO 1 AT 26.5 DEGREES ANGLE OF ATTACK AND
5 DEGREES OF SIDESLIP (FROM REFERENCE 73).
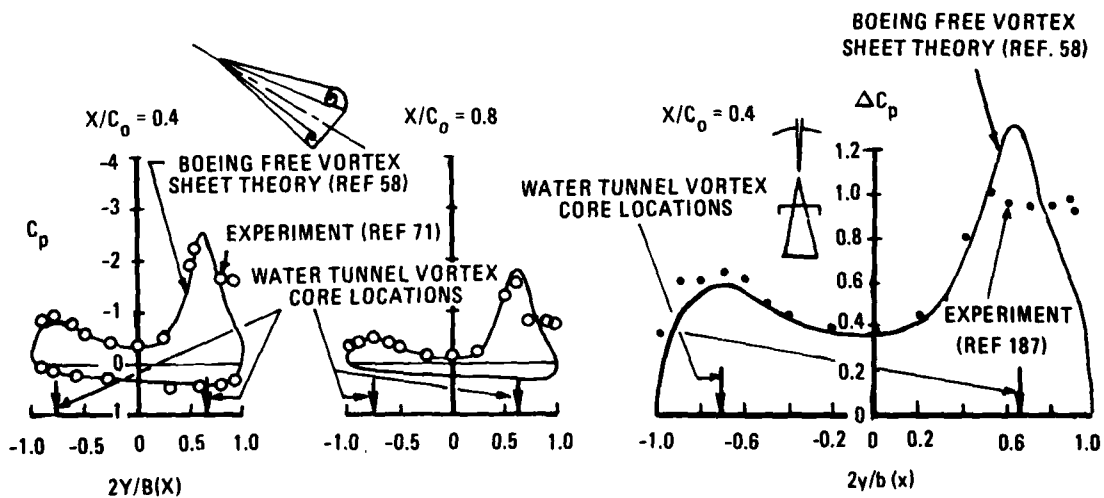
(b) ASPECT RATIO 1.15; M = 0.16;
α = 20 DEGREES; β = 10 DEGREES.

(c) ASPECT RATIO 0.71; M = 0;
α = 15 DEGREES; β = 5 DEGREES.

FIGURE 24. COMPARISON OF WATER TUNNEL YAWED DELTA WING
VORTEX CORE LOCATIONS WITH EXPERIMENTAL AND THEORETICAL
SURFACE PRESSURE DISTRIBUTIONS.

69
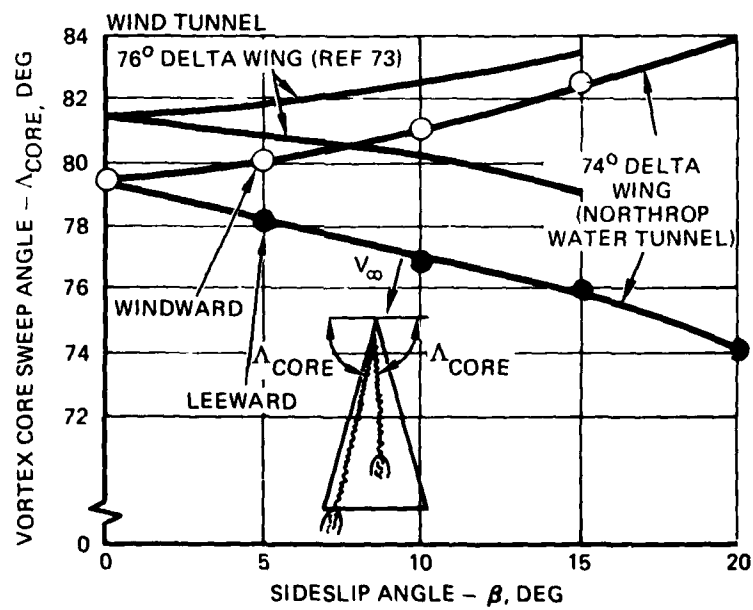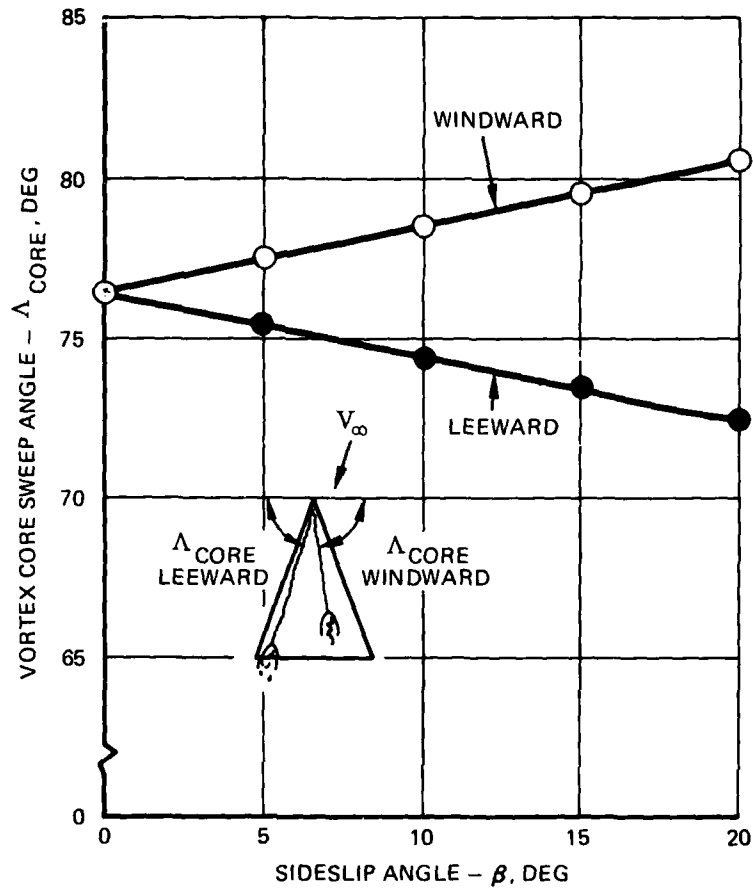
FIGURE 25. EFFECT OF SIDESLIP ON DELTA WING
VORTEX CORE POSITION – WATER TUNNEL
AND WIND TUNNEL RESULTS

70

$\alpha = 20^\circ \quad \beta = 0^\circ$

VORTEX
CORE

$V_\infty \longrightarrow$

$\alpha = 20^\circ \quad \beta = 15^\circ$

LEEWARD
VORTEX CORE

WINDWARD
VORTEX CORE

$V_\infty \longrightarrow$
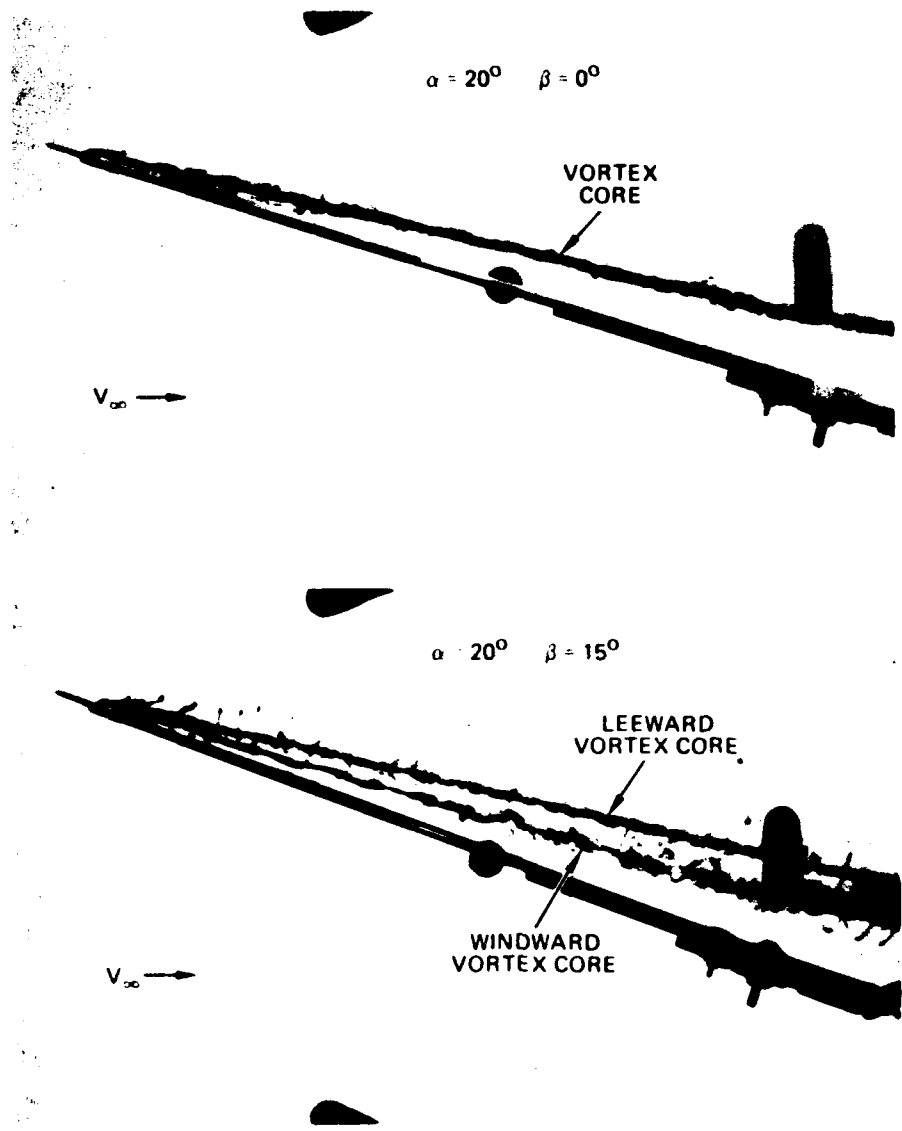
FIGURE 26. FLOW VISUALIZATION OF YAWED DELTA WING VORTEX CORES
(NORTHROP WATER TUNNEL)
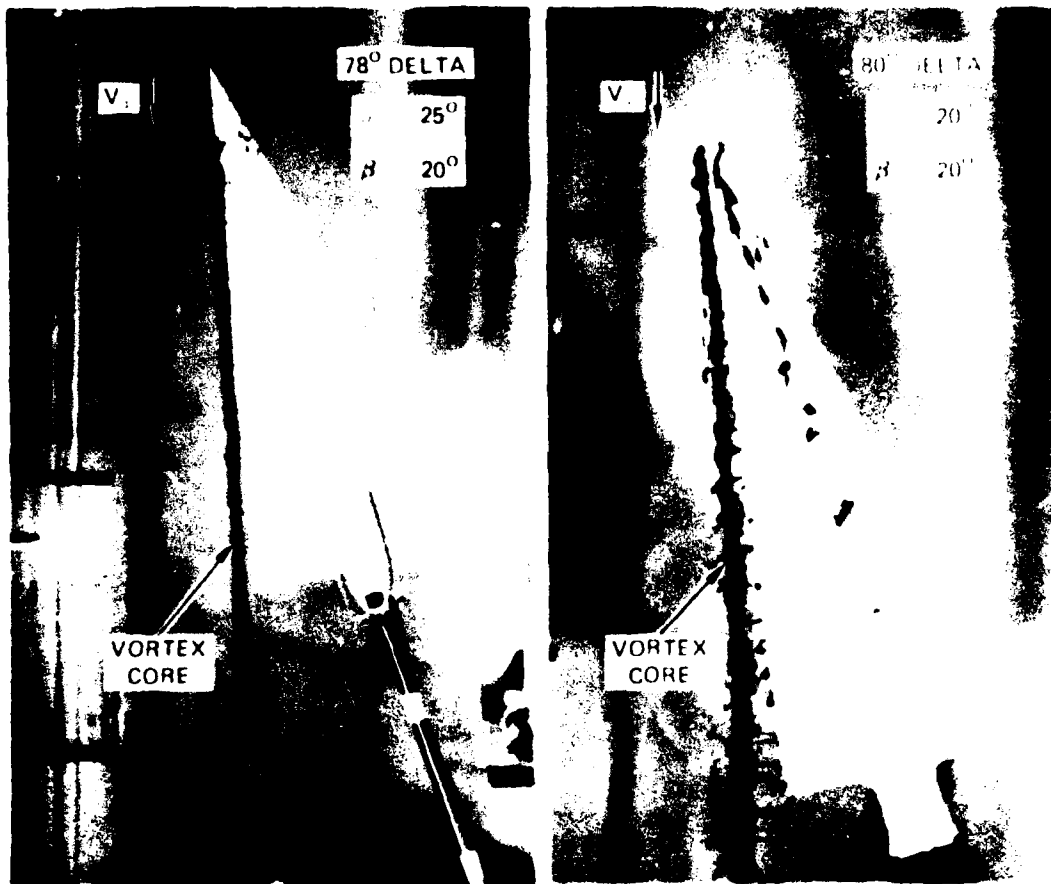
(a) LEEWARD VORTEX CORE TRAJECTORY AT LARGE ANGLE OF YAW (NORTHROP WATER TUNNEL)
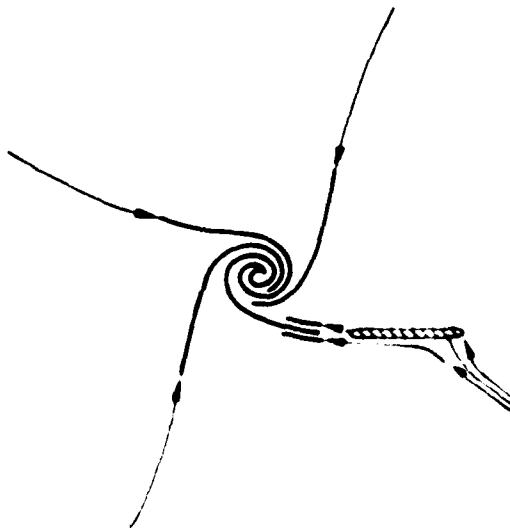
(b) THEORETICAL FLOW STREAMLINES (FROM REFERENCE 52)

FIGURE 27. DELTA WING VORTEX CHARACTERISTICS AT LARGE ANGLE OF YAW
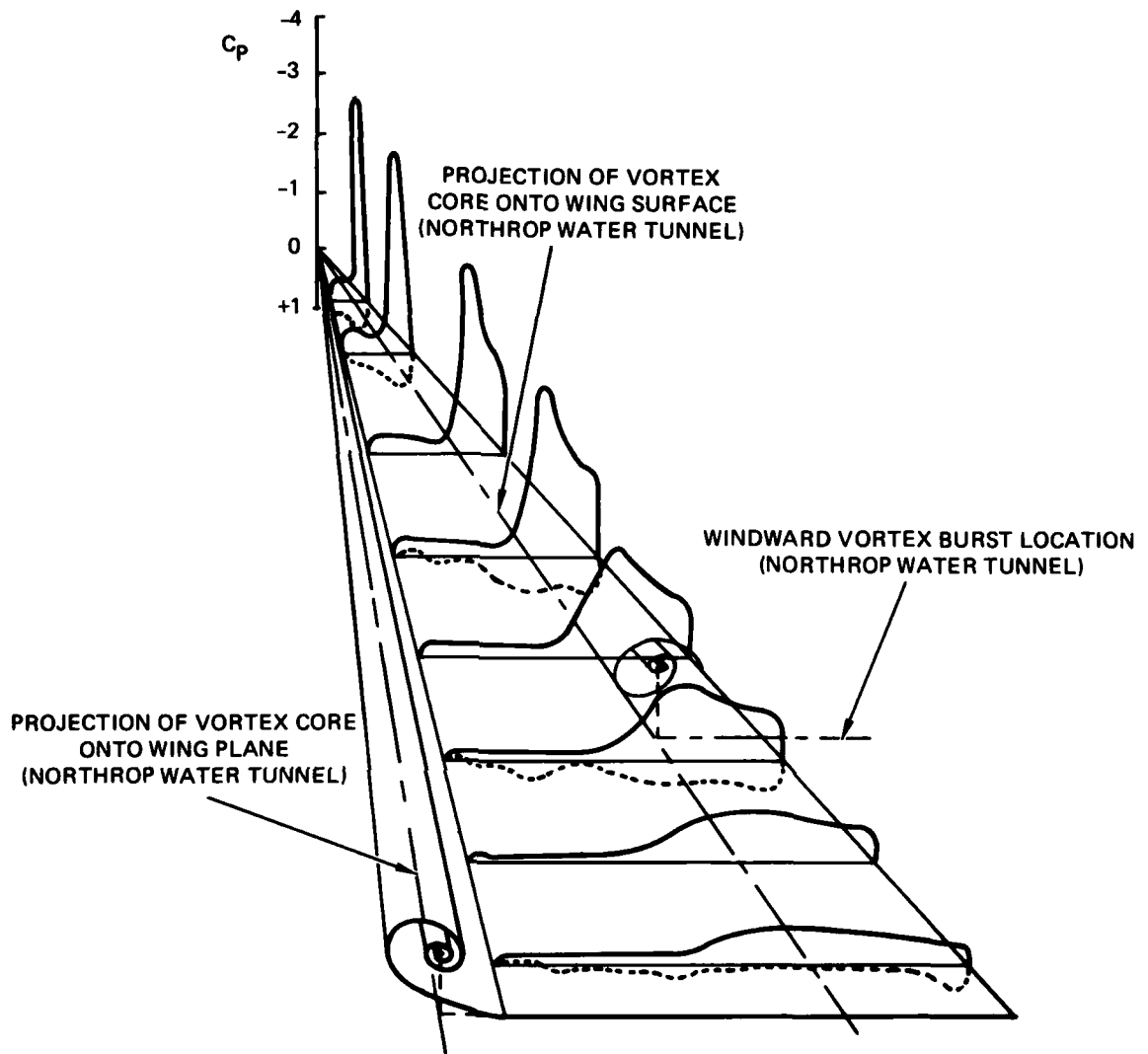
(C) PRESSURE DISTRIBUTIONS ON A FLAT-PLATE DELTA WING AT AN ANGLE OF ATTACK OF 20 DEGREES AND SIDESLIP ANGLE OF 25 DEGREES (FROM REFERENCE 71)

FIGURE 27. CONCLUDED

The Reynolds number insensitivity of the vortex sheet emanating from a sharp leading edge may be viewed in the following manner: For flows on surfaces -- a boundary layer, for example -- a disturbance tends to amplify within the boundary layer and to trigger transition to turbulence. On the other hand, free flows without boundary surfaces -- a free shear layer, for example -- tend to damp out disturbances and, in a sense, behave as if in a higher Reynolds number flow.

It is of interest to note that at flow conditions supporting the development of vortices on highly-swept delta wings in transonic, supersonic, and even hypersonic flow, vortex centerline locations are similar to the incompressible flow results (see Reference 7), as shown in Figures 28 and 29 (from References 74 and 75, respectively). Compressibility tends to reduce the scale of the vortical flow relative to the undisturbed boundary layer thickness, however, and the magnitude of the vortex-induced lift decreases with increased Mach number (Reference 76). Provided the sweep angle is such that the leading edge lies well inside the Mach angle, the flow exhibits the classical vortex structure at low speeds. With increase in Mach number towards hypersonic speeds, and with Mach lines approaching the leading edge, the lee-side flow changes gradually, allowing for an attached boundary layer from the edge inward, which requires a recompression to bring the streamlines back to the axial direction as the plane of symmetry is approached. This results in embedded shocks (if the Mach number is sufficiently high) which bound the vortex structure (see Reference 77).

Surface Boundary Layer Flow

Flow regime (2), the boundary layer flow near the wing, is viscosity-dominated. The flow at the wing surface below the leading-edge vortices is directed outwards. The steep pressure
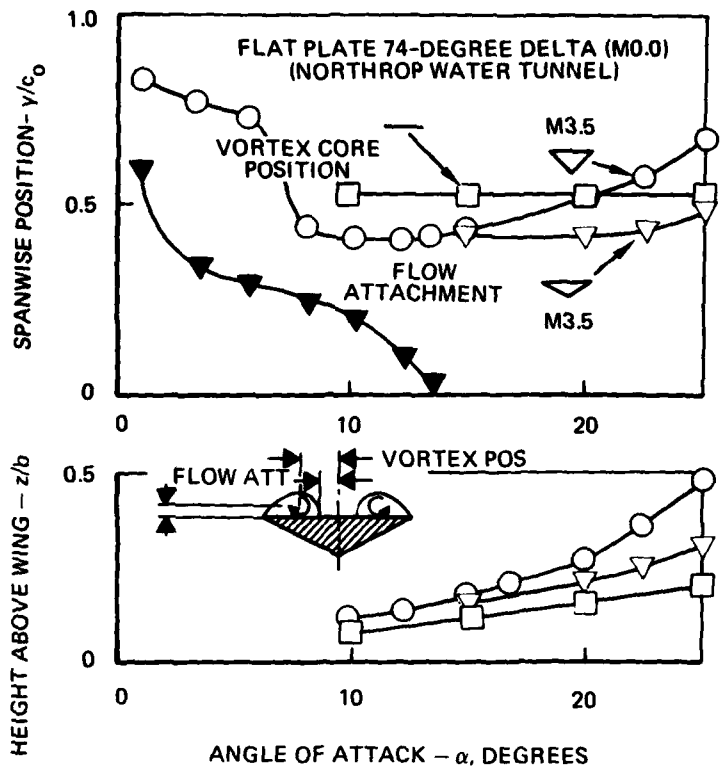
FIGURE 28. COMPARISON OF VORTEX CORE CENTERLINE POSITION IN INCOMPRESSIBLE
AND COMPRESSIBLE FLOW (REFERENCE 74) FOR A 74-DEGREE DELTA WING
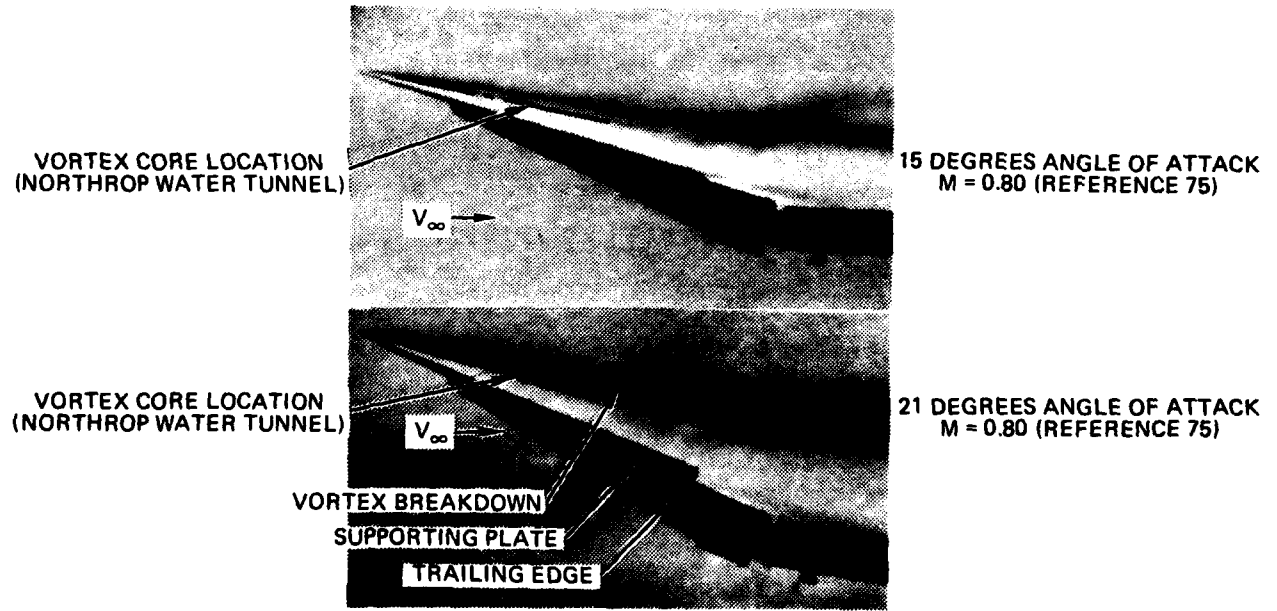
FIGURE 29. COMPARISON OF VORTEX CORE VERTICAL LOCATIONS IN INCOMPRESSIBLE
AND COMPRESSIBLE FLOWS FOR A 63.4-DEGREE DELTA WING

gradient between the location for minimum pressure and the leading edge causes flow separation which takes the form of a small secondary vortex. At the upper surface of the wing this secondary vortex induces additional velocities with a corresponding modification of the pressure distribution as sketched in Figure 30. Reference 78 has shown that patterns of surface oil flow on the upper surface of sharp-edge delta wings at incidence were independent of Reynolds number, except for the position of the line along which secondary separation takes place as shown in the surface sublimation photograph in Figure 31. As the surface pattern inboard of this line would also change if there was an appreciable change in the position of the vortex centerline, it appeared in Reference 78 that the movement of the separation line was not associated with a significant movement of the vortex core but only with a varying thickness of the boundary layer. Wind tunnel studies were made in Reference 79 using transition wire near the surface to delay boundary layer separation. Smoke trails of the vortex cores were in essentially the same location when compared with flow visualization without the transition wires. No substantial changes in forces and moments were observed in similar tests conducted in Reference 71. These results suggest that although the secondary separation affects the surface pressure distribution, the integrated effects, according to these studies, remain essentially the same.

Slight differences in core positions do exist, however, between laminar and turbulent boundary layer flow, as shown in Figure 32 (from Reference 52). Reference 63 has indicated that the primary vortex core position in the laminar case is upwards and inwards relative to the turbulent case due to the displacement effect of the secondary vortex. Compared with the pressure distribution for laminar boundary layers, much higher suction peaks are attained and the position of the pressure minimum is more outwards in the turbulent case. The relative pressure minima in the region of the secondary vortex are much

76
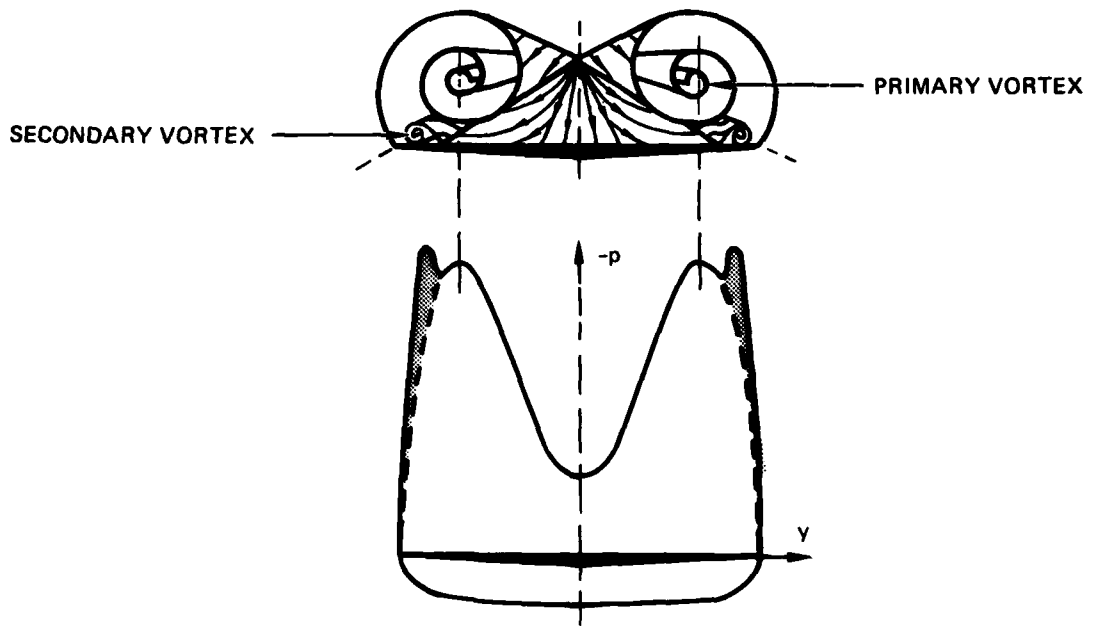
FIGURE 30. SECONDARY SEPARATION EFFECT ON SURFACE PRESSURE DISTRIBUTION (SCHEMATIC)

FIGURE 31. SECONDARY SEPARATION ON A 63.5-DEGREE DELTA WING AT 15-DEGREES ANGLE OF ATTACK AND M = 0.70 (FROM REFERENCE 195)

(A) SKIN-FRICTION LINE PATTERN ON UPPER
SURFACE OF SLENDER WING AT LOW
SPEEDS – 15 DEGREES ANGLE OF ATTACK

(B) PRESSURE DISTRIBUTIONS OVER A
THIN DELTA WING AT LOW SPEEDS
WITH LAMINAR AND TURBULENT FLOWS
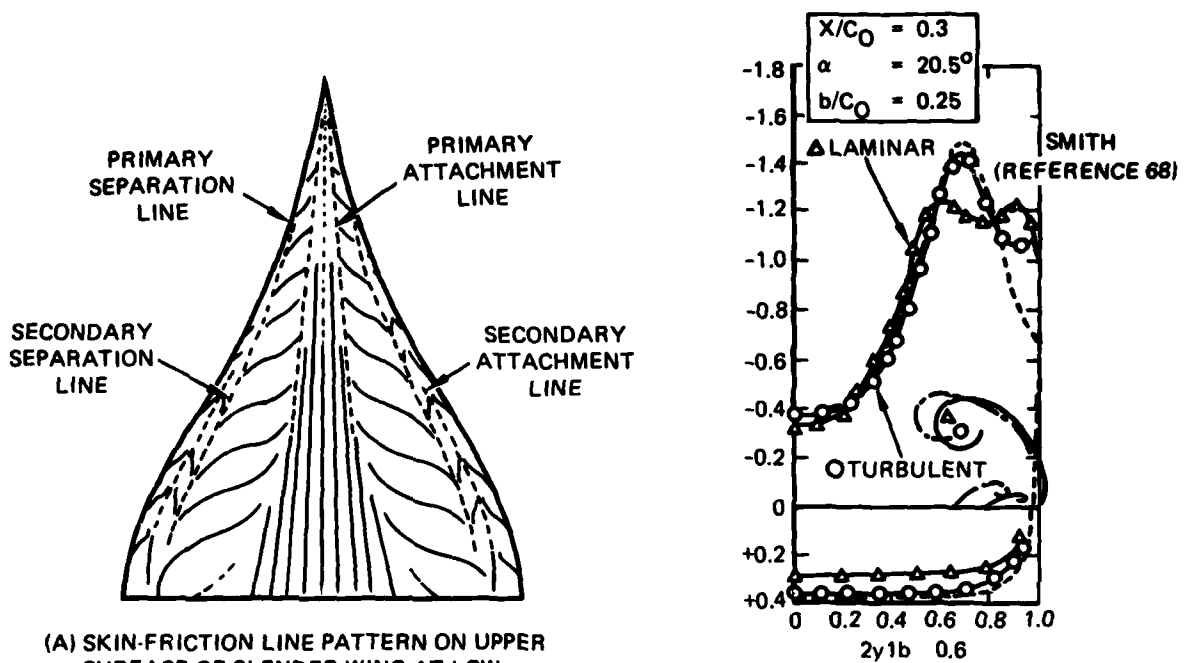
FIGURE 32. SURFACE PRESSURES AND SKIN-FRICTION LINES ON SLENDER
WINGS WITH SUBSONIC LEADING EDGES (FROM REFERENCE 52)
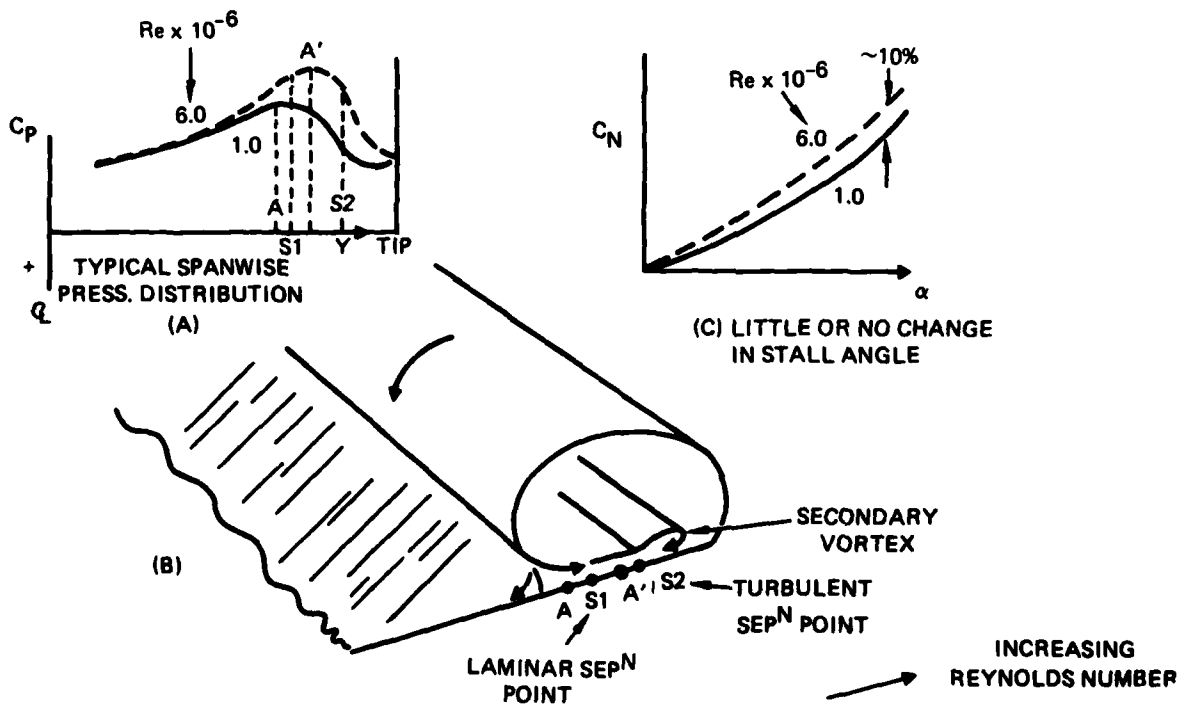
FIGURE 33. REYNOLDS NUMBER EFFECTS ON DELTA WING CHARACTERISTICS –
ASPECT RATIO 0.52 (FROM REFERENCE 80)

78
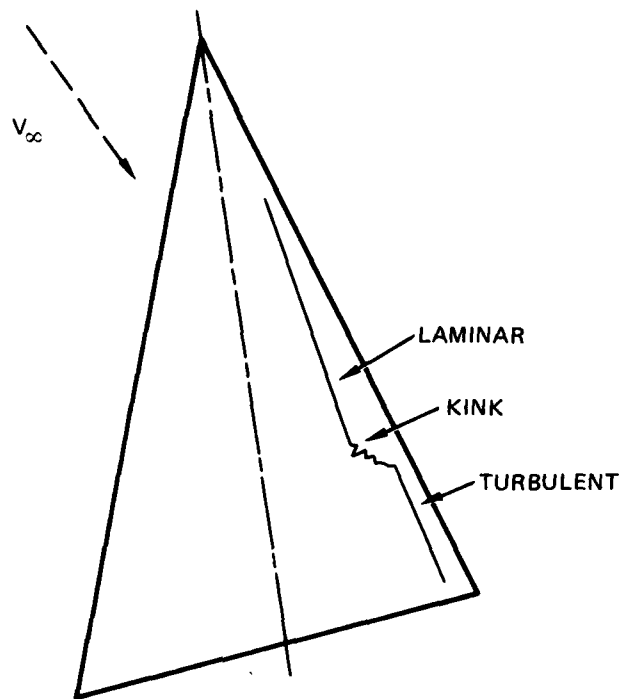
(d) LOCI OF SECONDARY SEPARATION POINTS

FIGURE 33. CONCLUDED
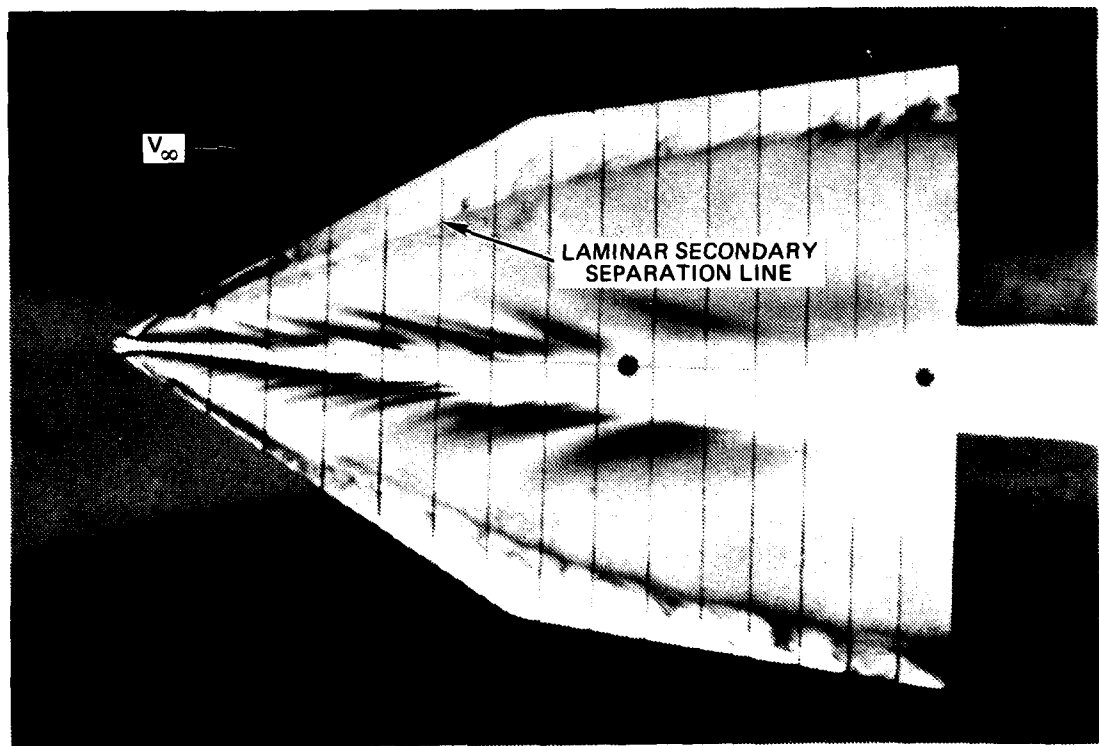
80-00255

FIGURE 34. UPPER SURFACE FLOW PATTERN ON A SLENDER WING
(NORTHROP WATER TUNNEL)

lower than in the laminar case. However, the integrated pressures are about the same in both the laminar and turbulent flows.

Some contradictory evidence on the effects of Reynolds number is provided in Reference 80. Data on a slender delta wing reveal measurable changes in the normal force due to increased Reynolds number (Figure 33). Boundary layer transition to turbulence results in a kink in the secondary separation line as sketched in Figure 33, and the increased suction over the newly turbulent region causes increased loading on the wing. The normal force increases with Reynolds number, especially at the higher angles of attack where the vortex system is large. As discussed in Reference 80, full-scale flow conditions on the upper surface of a delta wing at high angle of attack will not be correctly simulated by the traditional procedure of applying grit near the leading edge. The best position for grit will be somewhere just outboard of the spanwise location where the lower surface boundary layer fluid first attaches to the upper surface. Since vortex size varies with angle of attack, however, it may be necessary to apply grit to a substantial portion of the upper surface.

Based on the above discussions, in water tunnel tests, the secondary vortex and secondary separation line as depicted in the flow visualization photograph in Figure 34 can at most be observed in a qualitative sense.

Whether or not a tertiary vortex, rotating in the same sense as the primary vortex, is formed at all depends on the pressure gradient in the pressure distribution due to the primary and secondary vortices. Data from Reference 81 show that tertiary vortices apparently only occur when a laminar boundary layer separates along the secondary separation lin . A reason for this is that strong secondary vortices are rmed if there is a large separation between the secondary separation line and the leading edge, that is, if there is

80

separation of the laminar boundary layers. These then produce the corresponding large pressure gradients, such that the flow separates again. Turbulent boundary layer separation usually only occurs in the vicinity of the leading edge, as shown quite clearly in the surface oil flow patterns in Figure 35 (from Reference 63), therefore, only a small secondary vortex is formed which produces no additional separation. At the transition point between laminar and turbulent secondary separations, where the separation line has a break, the tertiary vortex *formed along the front part of the wing* disappears. (NOTE: As will be discussed in a subsequent section of this report, a completely analogous flow phenomenon appears to occur on the lee-side of slender bodies at high angles of attack.)

Physical Interpretation of Vortex Structure and Vortex Growth

Prior to a detailed discussion of flow regime (3) which deals with the internal structure of the vortex flow and, specifically, the vortex core, a physical interpretation of the observed vortex structure embracing the whole of the vortex from the outer spiral region to the inner diffusive subcore is provided. The discussion is based on the physics of the flow as described in Reference 82.

In a viscous fluid, vorticity is transported by convection and diffusion. At high Reynolds numbers, a significant difference in the scale of the two transport processes exists, the ratio of the scales of diffusion and convection being of the order $1/Re^{1/2}$. The latter term is also a measure of the boundary layer thickness. The rate of expansion of the vortex with distance x along the axis is of the order ℓ/x, where ℓ is the lateral scale or "diameter" of the large-scale structure of the vortex. In vortices studied experimentally, ℓ/x is typically much greater than $1/Re^{1/2}$. In the Northrop water tunnel,

Re = 0.9 X 10^6

(a) LOWER SURFACE
(b) UPPER SURFACE
(1) SECONDARY SEPARATION LINE

Re = 2.0 X 10^6
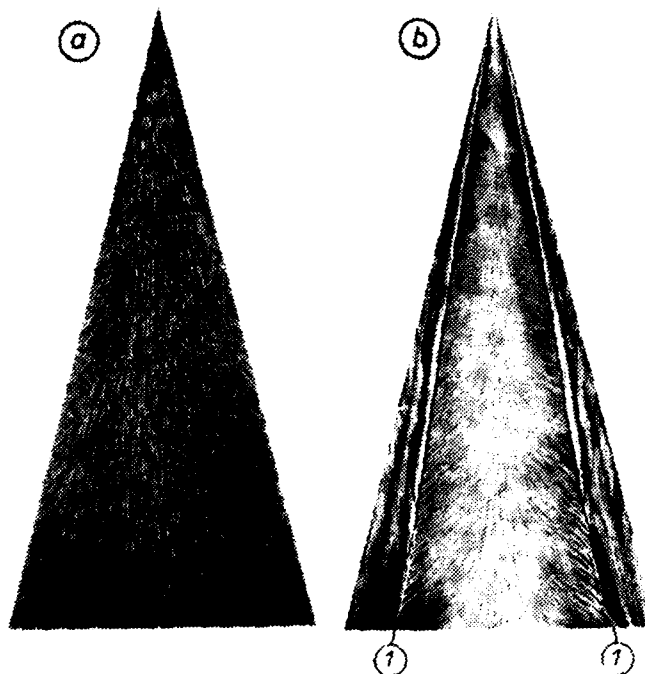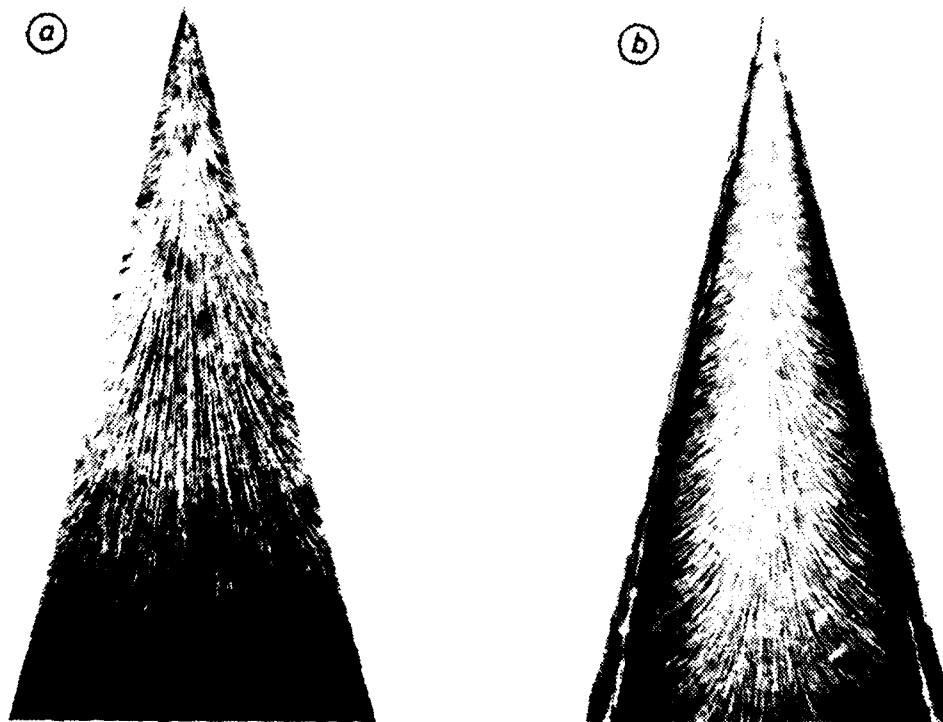
FIGURE 35. WIND TUNNEL SURFACE OIL FLOW PATTERNS IN LAMINAR AND TURBULENT
FLOWS FOR AN ASPECT RATIO 1 WING AT 20.5 DEGREES ANGLE OF ATTACK
(FROM REFERENCE 63)

for example, on a 0.305-meter slender wing at 20 degrees angle of attack, ℓ/x at the trailing edge is approximately 0.24 whereas $1/Re^{1/2} = 0.006$. Consequently, even at the low Reynolds numbers typical of water tunnels, the condition that $\ell/x \gg 1/Re^{1/2}$ is generally satisfied, in other words, the size of the vortex is much greater than the undisturbed boundary layer thickness. So, it appears that in these cases, the large-scale vortex structure must have been determined primarily by the convective transport mechanism and is likely to have been largely independent of Reynolds number.

Convection, though essentially a large-scale process, partially determines the small-scale structure of the vortex. At infinite Reynolds number the vortex is formed solely by convection, since diffusion is not present. A vortex sheet is shed from the wing leading edge which rolls up into an expanding spiral stream surface. The form of the spiral trace that this surface makes at any cross-section is defined by the spacing d between successive turns of the spiral as shown in Figure 36 from Reference 82. Therefore, d is a local measure of an essentially small-scale structure associated solely with convection.

Diffusion of vorticity occurs at finite Reynolds number, however, and the spiral vortex sheet becomes a vortex layer of finite thickness. The merging of successive spiral turns indicates that the small-scale structure is now determined both by convection and diffusion, the relative significance of which depends on the relative magnitude of their respective length scales d (convection) and $(\nu x/U_\infty)^{1/2}$ (diffusion), as shown in Figure 36.

Three distinct forms of small-scale structure are depicted in Figure 36. In the outer region where $d \gg (\nu x/U_\infty)^{1/2}$ discrete turns of the spiral remain in evidence. Diffusion is unconstrained since the neighboring turns are not yet merging. Consequently, the detailed structure of the layer exhibits
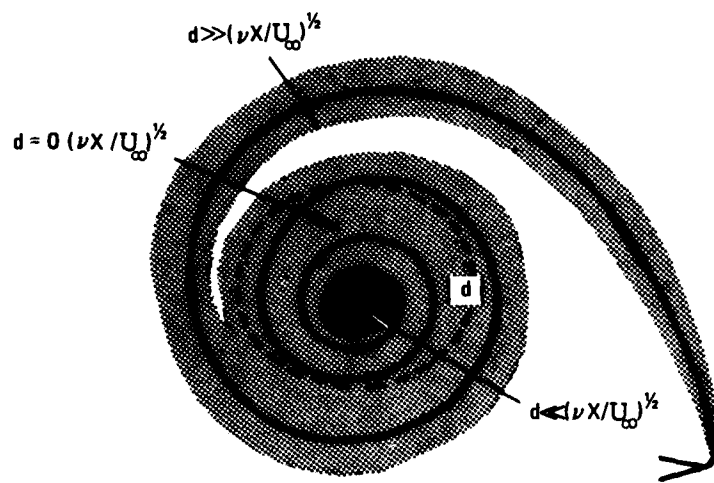
FIGURE 36. SKETCH OF VORTEX FLOW REGIMES (FROM REFERENCE 82).
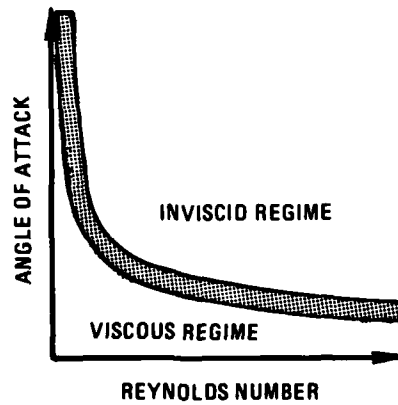
FIGURE 37. INVISCID AND VISCOUS REGIMES OF A
VORTEX FLOW (FROM REFERENCE 82).

scale effect. For example, Reference 88 has observed in wind tunnel tests that the outer turn of the spiral vortex layer becomes more sharply defined at higher Reynolds numbers.

Inside this outer region, as d and $(\nu x/U_\infty)^{1/2}$ become of comparable magnitude, the turns of the spiral merge. The rate of diffusion decreases since the radial gradient of vorticity is greatly reduced. The diffusion mechanism is constrained due to the close spacing of the neighboring spiral turns and, in essence, the convective transport mechanism remains dominant long after the spiral structure is no longer in direct evidence. With diffusion inhibited by constraint, there is little evidence of scale effect.

A marked Reynolds number effect is evident, however, in the region of the vortex axis where $d \ll (\nu x/U_\infty)^{1/2}$ because the entire structure of this region is dominated by diffusion. This sub-core region is quite small, however, its lateral extent or "diameter" being of the order of the undisturbed boundary layer thickness. (The sub-core is to be distinquished from the rotational core, as will be discussed in the next section.)

Although the boundaries between the three regions just described are expected to lie closer to the vortex axis with increased Reynolds number, scale effect is evident only in the small-scale structure itself. Consequently, provided flow separation occurs at a salient edge, the flow properties associated primarily with the large-scale structure, for example the strength and location of the vortex, are expected to be insensitive to changes in the value of the Reynolds number.

The kind of structure inferred from the arguments in Reference 82 is strictly applicable only at large Reynolds numbers (typical of wind tunnels and flight) and where the

lateral scale of the vortex structure as a whole greatly exceeds the diffusive rate of expansion of an element of vorticity relative to the rate of convection. As Reynolds number is reduced into the water tunnel range, the boundaries between the three discrete regions are expected to be displaced outwards. Yet, as was shown previously, l/x is still much greater than $1/Re^{1/2}$. This implies that the vortex structure is still primarily convective and relatively insensitive to Reynolds number changes.

It should be noted, however, that as Reynolds number is further reduced and the boundary of the inner core region expands sufficiently to approach the boundary of the vortex as a whole, the lateral scale of the vortex l/x becomes of the order $1/Re^{1/2}$ and the vortex structure is diffusion dominated. In essence, the vortex is submerged in the boundary layer flow. This flow situation would correspond to Reynolds numbers approaching creep flow conditions.

Reference 82 identifies two essentially different vortex regimes:

(1) Viscous vortex submerged or partially submerged in the boundary layer.

(2) Predominately inviscid vortex, large relative to the local boundary layer thickness, which can be regarded as a vortex sheet subject to relatively minor modification due to viscous diffusion. (This is analogous to the modification of the flow past a body at high Reynolds number due to the presence of the boundary layers.)

In addition to the dominance of diffusion at very low *Reynolds numbers*, there is also an angle of attack range at a given Reynolds number within which the vortices are of the

86

viscous type. As a result, a relationship can be envisioned between Reynolds number and angle of attack which defines whether a vortex is of the inviscid or viscous type. This is sketched in Figure 37 (from Reference 82). As will be shown later in this report, water tunnel simulation of vortex flows at low angles of attack can be unrepresentative because the vortices are of the viscous type, unlike the inviscid-type vortices generally observed at high Reynolds numbers in wind tunnels and flight. At high angles of attack in a water tunnel, the flow field is vortex-dominated and, hence, good agreement is observed with high Reynolds number results in air. In general, water tunnel experience indicates that the vortex sub-core height above the surface must be of the order of ten boundary layer thicknesses or more in order to be in the inviscid regime depicted in Figure 37.

It should be noted that near the wing apex, the local Reynolds number is quite small and, consequently, the vortex is of the viscous type. The presence of the viscous region near the apex is presumably not felt to any great extent, however, well within the inviscid region of the vortex further down-stream. Results have been obtained in water tunnel studies in Reference 89 which indicate that the presence of a thick laminar boundary layer near the apex of a delta wing apparently has negligible effect on the behavior of the vortex flow.

Vorticity Flow Within Vortex Sheet and Vortex Core

Flow regime (3), the vorticity flow within the vortex sheet and vortex core, deals with the internal structure of the vortex flow itself, as sketched in Figure 38, which depicts a vortex sheet of finite thickness. The thickness of the shear layer is negligible near the leading edge and as a first approximation the layer is modeled as a sheet of infinitesimal thickness which contains the vorticity shed at the edge. As the path length along the streamline emanating from the
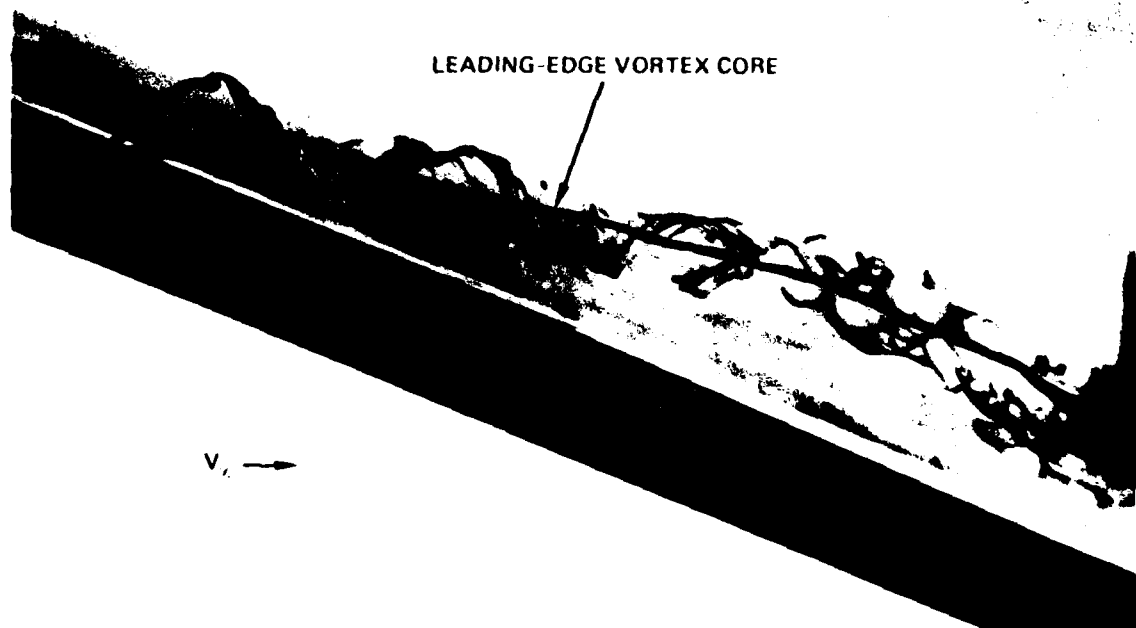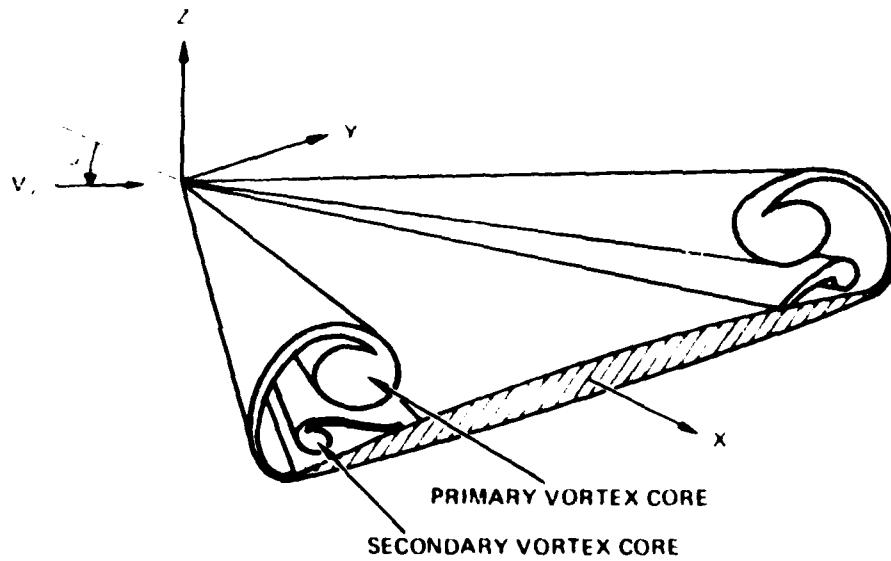
**FIGURE 38. SCHEMATIC OF VORTEX SHEET OF FINITE THICKNESS
AND CLOSE-UP VIEW OF CONCENTRATED CORE**

leading edge becomes much greater than a characteristic length L, a distinct shear layer is no longer observed since a region of continuously-distributed vorticity now exists which is called the vortex core. As indicated in Reference 83, the cross-sectional size of the rotational core is much greater than the laminar boundary layer thickness (which is proportional to $L/Re^{1/2}$) and the cross-sectional size and strength of the vortex core are weak functions of the Reynolds number. Inside the rotational core, the flow is governed by the Euler equations (viscous terms are dropped from the Navier-Stokes equations), except for a very small region around the center with a diameter of the order of the boundary layer thickness ($L/Re^{1/2}$) where the viscous forces are large. This small sub-core is depicted in the flow visualization photographs in Figures 38 and 39. This inner, diffusion-dominated viscous core is very small, representing approximately 3-5 percent of the vortex "diameter" (Reference 58) within which very high axial velocities are often observed, as shown in Figures 40 to 42. A qualitative explanation for the high axial velocity along the core axis can be provided in terms of the familiar spiral sheet model of the vortex, for the inclination of the spiralling vortex lines to the axis is such as to make them all induce a downstream component of velocity along the axis. Figure 41 depicts local axial velocities along the vortex core axis determined in ONERA water tunnel tests (Reference 84), whereas Figure 42 presents vortex core mean axial velocities determined over finite distances along the core axis in the Northrop water tunnel. For comparison, local axial velocities determined in wind tunnel tests of delta wings in References 85 and 86 are also shown. It should be noted, however, that water tunnel and wind tunnel studies in References 87 and 88 have indicated a Reynolds number effect on core axial velocity, as depicted in Figure 42. The water tunnel results are useful, however, in that they reveal the high axial velocities along the core axis. To appreciate the size of the sub-core region, a relationship is used from Reference 90 for the vortex core

VORTEX CORE BREAKDOWN

VORTEX CORE

WING UPPER SURFACE

V_∞
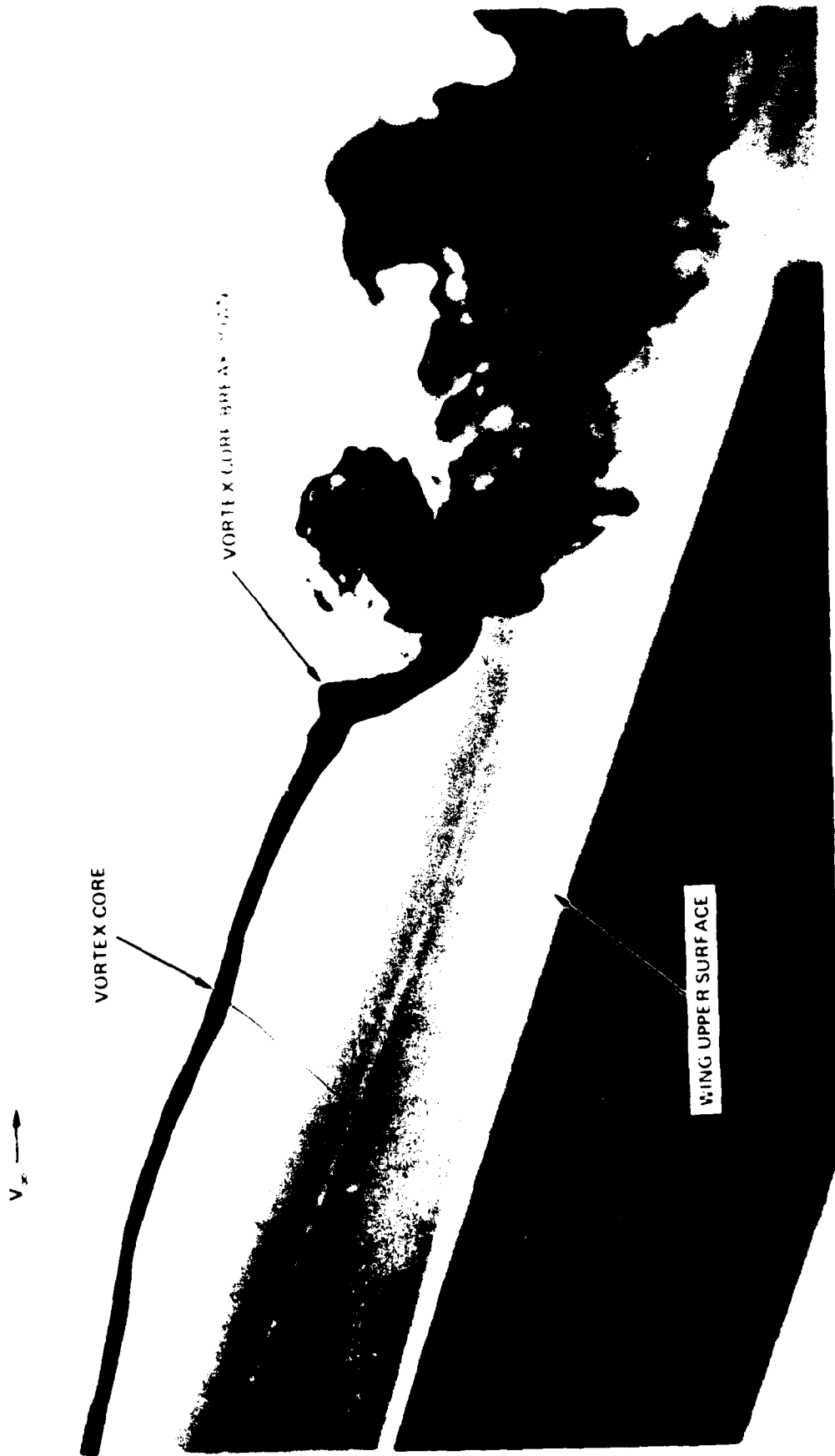
FIGURE 39. FLOW VISUALIZATION PHOTOGRAPH OF LEADING-EDGE VORTEX CORE AND
CORE BREAKDOWN (NORTHROP WATER TUNNEL)

FIGURE 40 CLOSE UP VIEW OF LEADING EDGE VORTEX CORE WITH HIGH VELOCITIES ALONG THE VORTEX AXIS (NORTHROP WATER TUNNEL)
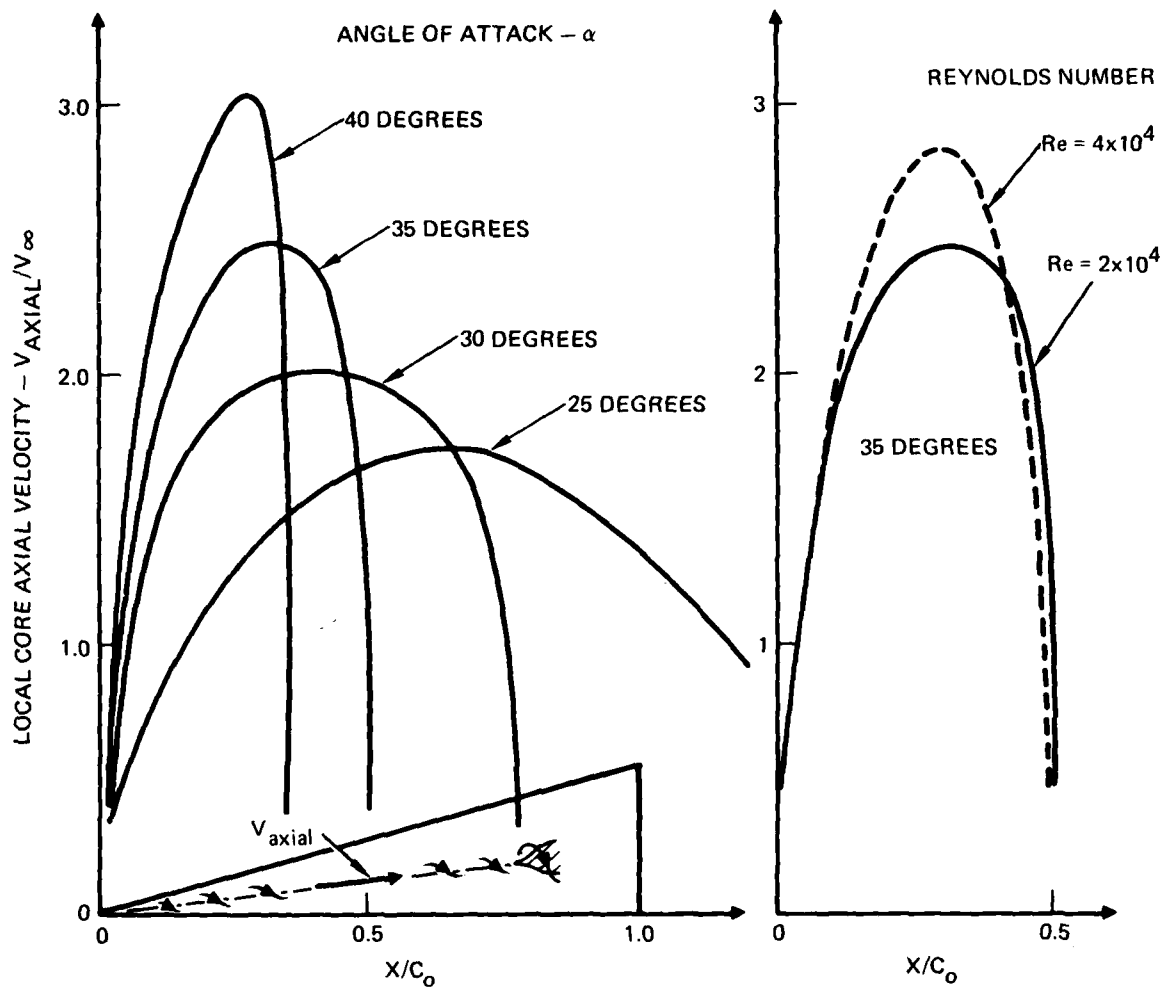
FIGURE 41. LOCAL AXIAL VELOCITIES ALONG CORE AXIS FOR AN ASPECT
RATIO 1.07 WING (FROM REFERENCE 84)
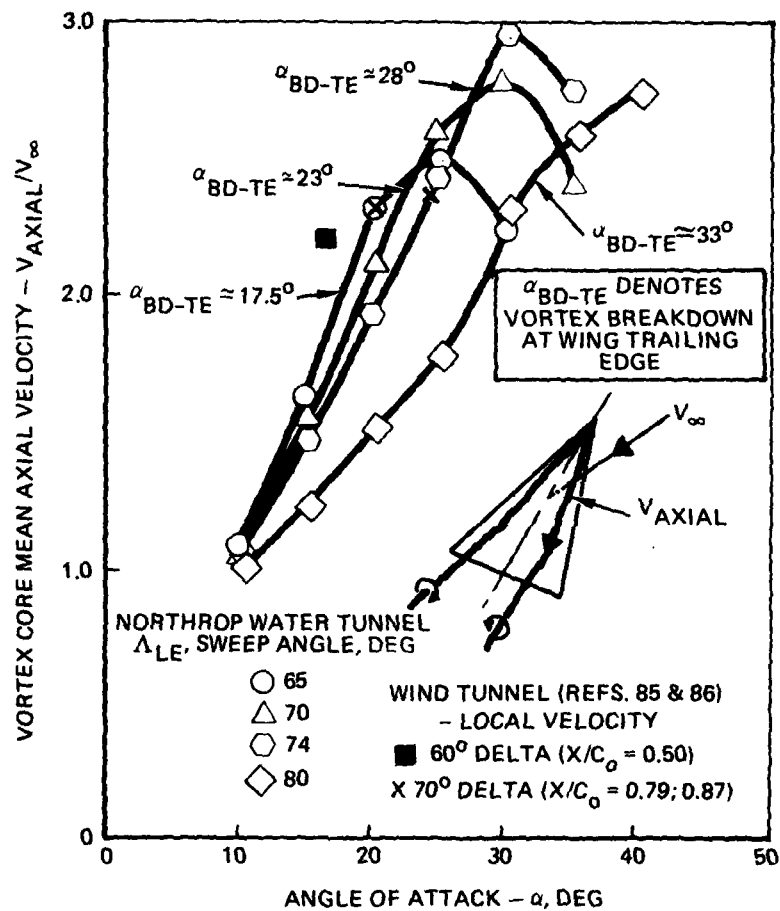
a) MEAN AXIAL VELOCITY — NORTHROP WATER TUNNEL

FIGURE 42. AXIAL VELOCITIES ALONG CORE AXIS
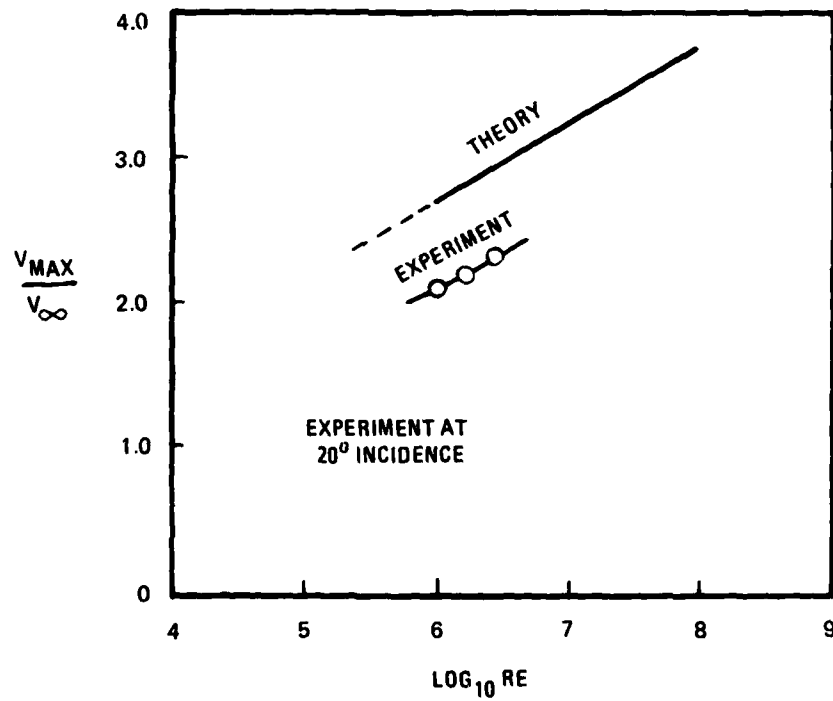
(b) VORTEX CORE AXIAL VELOCITY VERSUS REYNOLDS NUMBER.

FIGURE 42. CONCLUDED.

radius expressed as a function of downstream distance, $r(x) \sim (\nu x/U_\infty)^{1/2}$. In a low Reynolds number water tunnel, the radius at mid-chord of a 0.305-meter slender wing is then of the order of 0.136cm, which is in reasonable agreement with the estimated core radius of 0.12cm made during observation in the Northrop water tunnel (see Figure 40). The "diameter" of the vortex flow at this location is roughly 5.44 cm. The flow situation can, therefore, be approximated as inviscid and irrotational with embedded regions of inviscid rotational flow of infinitesimal extent that represent the rolled-up portions of the shear layer. Viscous dissipation is of significance only in a relatively small sub-core (see Reference 83).

Vortex cores are regions of high vorticity that can be considered roughly axisymmetric and of continuously-distributed vorticity. Within the core are appreciable axial and circumferential, or swirl, velocity components which are strongly coupled. An important physical feature to note concerning a vortex core is its highly responsive nature to external disturbances, such that small perturbations outside the core can trigger large responses within the core itself. Figure 43 illustrates an idealization of a viscous vortex, where the small diffusion-dominated central core region is approximated as a rigid body of rotation surrounded by a potential vortex flow. Initial axial velocity profile is assumed uniform (that is, $U_{axial}/U_\infty = 1.0$). The corresponding swirl velocity profile for each region is depicted in the second sketch where the swirl velocity varies directly with the radius within the inner core region and inversely with the radius in the outer, or potential, flow region. The corresponding pressure distribution across the vortex is shown in the third sketch which provides a plausible explanation for a phenomenon that has been observed in Northrop wind tunnel flow visualization studies: smoke introduced into the vicinity of a vortex core assumes a location along the outer edge of the viscous core due to the matching of pressures between the outer and inner flow regimes, thereby depicting a hollow core.

95
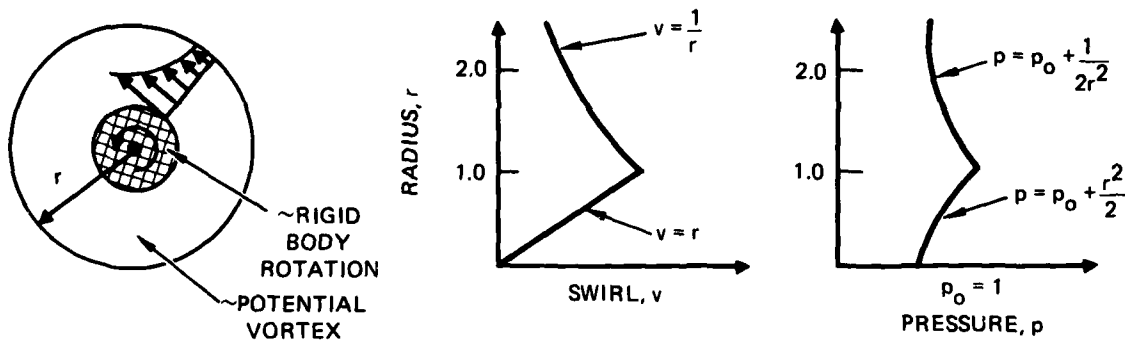
(A) IDEALIZATION OF A VISCOUS VORTEX
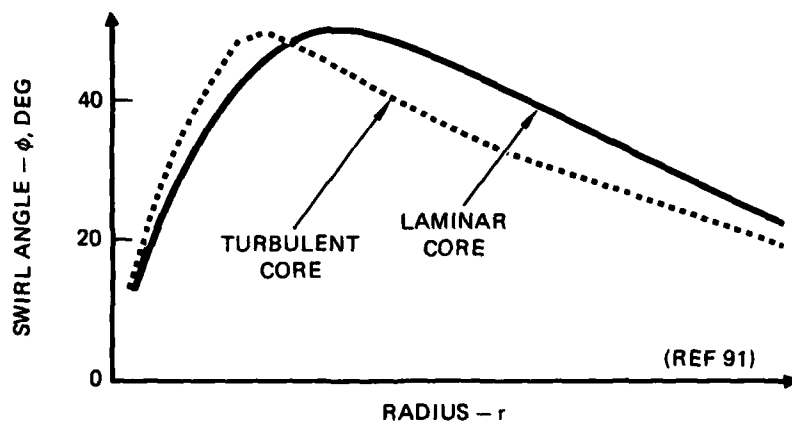
B) EFFECT OF TURBULENCE ON SWIRL ANGLE DISTRIBUTION

FIGURE 43. VORTEX CORE CHARACTERISTICS

In a viscous vortex, the swirl angle, $\varphi = \tan^{-1}(v/u)$, where v and u are the swirl and axial velocities, respectively, increases from zero at the axis to a maximum at the radial distance where the swirl velocity is nearly maximum, and subsequently decreases to zero with increased radial distance. The point at which the swirl angle achieves a maximum value corresponds to the outer edge of the viscous core depicted in Figure 43. Swirl angle is of critical importance to vortex stability and will be discussed subsequently in more detail in later paragraphs.

Prior to a detailed discussion of vortex breakdown, which follows in the next section, a brief discussion of the effects of turbulence and compressibility is warranted. Theoretical models of vortex cores have usually assumed a laminar core. However, most vortex cores are turbulent in which the motion is irregular and the rate of diffusion is much greater than if the flow were laminar. Many properties of vortex cores, however, depend on rotation and not diffusion. Consequently, turbulent core calculations often assume a constant eddy viscosity which, in some cases, is assumed at several times the value of the kinematic viscosity, and a set of governing equations identical in form to the laminar equations is solved. The effect of turbulence is to reduce the radius of the central core, as can be seen from Figure 43 depicting the radial location for maximum swirl angle for both laminar and turbulent cores. Wind tunnel results in Reference 86 on a 60-degree delta wing indicate that for the case of a turbulent leading-edge vortex, the breakdown position (where vortex breakdown is characterized by a sudden deceleration and stagnation of the axial flow and expansion of the core as if a solid obstacle were present in the flow) moves aft relative to the laminar core case. Water tunnel and wind tunnel results obtained in Reference 26, however, at Reynolds numbers from 1 $\times$ 10^4 to 2 $\times$ 10^6, which cover the range of laminar to turbulent cores, reveal no discernible effect on vortex core stability.

97

Compressibility results in a marked reduction in the responsiveness of the internal core structure to changes in the conditions external to the core, thus indicating increased damping within the core. An interesting point to note is that the solution for an inviscid compressible core of a leading-edge vortex gives finite axial velocity and zero circumferential velocity at the core axis, in contrast to the infinite values derived from the incompressible-flow equations (see Reference 91). An additional effect associated with compressibility is the extremely low core pressures which approach a vacuum.

Vortex core behavior is quite complex and the introduction of turbulence and compressibility effects makes a solution of the governing equations virtually intractable. A great deal of information can be derived from solutions of simplified sets of equations, which closely approximate the real core behavior. Consequently, several theories have been developed which assume steady, laminar, incompressible flow with appropriate boundary conditions and provide insight into key parameters which affect the development and stability (breakdown characteristics) of the vortex core. To augment these studies, experimental emphasis was placed on easily-controllable experiments in cylindrical tubes.

4.3.3 Vortex Core Breakdown - Theory and Experiment

Three general themes are evident in the theoretical explanations of vortex breakdown: (1) analogy to the separation of a two-dimensional boundary layer; (2) a consequence of a hydrodynamic instability; and (3) the existence of a critical state (see Reference 91 for a complete description of each hypothesis). Several parameters are common to each theory, among these are: sensitivity of breakdown position to swirl changes, the pressure gradient along the edge of the core, and the external conditions. The observed physical features of

98

vortex core breakdown include: (1) high swirl, for example maximum swirl angles ($\emptyset$) generally greater than 40 degrees are observed just upstream of breakdown; (2) a divergence of the stream tubes in the core immediately upstream of breakdown; and (3) an external pressure gradient in the axial direction. The occurrence of core breakdown depends on a delicate balance between the swirl magnitude, the amount of flow divergence, and the external pressure gradient. For example, core viscous effects can result in a divergence of the outer stream tubes, in the absence of an external pressure gradient, and can promote breakdown, because core stream tube divergence itself imposes an adverse pressure gradient within the viscous core. The larger the adverse pressure gradient (or degree of flow divergence) the less is the swirl required for breakdown.

The question arises, then, under what flow conditions does the water tunnel provide a realistic representation of the vortex core breakdown phenomena experienced in wind tunnel and flight tests. The highly viscous nature of the vortex inner core suggests that the low Reynolds number laminar core behavior in the water tunnel will be quite unlike the turbulent core behavior at high Reynolds number. The correlations that have been obtained to date, however, suggest that under certain conditions the relative significance of the key parameters is simulated in the water tunnel. Experiment provides insight into the relative importance of inertia, viscous, and pressure terms under particular external aerodynamic conditions. Water tunnel experience suggests that the pressure gradient in the external flow field, which appears the dominant vortex flow parameter at high angles of attack, is well-simulated in a water tunnel, thereby permitting good correlation with wind tunnel and flight results. By way of analogy, boundary layer separation can occur in the vicinity of a shock, independently of upstream boundary layer thickness, which is analogous to a vortex core traversing a large adverse pressure field over a wing at high angle of attack, where vortex breakdown occurs regardless of the value of the Reynolds number.

99

The following discussion presents a detailed review of theoretical and experimental studies of the <u>third flow phenomenon</u> which must be simulated in a water tunnel for proper correlation with high Reynolds number results: <u>vortex core breakdown (or burst)</u>.

Theoretical Studies of Vortex Core Breakdown

Vortex flows are subject to major structural changes involving large disturbances when a critical value of the ratio of swirl velocity to axial velocity is reached. The three spatial regimes of the vortex breakdown flow field are, according to Reference 92:

I. Approach flow consisting of a thin concentrated vortex core (viscous sub-core) embedded in an approximately irrotational flow. Changes in the approach flow with axial distance are gradual and the flow is either laminar or has low turbulent intensities. Axial velocity profiles are jet-like.

II. Breakdown region occupying an axial interval of about five core diameters involving rapid changes in the axial direction. There are three sub-regions: (1) the approach flow is decelerated and a stagnation point is formed on the axis, (2) reversed flow occurs near the axis, and (3) the original direction of the axial flow is restored marked by a large increase in turbulent intensity or, for laminar approach flows, by signs of transition to turbulence.

III. New vortex structure with expanded core downstream of the breakdown zone. Again, axial variations are gradual. Axial velocity profiles resemble a conventional wake behind a solid obstacle with centerline speeds less than those outside the core and the flow is turbulent.

100

The significance of pressure gradients on core behavior, which will be discussed in great detail later in this report, is mentioned briefly at this point. Vortex breakdown can be promoted by an adverse pressure gradient. Pressure gradients may be impressed upon the vortex core by a deceleration of the outer flow, from pressure differences along a vortex core caused by a sudden expansion, or from a pressure rise over the rear area of a wing. Reference 91 has shown that when an adverse pressure gradient is increased, less swirl is required to maintain a breakdown or, if the same level of swirl is maintained, the breakdown is moved upstream.

Quantitative experimental measurements of vortex core characteristics are prohibitive due to the high responsiveness of the core to external disturbances. Non-intrusive techniques (laser doppler method) are quite promising but the complexity and laboriousness of such measurements require further advancement of the state-of-the-art. Consequently, many analytical studies have been made of vortex development and breakdown phenomena. Analytic approaches range from a solution of the steady, incompressible Navier-Stokes equations (Reference 93) to numerous solutions of the quasi-cylindrical equations (References 94 to 96).

The theoretical approach in Reference 97, which considers high Reynolds number ($\sim 10^4$) based on core radius, features a viscous parabolic subset of the Navier-Stokes equations. The quasi-cylindrical vortex equations, analogous to the boundary layer equations, are used to compute vortex flows as long as their stream surface angle remains small. At high swirl values, singularities are encountered which indicate a failure of the quasi-cylindrical approach. Accordingly, this is associated with the occurrence of physical axisymmetric vortex breakdown. Reference 97 indicates that the quasi-cylindrical approximation can be correctly applied upstream to a distance of the order of the vortex breakdown

101

bubble diameter ahead of the stagnation point. The exact bubble shape and the external flow are well determined almost solely by the _inviscid flowfield_. Flow in the neighborhood of the stagnation point and in and around the bubble can be treated using the equation for inviscid rotating flow.

A dimensional analysis of the steady incompressible Navier-Stokes equations with rotational symmetry (Reference 97) reveals the well-known governing parameters: Reynolds number based on core radius $(U_\infty r_c / \nu)$, swirl parameter (v_c / U_∞) and core stream surface angle $(\gamma = \tan^{-1} w_c / u_c)$. Here, U_∞ is the external flow axial velocity and v_c, w_c, and u_c, are the swirl, radial, and axial velocities at the edge of the inner core, respectively. The quasi-cylindrical equations are a simplified set which describe slender vortex flows (large swirl: $v_c / U_\infty = 0(1)$; thin core: $\tan \gamma \ll 1$; and high Reynolds number: $(U_\infty r_c / \nu) \cdot \tan \gamma = 0(1))$. Viscous terms are retained in the radial and axial momentum equations with the swirl momentum equation reducing to:

$$\frac{v^2}{r} = \frac{1}{\rho} \frac{\partial p}{\partial r} \qquad \text{Equation 4}$$

Equation 4, which is exact only for _slowly expanding cores in the limit of high Reynolds numbers_, is an analytic expression for the balance between the fluid particle's centrifugal acceleration and the restraining pressure forces. Integration of Equation 4 from the limits r=0 (core axis) to r=∞ followed by differentiation with respect to the axial coordinate z yields:

$$\frac{\partial p_0}{\partial z} = -2\rho \int_0^\infty \frac{v}{r} \frac{\partial v}{\partial z} \partial r \qquad \text{Equation 5}$$

where p_0 is the pressure at the core axis. An assumption is made that the _external pressure gradient is zero_. Equations

102

4 and 5 illustrate the coupling between the axial and swirl forces. When the stream surface angle of this rotationally-symmetric vortex flow becomes appreciable, that is, when $\tan \gamma = 0(1)$, the set of equations represents inviscid flow, indicating the dominance of inertia and pressure terms. The vortex breakdown phenomenon is characterized by streamline expansion and core axial velocity stagnation and, therefore, is subject to this analysis.

An appreciation for the strong coupling between the axial and swirl components can be gained from further examination of Equation 5. Accordingly, the variation of axial pressure gradient across the core can be expressed as (see Reference 91):

$$\left(\frac{\partial p}{\partial z}\right)_{r=o} - \left(\frac{\partial p}{\partial z}\right)_{r=r_c} \sim \rho \gamma \Gamma^2 / r_c^2 \qquad \text{Equation 6}$$

where Γ represents the magnitude of the circulation. This expression indicates that the square of the circulation is a measure of the degree to which the adverse pressure gradient along the axis will exceed the pressure gradient along the outside edge of the vortex if the stream surfaces diverge (large γ). (An analogy of vortex breakdown with boundary layer separation is not appropriate in this case since in the conventional boundary layer situation the pressure variation across the layer is negligibly small and has no effect on the development of the layer.)

Swirl has a pronounced effect on the velocity distributions on the vortex axis. At a critical value of swirl, the high swirl permits a much greater upstream penetration of downstream velocity and pressure disturbances, that is, upstream decay of disturbances diminishes with increasing swirl. As described in Reference 97, there is one particular swirl parameter value dividing a vortex flow which decays in a

wake-like manner from another which breaks down, as shown in Figure 44. This dividing swirl parameter is a function of the vortex velocity profiles. Leading-edge and trailing vortices on wings are, as described in Reference 97, usually of the breakdown-stable type (1a), where vortex flows show smooth viscous decay of all velocity profiles to the surrounding free-stream velocity, but may change to the stagnating type (1b), characterized by increasingly rapid deceleration on the axis, increasing swirl, and eventual failure of the computation, as a result of either higher swirl (increased angle of attack) or adverse pressure gradient (negative external axial velocity and/or external circulation gradients which will be discussed in detail subsequently).

Of the three parameters discussed to this point, Reynolds number, swirl parameter, and core stream surface angle, Reynolds number is the more important parameter in understanding the characteristic difference of vortex development and breakdown in the water tunnel, wind tunnel and in flight. For large Reynolds numbers, the development of the vortex can be described by the quasi-cylindrical equations for flow up to large expansions or contractions, vortex breakdown being indicated by termination of the numerical solutions. These equations are indicative of wind tunnel and flight conditions where the Reynolds number is characteristically large. In a water tunnel, however, the Reynolds number is relatively small and, therefore, the viscous terms can be as important as the inertia terms. This effect is shown in Figure 45 which presents results from solutions of the Navier-Stokes equations for identical initial axial and swirl distributions. At low core Reynolds numbers, a Reynolds number effect on the axial velocity distribution is quite evident. The results also indicate, however, that above some critical Reynolds number those solutions which exhibit breakdown at low Reynolds number (indicated by negative axial velocity) should continue to do so as the Reynolds number is increased. These results were
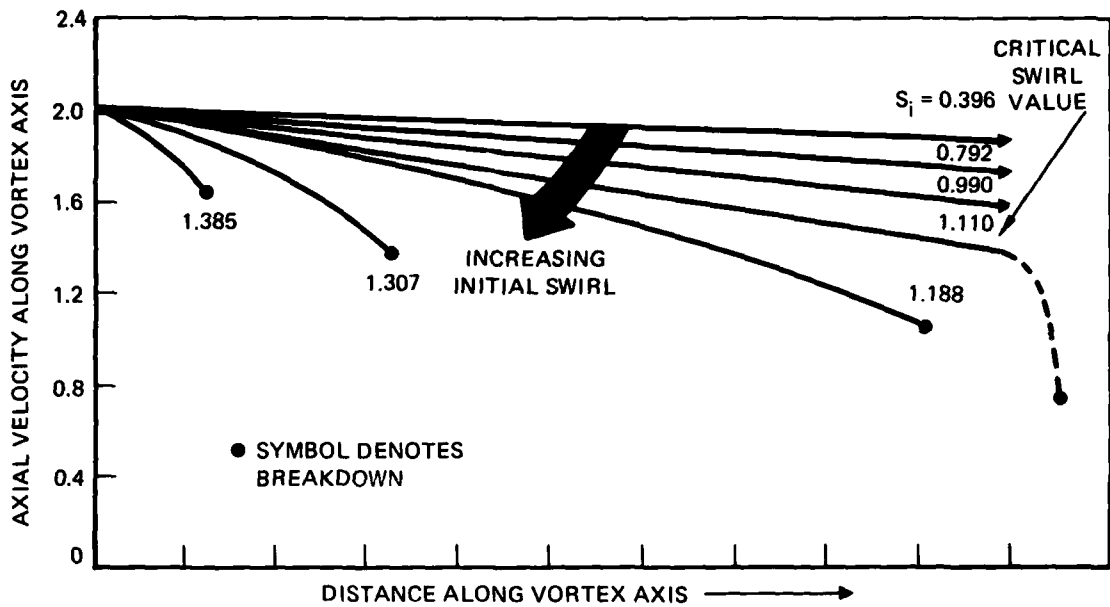
FIGURE 44. EFFECT OF SWIRL AS AN INITIAL BOUNDARY CONDITION ON THE
AXIAL VELOCITY ALONG THE VORTEX AXIS
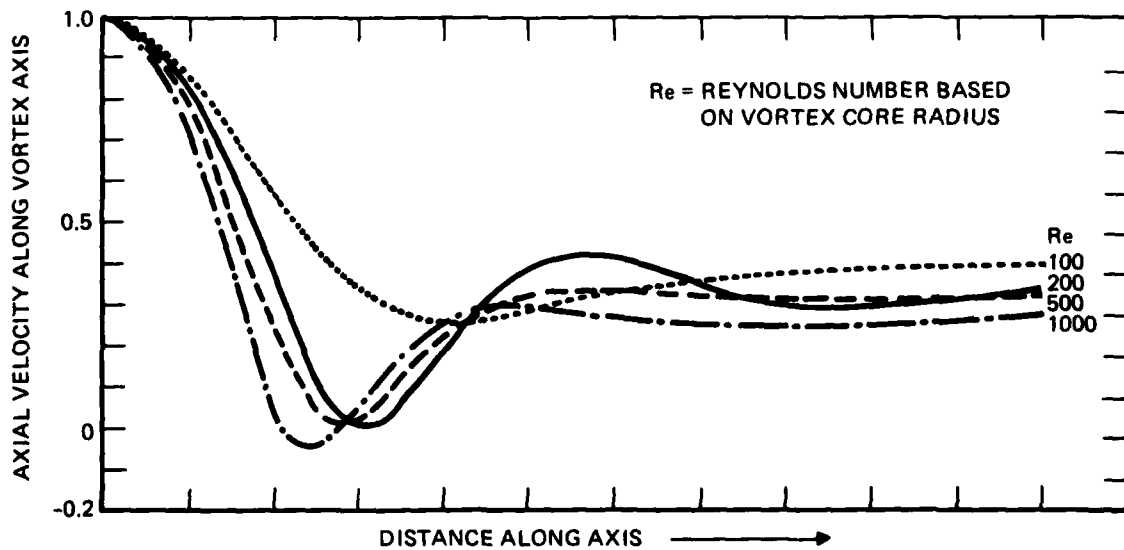
FIGURE 45. EFFECT OF REYNOLDS NUMBER ON AXIAL VELOCITY ON THE
VORTEX CORE AXIS

105

obtained from an alternative approach taken in Reference 93
where solutions of the Navier-Stokes equations for vortex
breakdown were obtained for core Reynolds numbers up to 200
(which is, at best, moderate; for example, typical Reynolds
numbers (based on core radius)in a water tunnel are of the
order 125). This numerical approach was developed as an
alternative to the quasi-cylindrical approximation because,
according to Reference 93, it was not clear that failure of the
quasi-cylindrical equations requires fully reversed flow, as is
encountered in vortex breakdown, since a computational failure
represents only the inability of the approximation to deal with
large axial gradients. The results from Reference 93, never-
theless, show similar trends. The appearance in a vortex core
of a large decrease in axial velocity is critically dependent
on the magnitude of the initial swirl. The strong coupling
between swirl and axial velocity components is shown in Figure
46. The axial velocity retardation arising from viscous
dissipation of the swirl is large enough to require a signi-
ficant amount of radial outflow. This decreases the swirl
velocities near the axis and, therefore, supports a very much
larger adverse pressure and an increased reduction of axial
velocity.

A fourth important parameter affecting vortex core
behavior is related to the external aerodynamic conditions.
Simulation of the pressure field in the external flow is of
critical importance when attempting to correlate water tunnel
results to high Reynolds-number data. At high angles of
attack, the effect of the external conditions on leading-edge
vortex stability is quite large.

The numerical solutions of the quasi-cylindrical equa-
tions for various external velocity gradients are shown in
Figure 47 for fixed initial swirl and with a uniform axial
velocity (U_{axial}/U_∞ =1.0). The velocity gradients assumed in
Reference 97 are quite small and consequently, the results
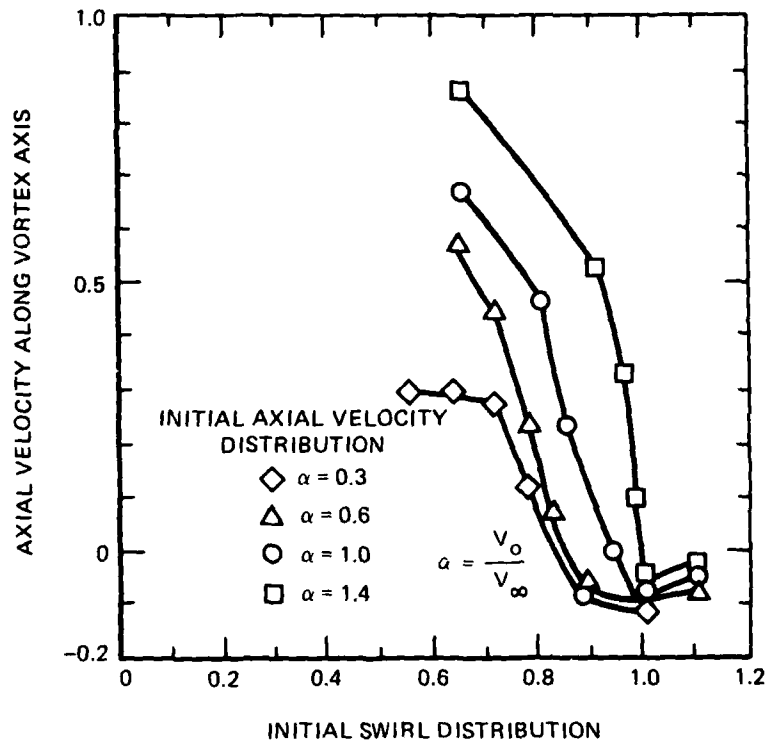
FIGURE 46. EFFECT OF INITIAL AXIAL VELOCITY AND SWIRL DISTRIBUTIONS ON AXIAL VELOCITY ALONG THE VORTEX AXIS: RE = 200
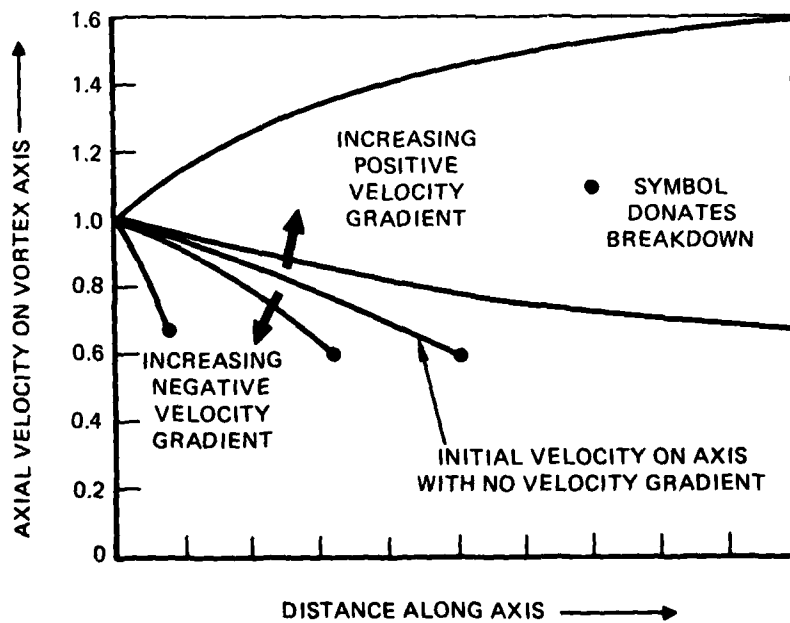
FIGURE 47. EFFECT OF VELOCITY GRADIENT ON AXIAL VELOCITY ON THE VORTEX AXIS (REFERENCE 97)

illustrate the significant effect which even very small external velocity gradients can have on the velocity on the axis. Furthermore, numerical results show that the core flow is mainly responsible for eventual breakdown and is easily influenced by external flow conditions. External flow gradients are felt through their effects on both the external pressure distribution and the swirl parameter. The numerical results shown in Figure 48 indicate that a vortex flow initially of stagnating type (1b) can be permanently stabilized by very small external velocity gradients. Conversely, negative velocity gradients reduce the critical swirl value and cause premature vortex breakdown. Such a flow condition is encountered over a lifting surface or slender body particularly at high angles of attack.

The effects of external pressure gradients are also documented in recent studies in Reference 86 in which the method of numerical calculation in Reference 91 was modified to account for turbulence. The concept of eddy viscosity was introduced and a set of quasi-two-dimensional equations was solved numerically. Initial and boundary conditions for a slender wing at angle of attack are specified from experimental results. Formulation of the theoretical approach was aided by experiment, typical results being shown in Figure 49 which presents axial and circumferential velocity distributions before and after breakdown on a delta wing, revealing the significant change in axial velocity profile due to breakdown. Conclusions reached in this numerical study of vortex breakdown are that the majority of phenomena in the flow field created by a delta wing leading-edge vortex is dominated by potential flow effects, that is, the pressure gradient. The numerical procedure is equivalent to the calculation of the flow field when a vortex with a certain initial condition, as determined from experiment, is placed in a potential flow field with a specified pressure gradient. Results confirm that despite a very

108
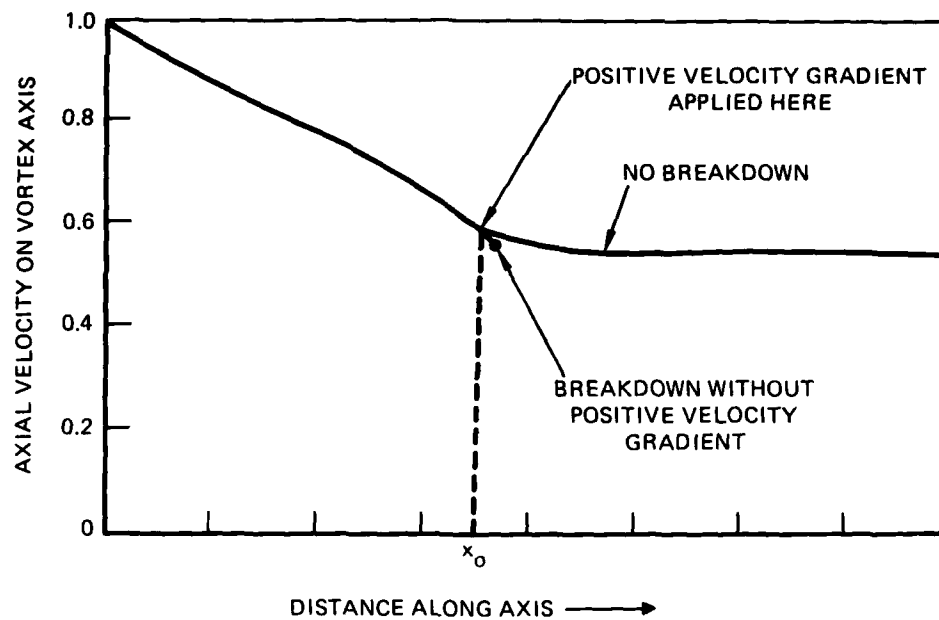
FIGURE 48. EFFECT OF SMALL POSITIVE VELOCITY GRADIENT ON AXIAL
VELOCITY ON THE VORTEX AXIS
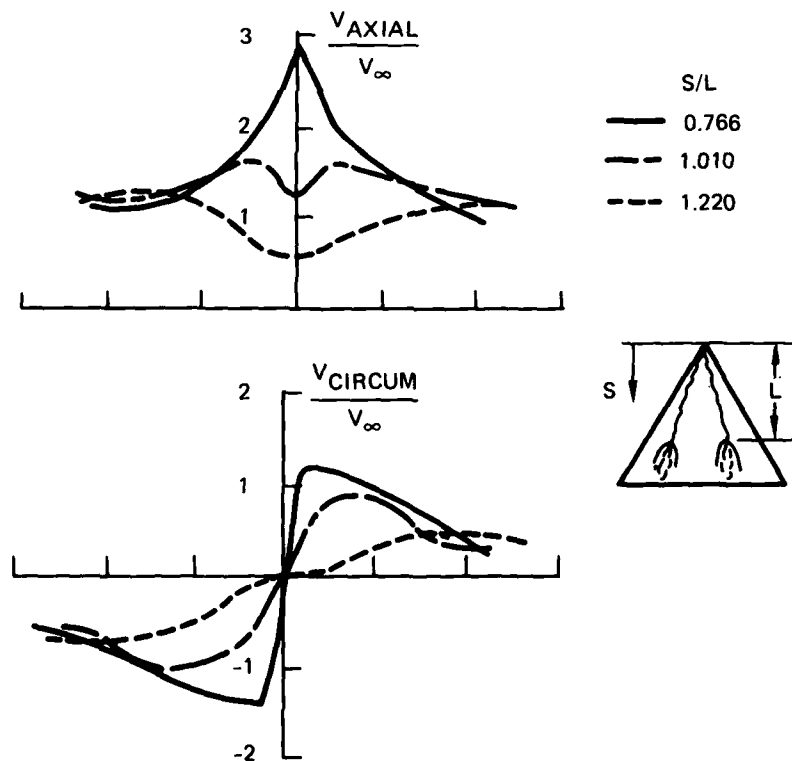
FIGURE 49. AXIAL AND CIRCUMFERENTIAL VELOCITY COMPONENTS BEFORE
AND AFTER BREAKDOWN (FROM REFERENCE 86)

109

small pressure increase outside the core, a sharp pressure gradient is created in the vortex central axis. The vortex growth, development, and breakdown are mostly subject to the pressure gradient associated with the external potential flow field. In contrast, for the case in which a vortex flow is embedded in an essentially irrotational flow where the pressure gradient in the outer flow vanishes (a wing tip vortex, for example), the vortex changes form only in response to viscous effects. At Reynolds numbers occurring in practice, hundreds of vortex-core diameters are required for significant structural changes due to viscosity (see References 91, 94, and 98).

Experimental Studies of Vortex Core Breakdown

Experimental results from Reference 29 provide confirmation of the large effect on vortex stability of adverse pressure gradients. Data were obtained using cylindrical tubes of varying degree of divergence, that is, varying pressure gradient, and typical results are shown in Figure 50.

Pressure measurements made on delta wings in Reference 26 provide insight into vortex behavior at high angles of attack. Under a laminar vortex there is, with increasing distance from the apex, a rising surface pressure. At a fixed position, the pressure gradient increases with incidence, as seen in Figure 51. As pointed out in Reference 52, on a lifting wing the external flow is marked by large pressure changes, especially at subsonic and transonic speeds where most of the lift is generated by suction forces, that is, pressures less than that of the free-stream. Downstream of the suction region, pressure must rise steeply so as to come back to some value near that of the mainstream at the trailing edge of the wing. A leading-edge vortex is subjected to this pressure recovery near the trailing edge which becomes more
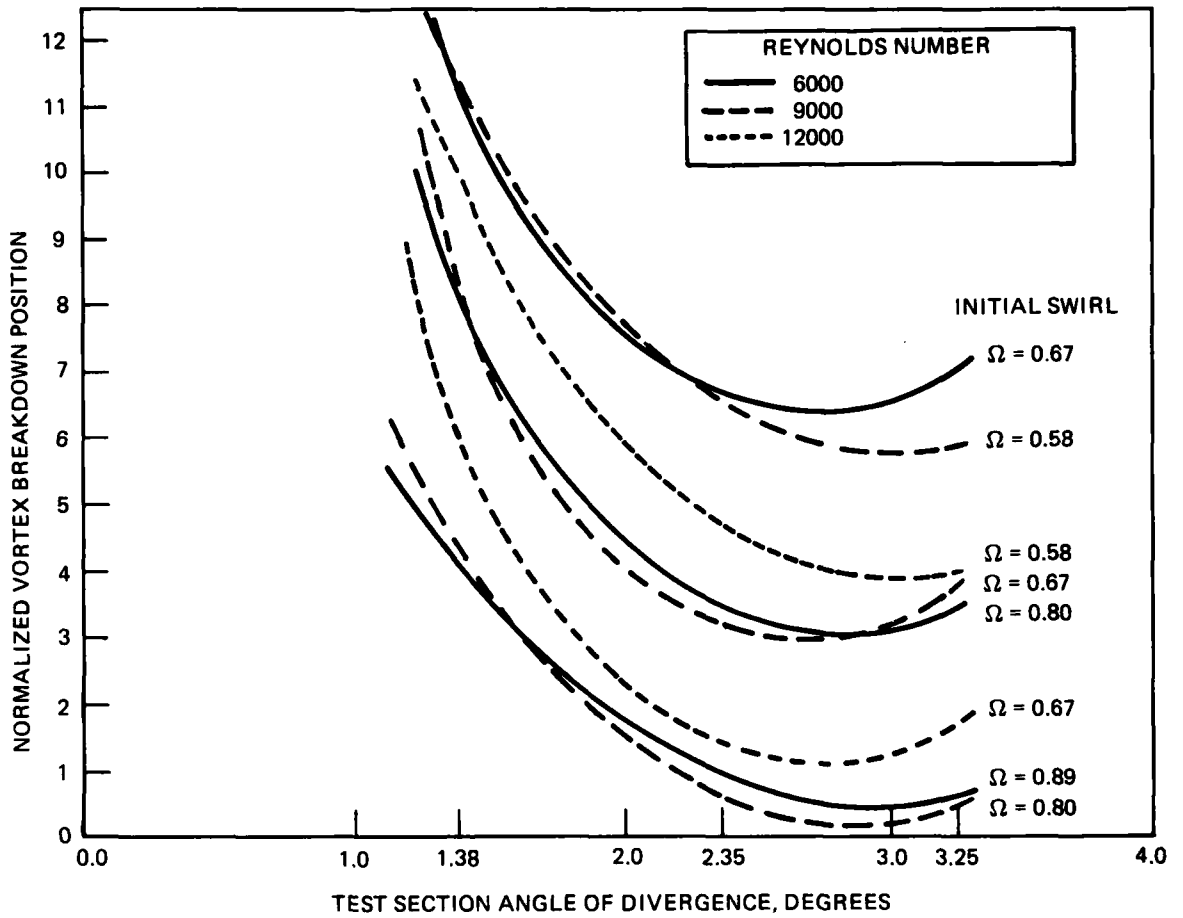
FIGURE 50. EFFECT OF TEST SECTION DIVERGENCE ANGLE ON NORMALIZED
BREAKDOWN POSITION (REFERENCE 29)

111
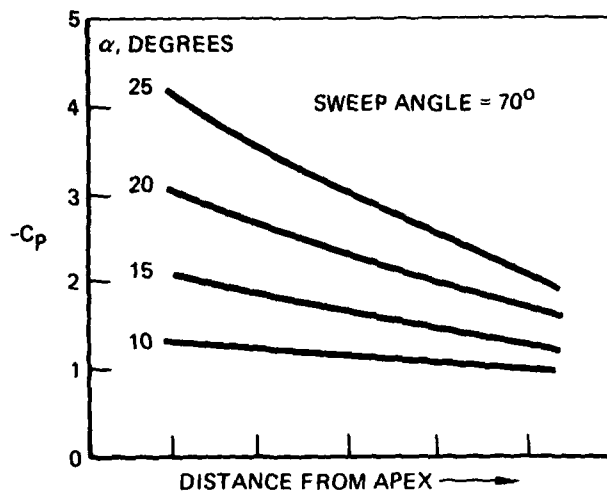
(a) 70-DEGREE DELTA WING SURFACE
PRESSURES UNDER VORTEX CORE
(FROM REFERENCE 26)
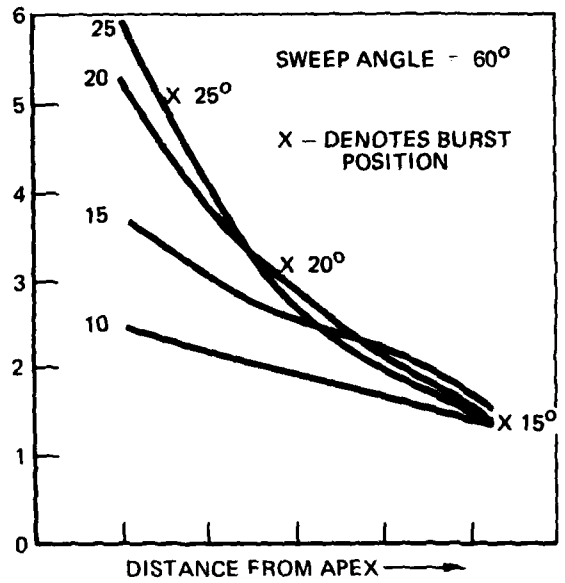
(b) 60-DEGREE DELTA WING SURFACE
PRESSURES UNDER VORTEX CORE
(FROM REFERENCE 26)
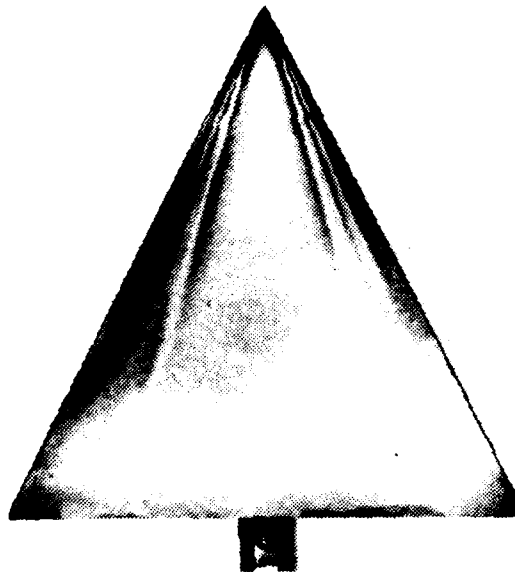
(c) 63.5-DEGREE DELTA WING — SURFACE
SUBLIMATION SHOWING EFFECT OF BURST
(FROM REFERENCE 195)

FIGURE 51. SURFACE PRESSURE DISTRIBUTION ALONG SUCTION RIDGE,
INCLUDING EFFECT OF BURST

112

pronounced as leading-edge sweep is decreased (see Figure 51). Eventually, this trailing-edge pressure recovery is sufficient to promote vortex breakdown, as illustrated in Figure 51 which shows surface sublimation on a delta wing. Note the sudden expansion of the vortex as implied by the flow patterns. Observations in Reference 26 reveal pressure gradients close to the observed position of the burst much steeper than that to be expected in the absence of burst. In addition, downstream of burst, the pressure tends to a value which is independent of incidence. Extensive measurements in the wake region of vortex breakdown (Reference 99) indicate that the qualitative features of breakdown appear to be independent of Reynolds number. Results from Reference 26 show that surface pressures, unlike surface flow patterns, begin to be affected even when the burst position is downstream of the measuring station.

The effect of imposing an adverse pressure gradient on vortex core stability is shown in Figure 52 in which water tunnel data are presented showing the effect of a downstream obstacle on the vortex burst characteristics of an 80-degree delta wing. A large effect on vortex stability is evident, which increases with decreased distance between the obstacle and wing trailing edge. An important point to note is that the downstream pressure gradient is imposed on a region forward of the wing trailing edge. This upstream effect of a downstream disturbance indicates that consideration must be given to potentially-large effects of the model support arrangement in a water tunnel or wind tunnel. For example, Reference 73 has shown in a wind tunnel large effects on vortex behavior of a downstream obstacle (see Figure 53); significant interference on powerful vortical motions has been experienced due to a wind tunnel "C-strut" arrangement (Reference 100); and Northrop water tunnel results reveal large differences in delta wing burst point aft of the trailing edge depending on whether a "straight" sting or "offset" sting arrangement are used (see
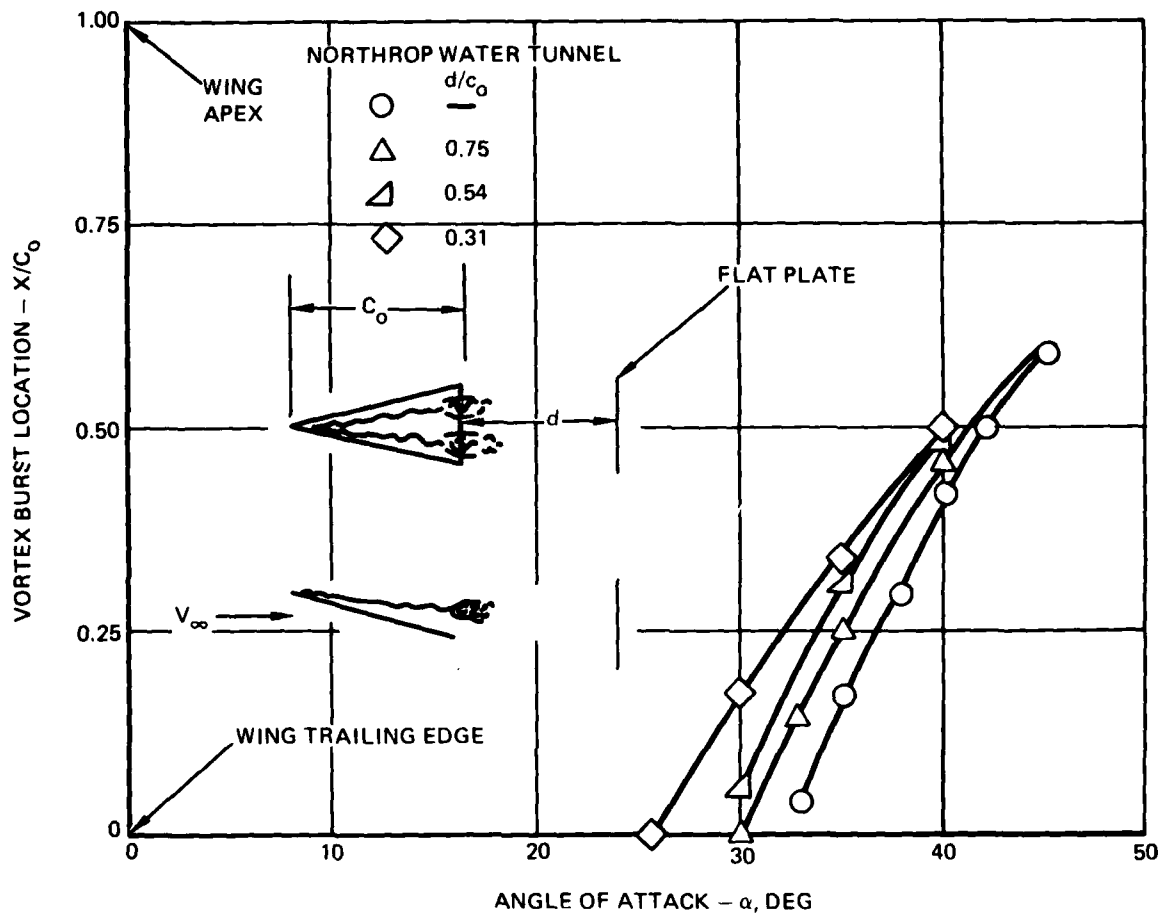
FIGURE 52. EFFECT OF DOWNSTREAM OBSTACLE ON VORTEX STABILITY FOR AN ASPECT RATIO 0.706 DELTA WING (NORTHROP WATER TUNNEL)
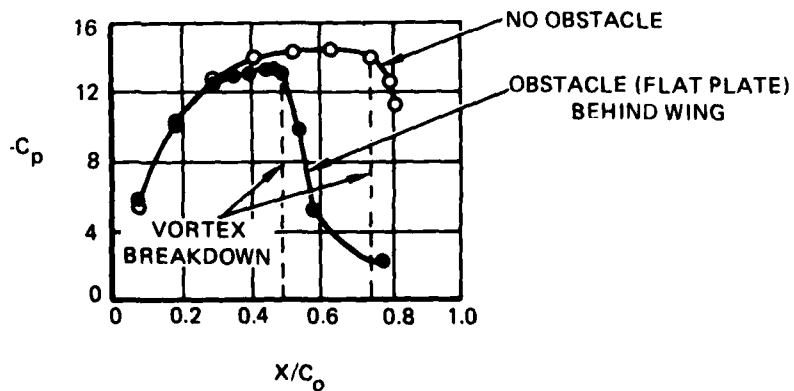
FIGURE 53. EFFECT OF DOWNSTREAM OBSTACLE ON SURFACE PRESSURE DISTRIBUTION ON AN ASPECT RATIO 1 WING AT 31 DEGREES ANGLE OF ATTACK (FROM REFERENCE 73)

Figure 54). Conversely, a favorable pressure gradient, as might be provided by a propulsive lift device, for example, or downstream suction (Reference 81), can prevent a flow from breaking down (See Figure 48).

Reference 26 discusses the balance of three factors which determine the pressure distribution along the vortex axis: (1) increasing vortex strength tending to provide falling axial pressure, (2) diffusion of vorticity within the viscous core tending to give a rising axial pressure and (3) flow deceleration (associated with the trailing edge) of the longitudinal component in the irrotational flow tending to cause a rising axial pressure. Ignoring (3),the balance between (1) and (2) would be expected to change even before the trailing edge is reached because both the rate of generation of vorticity and the rate at which this is added to the vortex are *falling*. Eventually, in the wake, diffusion of vorticity is the dominant factor resulting in rising axial pressure.

The significance of factor (3), pressure recovery in the irrotational flow, can be envisioned as follows. External flow retardation leads to an expansion of the rotational core quite apart from that caused by diffusion. Constancy of circulation requires a reduction of the rotational velocities within the core which augments the axial pressure rise. Due to the characteristically low total pressure near the core axis, the axial flow is easily stagnated. The mutual interactions between axial deceleration, vortex expansion, and pressure rise can lead to a critical condition corresponding to breakdown of the core structure. Thus, it can be seen that a gradual pressure increase in the outer regions of the flow surrounding a vortex core can induce a much steeper rise along a streamline near the axis. In general, if the trailing edge pressure recovery is insufficient to stagnate the axial flow, a burst would not occur in the vicinity of the wing but may occur

(a)STRAIGHT STING.

V,

VORTEX CORE

(b) OFFSET STING.

V,

VORTEX CORE

VORTEX BURST

V,

VORTEX CORE
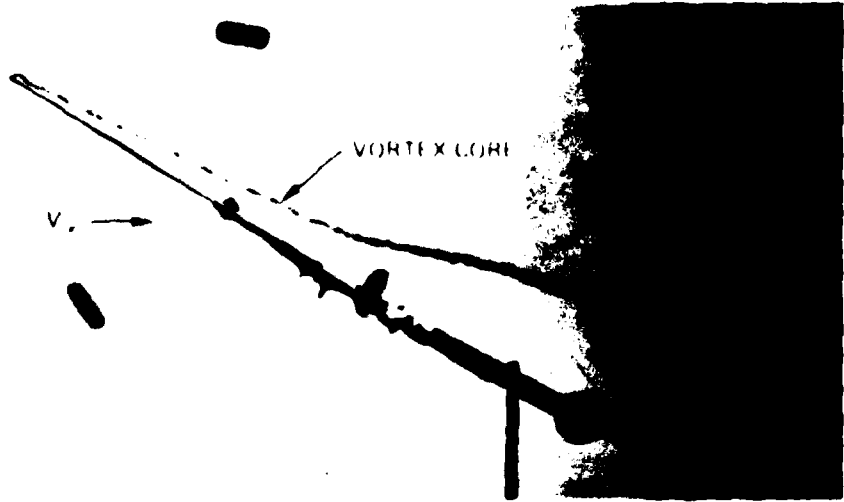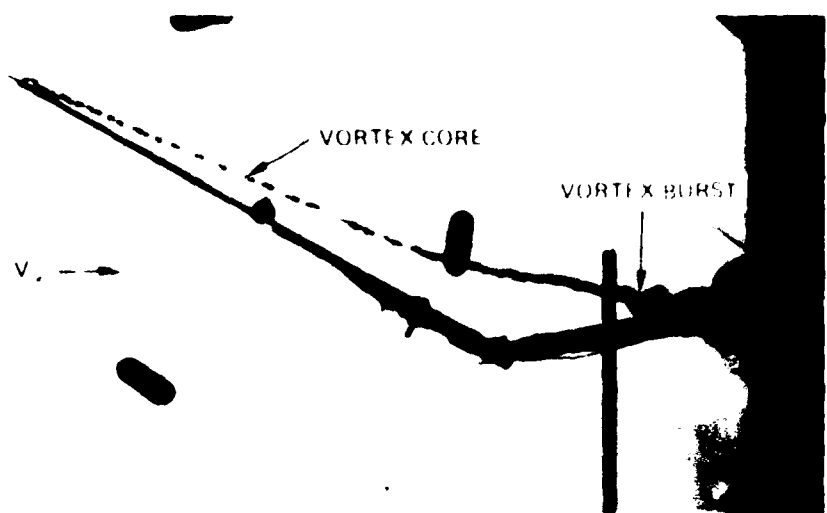
VORTEX BURST

(c)OFFSET STING
CLOSE-UP VIEW OF
CORE BURSTING
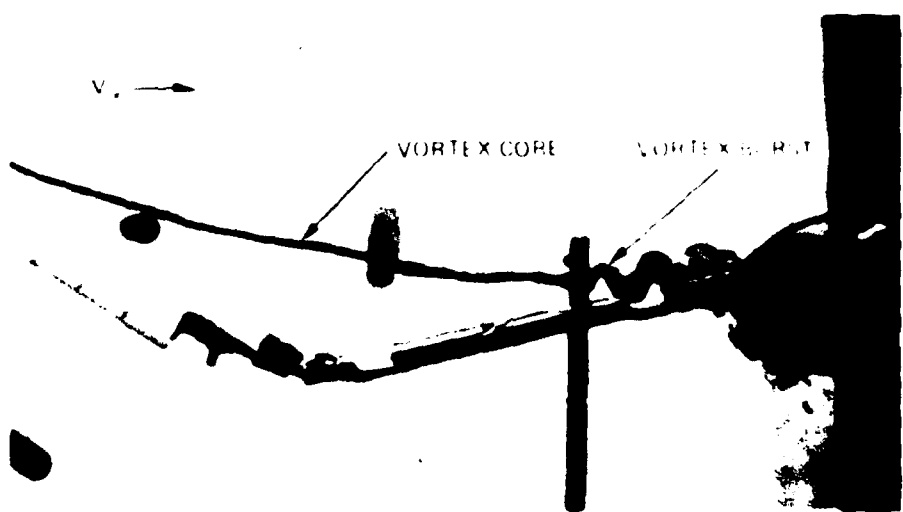
FIGURE 54 PROMOTION OF VORTEX BURST DUE TO MODEL SUPPORT ARRANGEMENT
(NORTHROP WATER TUNNEL)

during a subsequent axial pressure rise due to vorticity diffusion in the wake. This statement is corroborated by the flow visualization photograph in Figure 55 which depicts the high-swirl vortex shed from the tip of a forward-swept wing. Adverse external pressure gradients in this region are negligible and the vortex core exhibits a gradual increase in diameter with distance downstream, which can be attributed to core viscous effects.

The effect of compressibility on the external flow conditions is to reduce the adverse pressure field over a slender lifting surface such as a delta wing, enabling the vortex core to penetrate farther downstream. That is, increased Mach number requires increased angle of attack to establish streamwise pressure gradients strong enough to trigger bursting, as can be seen in the wind tunnel data on a low aspect ratio wing in Figure 56 (from Reference 80). However, the presence of a shock wave would promote vortex bursting. Although increased Mach number tends to delay core breakdown and, hence, delay wing stall, the compressibility effect on suction is to decrease the pre-stall normal force, as illustrated in Figure 57. This decrease of upper surface suction due to increased Mach number may be due to less vorticity available from the lower surface boundary layer for diffusion through the vortex to generate circulation (see Reference 80).

The strong effects of external axial pressure gradients on vortex flows have thus been well established in experiment and in numerical computations. A truly impressive correlation of water tunnel data with flight data is shown in Figure 58 which shows the occurrence of vortex breakdown on a current fighter aircraft at high angle of attack. At a similar angle of attack, the water tunnel model exhibits vortex bursting over the wing panel at a location quite comparable to the full-scale aircraft. Under these flow conditions, the large disparity in

117

FIGURE 55. VORTEX CORE BEHAVIOR IN THE ABSENCE OF AN EXTERNAL PRESSURE
GRADIENT (NORTHROP WATER TUNNEL)
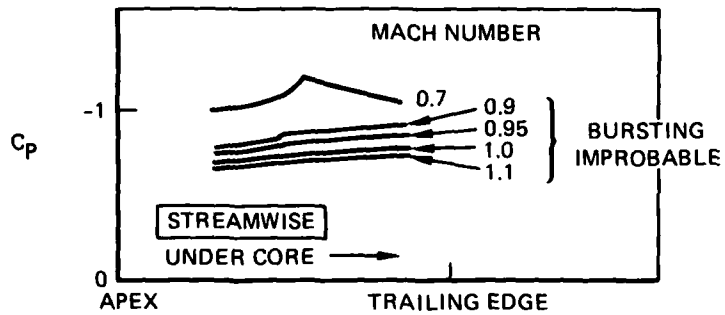
FIGURE 56. MACH NUMBER EFFECT ON SURFACE PRESSURE UNDER VORTEX
CORE: ASPECT RATIO ≈ 0.5; 30 DEGREES ANGLE OF ATTACK
(FROM REFERENCE 80)
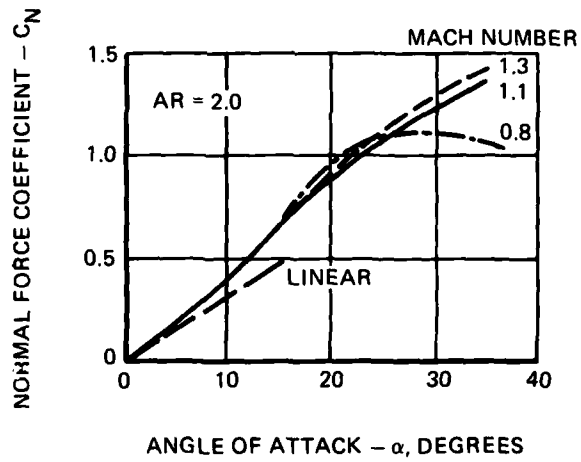
FIGURE 57. MACH NUMBER EFFECT ON NORMAL FORCE; ASPECT RATIO 2
DELTA WING (FROM REFERENCE 80)

119
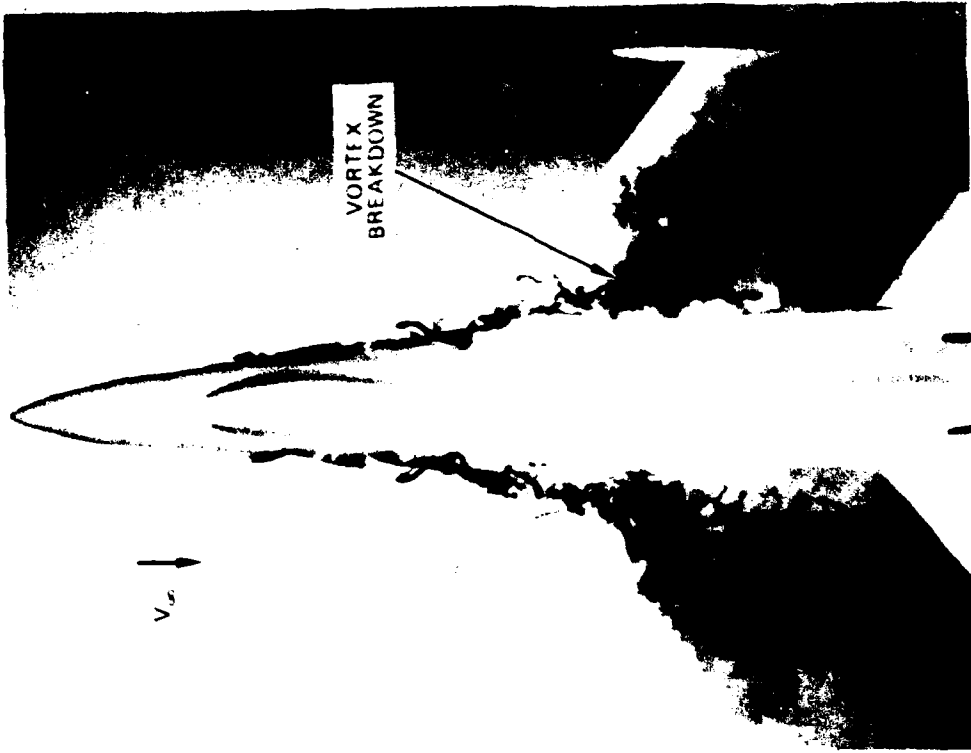
VORTEX
BREAKDOWN

(b) NORTHROP WATER TUNNEL

V∞
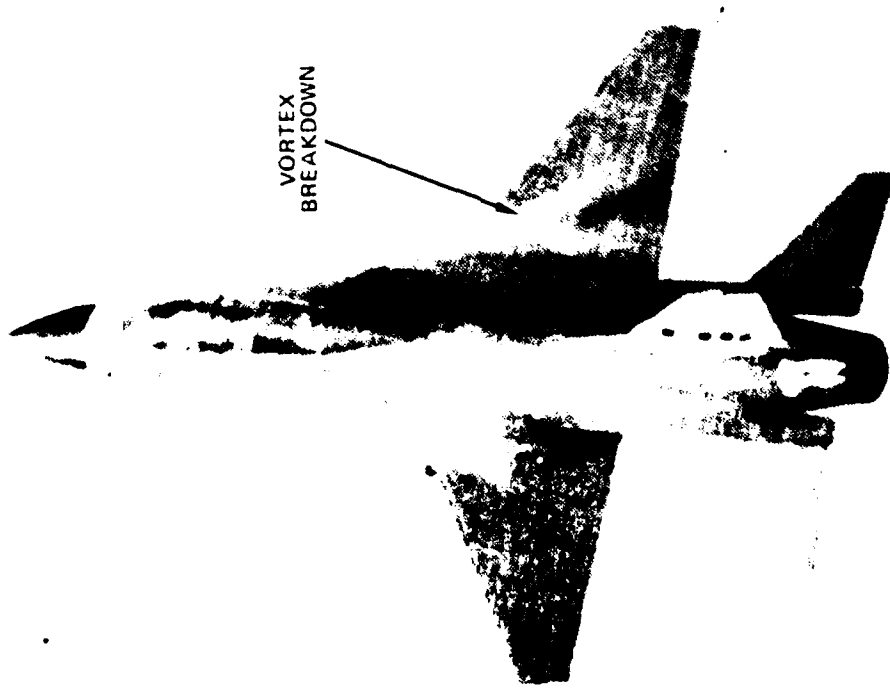
VORTEX
BREAKDOWN

(a) FLIGHT (PHOTOGRAPH COURTESY OF AVIATION WEEK &
SPACE TECHNOLOGY)

FIGURE 58. CORRELATION OF VORTEX BREAKDOWN ON A CURRENT FIGHTER AIRCRAFT
IN A WATER TUNNEL AND IN FLIGHT AT APPROXIMATELY 26 DEGREES ANGLE OF ATTACK

vortex core Reynolds number between water tunnel and flight appears irrelevant due to the dominance of the adverse pressure gradient in the external potential flow field at high angles of attack. Therefore, provided flow separation occurs from a sharp leading edge, the water tunnel is expected to provide a realistic representation of the wake shed from a wing and, consequently, the pressure field through which a vortex core must traverse. Although there is as yet no theoretical verification that this parameter is the dominant one, it is upon this premise, which is supported by the wealth of theoretical and experimental studies just cited, that correlations can be made between low-Reynolds number vortex stability (that is, breakdown) characteristics in water with high Reynolds number vortical motions in air. In addition, in the event of massive flow separation, the phenomenological aspects of vortical motions at high Reynolds numbers in air can, in many cases, be assessed in a low Reynolds number hydrodynamic test facility.

Since slender wings and bodies are topologically equivalent objects (Reference 54), it is reasonable to expect that much of the discussions pertaining to slender wing vortex behavior should find a counterpart in the behavior of the flow over slender bodies. The following paragraphs present reviews of representative theoretical and experimental studies pertaining to body vortices, followed by a discussion of slender body vortex flow simulation in a water tunnel facility. Emphasis is placed on asymmetric vortex shedding at high angles of attack.

4.4 SLENDER BODY VORTICAL FLOWS - THEORY AND EXPERIMENT

The cross-flow or impulsive flow analogy described in Reference 101 has been utilized extensively to explain the development of a three-dimensional vortex wake shed by slender bodies at moderate-to-high angles of attack. According to the analogy, the progressive development of the wake along the body when viewed in cross-flow planes is similar to the growth

121

with time of the flow past a two-dimensional cylinder started impulsively from rest. Close to the body nose no wake exists, whereas farther downstream two symmetrically disposed vortices form on the leeside. These vortices are fed by vortex sheets containing boundary layer fluid which has separated from the body (see Figure 59). Farther aft along the body, first one and then the other of these vortices detach and move downstream at an angle to the free-stream. Other vortices form on the leeside of the body at increasing distance and behave in a similar manner as illustrated in Figure 60. This flow phenomenon continues along the body length and a flow cross-section far from the nose resembles a vortex street. The flow pattern just described is essentially a space-time plot of the flow past a two-dimensional cylinder started impulsively from rest.

As described in Reference 102 for an asymmetrical flow pattern in incompressible flow at high angles of attack, the angle between the body centerline and the vortex core trajectories can be used to determine vortex strength, whereas the spacing of the vortex paths is a measure of the Strouhal number of the wake from a circular cylinder with identical cross-flow conditions. A theoretical approach based on analogy with a Karman vortex street has certain restrictions on its applicability, however, since an infinite vortex street is required and all vortices must have the same strength. The actual flow situation on a body at incidence, however, is markedly different since the strength of each vortex is determined from the circulation generated in the boundary layer fluid which was initially located along a well-defined section at the body surface. Only when the downstream influence of the nose on the body pressure distribution is negligible will the boundary layer behavior be the same on each body section and the vortex strengths be identical. Vortices generated from the boundary layer upstream of this region will

122
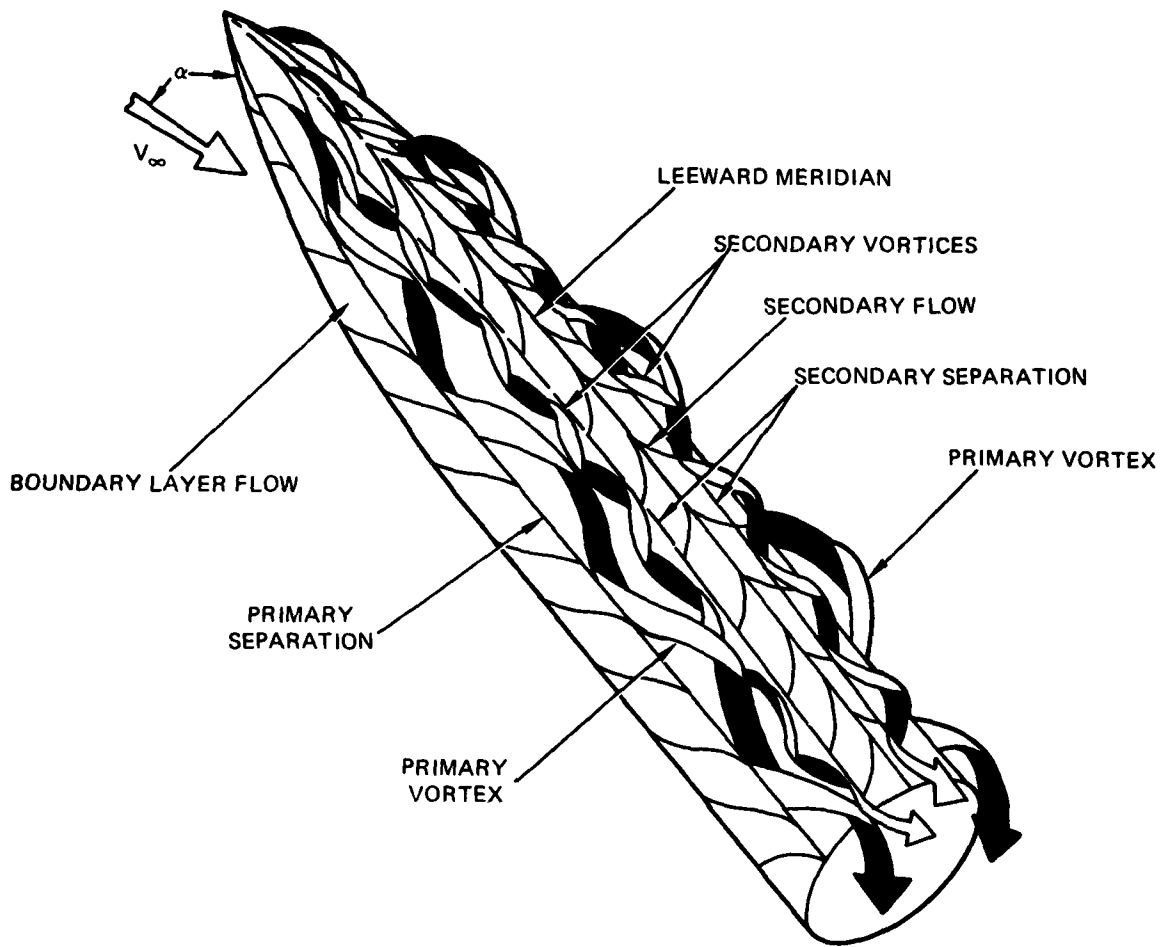
FIGURE 59. VORTEX SHEDDING ON A SLENDER BODY (SCHEMATIC FROM REF 105)
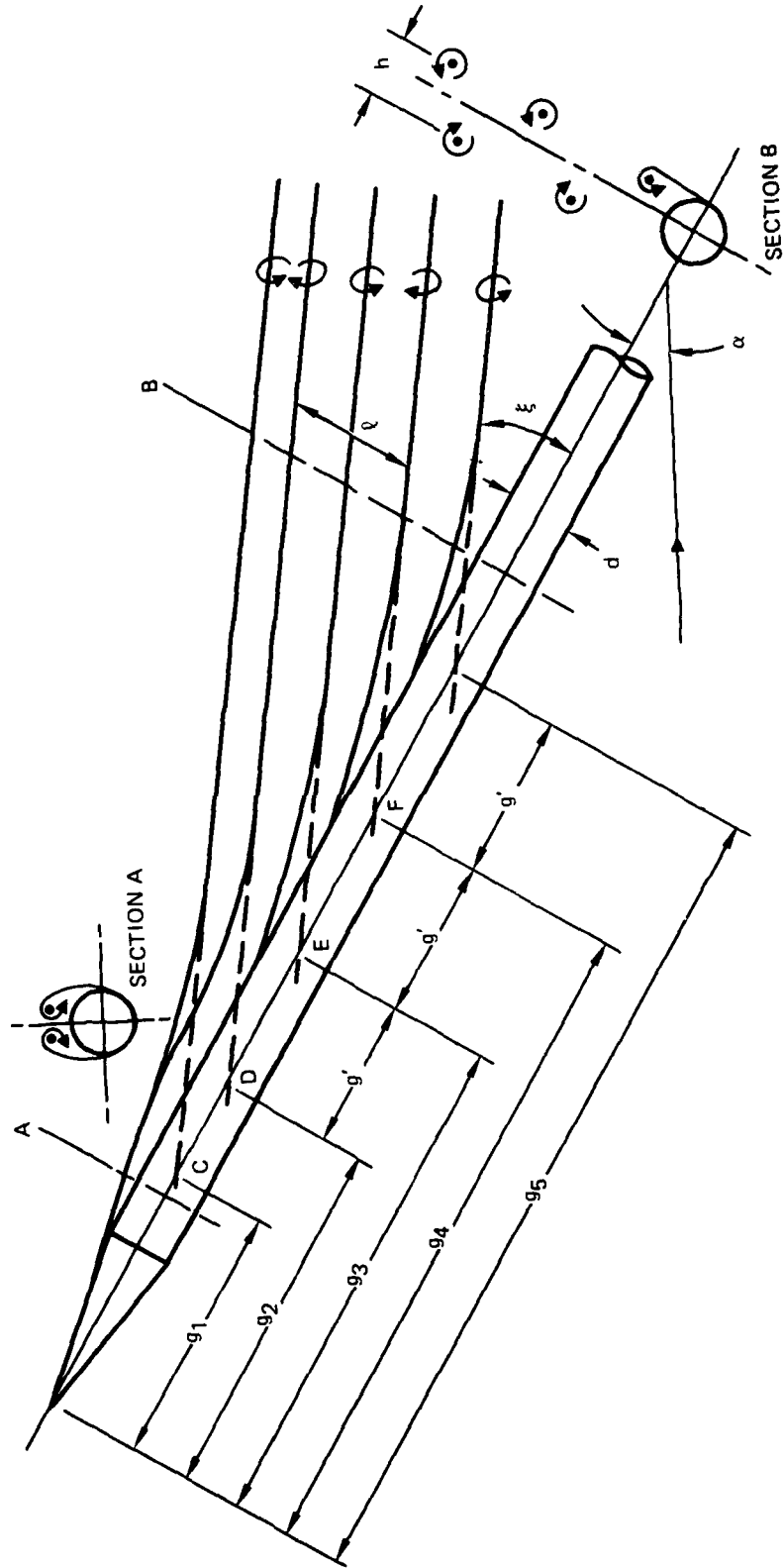
FIGURE 60. SCHEMATIC OF VORTEX WAKE FROM SLENDER BODY AT INCIDENCE (FROM REFERENCE 102)

124

have strengths differing from those generated downstream. The first two vortices contain boundary layer fluid from the nose and cannot be considered as part of the Karman vortex street. Hence, in this theoretical approach, only the third and ensuing vortices are considered.

An analytic method was developed in Reference 103 using the unsteady cross-flow analogy where the asymmetric wake in the cross-flow plane is described by a large number of point vortices. For high Reynolds number flow, Stratford's turbulent separation criterion is used to specify the location at which point vortices are fed from the boundary layer into the wake. A solution to the problem is obtained by assuming that for high Reynolds numbers the flow may be divided into two regions: (1) a viscous inner flow near the cylinder and (2) an essentially inviscid outer flow elsewhere. The outer flow consists of the classical potential flow about a circular cylinder superimposed with the potential flow of a number of ideal point vortices which describe the wake. The inner flow consists of a boundary layer and a rear shear layer and is the source of vorticity in the outer flow. In this solution scheme, the small perturbation leading to the development of an asymmetric wake is modeled by reducing by 10 percent the vorticity flux out of the boundary layer along one side of the missile nose.

This so-called "vortex cloud" approach was adopted in Reference 104 in which potential flow methods and slender body theory were used to model the steady three-dimensional flow as an unsteady two-dimensional problem. An asymmetric vortex shedding model for non-circular cross-sections was also developed. A modified, semi-empirical Stratford criteria based on surface pressure and run length is used to calculate the location of the primary separation points. For bodies with a vertical plane of symmetry, some form of asymmetric disturbance is necessary to perturb the symmetric solution. Typically, the disturbance takes the form of rotating the computed separation points through a small angle of the order of

125

0.5 degrees over the first 5 to 10 percent of the nose length. Thereafter, the separation point locations calculated from the modified Stratford criteria are used. Computed results reveal the flow to be very sensitive to small disturbances in the separation points. No initial disturbance is required on non-circular bodies in sideslip.

As discussed in Reference 105, the majority of theoretical approaches to predict vortex-induced asymmetric loads have until now been based upon inviscid flow modeling of the vortices generated for subcritical (laminar) conditions on the cylindrical aftbody. A severe problem exists, however, due to neglecting the dominating influence of the slender pointed apex as shown in Figures 61 and 62. Since the theoretical assumptions do not apply to practical geometries having pointed, slender noses, the angles of attack for onset of vortex asymmetry as *predicted by* theory (based on the impulsive-flow analogy) are typically half the angles obtained in experiment.

The theoretical approach in Reference 105, which describes a method of predicting maximum vortex-induced sideloads, is based on the premise that the largest aerodynamic loads occur in the critical Reynolds number regime where subcritical (laminar) and supercritical (turbulent) separations can co-exist. Consideration is made of the nose region which, as indicated by experiment, generates the largest side load and also controls the asymmetric vortex geometry that can exist on the aftbody.

While the effects of boundary layer transition along the forebody surface may well modulate the development of the leeside flow, Reference 106 does not consider it to be the primary driver of flow asymmetry. Reference 106 suggests that initial development of asymmetry in the vortex flow may be related to the stability of the velocity profiles in the

126
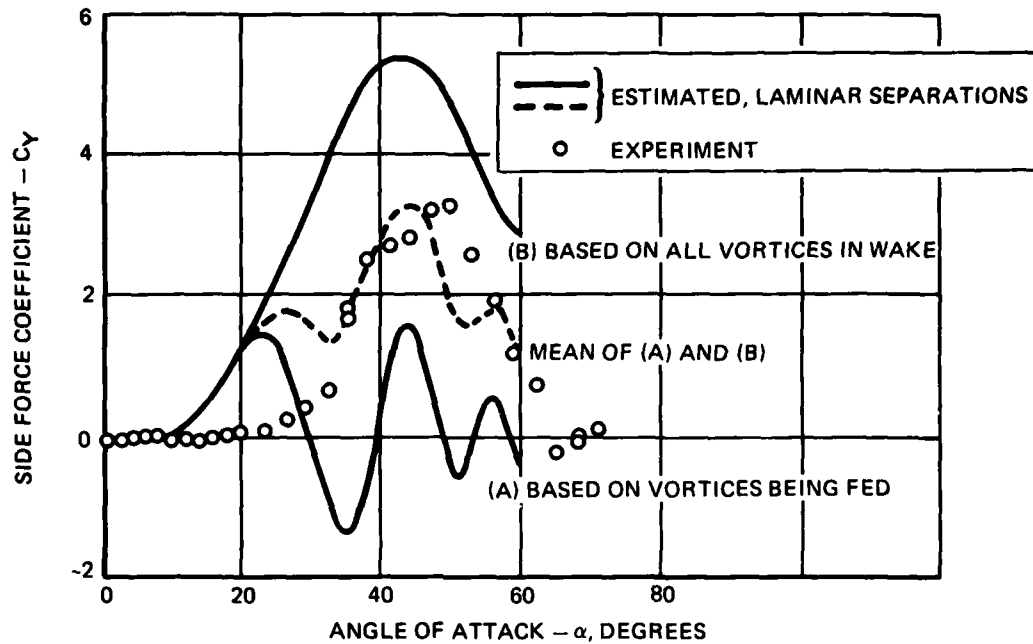
FIGURE 61. COMPARISON BETWEEN PREDICTED AND EXPERIMENTAL
VORTEX-INDUCED SIDE LOADS ON A 10 CALIBERS LONG 15-DEGREE
CONE-CYLINDER AT M = 0.5 AND Re_d = 0.09 x 10^6
(FROM REFERENCE 105)
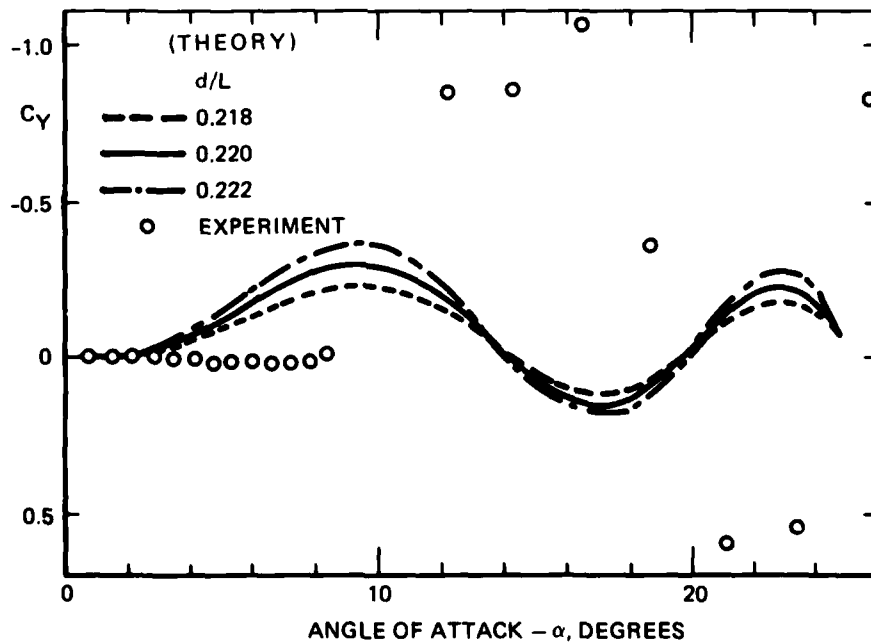
FIGURE 62. COMPARISON BETWEEN PREDICTED AND EXPERIMENTAL SIDE FORCE
ON A 17 CALIBERS LONG 3.7-DEGREE CONE-CYLINDER AT M = 0.5 AND
Re_d = 1.4 x 10^6 (FROM REFERENCE 105)

127

vicinity of an enclosing saddle singular point that exists in the cross-flow above the body vortices and the subsequent amplification of asymmetric disturbances in this region. The structure and fluid mechanisms of the leeward separated flow fields are conceptualized using topological ideas. Flow structures consistent with physical fact are constructed by invoking the rules of topology coupled with ideas from the impulsive-flow analogy.

At present, however, no pure theoretical means (as opposed to semi-empirical) for predicting onset of vortex asymmetry is available. As discussed in Reference 107, the theoretical state of the art for calculating steady asymmetric vortex patterns around bodies of revolution, let alone non-circular bodies, at low speeds is semi-empirical.

Experimental studies indicate that, starting at low angles of attack, flow on the leeward side of a slender body separates, vorticity sheets are formed by boundary layer fluid leaving the body surface, and regions of concentrated vorticity are formed. As shown in the water tunnel photographs from Reference 108 in Figure 63, these regions of concentrated vorticity are symmetric at moderate angles of attack, but as angle of attack is increased an asymmetric vortex pattern is formed. At some point, the vortex sheet breaks away from the body forming a free vortex and a new vortex starts forming immediately. There is an important connection between boundary layer vorticity at separation and free vortex strength since the vorticity fluxes contained in the primary separating boundary layers supply most, but not quite all, of the vorticity in the various free vortices (some vorticity enters the vortices from the boundary layers on the rear of the body). A series of free vortices of alternate sign are generated along the body and large side forces and yawing moments are the result of the asymmetric vortex flow field. Furthermore, a bistable vortex switching phenomenon can occur in addition to vortex core breakdown at high angles of attack.

128

(a) SYMMETRIC VORTICES

FIGURE 63. WATER TUNNEL FLOW VISUALIZATION OF BODY VORTEX SHEDDING AT
VERY LOW REYNOLDS NUMBER. $Re_d \approx 400$ (FROM REFERENCE 108)
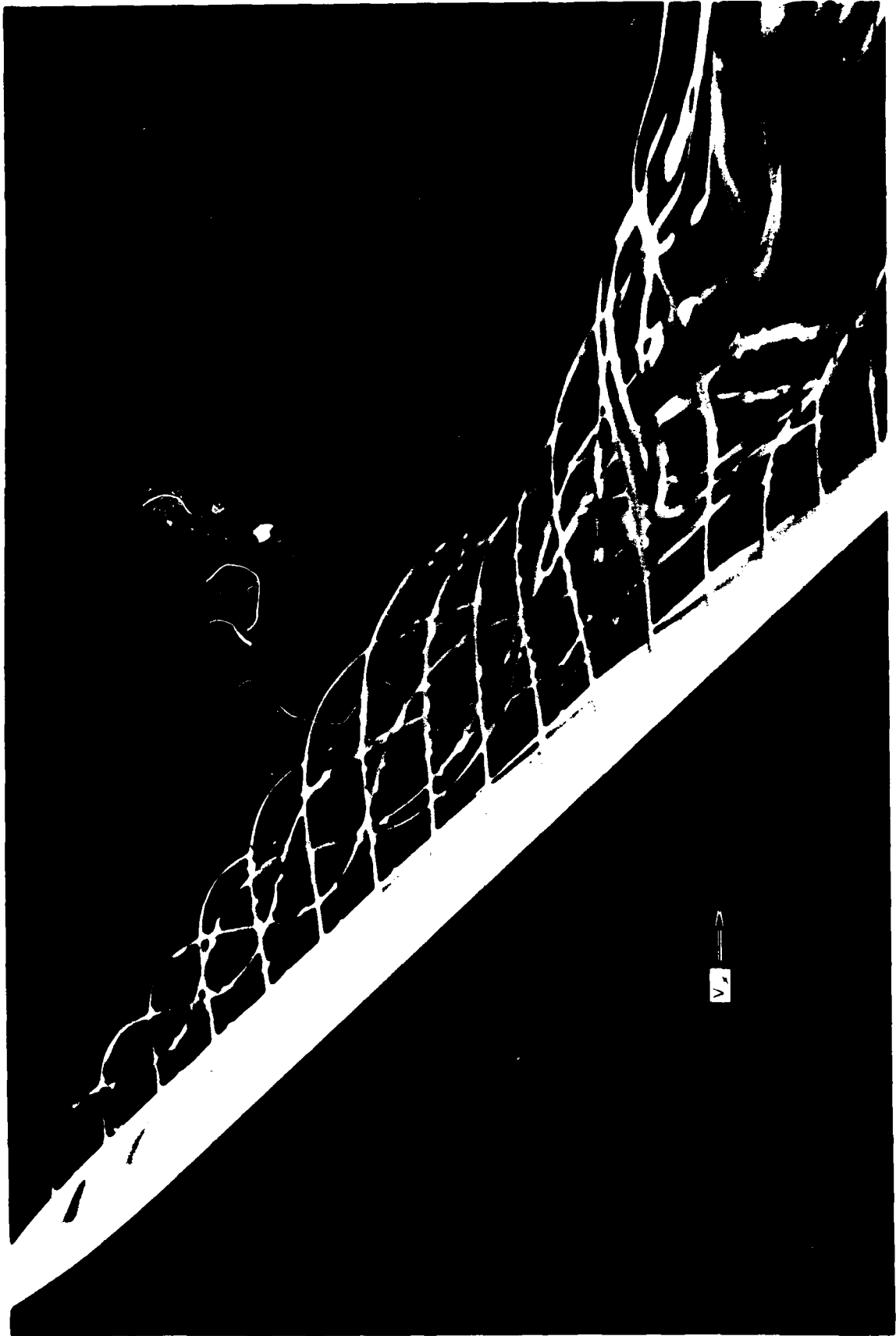
(b) ASYMMETRIC VORTICES

FIGURE 63. CONCLUDED

Reynolds number has a dominating influence on the side force induced by asymmetric vortices (see Figure 64, from Reference 109). The nose-induced asymmetric loads are of great magnitude, often exceeding the normal force. Experimental results from various sources indicate that the asymmetric vortices on the aft body have only limited influence on the flow over the nose. However, the dominance of the nose vortex pattern is evident in that the asymmetric aft body vortices must align themselves in accordance with the pattern set up by the nose vortices.

The flow process leading to vortex asymmetry may be somewhat different in the case of a pointed, slender nose from that on a cylindrical aft body (Reference 105). It has been pointed out (Reference 110) that there is a similarity of vortex asymmetry on slender bodies and delta wings since, in each case, a basic inviscid hydrodynamic instability resulting from a crowding together of the vortices near the apex appears to be a significant factor. It has been proposed by some researchers (Reference 110) that asymmetry in the separation points on a body of revolution would not necessarily be an essential feature of vortex asymmetry. This is analogous to conditions for corresponding vortex asymmetry in two-dimensional flow where separation point movement is not a prerequisite for the establishment of the von Karman vortex street.

It can be seen, then, that asymmetric vortex shedding occurs even when the separation point is fixed by the geometry. However, the generated forces are highly-dependent upon the separation point degree of freedom. When the geometry fixes separation symmetrically, it is expected that the generated asymmetric forces will be much less than the case where separation point location is free to move. It thus appears that both "vortex crowding" and separation point degree of freedom are important features in vortex-induced asymmetric loads.

131
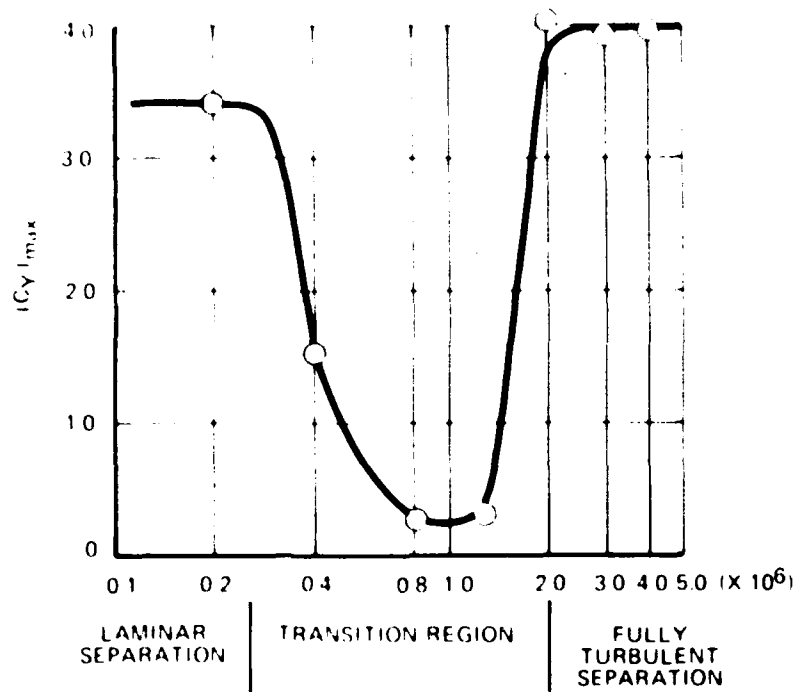
FIGURE 64. VARIATION OF MAXIMUM SIDE FORCE WITH
REYNOLDS NUMBER FOR l/d = 6 OGIVE CYLINDER AT
σ = 55 DEGREES (REFERENCE 109)
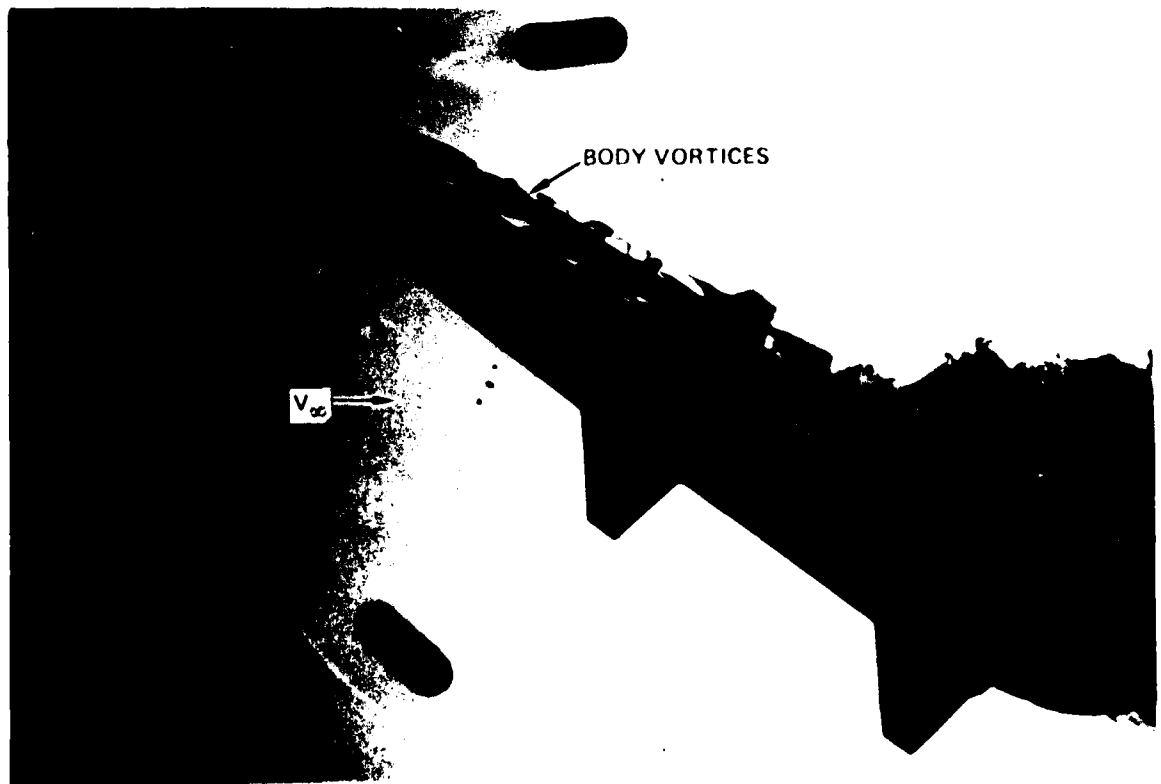
(a) CRUCIFORM MISSILE CONFIGURATION

FIGURE 65. SLENDER BODY VORTICAL FLOW
(NORTHROP WATER TUNNEL)

BODY VORTICES

(b) FIGHTER CONFIGURATION

FIGURE 65. CONCLUDED

133

4.5   SLENDER BODY VORTEX FLOW SIMULATION

As in the case of leading-edge vortices, the flow
phenomena which must be simulated in the water tunnel in order
to ensure correlation of forebody vortices at high angles of
attack are: (1) vortex generation, (2) vortex sheet and core
location or trajectory, and (3) vortex core breakdown.

4.5.1   Vortex Generation

Regarding the first factor, vortex generation, if the
pressure gradients on a slender body at angle of attack are
sufficiently adverse and sustained, the three-dimensional
boundary layer will converge, thicken, and eventually separate
along a line on the surface oblique to the local stream direc-
tion.   The three-dimensional separated shear layers roll up
into vortical motions (see Figure 65).   Separation point
location is a function of the Reynolds number and, conse-
quently, at Reynolds numbers typical of the water tunnel
(10^3 to 10^4), characteristically well below the transition
Reynolds number, generation of nose and aft body vortices   is
expected to occur at lower angles of attack relative to tests
conducted at wind tunnel and flight Reynolds numbers (10^5 to
10^6 and 10^7 to 10^8, respectively).   This is, indeed, the case
as was shown in water tunnel studies in Reference 44 which
indicated that increased Reynolds number tends to delay
vortex formation, as shown in Figure 66.   This flow situation
appears analogous to the flow about a slender wing having a
blunt leading edge, where at low Reynolds numbers the flow
separates and rolls up into a spiral vortex sheet, whereas at
higher Reynolds numbers flow separation is delayed and, once a
vortex is shed, it is generated farther aft.   It has been
pointed out, however, in Reference 111, that near the apex of a
slender nose the cross-flow Reynolds number is low due to small
body diameter and separation may be laminar even though Rey-
nolds number based on maximum body diameter indicates turbulent

134
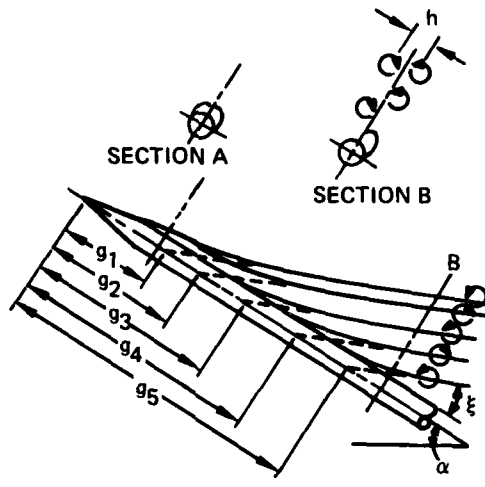
(A) SKETCH OF THE VORTEX WAKE OVER A SLENDER BODY
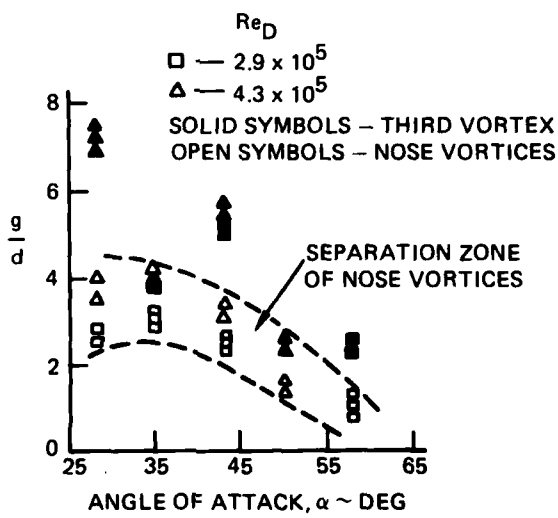
(B) STARTING POSITIONS OF THE BODY VORTICES

**FIGURE 66. EFFECT OF REYNOLDS NUMBER ON BODY VORTEX SHEDDING
(FROM REFERENCE 44)**

separation. Such a phenomenon has been observed in Northrop wind tunnel oil flow studies of the F-5F as shown in Figure 67. Reynolds number based on maximum body width corresponds to near-critical conditions, yet the surface oil flow patterns reveal subcritical (laminar)separation over the forward region of the body followed by transition to turbulence farther aft (as evidenced by the "kink" or discontinuity in the primary separation line). Also, as pointed out in Reference 105, the favorable pressure gradient over the nose may inhibit transi- tion to some extent. Simulation of body vortices is far from straightforward, however, and at this point it must be conjec- tured that in the critical area of the nose, vortex generation may be reasonably represented in the water tunnel due to laminar separation near the nose region in all cases. Subse- quent examples of water tunnel results will support this contention.

In laminar, incompressible flow about simple bodies at angle of attack, where the effects of axial pressure gradients are negligible in comparison with the circumferential gra- dients, calculated three-dimensional separation lines (Refer- ence 112) agree quite well with water tunnel studies on right-circular and elliptic cones in Reference 113. In turbu- lent but still low-speed boundary layers, prediction of separation lines is at present prohibitively complex. It is interesting to note, however, the laminar flow of a slender ellipsoid at high angle of attack investigated at ONERA in Reference 114 bears close similarity to high Reynolds number turbulent flow results in Reference 115.

4.5.2 Vortex Sheet and Core Location

The sheets of vorticity which spring from the separation lines along the sides of the body roll up into two vortex cores of concentrated vorticity, as shown in Figure 68. The flow

136
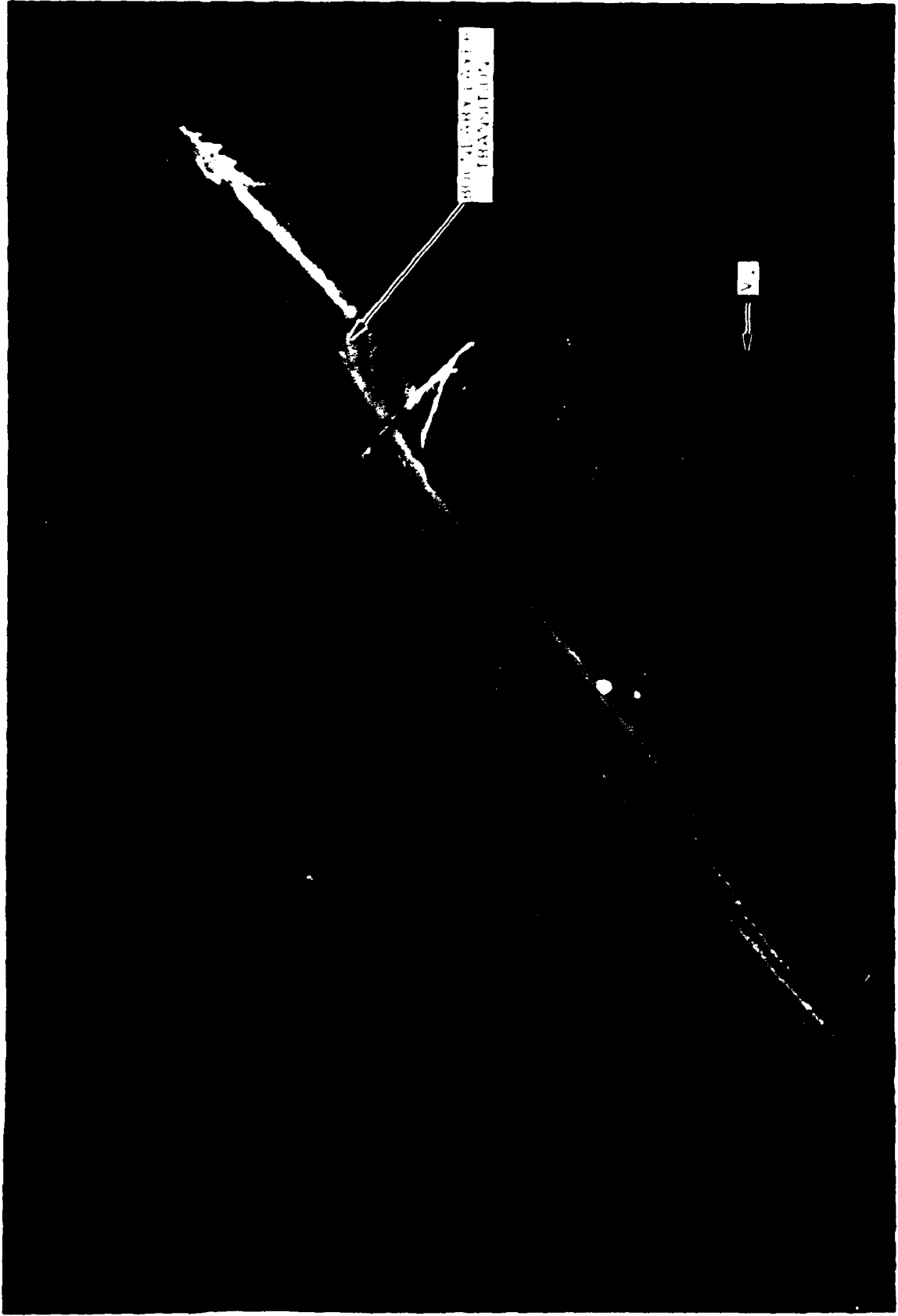
FIGURE 67 WIND TUNNEL SURFACE OIL FLOW PATTERNS ON A SLENDER FOREBODY
(NORTHROP WIND TUNNEL)

PRIMARY
APEX VORTEX
PAIR
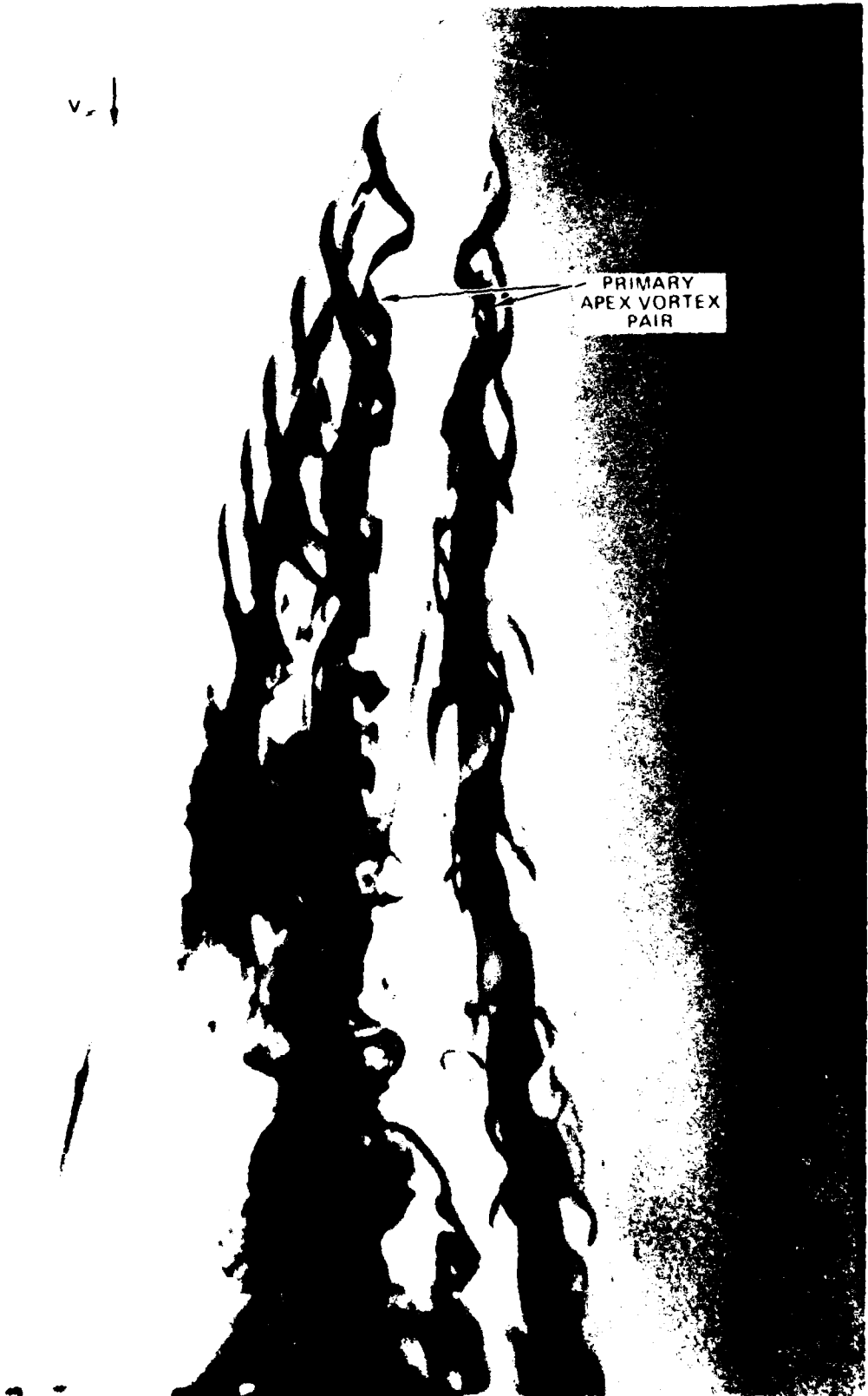
FIGURE 68. CONCENTRATED VORTEX CORES ON
A SLENDER BODY (NORTHROP WATER TUNNEL)

can, in general, be divided into three regions: (1) the inviscid flow outside the surface boundary layer, vortex sheet (free shear layer) and vortex core, (2) the boundary layer flow near the body, and (3) the vorticity flow inside the vortex sheet and vortex core. Each regime has its own specific characteristics.

Inviscid Flow Regime

Regarding flow regime (1), unlike the slender wing with sharp leading edge, it is not possible to utilize solely the potential flow equation subject to the boundary conditions that the normal velocity at the outer edge of the surface boundary layer is zero and the normal velocity and pressure differential across the vortex sheet are zero. Since the vortex sheets originate from separation lines on the body sides which are not known a priori, the strength and location of the vortex sheets and vortex cores vary with the Reynolds number. The effects of Reynolds number on normal force and local side force coefficient are presented in Figures 69 and 70. Caution must be exercised, then, when body vortices are studied at subcritical conditions in a water tunnel.

Comparison of the primary apex vortex core trajectories obtained in water tunnel and wind tunnel facilities, taken from Reference 116, are shown in Figures 71 and 72. It can be seen that the vertical positions are in fair agreement whereas the lateral positions are not, the water tunnel results indicating a much wider lateral separation between the cores. Similar effects are seen in Figure 73 from Reference 54. The sketches in Figure 74 provide an explanation for the trends shown in Figures 71 to 73. At low Reynolds number, the laminar boundary layer separates in the presence of an increasing pressure field whereas at higher Reynolds numbers at which transition to turbulence occurs, turbulent boundary layer separation is delayed. As a result, the low Reynolds number

139
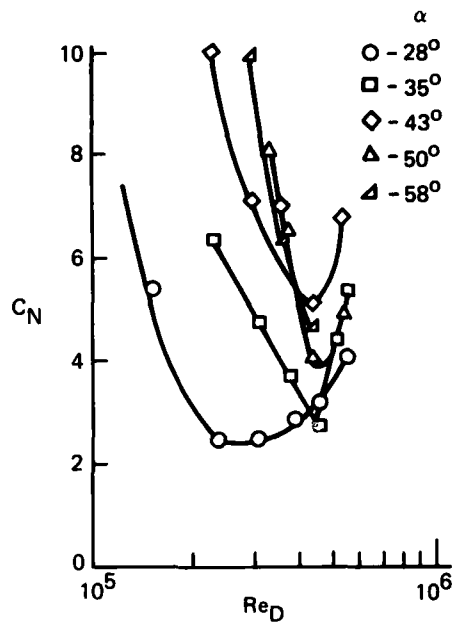
FIGURE 69. REYNOLDS NUMBER EFFECT ON NORMAL FORCE (FROM REFERENCE 44)
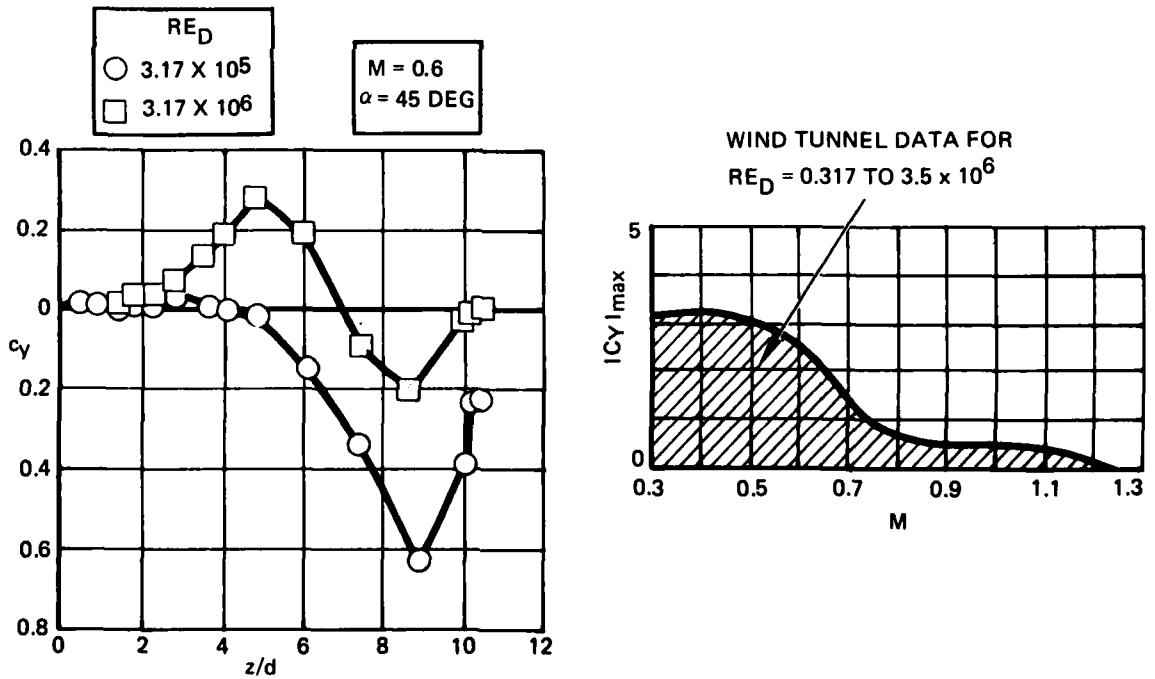
A) SIDE FORCE DISTRIBUTION ON AN OGIVE CYLINDER

FIGURE 70. REYNOLDS NUMBER EFFECT ON SIDE FORCE DISTRIBUTION AND DIRECTIONAL STABILITY PARAMETER (FROM REF 105)
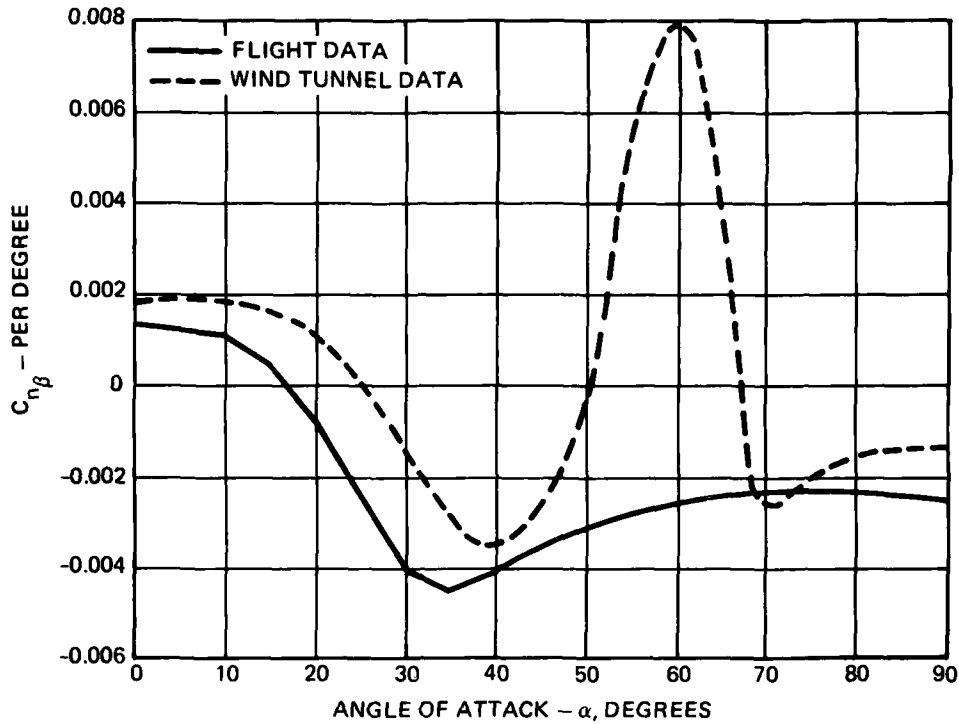
(B) DIRECTIONAL STABILITY OF A SLENDER-NOSED FIGHTER

FIGURE 70. CONCLUDED
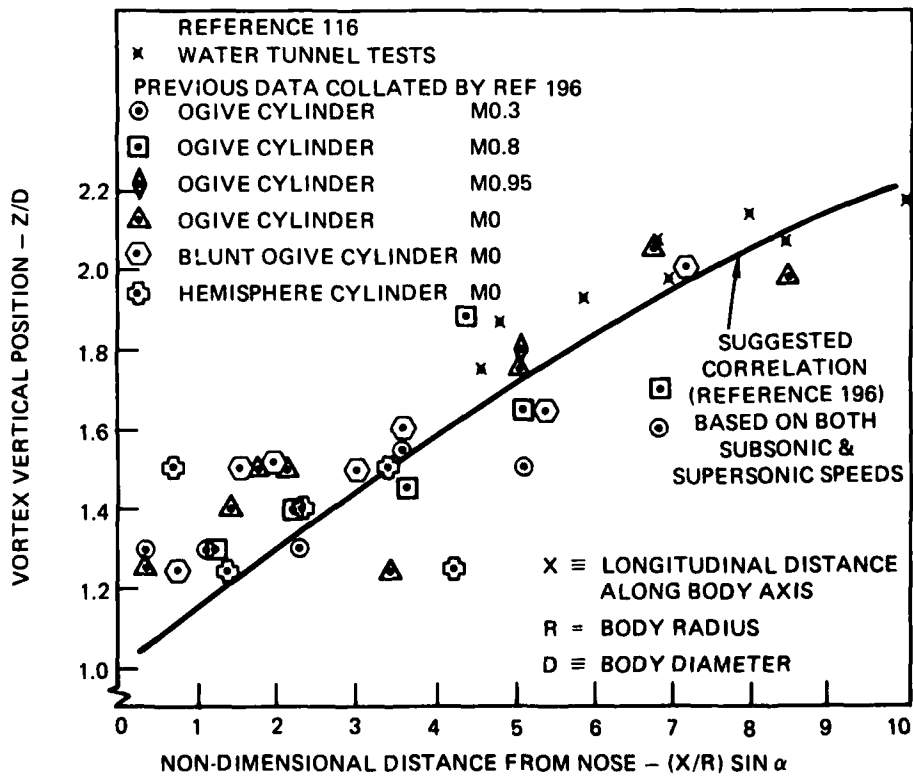
**FIGURE 71. VORTEX CORE VERTICAL LOCATIONS ON A SLENDER BODY
(FROM REFERENCE 116)**
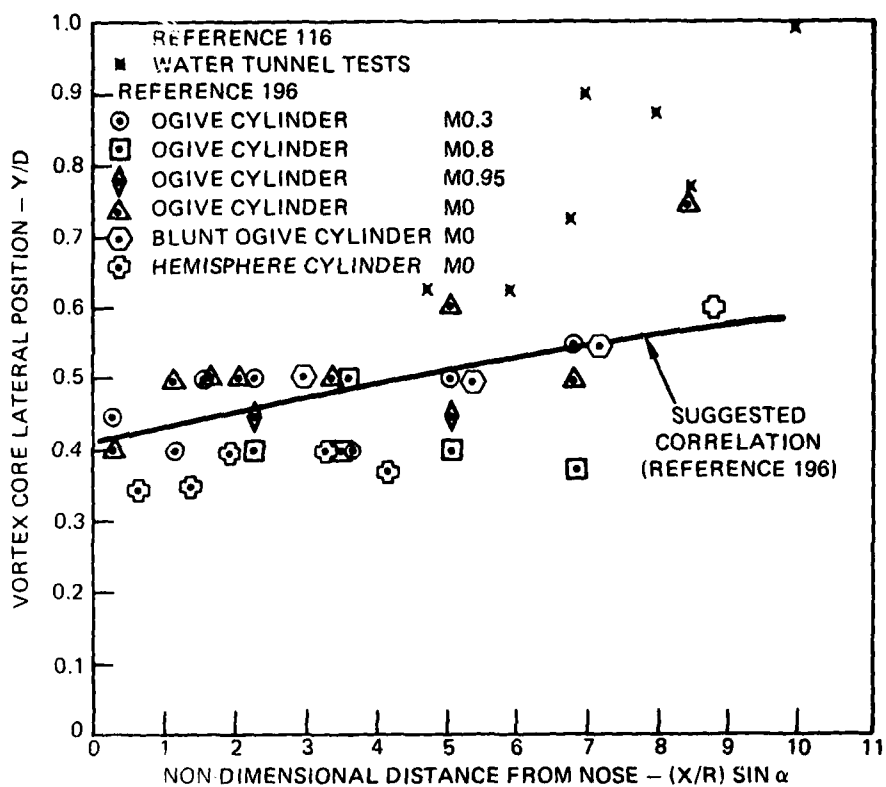
FIGURE 72. VORTEX CORE LATERAL LOCATIONS ON A SLENDER BODY (FROM REFERENCE 116)
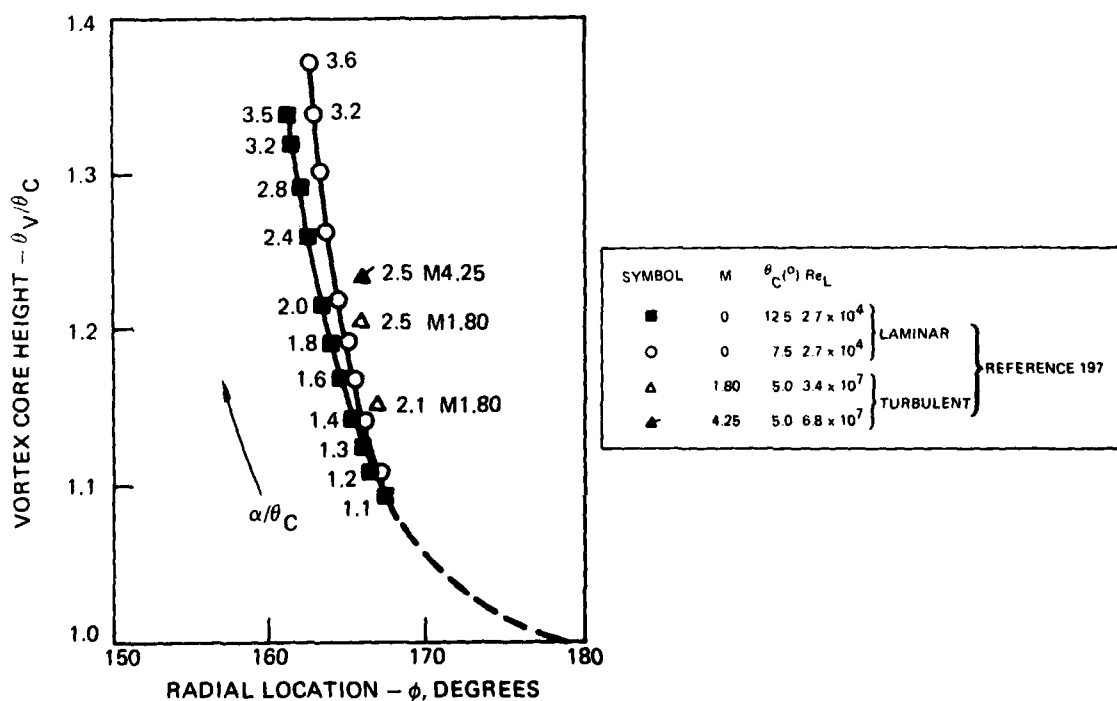
FIGURE 73. COMPARISON OF BODY VORTEX CORE LOCATIONS IN LAMINAR AND TURBULENT FLOWS (FROM REFERENCE 54)

142
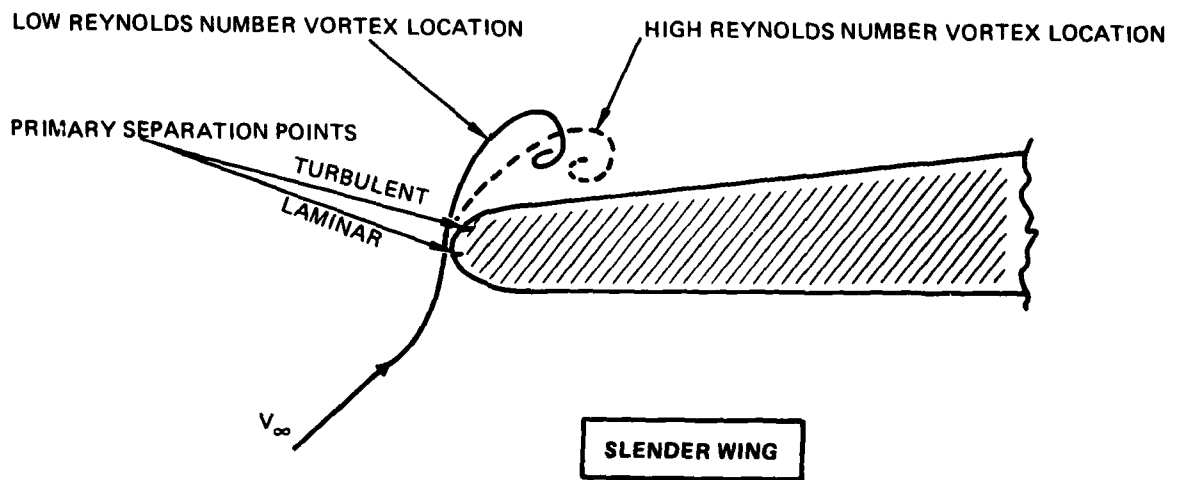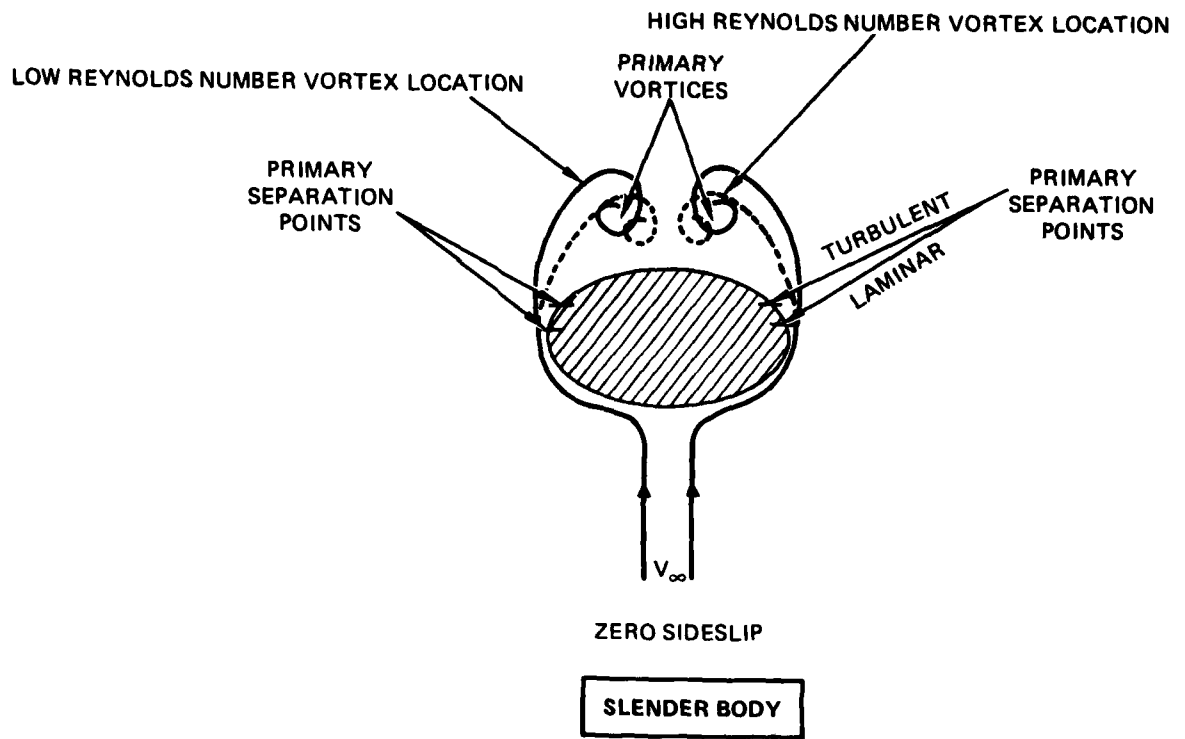
FIGURE 74. SKETCHES OF VORTEX LOCATIONS ON A SLENDER BODY AND SLENDER WING AT LOW AND HIGH REYNOLDS NUMBERS

143

case is expected to provide vortex sheet and vortex core locations that are further from the body and more widely spaced relative to the high Reynolds number flow situation, in a manner similar to that depicted in Figure 74 for a slender wing with large leading-edge radius. Body geometries are, however, likely to create a larger variation with Reynolds number of lateral spacing than vertical position. It is evident, therefore, for body geometries without fixed separation, the water tunnel results reveal the phenomenological aspects of the flow field but quantitative comparisons with high Reynolds number data are not possible.

On slender bodies, as angle of attack is increased, asymmetric vortex shedding occurs in a symmetric flight condition, as illustrated in Figure 75. Reference 110 has suggested that this flow situation is caused by an inviscid hydrodynamic instability due to the crowding together of the vortices near the apex. This is supported by data on slender delta wings (Reference 117) where asymmetric vortices have been observed despite a sharp edge of separation, as shown in Figure 76. The role of the separation point degree of freedom on a slender body is to reduce the angle of attack at which asymmetric vortices appear. For example, wind tunnel data on a slender nose shape in Reference 118 have shown that at a Reynolds number, Re_d, of 3.17×10^5 the body vortices remain nearly symmetric for about half the body length, as indicated by sectional side force distributions and vapor screen photographs, whereas at high Reynolds number, 3.17×10^6, the vortices become asymmetric nearly immediately. It would appear, then, that both the hydrodynamic instability and separation point degree of freedom play important parts in the development of flow asymmetries on bodies at high angles of attack. Consequently, differences are to be expected when comparing vortex asymmetry onset in the water tunnel with results obtained in wind tunnels and in flight. The increased lateral spacing of the vortex cores due to the laminar boundary

144

ASYMMETRIC FOREBODY VORTICES

V.

FIGURE 75. ASYMMETRIC FOREBODY VORTEX SHEDDING AT ZERO SIDESLIP (NORTHROP WATER TUNNEL)

(a) VORTEX ASYMMETRY ON AN OGIVE CYLINDER BODY
AT M0.0 (NORTHROP WATER TUNNEL)
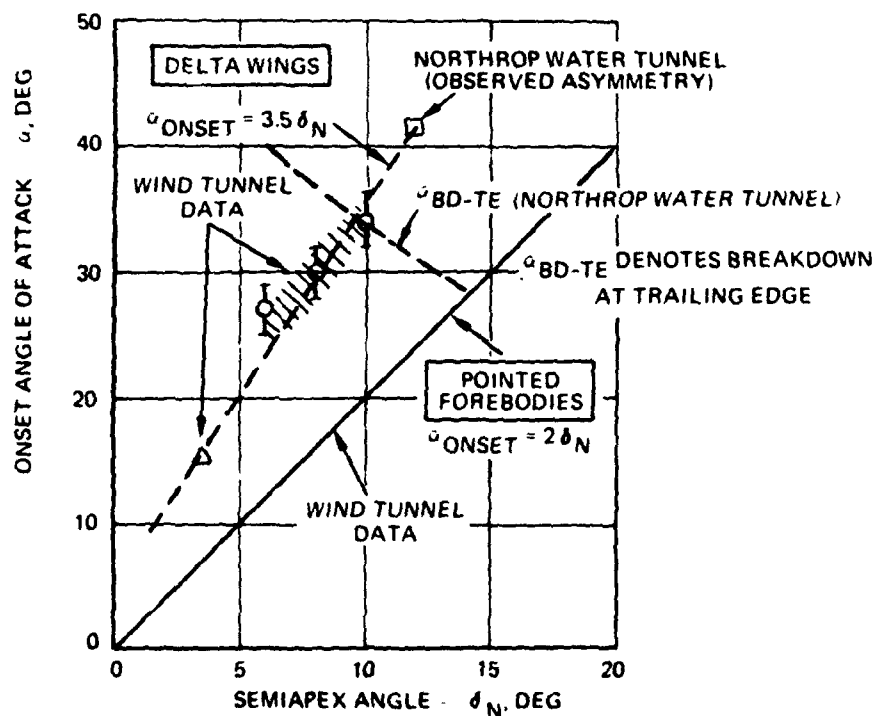
(b) ONSET OF VORTEX ASYMMETRY –
SLENDER WINGS AND BODIES
(REFERENCE 110)

FIGURE 76. DELTA WING AND FOREBODY VORTEX ASYMMETRY

146

layer separation on each side of the windward generator observed in a hydrodynamic facility should increase the angle of onset of vortex asymmetry relative to higher Reynolds number tests. This contention is supported by the data presented in Figure 77 which indicate that the water tunnel results are consistently higher than data obtained in a wind tunnel. The trends are similar, however, in that the water tunnel reveals the effects of increased forebody fineness ratio and afterbody length in reducing the asymmetry onset angle. These results suggest that, despite the separation point degree of freedom, once the vortices are shed from the body the vortex behavior is essentially insensitive to Reynolds number changes.

A vortex core switching phenomenon is sometimes observed. At very high angles of attack (~70 degrees) it is due to incipient Karman vortex shedding but at moderate angles of attack may be caused by support effects or free-stream turbulence (Reference 119). The phenomenon has been observed both in water tunnels (see Figures 78 and 79, for example) and wind tunnels. There is also evidence of sensitivity to tiny imperfections in axisymmetric test models. The flow instability observed on a cruciform missile arrangement within a very small angle of attack range in the Northrop water tunnel, depicted in Figure 80, involved highly oscillatory vortex core behavior and alternate bursting of the primary vortex cores which appeared to be due, in part, to the vortices traversing alternately favorable and adverse pressure fields near the top-mounted fin. This unsteady phenomenon will be described in detail in the section on Unsteady Flows.

At very high angles of attack, approaching 90 degrees, subcritical separation on a slender body results in the classical time-dependent Karman vortex street as illustrated in Figure 81. Supercritical separation produces a similar flow but with a different frequency. In the critical and post-critical regions, the wake flow is random.
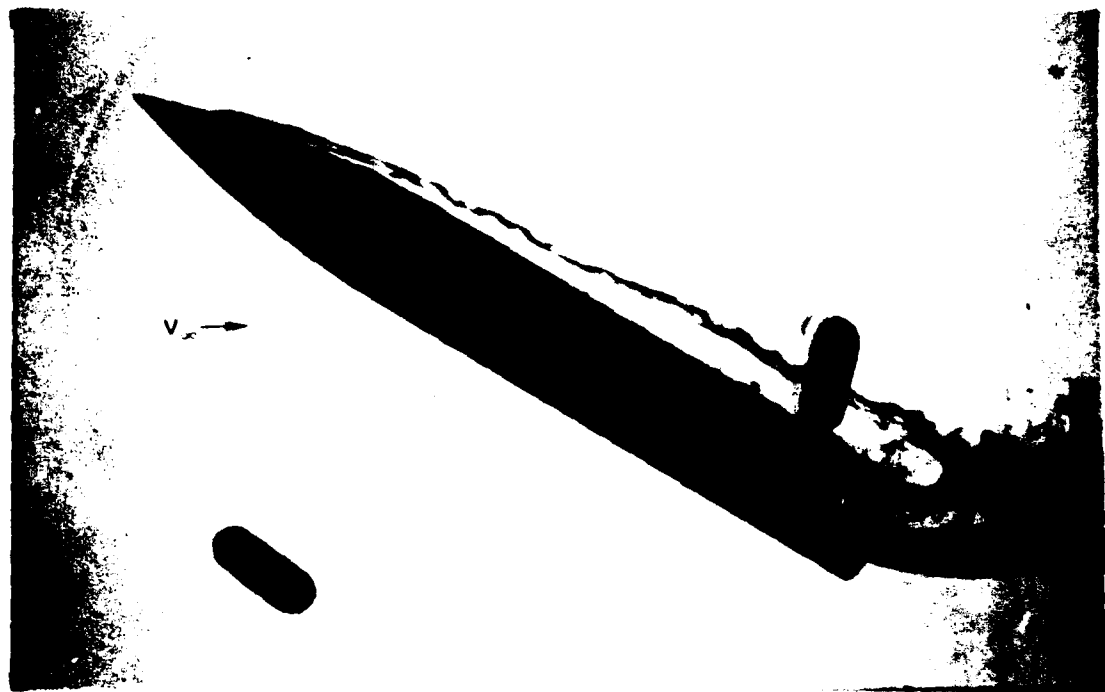
(a) TYPICAL NORTHROP WATER TUNNEL OGIVE CYLINDER
MODEL AT MODERATE ANGLE OF ATTACK
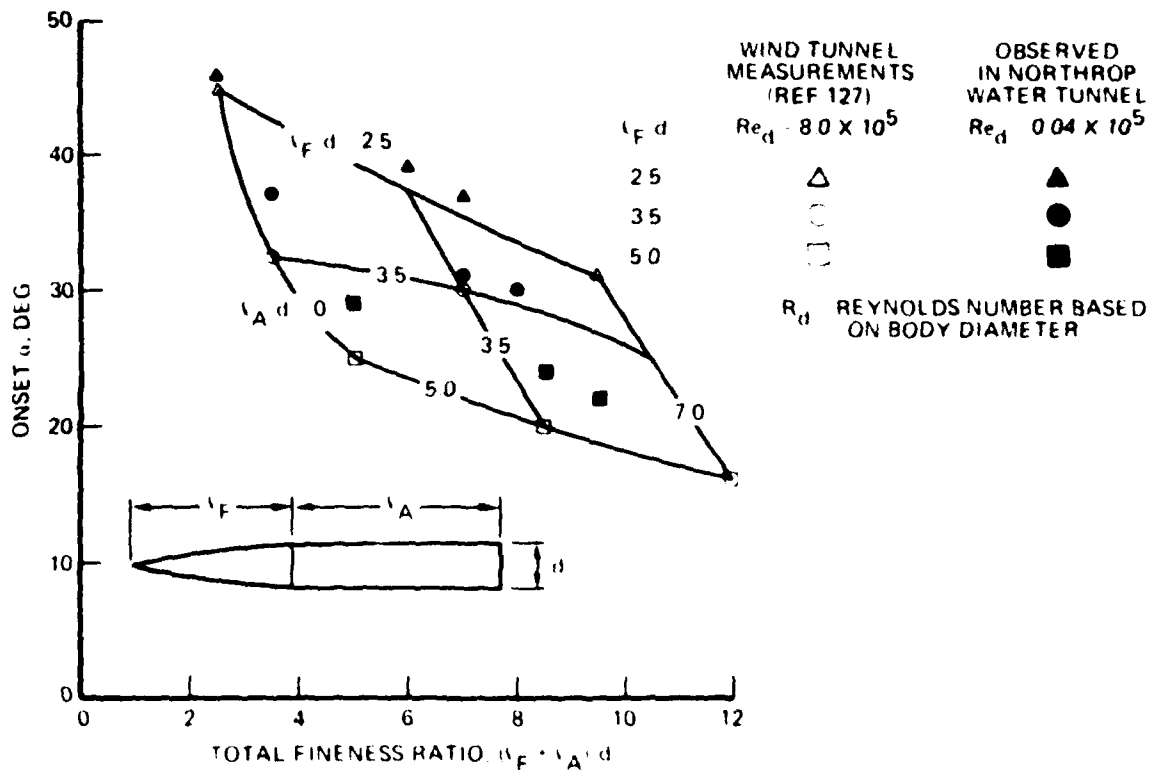
(b) EFFECTS OF FOREBODY AND AFTERBODY FINENESS RATIO
ON ONSET ANGLE OF ATTACK OF VORTEX ASYMMETRY

FIGURE 77. COMPARISON OF WATER TUNNEL AND WIND TUNNEL
RESULTS ON SLENDER BODY VORTEX ASYMMETRY ONSET

FIGURE 78. WATER TUNNEL FLOW VISUALIZATION OF UNSTEADY VORTEX SHEDDING (FROM REFERENCE 108)

FIGURE 79. WATER TUNNEL FLOW VISUALIZATION OF UNSTEADY FOREBODY VORTEX SHEDDING (NORTHROP WATER TUNNEL)
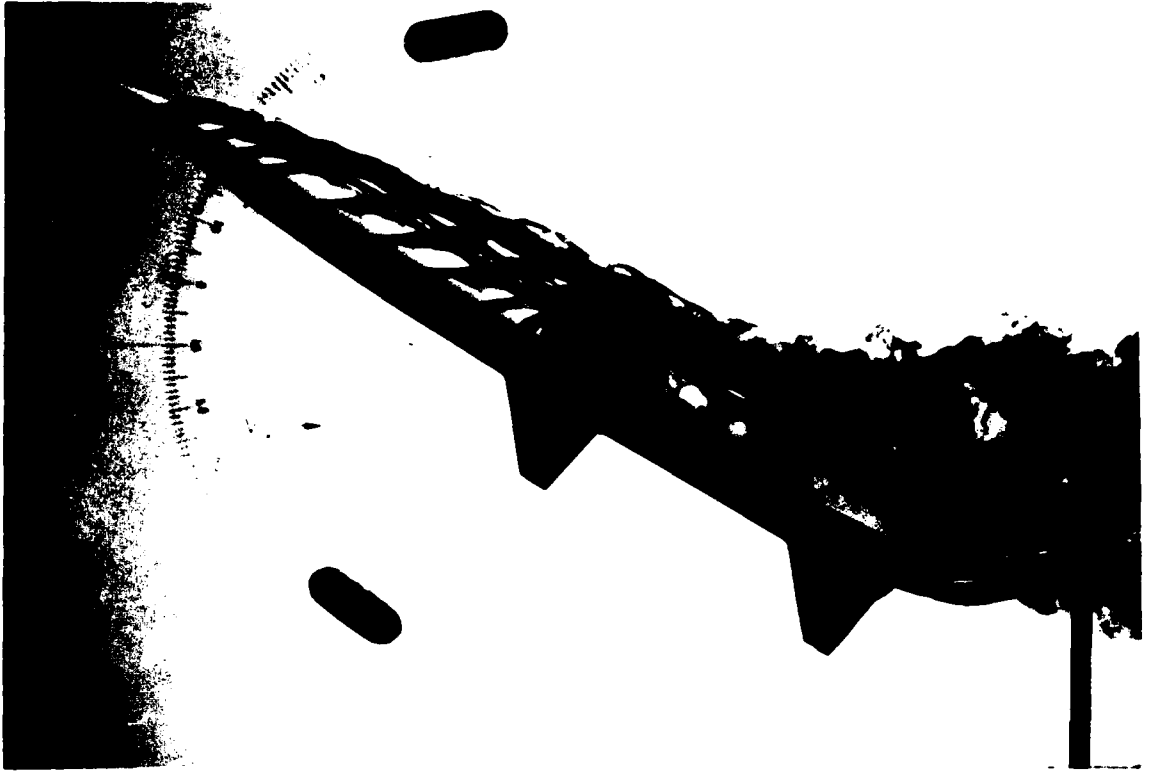
FIGURE 80 CRUCIFORM MISSILE CONFIGURATION EXHIBITING OSCILLATORY VORTEX CORE
BEHAVIOR (NORTHROP WATER TUNNEL)

FIGURE 81. SUBCRITICAL SEPARATION ON A SLENDER BODY AT 90 DEGREES ANGLE OF ATTACK (FROM REFERENCE 108)

Surface Boundary Layer Flow

Flow regime (2), the boundary layer flow near the body, is viscosity-dominated. This involves not only separation of the primary boundary layers that develop on each side of the windward generator but also secondary separations of the leeward boundary layer as well, as sketched in Figure 82. The dividing surfaces emanating from the separation lines on the body surface roll up, respectively, into the primary and secondary vortices. These secondary vortices, which have rotational sense opposite to that of the primary vortices, make a significant contribution to the normal force, which is reduced when the secondary suction peak is lost. The position of the secondary vortex is governed by the Reynolds number of the secondary flow. When transition occurs in the secondary flow, the secondary vortex will move outboard, similar to the behavior on a delta wing. It may be conjectured that the movement of the secondary vortex core will affect the location of the primary apex vortex core in a manner similar to that on a slender wing, although to perhaps a lesser extent due to body geometry.

At low Reynolds numbers in the water tunnel, a tertiary vortex is observed which rotates in the same sense as the primary vortex. The flow situation is shown in Figures 83 and 84 from Northrop and ONERA studies (Reference 120), respectively. Laminar separation of the primary and secondary boundary layer flows enables the development of the tertiary vortices, similar to the flow situation described for delta wings. As Reynolds number is increased, however, into the transition region, the separation point moves outboard and sufficient space is no longer available for the rolling up of a third vortex system, which explains why these vortices have generally not been observed in wind tunnel tests. Hence, as in the case of delta wings, the secondary and tertiary vortex

153
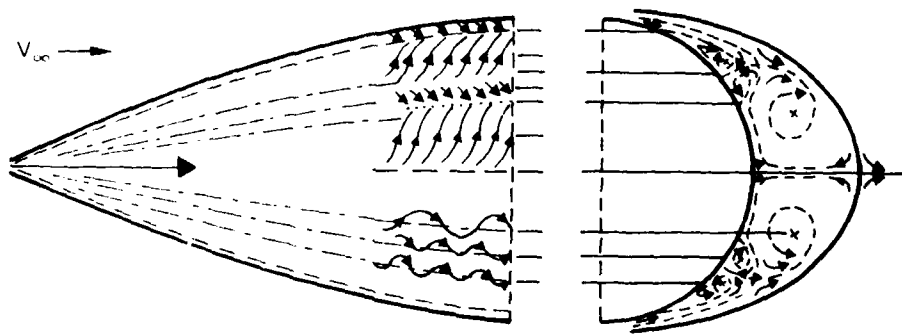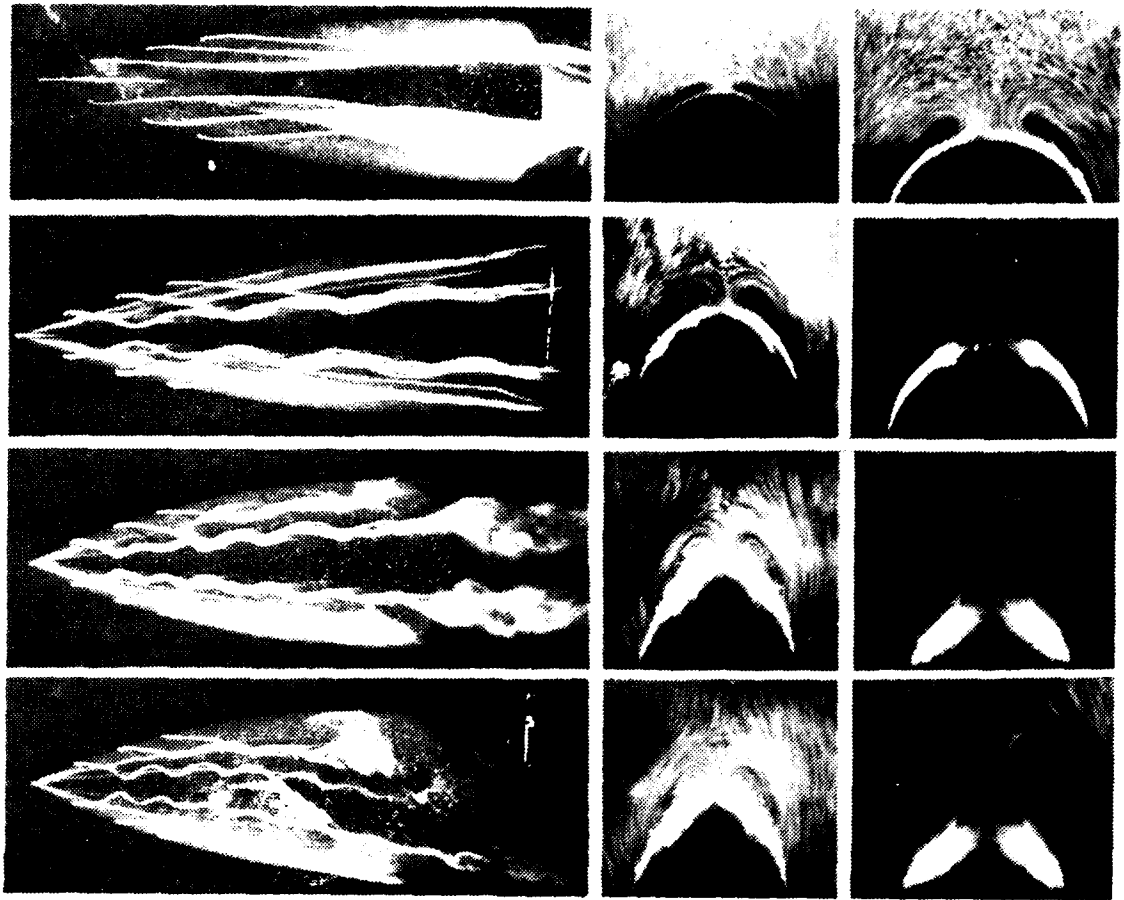
FIGURE 82. PRIMARY AND SECONDARY BOUNDARY LAYER SEPARATION ON
A SLENDER BODY (FROM REFERENCE 120)

FIGURE 83. TERTIARY VORTEX FORMATION ON A SLENDER BODY IN LAMINAR FLOW
(NORTHROP WATER TUNNEL)

PRIMARY VORTICES
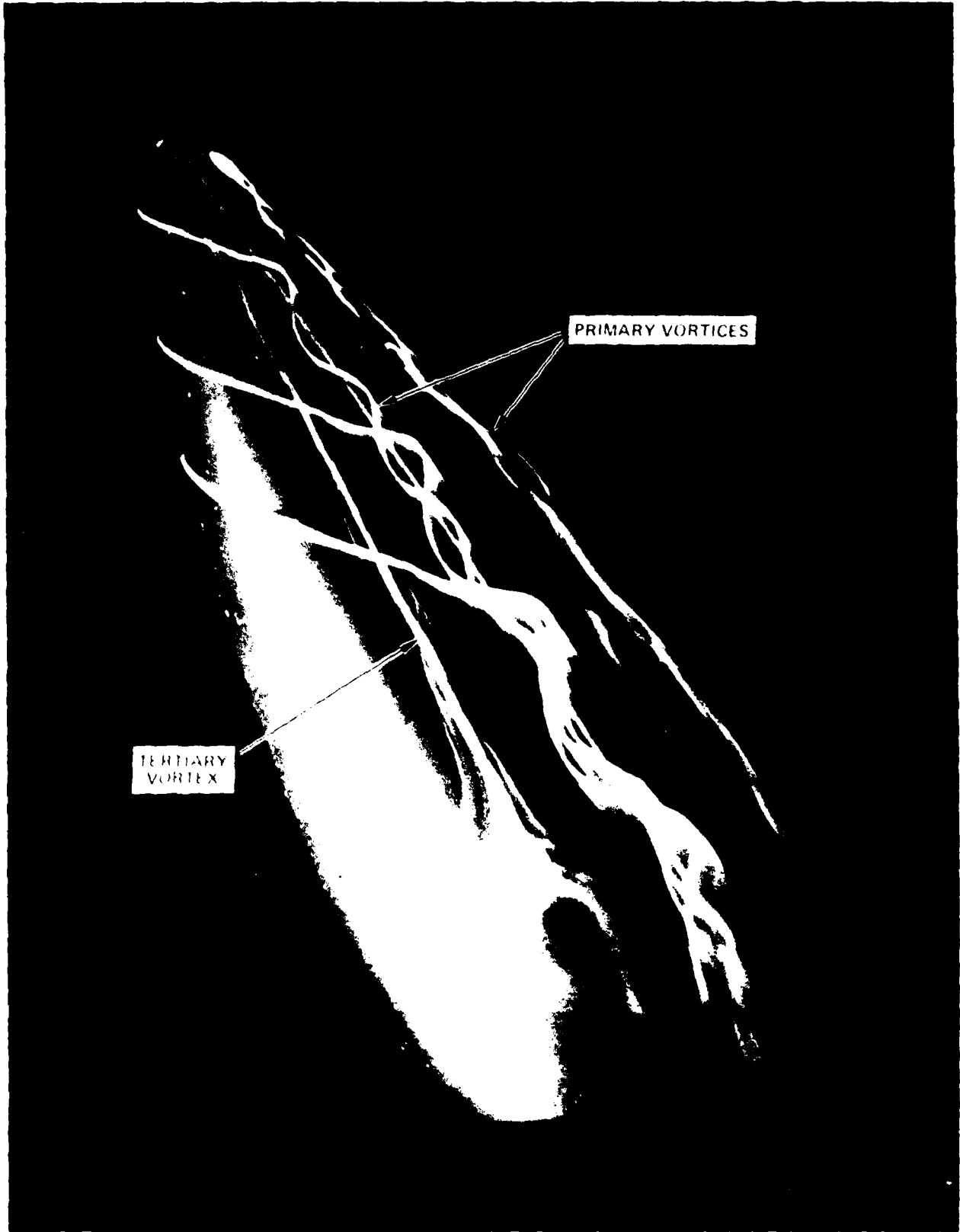
TERTIARY VORTEX

FIGURE 84 TERTIARY VORTEX FORMATION ON A SLENDER BODY IN LAMINAR FLOW
(FROM REFERENCE 120)

flows are of qualitative significance only, when observed in a water tunnel.

Vortex Flow Internal Structure

Flow region (3) deals with the internal structure of the vortex flow itself. Although water tunnel simulation of body vortex sheet and core locations and vortex strength are subject to the limitations just discussed, once the vortex is shed from the body it is then subject to essentially potential flow effects, and body vortex core stability at high angles of attack is expected to be governed by the adverse pressure gradient in the external flow field, as was the case for leading-edge vortices shed from slender wings. On bodies alone, since the separation point location is a function of the Reynolds number, the body wake and, hence, pressure gradient are also expected to vary with Reynolds number. Similarities do exist between water tunnel and wind tunnel tests, however. Reference 121 has indicated that breakdown (in a wind tunnel) of the primary nose vortices appears in the form of a relatively gradual structural change in the vortex core, in which the core expands with distance downstream followed by a diffused rotational flow. This is in complete agreement with studies made of tangent ogive-cylinders in the Northrop water tunnel, typical results being shown in Figure 85. The positive pressure gradient along the length of a slender body at high angle of attack is much less than that over a wing. Consequently, the nose vortex pair is better able to penetrate the body pressure field and exhibits no abrupt deceleration and stagnation of the vortex core axial flow until very high angles of attack are attained. For wing-body combinations, the nose vortex may, under certain conditions, penetrate the highly adverse pressure field associated with the wing wake and, consequently, core breakdown abruptly occurs, as seen in Figures 86 and 87. The outer periphery of the wing wake in Figure 87 can be defined by extending a line parallel

157
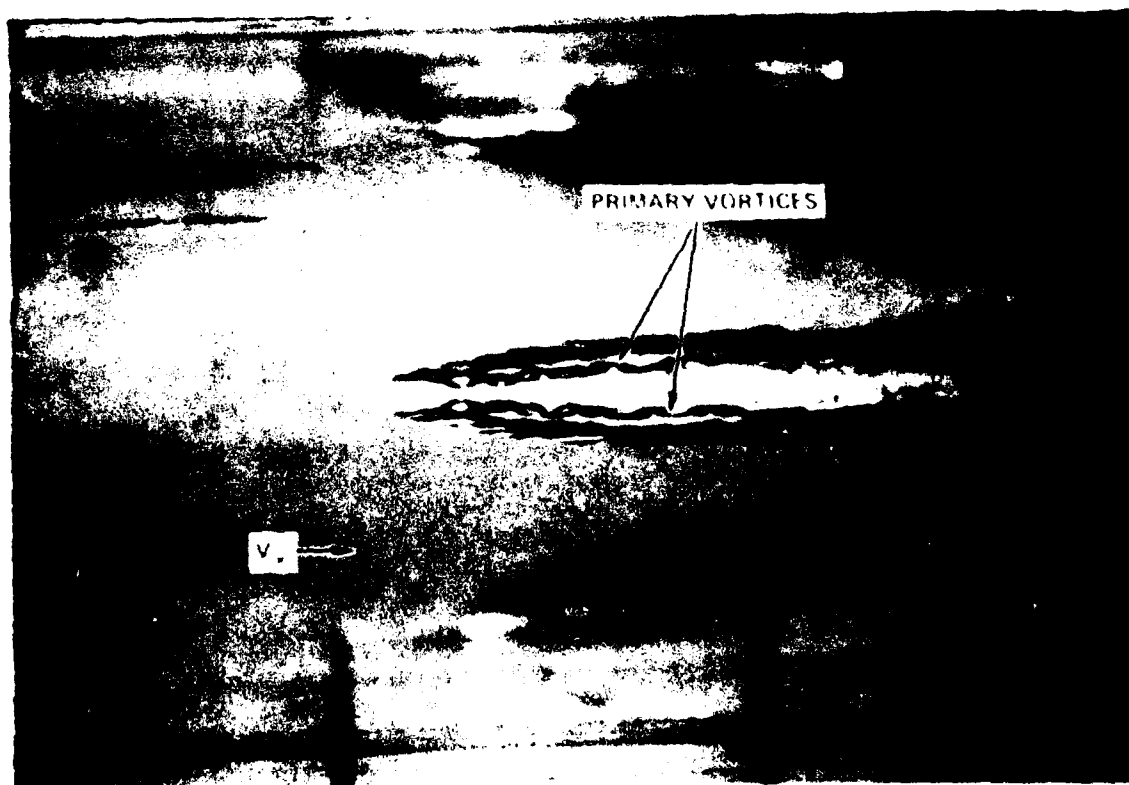
FIGURE 85 GRADUAL STRUCTURAL CHANGE IN VORTEX CORE ON BODY ALONE
(NORTHROP WATER TUNNEL)

FIGURE 86   ABRUPT STRUCTURAL CHANGE IN VORTEX CORE IN PRESENCE OF WING
PRESSURE FIELD NORTHROP WATER TUNNEL

VORTEX BURST

VORTEX ASYMMETRY

WING WAKE
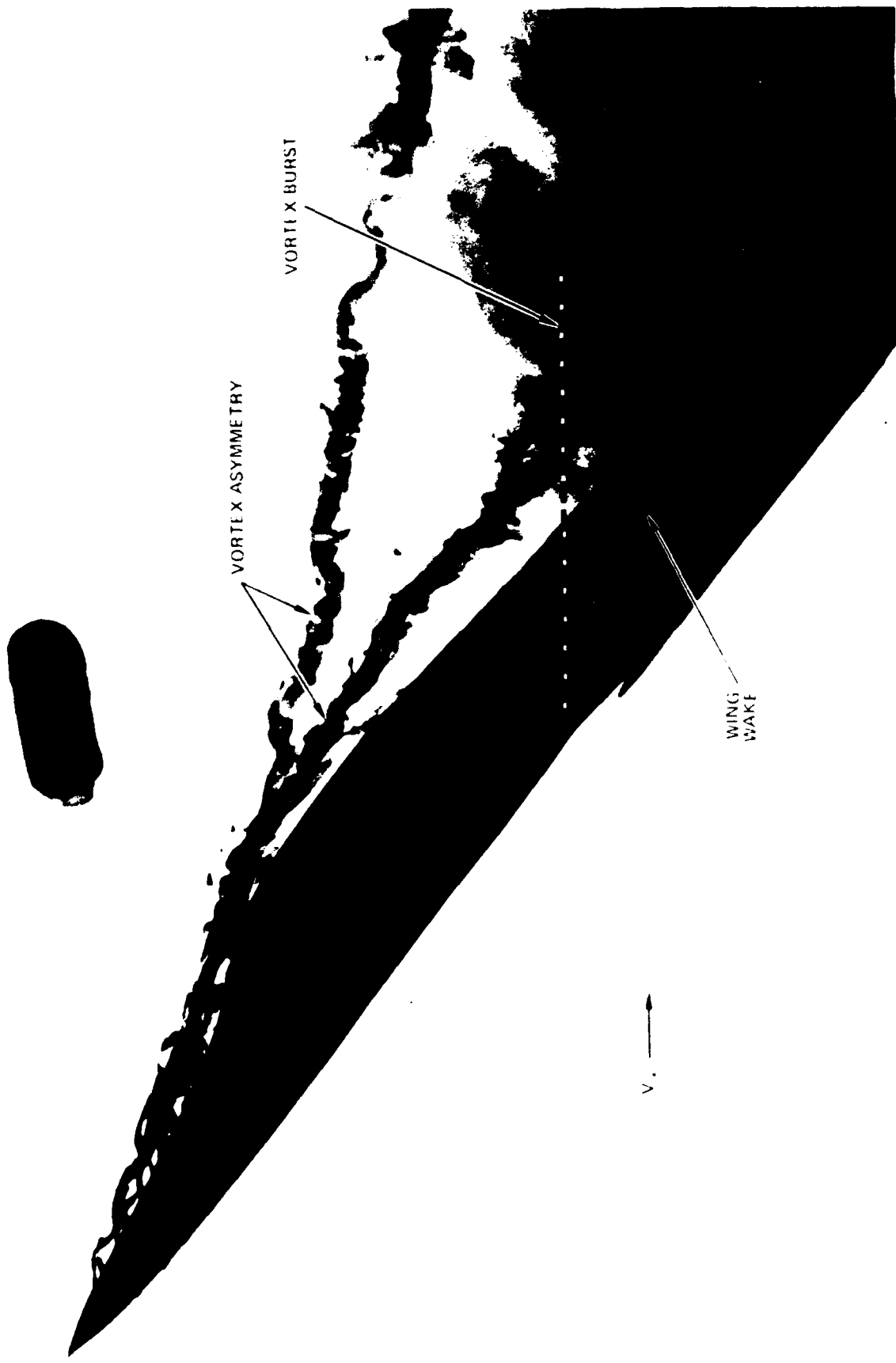
FIGURE 87. BODY VORTEX BEHAVIOR IN PRESENCE OF WING FLOW FIELD
FIGHTER CONFIGURATION (NORTHROP WATER TUNNEL)

to the free-stream from the wing leading edge as shown. It is evident in the photograph that the body vortex bursts immediately upon entering this high pressure field. (Note also the upper nose vortex in Figure 87 which traverses a relatively minor positive pressure gradient and, as a result, exhibits no major structural change, although core instability is evident.) A substantial shift in the positions of the body vortex cores due to the induced effect of a wing has also been observed in wind tunnel tests in Reference 122 using LDV equipment.

Compressibility Effects

Comments on compressibility effects on body vortices are appropriate at this point. The compressibility effects found in air for high Mach number flight cannot be properly modeled in the water tunnel, since water behaves as an incompressible fluid. Accordingly, the presence of shock waves and shock-induced separation cannot be studied in a hydrodynamic test facility. Keeping these limitations in mind, there are certain areas where the water tunnel can be used to gain understanding of separated flow fields on the leeward surface of vehicles in supersonic flight.

The vortices formed on bodies of revolution at angle of attack have been found to be present for freestream, supersonic Mach numbers (see References 123-125) and vortex core trajectories exhibit the same qualitative behavior as in incompressible flow.

The effect of Mach number on the vortices formed on bodies of revolution is dependent on the crossflow Mach number, $M_c = M \sin \alpha$. Changes in the vortex flow field due to compressibility begin at M_c of about 0.6 (Reference 126). Increases in the crossflow Mach number have been found to reduce the

161

vortex-induced side force on bodies at zero sideslip (see Figure 64). No significant vortex-induced side forces have been observed on cones or ogive cylinders at supersonic cross-flow Mach numbers (References 127 and 128). A symmetric pattern of shock waves develops which inhibits the influence of the asymmetric vortices from reaching any side area of the body. In addition, the experimental results in Reference 124 indicate that compressibility effects will reduce the concentrated circulation in a body vortex, making it more diffuse.

Despite the reduction in vortex-induced side force at zero sideslip with increasing Mach number, the fuselage vortices are still present to very high Mach numbers and can still influence the flow fields near downstream tail surfaces, for example. On blunt-nosed bodies, vortices were generated on the body aft of a bow shock and a shock wave in the nose region (Reference 125). Oil flow studies made at hypersonic speeds on the leeward side of delta-wing orbiter configurations (References 129 and 130) show the presence of a fuselage vortex pair, as was observed on the Space Shuttle Orbiter in low-Reynolds-number, $M \approx 0$, water tunnel studies in Reference 131.

The preceding discussions serve to point out the difficulty in simulating separation-induced vortex flows on slender bodies and, hence, the establishment of straightforward flow simulation guidelines. Quantitative comparisons of low-Reynolds-number body vortex flow behavior with high-Reynolds-number results in air appear unlikely due to the sensitivity of vortex development to Reynolds number, model imperfections, free-stream turbulence, model support system, etc. Emphasis should be placed on _qualitative_ comparisons since, as shown in this section and will be shown in Section 5, _trends_ observed in a water tunnel correlate, in general, extremely well with wind tunnel and flight phenomena pertaining to body vortex flows and their subsequent interactions with airframe components. For,

162

despite the large viscous effects near the body, at high angle of attack the primary vortical motions themselves are embedded in an essentially potential flow field.

The philosophy adopted by Von Karman Institute (VKI) researchers in Reference 132 regarding the applicability of results of water tunnel tests on a missile with wing-strake to transonic wind tunnel tests is worth noting here: "...that for flow over configurations in which extensive flow separation occurs, surprisingly good agreement in flow behavior is found." A similar attitude is expressed by British Aerospace Corporation (BAC) researchers in Reference 116: "It is thought, however, that for particular cases where aspects of the configuration shape dictate the flow details, or for conditions where large areas of separated flow are expected, then the use of water tunnel experiments is justified and will yield valuable qualitative results."

SECTION 5

TASK III - <u>IDENTIFICATION OF WATER TUNNEL APPLICATIONS TO</u>
<u>VORTEX FLOWS</u>

5.1   INTRODUCTION

Correlations of separation-induced vortex flow phenomena
observed in water at low Reynolds numbers with high Reynolds
number wind tunnel and flight test data have been extensively
documented yet little attention has been given to the reasons
why such correlations are possible and, in some cases, why the
correlations are <u>not</u> satisfactory.   The results of the study
presented in Section 4 provide insight into key parameters
(Reynolds number, external pressure gradient, etc.) which must
be considered when vortex flow studies are made in a hydrody-
namic facility. Whereas Section 4 was oriented more towards
simple wing and body geometries, the following paragraphs
address the questions associated with the study of practical
aerodynamic configurations such as advanced fighter aircraft
and missile configurations at high angles of attack.   Complex
vortex systems shed from non-circular forebodies and highly-
cambered and twisted wing - LEX planforms which may, or may
not, have sharp leading edges, and vortex system interactions
are considered.   Simulation of <u>steady</u> and <u>unsteady</u> vortical
motions are addressed.   The discussions are augmented by
several examples of vortex flow phenomena to which a water
tunnel has been applied, thereby enabling an identification of
water tunnel applications to a wide class of vortical flows.

5.2   LEADING-EDGE VORTICES IN STEADY FLOW

A water tunnel is employed to maximum advantage when
it is used for flow phenomena which are insensitive to changes
in Reynolds number. Vortices shed from the sharp edges of
slender wings and wing leading-edge extensions (LEXs) or
wing-body strakes at high angles of attack, as illustrated in
Figures 88 and 89, come under this category since it is
possible under certain conditions to properly simulate in a
water tunnel the flow phenomena of vortex generation, vortex
core location, and vortex core breakdown that are necessary for
correlation with high Reynolds number results. Provided flow
separation occurs from a sharp leading edge, the separation
point does not vary with Reynolds number. This means that the
water tunnel then provides a good representation of the
wake shed from a wing and, hence, of the adverse pressure
gradient (expressed in non-dimensional form) which a leading-
edge vortex must traverse.

Figure 90, which presents onset angle of attack for
vortex bursting at the trailing edge of delta wings obtained in
water tunnels, wind tunnels, and in flight, indicates that the
variation in onset angle at different Reynolds numbers is no
greater than the differences observed at the same Reynolds
number in different test facilities. Similar trends are shown
in Figure 91 which show the progression of delta wing vortex
bursting with angle of attack at different Reynolds number.

It is interesting to note that, at high angles of
attack, with several dye ports distributed along the leading
edge of a slender wing, the point along the leading edge at
which the vortex is no longer fed by vorticity shed from the
leading edge can be ascertained. Vortex core instability and
subsequent breakdown can then be observed shortly downstream.
These results concur with a theoretical exercise conducted in
Reference 133 in which a series of sine waves was used to

165

LEX VORTEX

FIGURE 88 WING LEADING EDGE EXTENSION (LEX) VORTEX FLOW (NORTHROP WATER TUNNEL)

LEX VORTEX

FIGURE 89. WING LEADING-EDGE EXTENSION (LEX) VORTEX FLOW (NORTHROP WATER TUNNEL)

			REYNOLDS NO. (BASED ON CENTER-LINE CHORD)
○	NORTHROP	WATER TUNNEL	4.1×10^4
◗	REFERENCE 134	WATER TUNNEL	9.8×10^3
+	REFERENCE 179	WATER TUNNEL	1.0×10^4
□	REFERENCE 135	WIND TUNNEL	1.5×10^6
△	REFERENCE 135	WIND TUNNEL	1.3×10^6
●	REFERENCE 141	WIND TUNNEL	9.0×10^5
✕	REFERENCE 137	WIND TUNNEL	$1.4 \ \& \ 1.7 \times 10^6$
◿	REFERENCE 73	WIND TUNNEL	2.0×10^6
◇	REFERENCE 135	FLIGHT	40.0×10^6
◆	REFERENCE 26	WATER TUNNEL	$1.0 \ \& \ 8.0 \times 10^4$
✳	REFERENCE 85	WIND TUNNEL	2.0×10^6
▲	REFERENCE 136	WIND TUNNEL	1.0×10^6
◆	REFERENCE 135	WATER TUNNEL	3.0×10^4
▨	REFERENCE 27	WATER TUNNEL	3.0×10^4
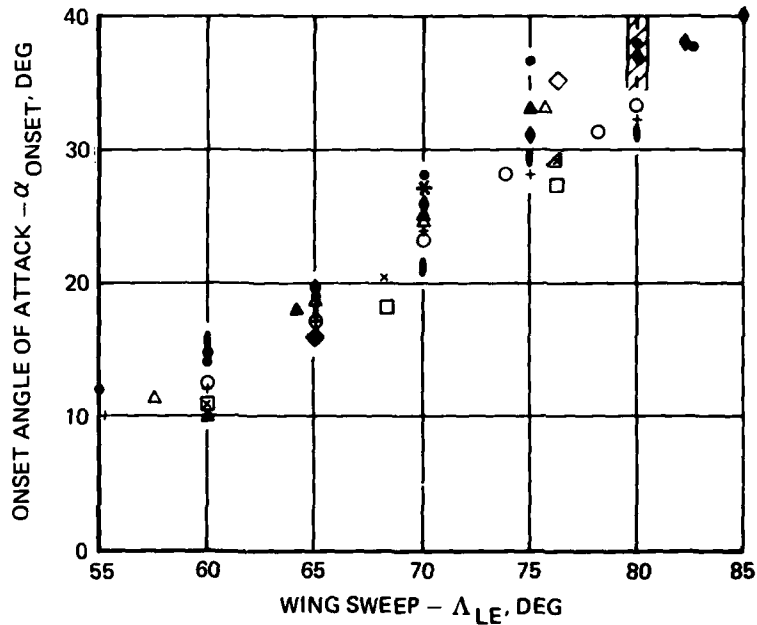
FIGURE 90. EFFECTS OF WING SWEEP AND REYNOLDS NUMBER ON DELTA WING VORTEX BREAKDOWN AT THE TRAILING EDGE
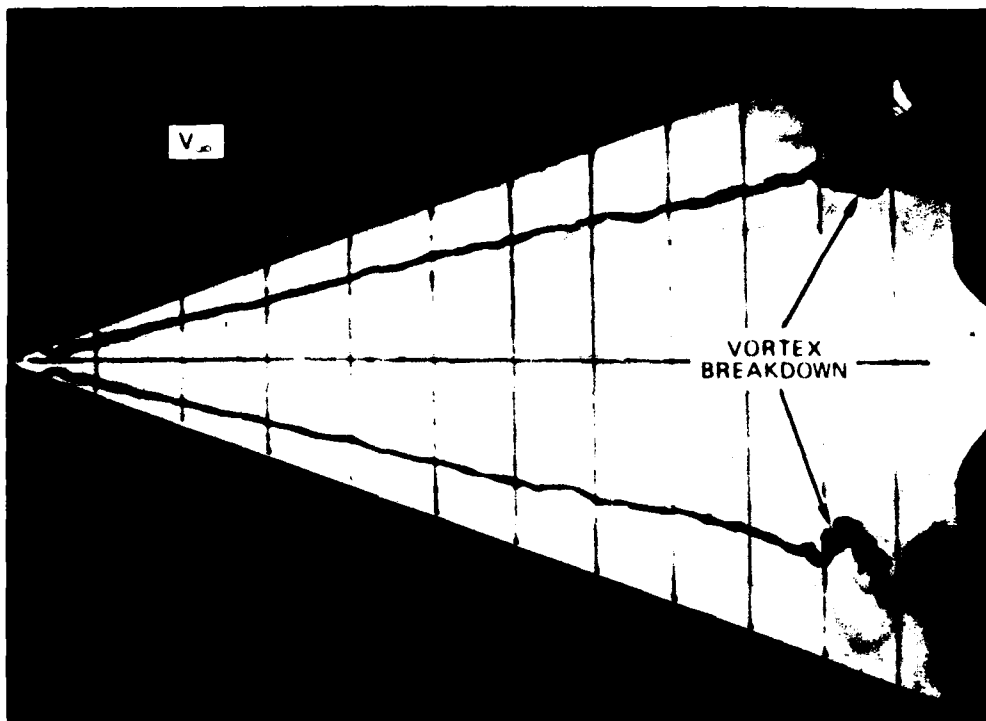
(a) TYPICAL VORTEX BREAKDOWN OVER AN ASPECT RATIO 1.46 WING
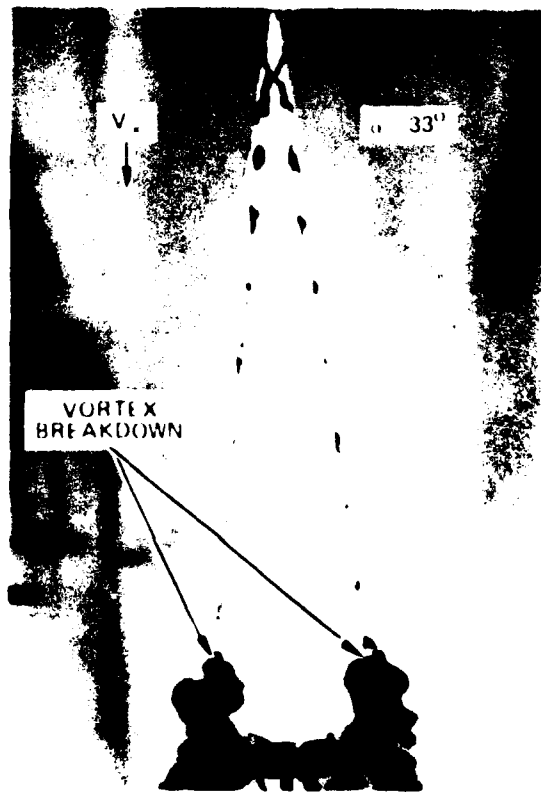
(b) PROGRESSION OF VORTEX BREAKDOWN ON AN ASPECT RATIO 0 71 WING

FIGURE 91. TYPICAL DELTA WING VORTEX BREAKDOWN CHARACTERISTICS
(NORTHROP WATER TUNNEL)

REYNOLDS NUMBER   REF

		REYNOLDS NUMBER	REF
■	NORTHROP	3×10^4	
(NO BLOCKAGE CORRECTION) ──△──	ONERA	$2 - 4 \times 10^4$	84
(WITH BLOCKAGE CORRECTION) ────	ONERA	$2 - 4 \times 10^4$	84
x	HUMMEL	2×10^6	136
●	WENTZ & KOHLMAN	10^6	141
O	EARNSHAW & LAWFORD	$0.4 \& 0.9 \times 10^6$	137

NORMALIZED VORTEX BREAKDOWN POSITION – X/C_o
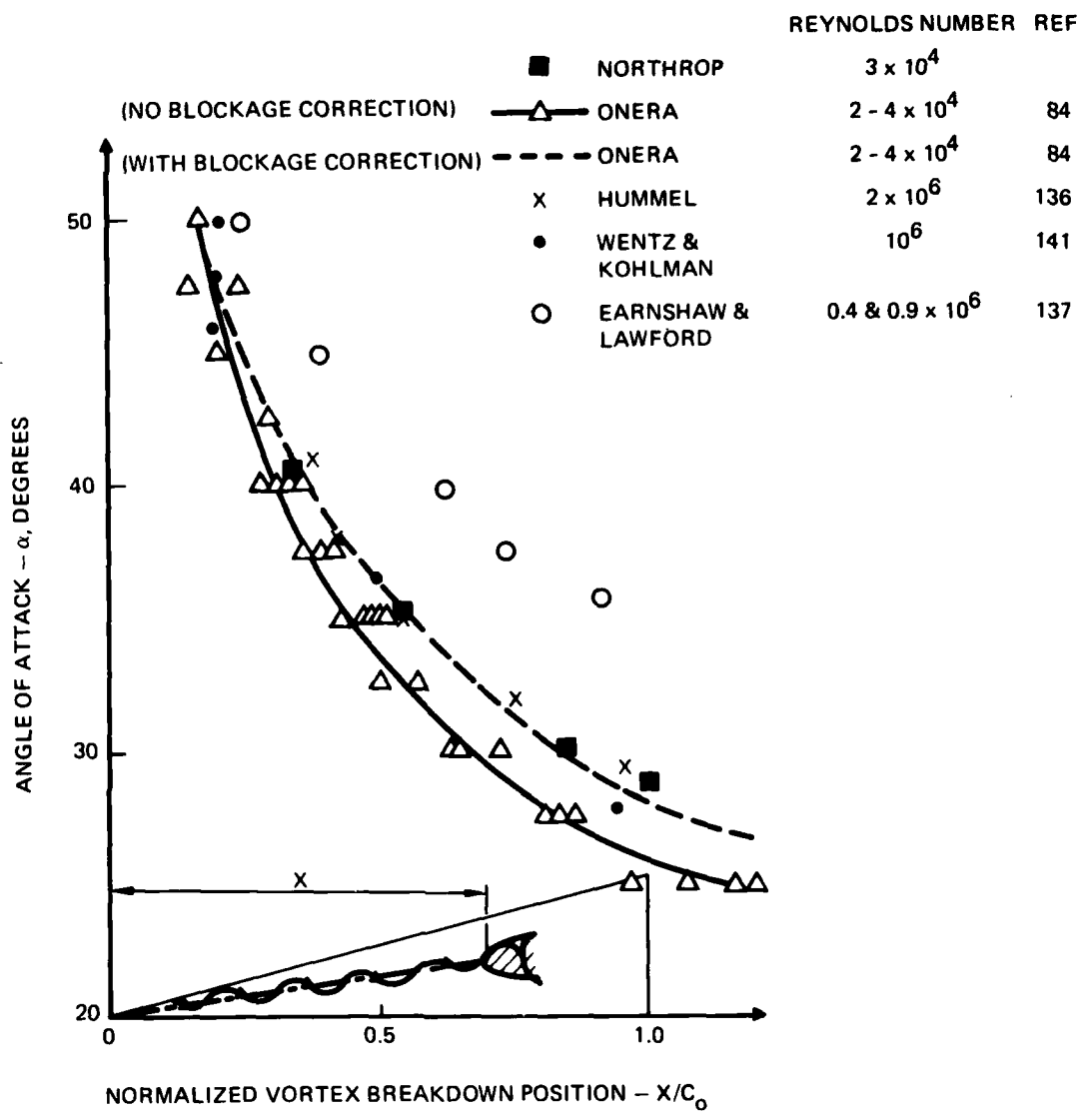
(C) COMPARISON OF WATER TUNNEL AND WIND TUNNEL VORTEX BREAKDOWN CHARACTERISTICS

FIGURE 91. CONCLUDED

170

represent the shed vorticity from a slender wing. It was found that shortly after the point at which new sine waves were no longer introduced, the concentrated "vorticity" exhibited a spiral-type disturbance similar to vortex core breakdown.

5.2.1 Water Tunnel Applications to Flat-Plate, Cambered, and Blunt-Nosed Wings

In many cases, the conditions described above are not fully-satisfied. When flow separation does not occur from a sharp edge, as would be the case on a thick wing with round leading edge or on a cambered wing, for example when a wing leading-edge flap is deflected, the separation point varies with the Reynolds number and, consequently, the size and structure of the wing wake in a water tunnel are less representative. Hence, the vortex behavior on blunt or cambered wings, though exhibiting the correct trends, is found to be of qualitative, rather than quantitative, value. This effect is illustrated in Figure 92, which presents water tunnel and wind tunnel data on the effect of wing leading-edge flap deflection angle on onset angle of attack for LEX vortex breakdown at the wing trailing edge. The low Reynolds number water tunnel results reveal the beneficial effect of a deflected leading-edge flap on vortex stability (see Figure 92) but do not predict the quantitative effects (that is, the flap benefits in a water tunnel are not as significant) as can be seen by comparison with the wind tunnel test data from Reference 138. Wind tunnel studies in Reference 139 on an aspect ratio 1.0 delta wing with elliptical edges indicate that leading-edge flow separation appears initially at aft stations and then becomes apparent at the forward stations at high angles of attack. This indicates that separation is a progressive phenomenon and, in this case, is relatively slow. Consequently, for results obtained in a water tunnel and wind tunnel at Reynolds numbers typical of the respective facilities, the
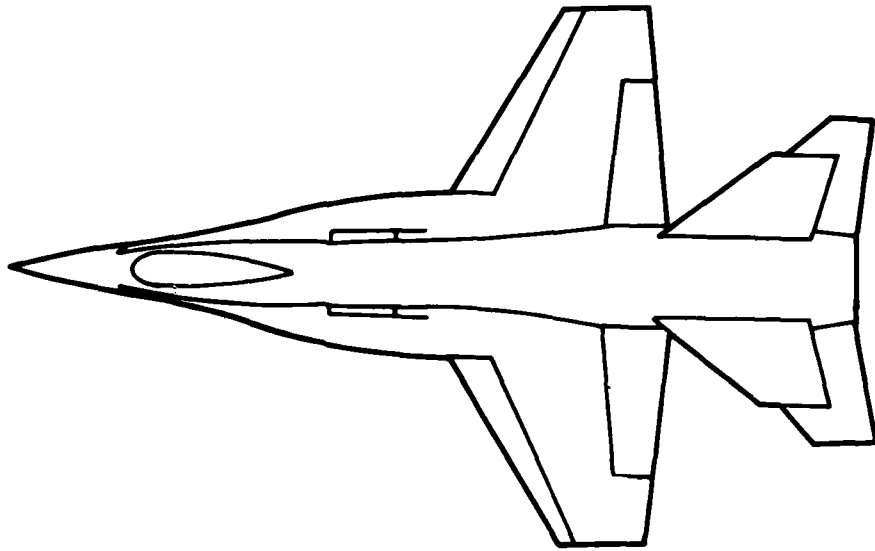
(A) SKETCH OF NORTHROP P-530 WIND TUNNEL MODEL
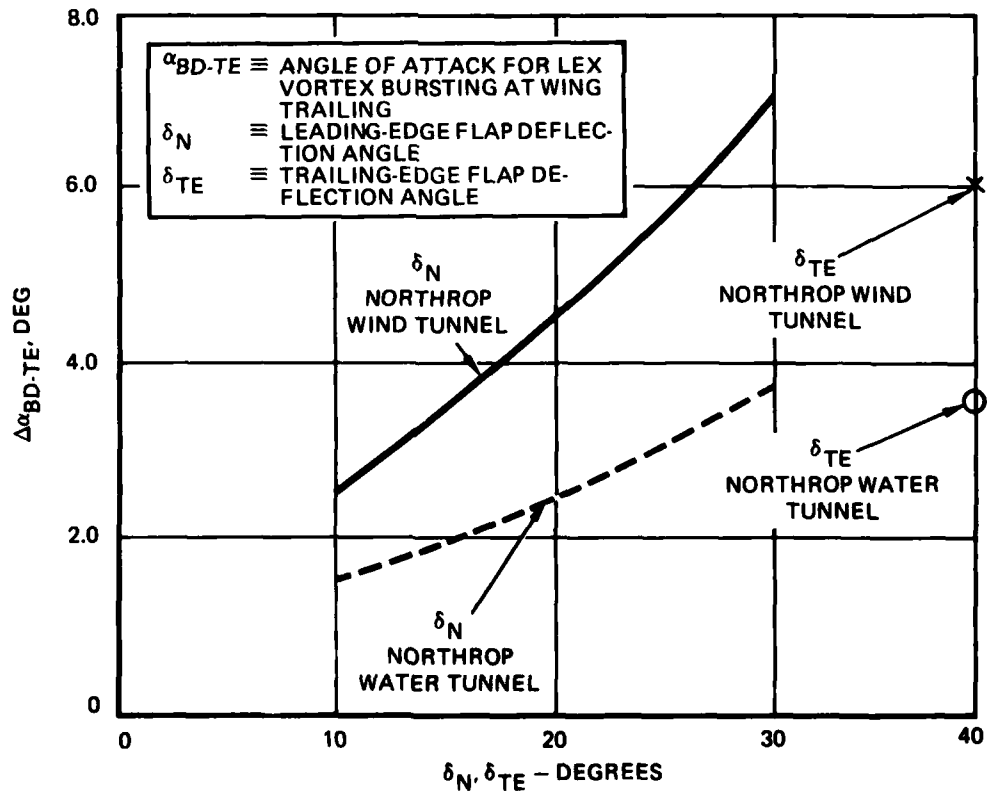
(B) EFFECTS OF LEADING- AND TRAILING-EDGE FLAPS ON LEX VORTEX STABILITY

FIGURE 92. DEFLECTED FLAP EFFECTS ON VORTEX BEHAVIOR

172
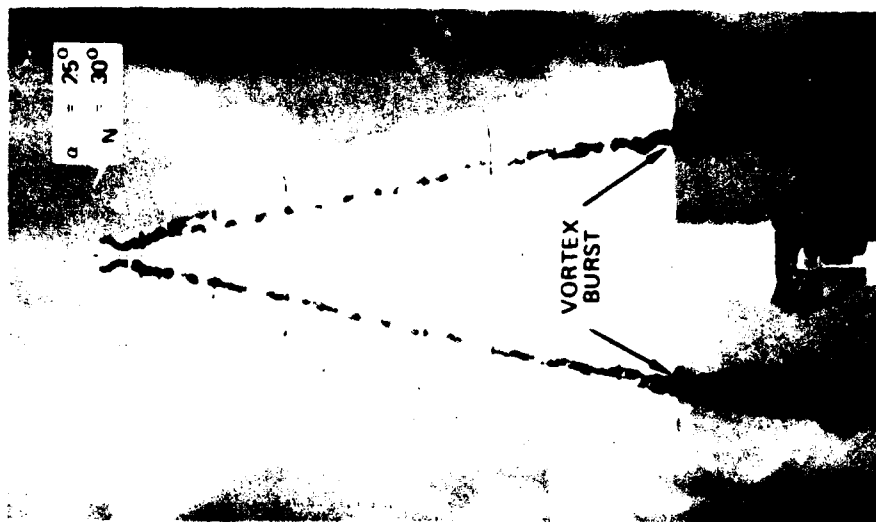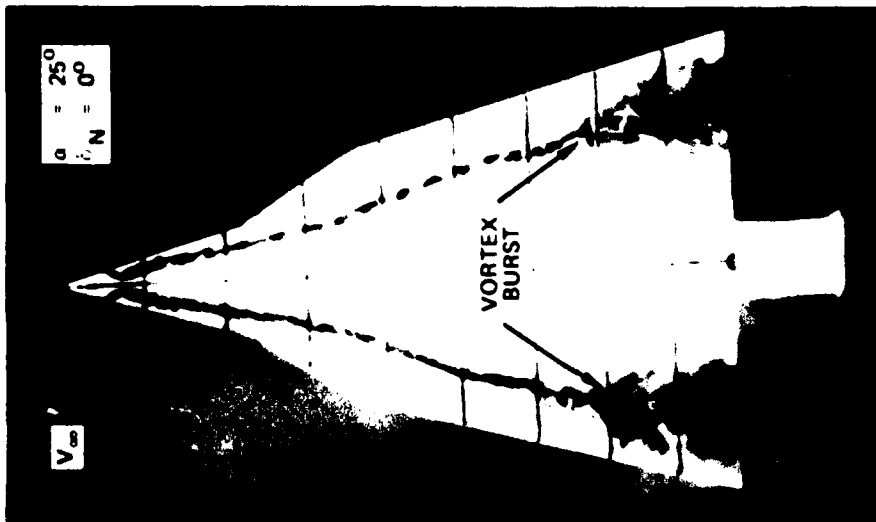
(c) NORTHROP WATER TUNNEL FLOW VISUALIZATION OF THE EFFECT OF DEFLECTED LEADING-EDGE FLAPS ON SLENDER WING VORTEX BEHAVIOR.

FIGURE 92. CONCLUDED

173

water tunnel would reveal earlier vortex formation, greater vortex-induced lift, and increased drag due to loss of suction resulting from flow separation at the leading edge.

Similar effects have been observed at ONERA (Reference 53) in water tunnel and wind tunnel tests of a rectangular variable - sweep wing. Reynolds number changes did not affect the qualitative behavior of the leading-edge vortex although differences were evident in the origin and principal location of the vortex.

The wind tunnel results in Reference 71 also indicated that vortex core definition (by water vapor) became more difficult for wings having apex or conical camber since the vortices do not increase in strength with distance from the apex in the same (theoretically linear) manner as a flat delta wing. These results have been confirmed in extensive studies of cambered wings in the Northrop water tunnel, an example from which is shown in Figure 93. The water tunnel studies reveal a reduction in vortex strength due to wing camber.

Water tunnel simulation of surface flow characteristics on flat-plate and cambered wings of low-to-moderate sweep (typical main wing sweep angles on fighter aircraft range from about 26 to 50 degrees) is inadequate because of laminar boundary layer separation in water as opposed to turbulent boundary layer separation characteristics at high Reynolds numbers in air. At higher values of wing sweep (typical of wing leading-edge extensions and supersonic cruise fighter wing planforms), flow separation characteristics are better simulated as will be discussed in detail in subsequent paragraphs.

Because the boundary layer on the upper surface of a wing in a low-speed water tunnel is laminar and has different separation characteristics to the turbulent boundary layer

174
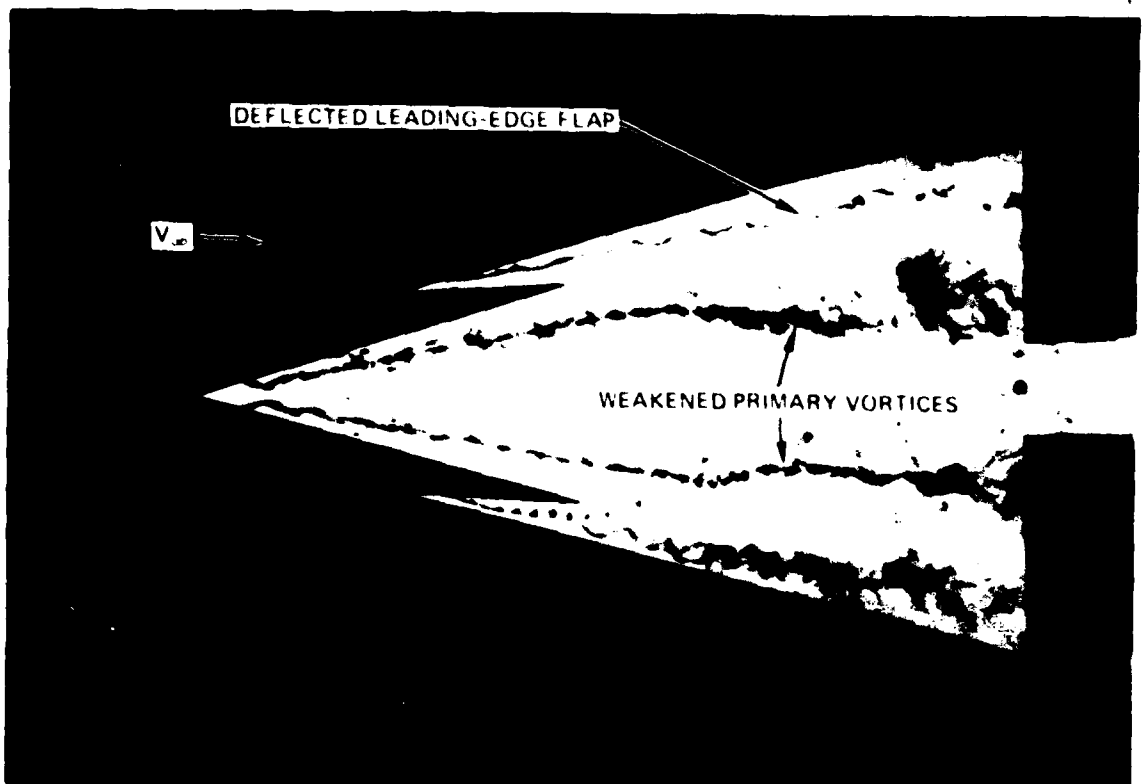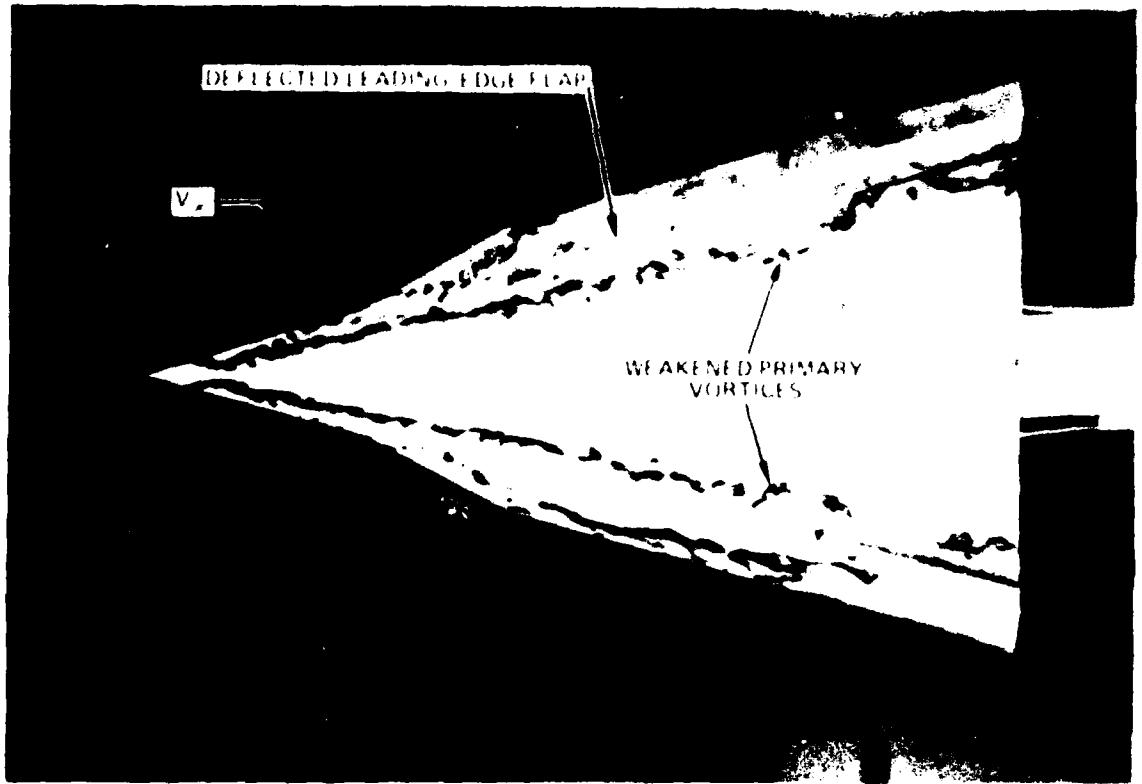
FIGURE 93. VORTEX FLOW ON SLENDER WINGS WITH CAMBER (NORTHROP WATER TUNNEL)

which occurs at high Reynolds number, the effects of a plain trailing-edge flap on vortex core trajectory and stability are not, in general, well-predicted, as shown by the limited available data in Figure 92. The adverse effect of a deflected trailing-edge flap on vortex stability is shown in a water tunnel, but the poor simulation of boundary layer separation characteristics "masks" the quantitative effect. Wind tunnel smoke flow studies of a fighter configuration with a LEX-wing geometry made in Reference 138 in the Northrop low-speed facility indicate that at low angles of attack (generally less than 10 degrees), the LEX vortex does not burst over the wing, as shown in Figure 94, and the vortex core exhibits a trajectory which conforms quite closely to the curvature of the wing (leading- and trailing-edge flaps are deflected). The vortex then continues downstream and can interact with other airframe components. However, at the same low angles of attack, the LEX vortex core in a water tunnel is influenced by the wake region produced by laminar separation from the rear portion of the wing. As shown in Figure 95, this alters the vortex path and also produces premature dissipation of the vortex due to entrainment of turbulent fluid from the separated wake. This discrepancy occurs on all wings, independent of sweep, at low angles of attack, unless steps are taken to simulate the correct boundary layer behavior by blowing or suction, for example. Special note will be made subsequently, however, of the improved agreement between water tunnel and wind tunnel results as (1) angle of attack is increased and (2) as wing sweep increases.

It can be seen, then, that at low angles of attack for flat-plate wings and for cambered wings or wings with blunt leading edges where flow separation does not occur at a salient edge, the results obtained in a water tunnel at low Reynolds number will not accurately simulate vortex sheet and core locations and vortex strength. For example, wind tunnel data obtained in Reference 140 at different Reynolds numbers on a

176

LEX VORTEX CORE

V_∞
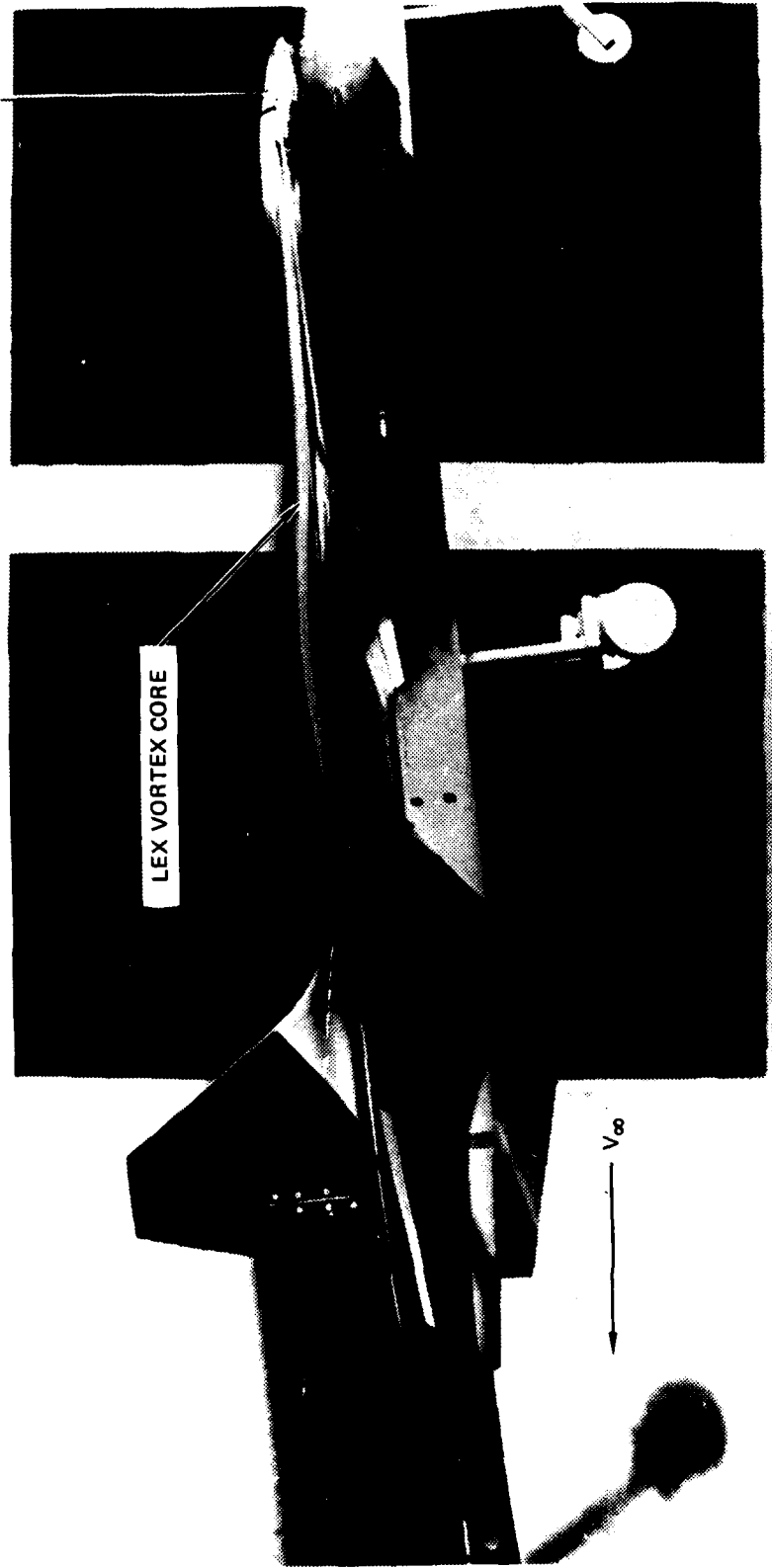
(a) SIDE VIEW — 6 DEGREES ANGLE OF ATTACK

FIGURE 94. NORTHROP WIND TUNNEL SMOKE FLOW VISUALIZATION OF A LEX VORTEX CORE AT LOW
ANGLE OF ATTACK (FROM REFERENCE 138)

LEX VORTEX CORE

V_∞
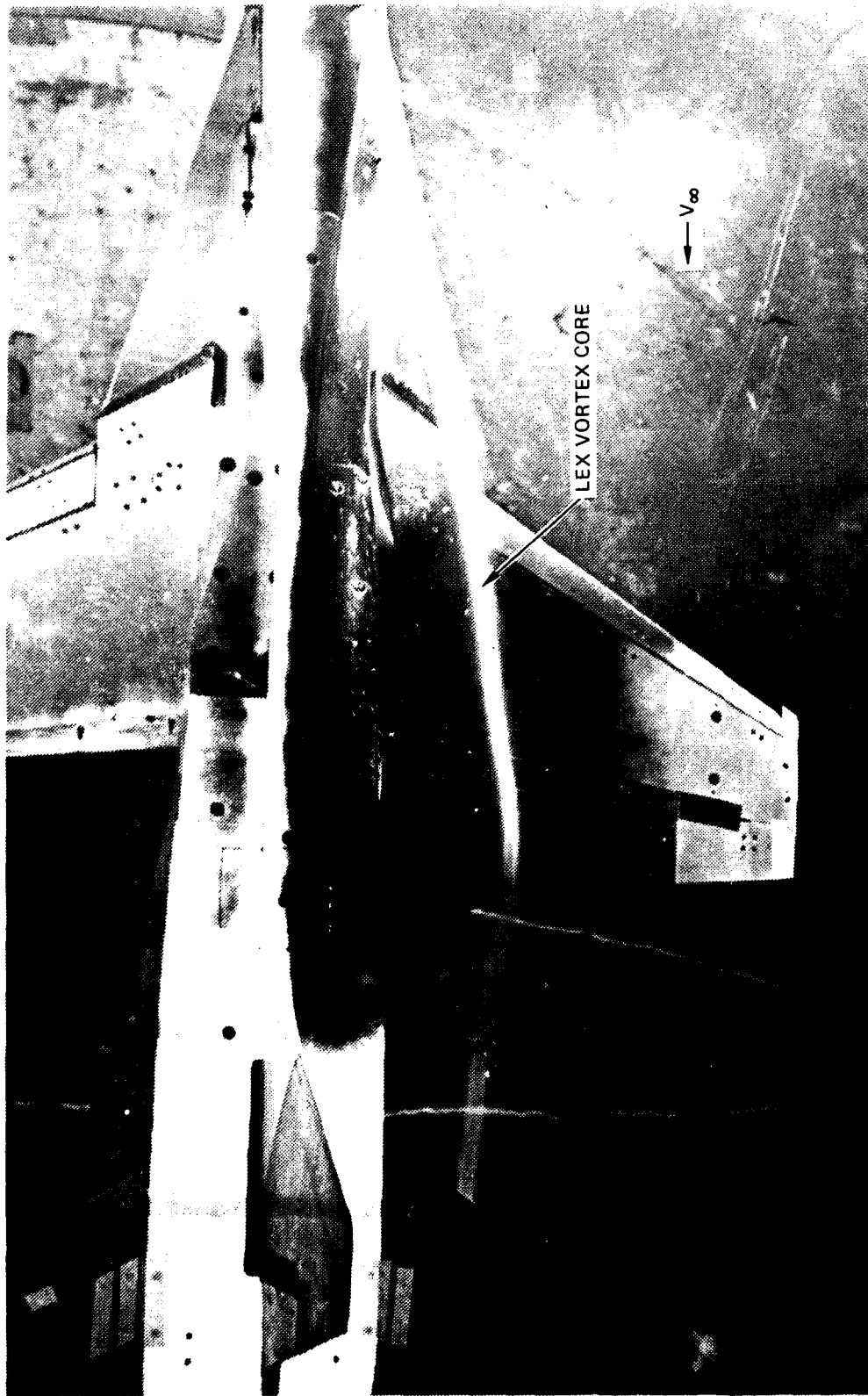
(b) PLANVIEW – 6 DEGREES ANGLE OF ATTACK

FIGURE 94. CONCLUDED

(c) CURRENT TWIN TAIL FIGHTER   8 DEGREES ANGLE OF ATTACK

FIGURE 95   NORTHROP WATER TUNNEL FLOW VISUALIZATION OF A LEX VORTEX CORE
AT LOW ANGLE OF ATTACK

$V_\infty \downarrow$

LEX VORTEX

PREMATURE
VORTEX
INSTABILITY
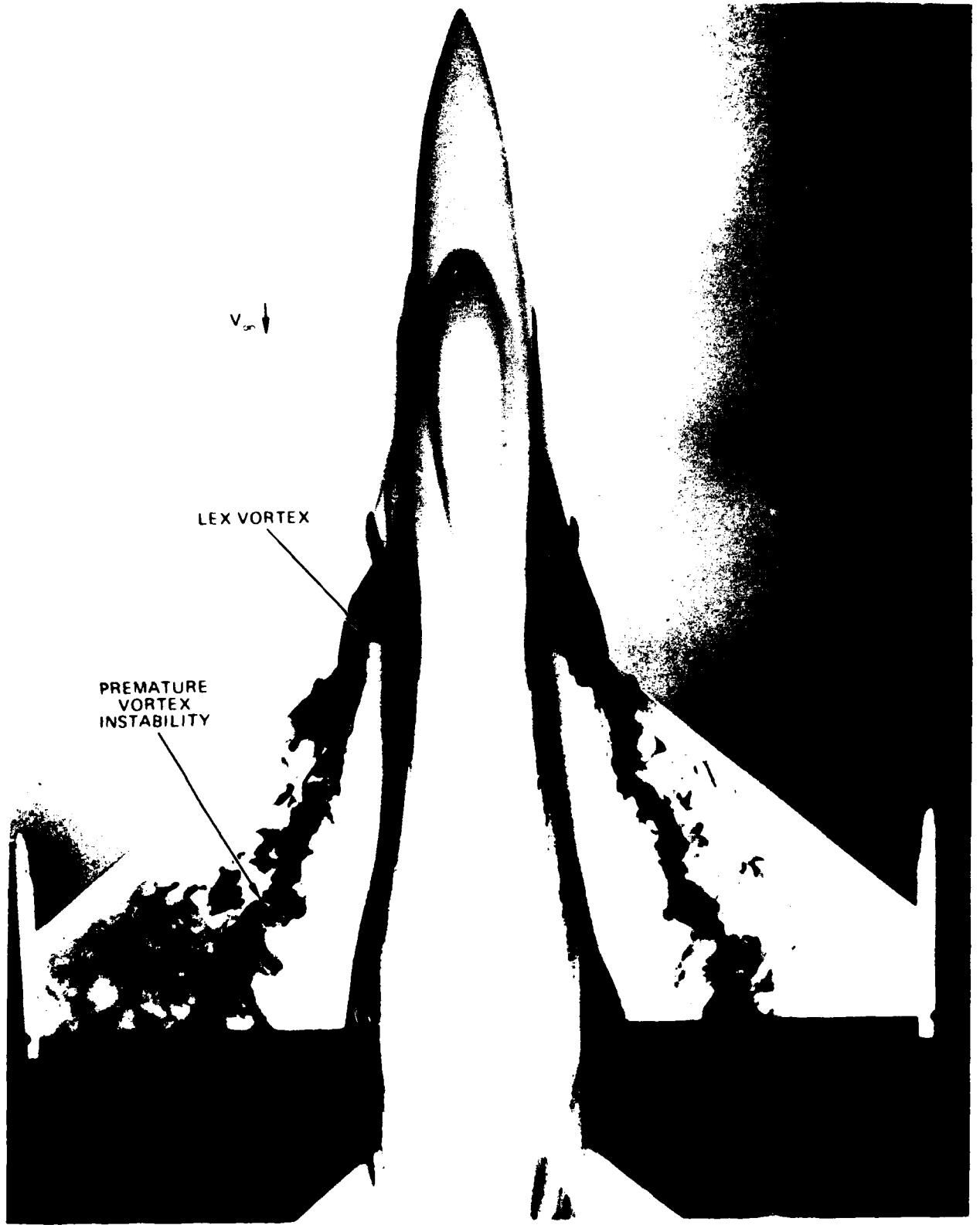
(b) CURRENT LIGHTWEIGHT FIGHTER – 8 DEGREES ANGLE OF ATTACK

FIGURE 95. CONCLUDED

180

60-degree cropped delta wing with blunt leading edge reveal
greatly increased lift at the low Reynolds number due to
early formation of a leading-edge vortex and, hence, develop-
ment of vortex-induced lift. In the case of blunt-nosed wings
or cambered wings, however, once the condition for which
separation occurs everywhere along the leading edge is reached,
it is considered that the fundamental character of the flow
will be quite similar to that observed at high Reynolds number.
(This was the justification for Northrop water tunnel studies
of the Space Shuttle Orbiter in Reference 131.) These comments
are pertinent to factor (1) above, that is, as angle of attack
increases, the strength of the vortex increases and the
vortex core path shifts upward and, thus, away from the separ-
ated boundary layer flow. For example, at angles of attack at
which breakdown of the vortex occurs forward of the wing
trailing edge, reasonably good correlations at all wing sweep
angles can be made (as evidenced by the agreement between
Northrop water tunnel data and wind tunnel measurements in
Reference 141 which cover a range of values of flat-plate,
delta wing sweep angle from 55 to 85 degrees). This is
presumably because the incorrect simulation of the flow near
the trailing edge is irrelevant. In other words, surface flows
at low angles of attack that are not yet vortex-dominated can
be more sensitive to Reynolds number effects. At high angles
of attack, the influence of the external pressure gradient on
the now vortex-dominated flow field is adequately represented
in a water tunnel.

Turning, now, to factor (2), as wing sweep is increased
(a) the pressure recovery near the trailing edge is reduced,
(b) surface flow patterns are better simulated, and (c) in-
creased angle of attack is required for core breakdown at
a given streamwise location. Reduced pressure rise near the
trailing edge affects vortex stability in that the core is
better able to penetrate the wing pressure field. This in turn

181

also reduces the tendency of the wing boundary layer to separate and, hence, results in better water tunnel simulation of the wing stall pattern. In other words, a "synergistic"-type effect occurs. Since higher angles of attack can be attained before core bursting is precipitated, vortex core entrainment of turbulent fluid due to interaction with the separated boundary layer is alleviated and, consequently, on a slender wing, vortex core trajectory, including interaction with downstream tail surfaces, and vortex stability can be well-represented in a water tunnel. For example, a flat-plate 75-degree delta wing requires an angle of attack of about 30 degrees for vortex bursting near the trailing edge. At angles of attack below this value, a stable core can be observed to stream past the trailing edge, as shown in Figure 96, and interact with downstream tail surfaces, for example. The importance on vortex stability of displacing the vortex above the wing boundary layer has been visualized in a water tunnel on an advanced fighter where, in sideslip conditions, the leeward LEX vortex core is displaced away from the wing surface relative to the zero-sideslip condition and has been observed to maintain its stability to a distance far downstream, at particular values of angle of attack, as illustrated in Figure 97. (At zero sideslip, the core exhibits premature instability and subsequent breakdown prior to reaching the trailing edge.)

LEX-Wing Geometries

The coupling of a low aspect ratio lifting surface with a moderate-to-high aspect ratio main wing panel (depicted in the flight photographs in Figures 98 and 99) poses an intriguing problem to water tunnel simulation. Figure 100 presents wind tunnel oil flow patterns on a LEX-wing fighter geometry at low, moderate, and high angles of attack. Care must be exercised at low angles of attack in a water tunnel due

LEADING-EDGE VORTEX CORE

WING TRAILING EDGE

V_8

FIGURE 96. STABLE VORTEX CORE OVER A SLENDER WING (NORTHROP WATER TUNNEL)

183
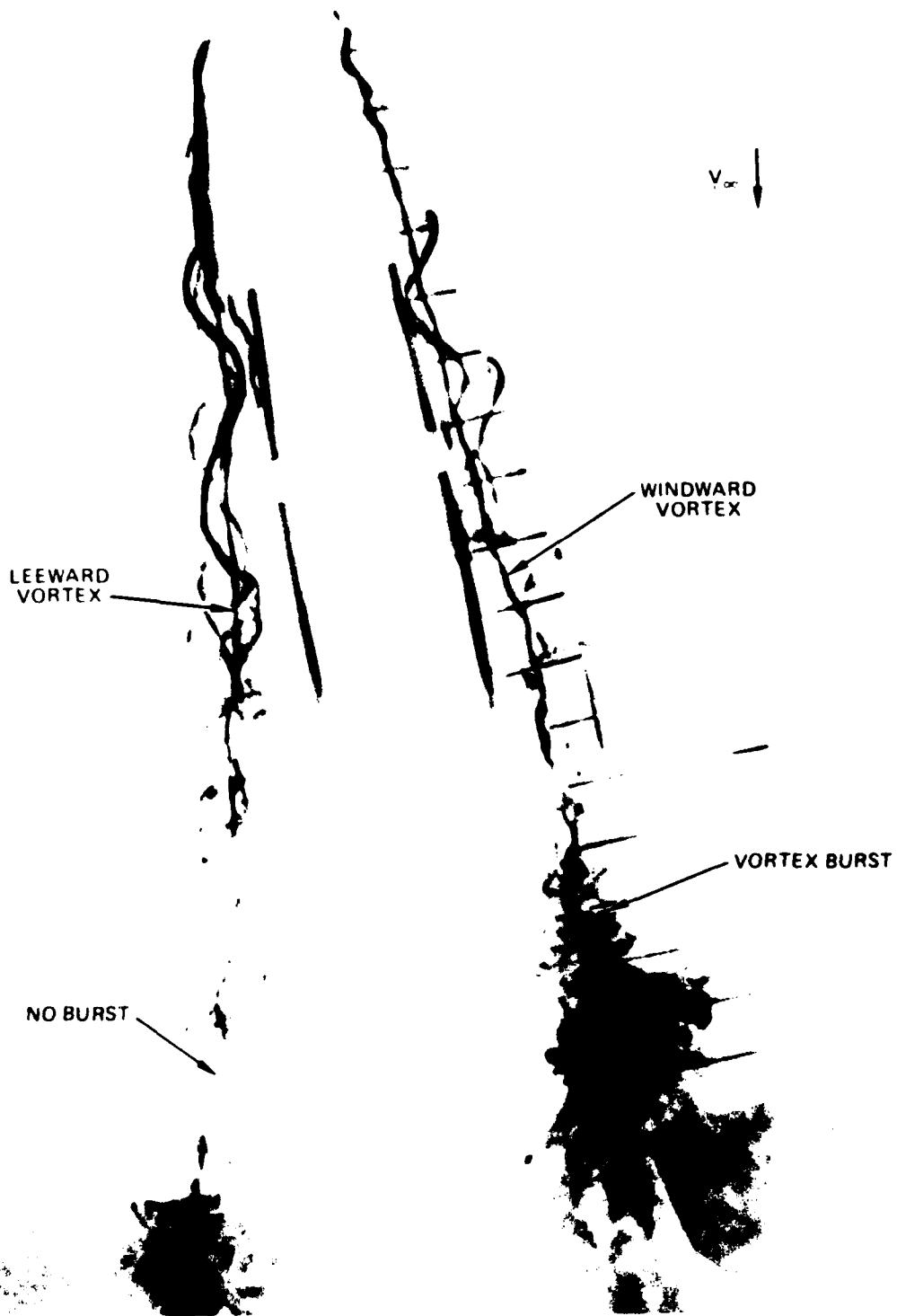
FIGURE 97. DISPLACEMENT OF LEEWARD VORTEX CORE AWAY FROM WING SURFACE DUE TO SIDESLIP (NORTHROP WATER TUNNEL)
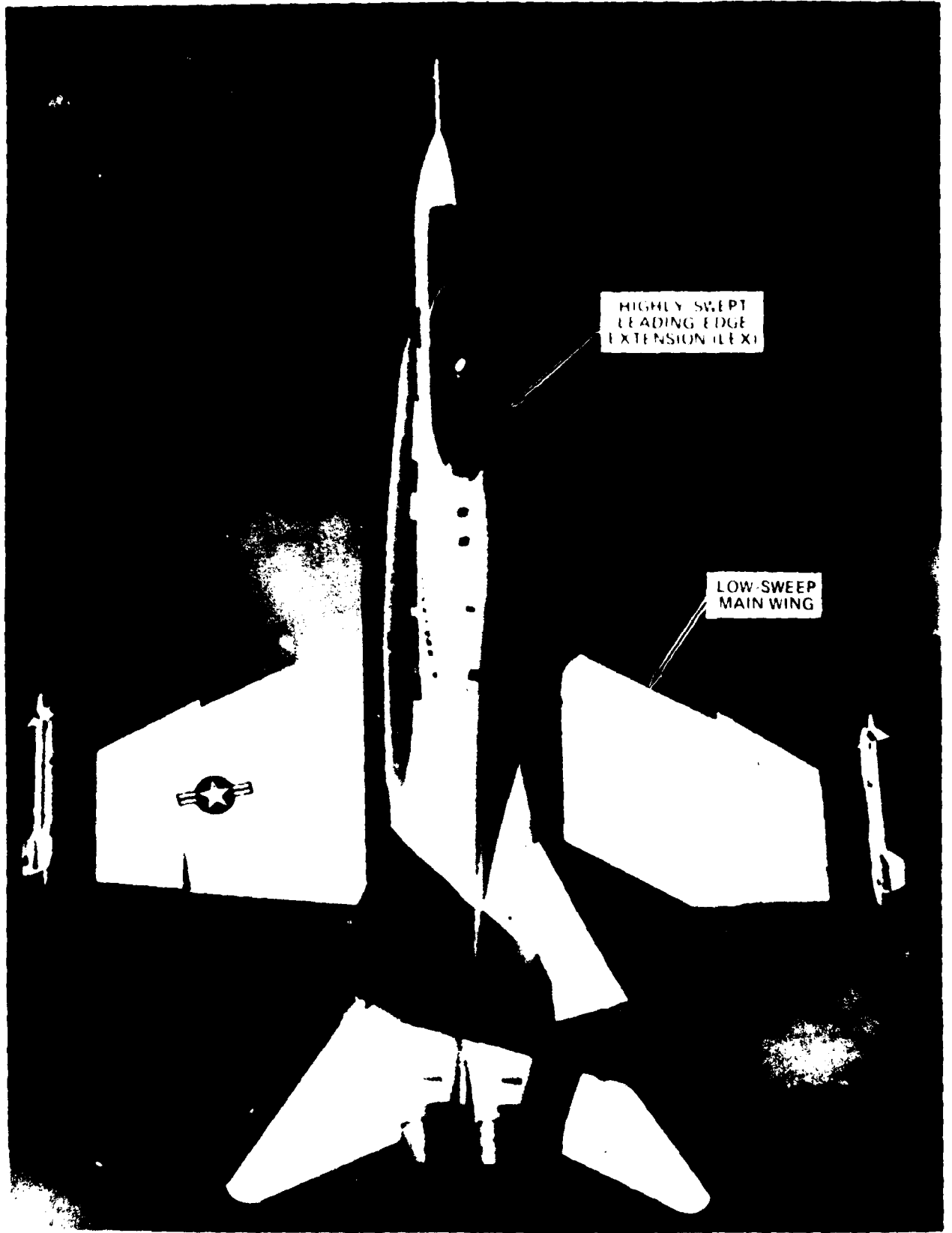
FIGURE 98. HYBRID WING (WING-LEX) GEOMETRY

FIGURE 99. HYBRID WING (WING-LEX) GEOMETRY

HIGHLY SWEPT
LEADING EDGE
EXTENSION

LOW SWEPT
MAIN WING

(a) 6 DEGREES ANGLE OF ATTACK

FIGURE 100. NORTHROP WIND TUNNEL SURFACE OIL FLOW PATTERNS ON THE NORTHROP YF-17

(b) 18 DEGREES ANGLE OF ATTACK

FIGURE 100. CONTINUED
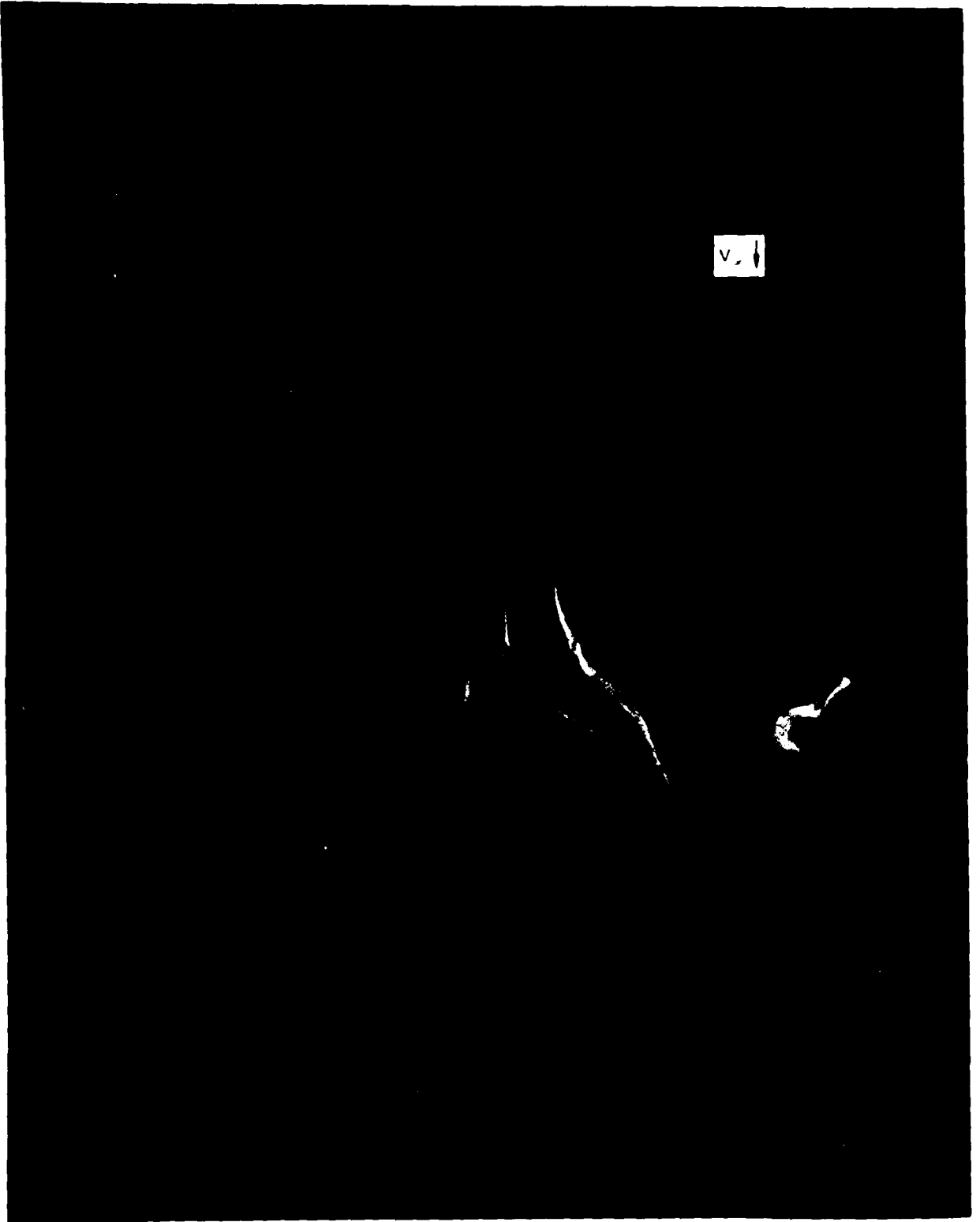
(c) 25 DEGREES ANGLE OF ATTACK

FIGURE 100. CONTINUED
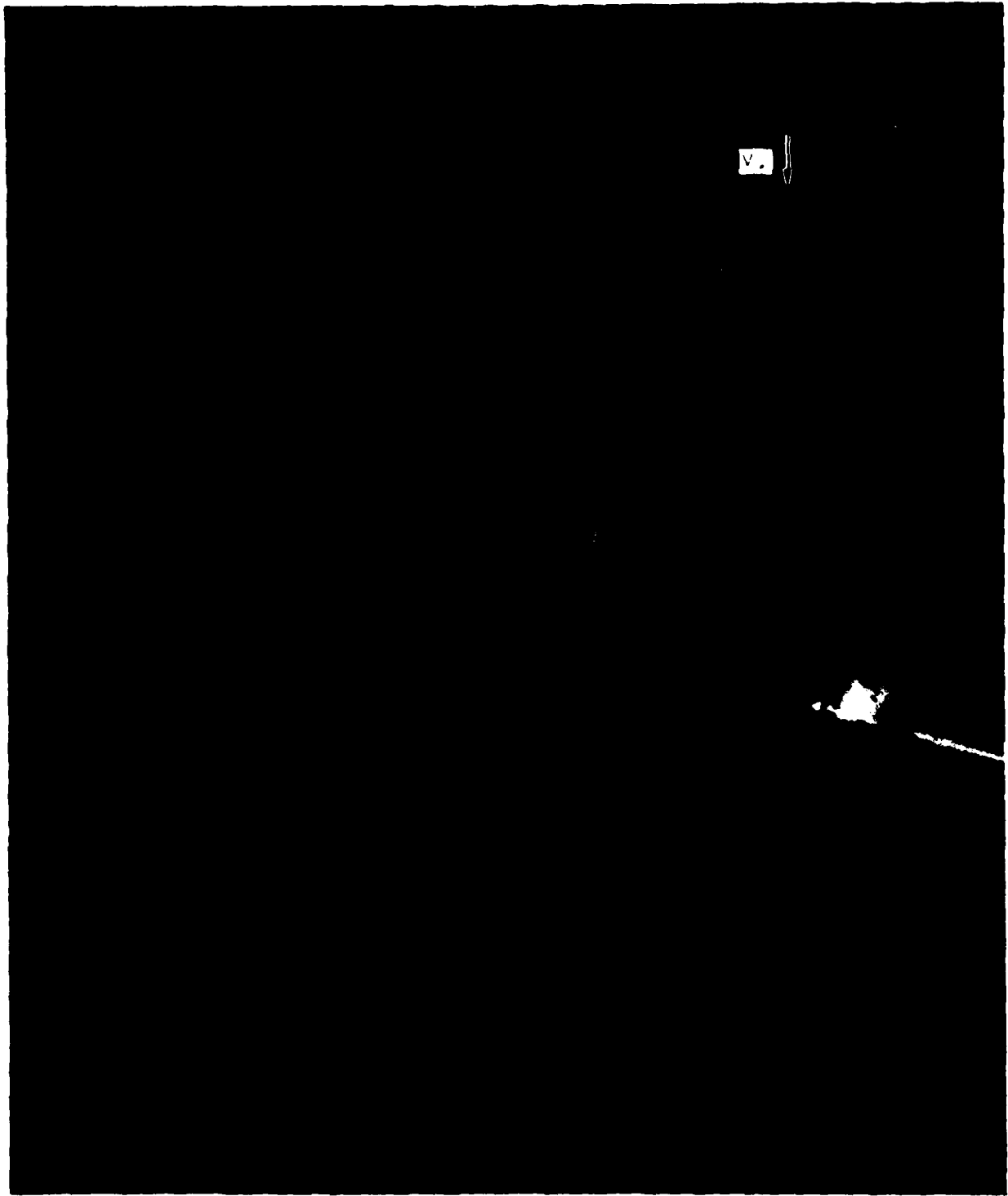
d. 65 DEGREES ANGLE OF ATTACK

FIGURE 100 CONCLUDED

to the laminar separation characteristics near the rear portion of the main wing, which is not evident in the wind tunnel surface flow patterns, that influence the stability of the LEX vortex. As angle of attack increases, the vortex increases in size, the core centerline shifts upwards from the wing and breakdown of the core flow occurs, as can be inferred from the wind tunnel oil flow results. Under these conditions, the water tunnel results are quite representative of the wind tunnel results. For example, the F-5F LEX vortex core behavior observed in the water tunnel, shown in Figure 101, is unrepresentative at low angles of attack but corresponds quite well to the lift and pitching moment trends at high angles of attack in a wind tunnel.

Due to the main wing pressure field, breakdown of the LEX (or forward wing on a double delta-type planform) vortex *breakdown is promoted* at a lower angle of attack relative to the LEX-alone case (see Figure 102). It should be noted, however, that on LEX-wing geometries, the vortex shed from a <u>large</u> LEX exhibits increased stability relative to a small LEX of the same planform at fixed angle of attack and, as a result, a discrete vortex core from a large LEX can in many cases be observed aft of the wing trailing edge even at low angles of attack, as shown in Figure 103. There is, however, a critical angle of attack below which the LEX vortex core in a water tunnel will exhibit premature instability as the relatively weak vortex entrains disproportionately more turbulent fluid from the separated boundary layer. This angle is dependent on: LEX size, LEX sweep, and main wing panel leading edge sweep, among other factors. In general, as main wing sweep angle increases, for a LEX of fixed size and geometry, the critical angle of attack below which vortex core-boundary layer interaction precludes simulation is reduced.

The induced upwash near the LEX-wing junction and favorable sidewash induced by the LEX vortex on the main wing

191

VORTEX BREAKDOWN

α 9°   α 11°   α 13°

α 15°   α 17°   α 19°

α 21°   α 23°   α 26°
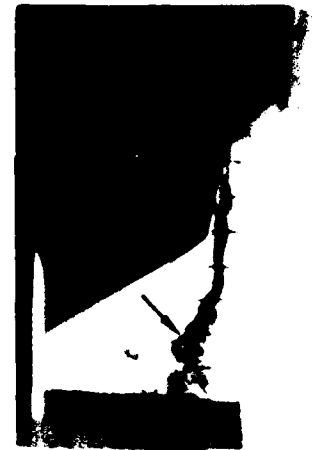
(a) PLANVIEW

FIGURE 101. NORTHROP WATER TUNNEL FLOW VISUALIZATION OF THE NORTHROP F-5F LEX VORTEX (INLETS BLOCKED)

9°   11°   13°

15°   17°   19°
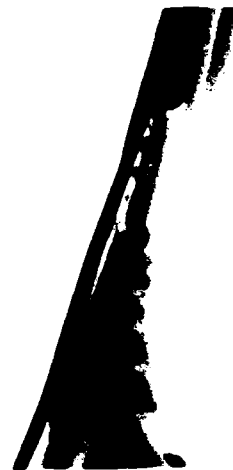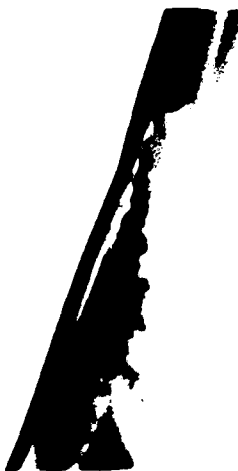
(b) SIDEVIEW

FIGURE 101 CONCLUDED
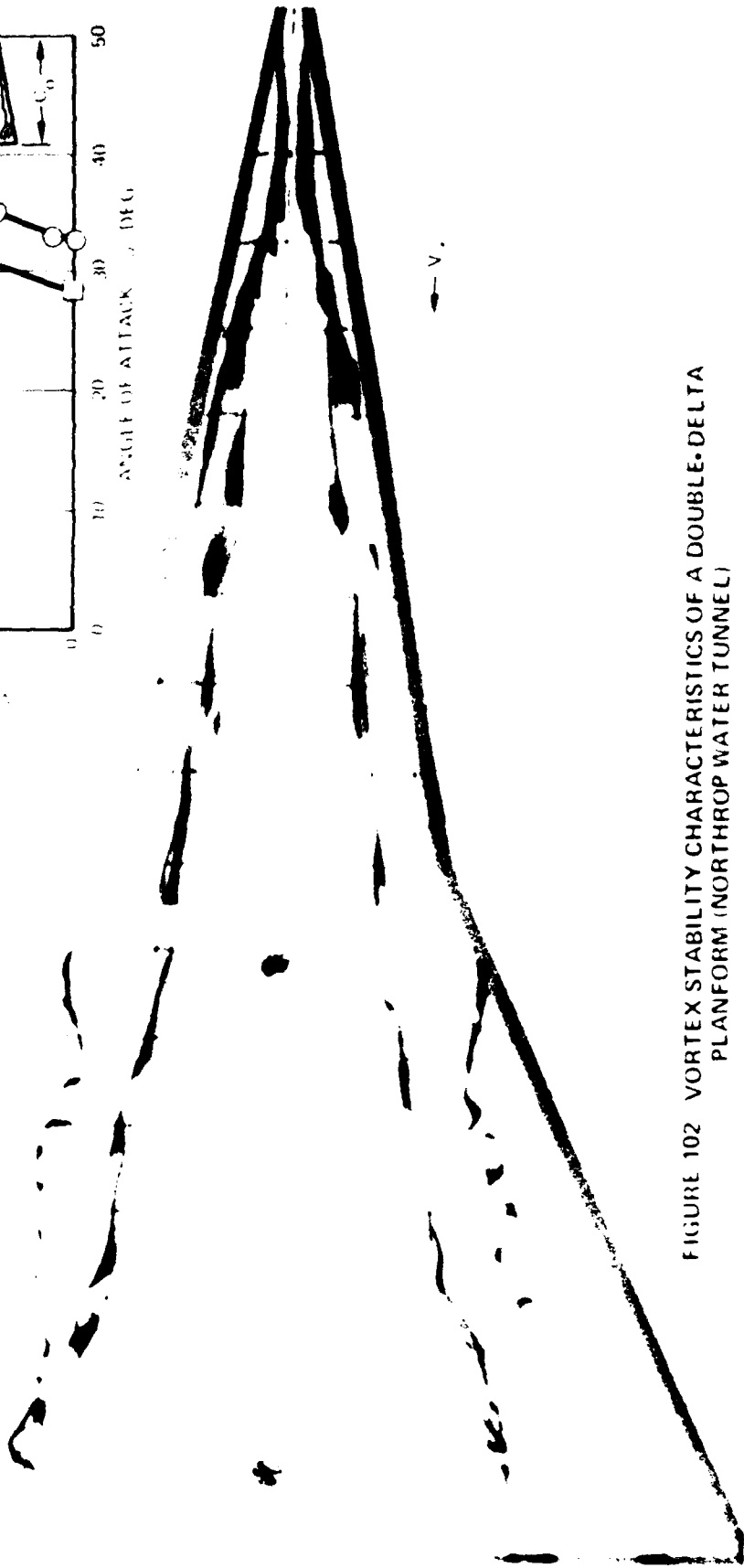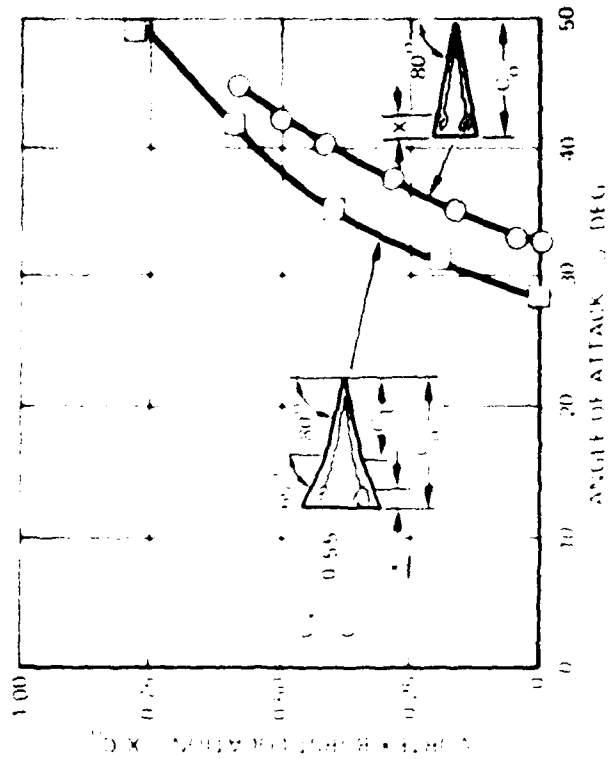
FIGURE 102 VORTEX STABILITY CHARACTERISTICS OF A DOUBLE-DELTA PLANFORM (NORTHROP WATER TUNNEL)

LEX VORTEX CORE

V, →

LEX VORTEX CORE

V, →
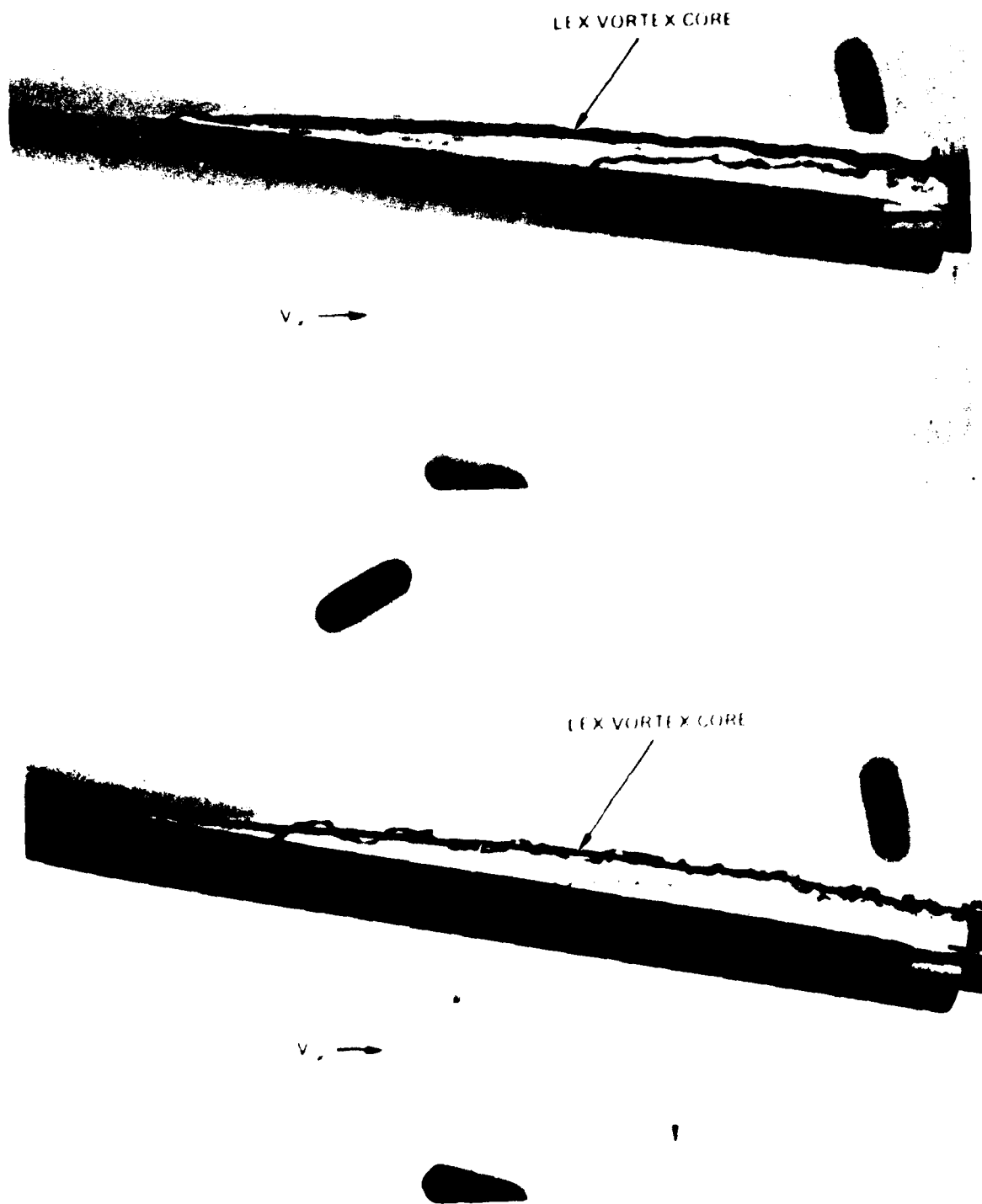
FIGURE 103 VORTEX FLOW SHED FROM A LARGE LEX AT LOW ANGLE OF ATTACK
(NORTHROP WATER TUNNEL)
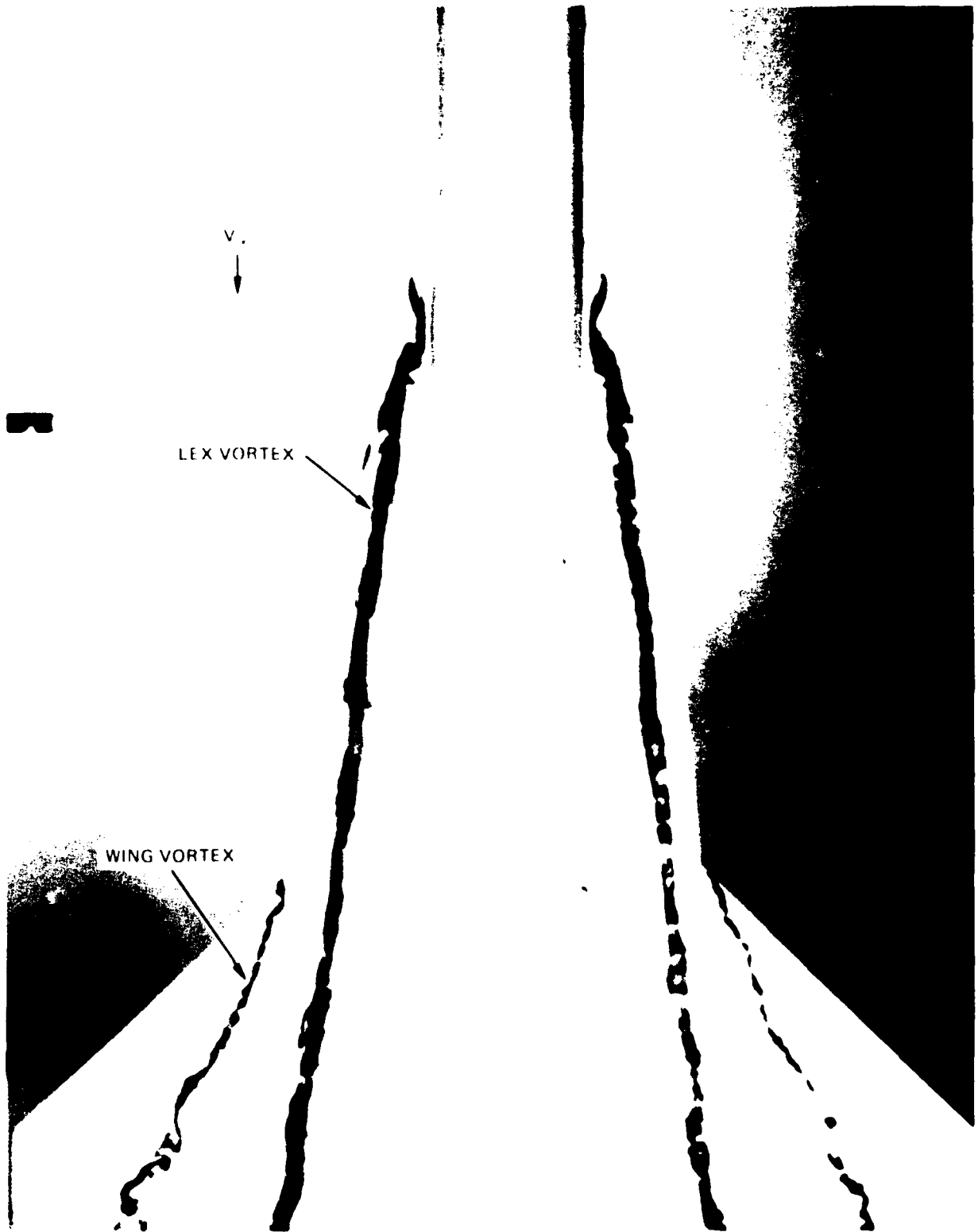
(a) GOTHIC LEX – PLANVIEW

FIGURE 104. LEX VORTEX-INDUCED EFFECT ON MAIN WING PANEL
(NORTHROP WATER TUNNEL)

WING VORTEX

LEX VORTEX

(b) GOTHIC LEX   SIDEVIEW

FIGURE 104. CONTINUED
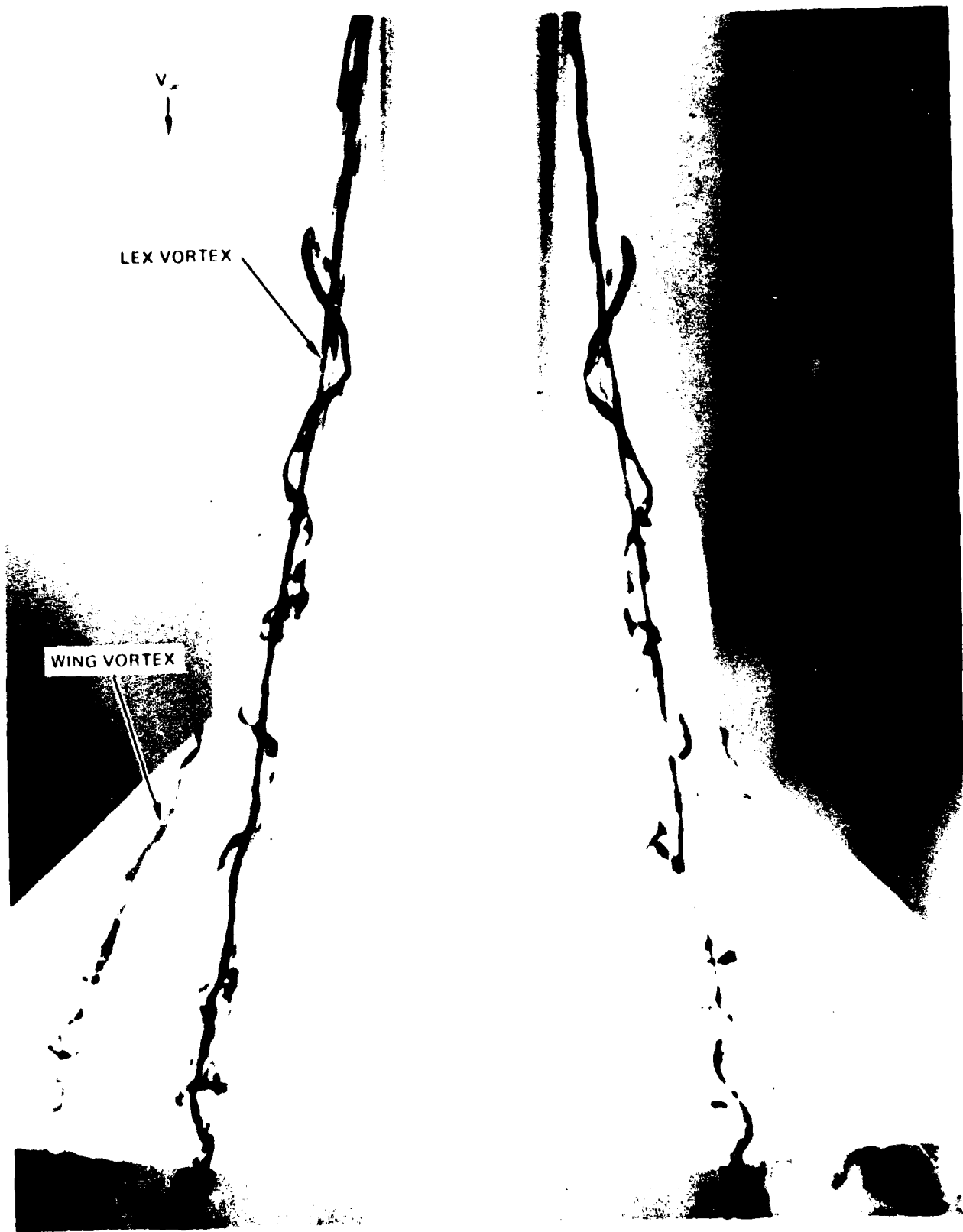
(c) REFLEXIVE LEX - PLANVIEW

FIGURE 104. CONCLUDED

panel can result in the development of a concentrated wing vortex, as shown in the water tunnel photographs in Figure 104. Excellent quantitative agreement is obtained between water tunnel and wind tunnel results regarding this induced effect on thin, sharp-edged wings as can be seen in Figure 105, where the wing vortex centerline location in the wind tunnel is ascertained by chordwise suction peaks at several spanwise locations (see Reference 142). A synergistic effect occurs on LEX-wing geometries, as described in Reference 143, due to the development of a discrete wing vortex in the presence of the LEX vortex. It seems reasonable, then, that the LEX vortex would be better able to penetrate the wing pressure field under these conditions. The critical angle of attack in the water tunnel on the fighter configuration shown previously in Figure 95 which has a wing leading-edge sweep of 26 degrees is higher than the critical angle observed on the configuration in Figure 104 having a wing sweep of 44 degrees since, on the latter, a vortex generated from a LEX of given size can more easily traverse the wing flow field.

The above discussion is relevant to the study of wing leading-edge discontinuities, snags, lower surface fences, etc. which have been shown in various investigations (see Reference 144) to generate concentrated vortices. Due to the relatively small size of these vortex-generating devices, however, difficulties have been encountered in water tunnel studies where a strong interaction occurs between the separated wing boundary layer and the vortical motions. These results indicate, then, the importance of the scale of the vortical motions relative to boundary layer thickness.

Canard-Wing Configurations

Closely-coupled canard-wing arrangements (Figure 106) require special consideration. Most canards feature leading-edge sweep angles in the 50-60 degree range. Such planforms

WATER TUNNEL

V_∞ ↓

$R_e = 2 \times 10^4$

WIND TUNNEL

$R_e = 1 \times 10^4$

WING VORTEX

WING FUSELAGE JUNCTION

WING LEX JUNCTION

DETERMINED FROM PEAK
PRESSURES (REFERENCE 14)
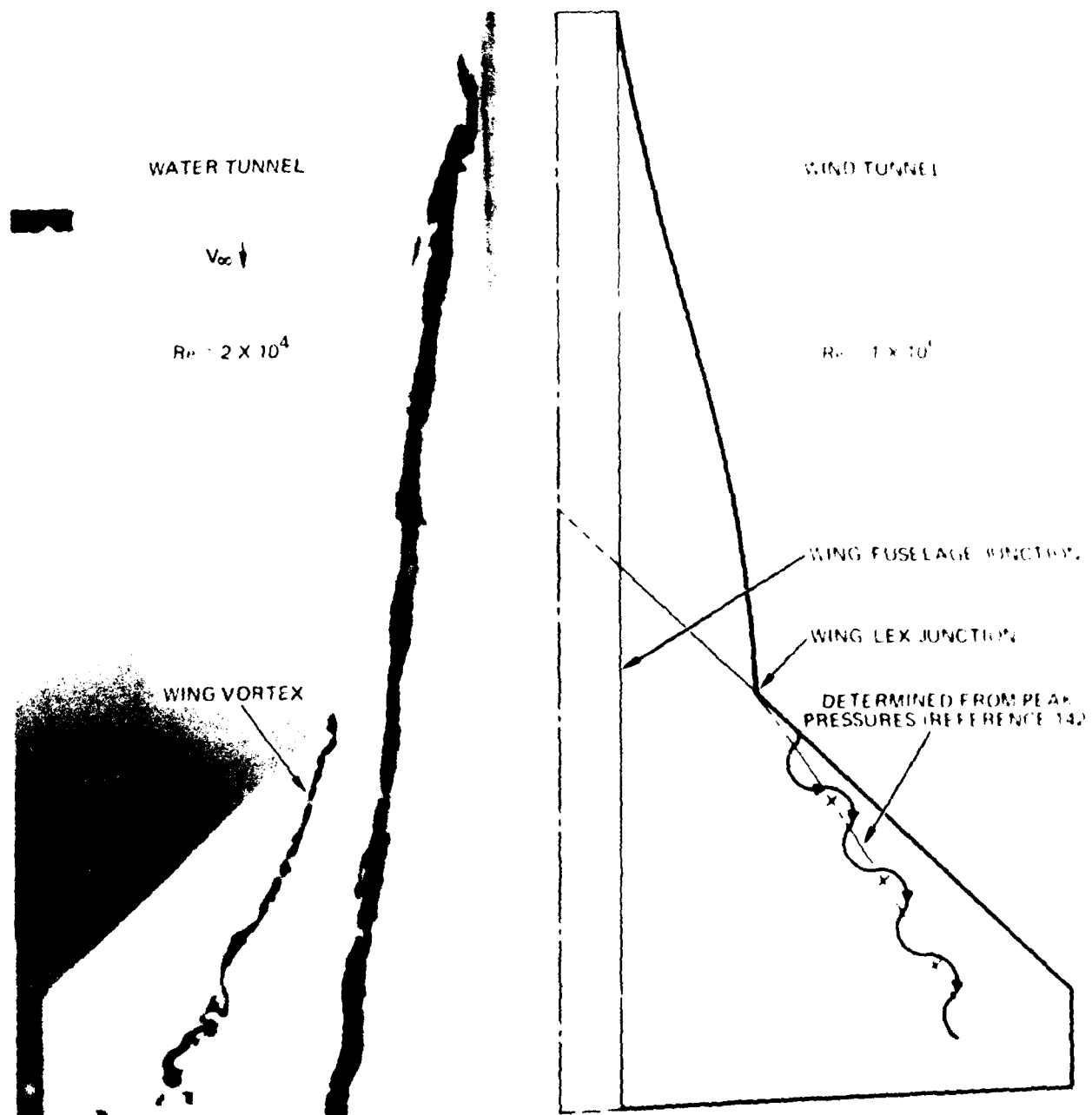
FIGURE 105. COMPARISON OF WATER TUNNEL AND WIND TUNNEL
MAIN WING PANEL VORTEX CENTERLINE LOCATION
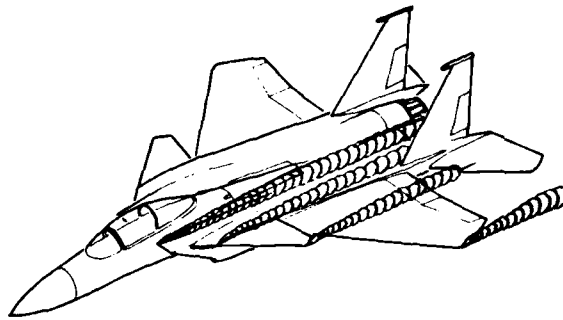
(a) VORTEX FORMATION AT LOW ANGLE OF ATTACK.
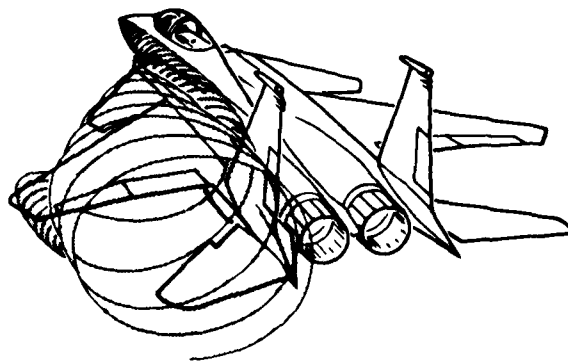
(b) VORTEX INTERACTIONS AT HIGH ANGLE OF ATTACK.

FIGURE 106. SKETCH OF CANARD – WING VORTEX FLOWS AT LOW AND HIGH
ANGLES OF ATTACK. (FROM REFERENCE 145).

develop much less vortex lift than a highly-swept LEX and, according to Northrop water tunnel data, vortex breakdown over wings of such sweep occurs at angles of attack of about 12 degrees or less. Even in the wind tunnel, it has proved difficult to assess the core structure on a wing of 55-degree sweep at low angles using a Schlieren system due to the very low density gradients (see Reference 141). Figure 107 (from Reference 146) indicates that for delta wings of aspect ratio 2.0 or greater, the percentage of vortex lift relative to total lift becomes quite small.

This suggests that the instability at low attitudes due to canard vortex core-boundary layer interaction and the lack of a discrete canard vortex passing over a trailing surface may also occur at Reynolds numbers typical of wind tunnel tests and, consequently, the water tunnel results may not be totally unrepresentative. Water tunnel studies of slender canards (70-degree sweep or greater) do reveal a concentrated vortex passing over a trailing lifting surface as shown in Figure 108.

At higher angles of attack, the water tunnel provides excellent insight into the effects of the canard downwash on the wing flow field; for example, the delay of vortex formation on the wing, the enhancement of the wing leading-edge vortex (once a vortex is formed), and the spanwise variation of the origin of the wing vortex with increased angle of attack in the presence of the canard surface, as was demonstrated in Northrop water tunnel studies of the HiMAT RPRV in Reference 147 and on the Swedish JAKT VIGGEN, illustrated in Figure 109. The latter water tunnel photograph depicts a concentrated wing vortex in the presence of a canard at an angle of attack of 30 degrees, well beyond the angle of attack for wing-alone stall.
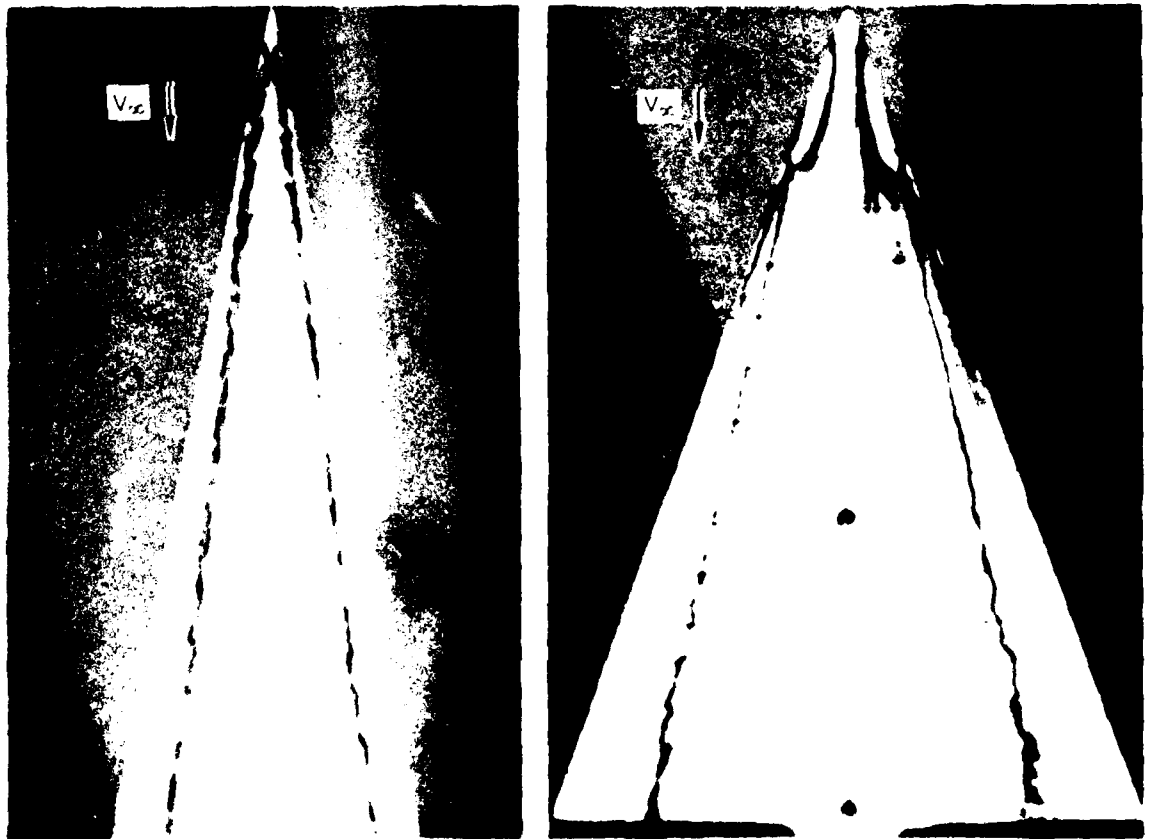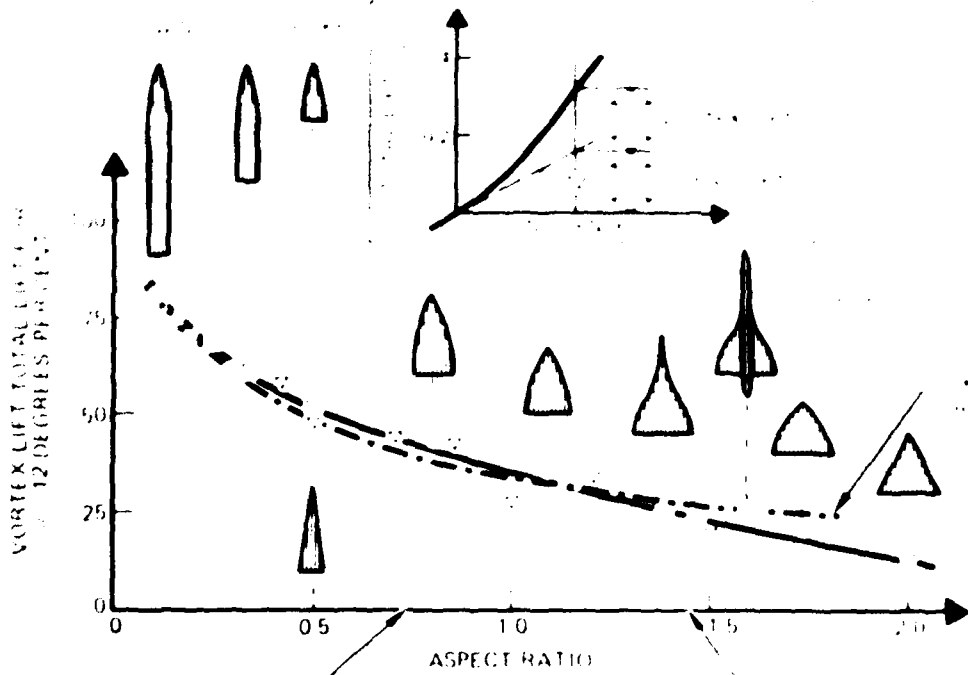
FIGURE 107 PERCENTAGE OF VORTEX LIFT TO TOTAL LIFT FOR WINGS
OF VARIOUS ASPECT RATIO FROM REF 146
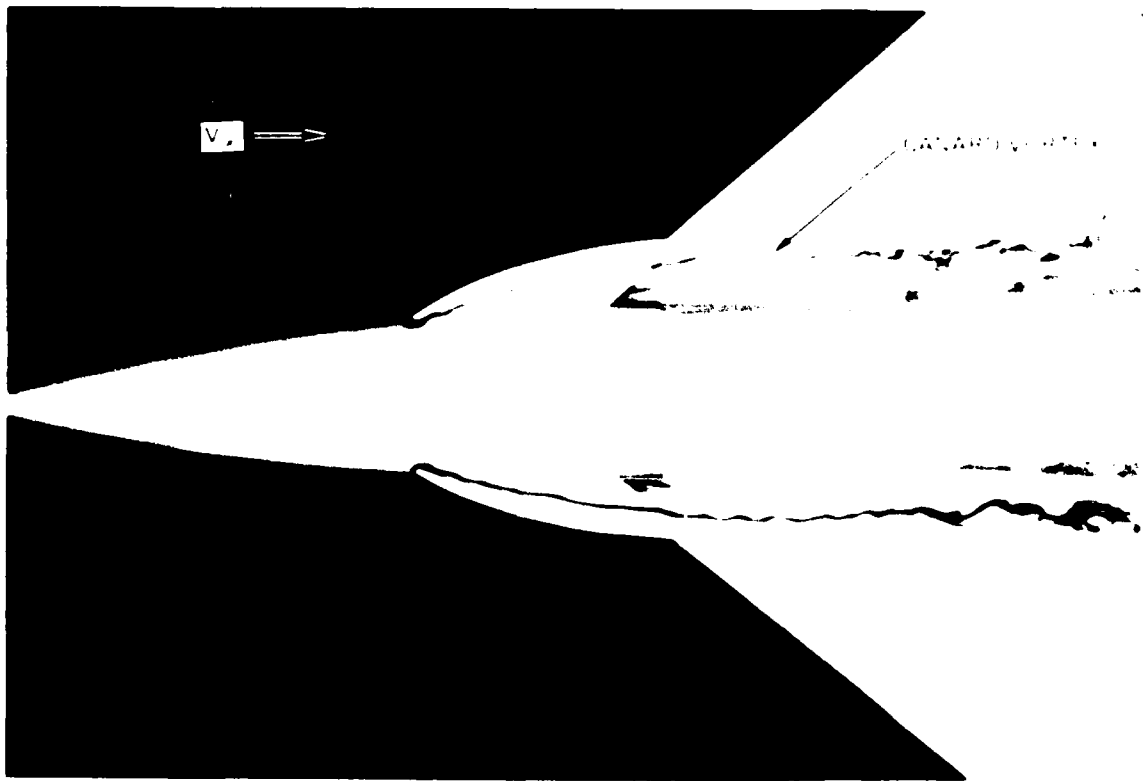
FIGURE 108. CONCENTRATED VORTEX SHED FROM A SLENDER CANARD AT 15 DEGREES ANGLE OF ATTACK (NORTHROP WATER TUNNEL)
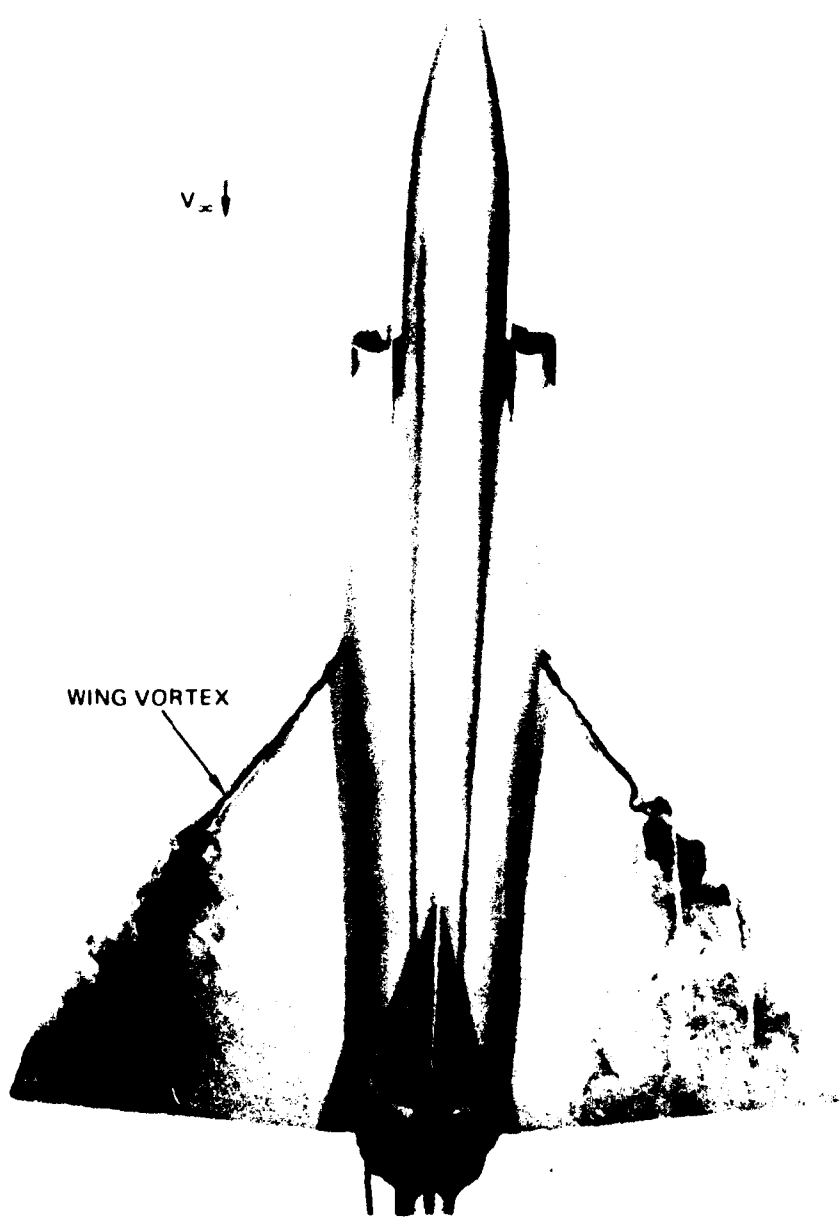
FIGURE 109. FLOW VISUALIZATION OF WING VORTEX ON THE SAAB-VIGGEN CANARD-WING
AIRCRAFT CONFIGURATION AT 30 DEGREES ANGLE OF ATTACK
(NORTHROP WATER TUNNEL)

General Guidelines

Guidelines concerning leading-edge vortex flow simulation on flat-wing and cambered lifting surfaces with sharp or blunt leading edges in a water tunnel have thus emerged. The <u>first guideline</u> concerns vortex behavior at <u>high angles of attack:</u> Once the flowfield becomes vortex-dominated and flow separation has occurred everywhere along the leading edge, the fundamental character of the flow field and, hence, vortex behavior are adequately simulated in a low-Reynolds-number water tunnel. This is also applicable to multiple lifting surface arrangements such as closely-coupled canard-wing geometries and their subsequent interactions. The <u>second guideline</u> pertains to vortex behavior at <u>low angles of attack.</u> Wing surface flows that are not yet vortex-dominated and wing geometries on which leading-edge separation does not occur simultaneously along the entire span are subject to relatively significant Reynolds number effects. Interaction of the vortex core with the wake region produced by laminar boundary layer separation on wing geometries which feature leading-edge separation point degree of freedom (which affects the wing wake size and structure) produce vortex flow characteristics that can at best be viewed in a qualitative sense.

5.2.2 <u>Representative Water Tunnel Studies of Leading-Edge Vortex Flows</u>

The following examples of vortex flow studies in the Northrop Water Tunnel provide <u>qualitative and quantitative</u> correlations with subsonic wind tunnel results.

<u>Lift Characteristics of Slender Wings</u>

A nonlinear variation of lift with angle of attack is evident on highly-swept planforms which can be attributed to

the development of leading-edge vortices, the strength of which increases with angle of attack. This vortex-induced lift effect is illustrated in Figure 110, where the low-speed wind tunnel data for 70-, 78-, and 80-degree delta wings are taken from Reference 117. Corresponding angles of attack for vortex breakdown at the wing trailing edge, α_{BD-TE} (see Figure 111), determined in the water tunnel, are also shown. For the 70-degree delta wing, α_{BD-TE} = 23 degrees correlates with an initial reduction in lift-curve slope. For the more highly-swept wings (78- and 80-degrees)a lift-curve slope reduction is evident despite the lack of vortex burst over the wing. This effect can be attributed to streamwise bending of the vortex core (nonlinear variation of core height above the wing) near the trailing edge as shown in Figure 112 and vortex contact (Reference 56), where the proximity of the vortex cores to each other results in a symmetric displacement of the cores above the wing. Development of maximum lift on the very highly-swept wings occurs at approximately the angle of attack for vortex breakdown at the trailing edge. When vortex burst occurs over the wing, the effect on lift is more significant the greater the sweep angle, due to the higher percentage of the nonlinear vortex lift relative to overall wing lift (see Figure 107).

Lateral Stability Characteristics of Slender Wings

The degree of vortex breakdown asymmetry in sideslip observed in a water tunnel, as depicted in Figure 113, correlates with lateral instabilities measured in wind tunnel tests of delta wings in Reference 117, as illustrated in Figure 114. Initial reduction in the slope of the effective dihedral parameter (C_{l_β}) versus angle of attack curve corresponds reasonably well with initial vortex breakdown asymmetry. Degree of asymmetry, $\Delta(x/c_o)$, is determined by the difference in burst location over the wing between windward and leeward sides, where burst location is measured from the wing trailing
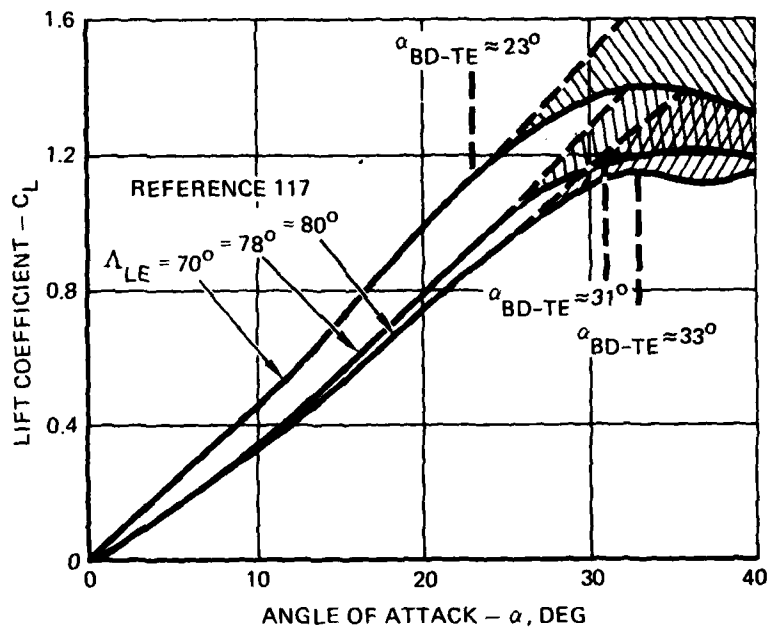
A) NONLINEAR VORTEX – INDUCED LIFT
EFFECTS – DELTA WINGS
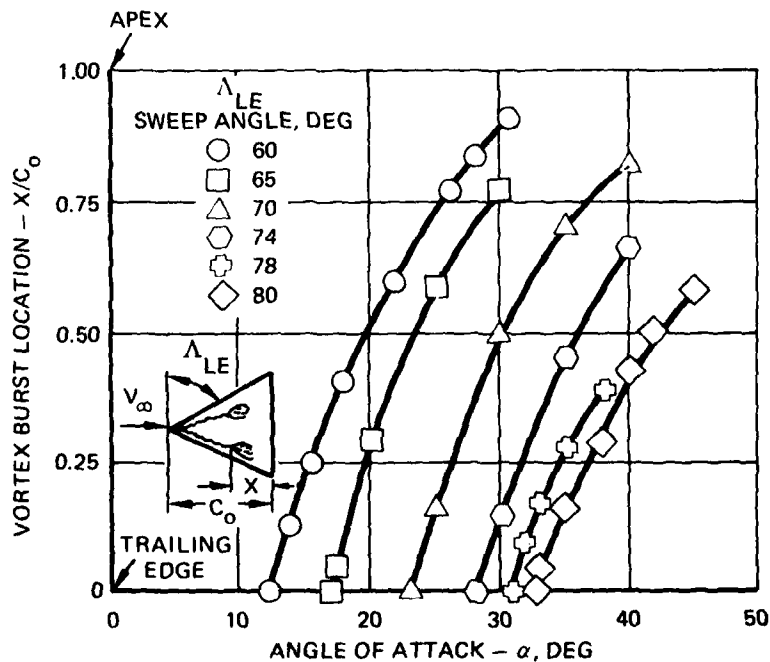
(B) WING SWEEP AND ANGLE OF ATTACK
EFFECTS ON VORTEX STABILITY

FIGURE 110   DELTA WING LIFT CHARACTERISTICS
AND CORRELATION WITH VORTEX
STABILITY CHARACTERISTICS

208
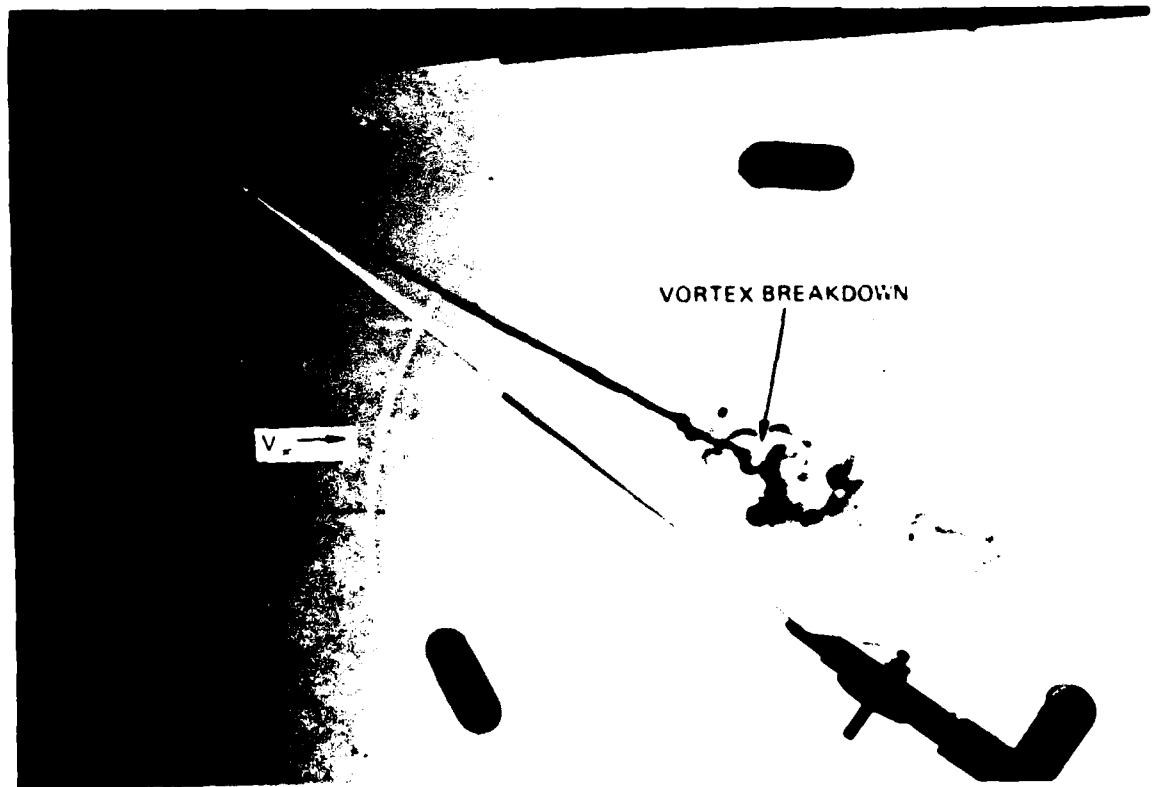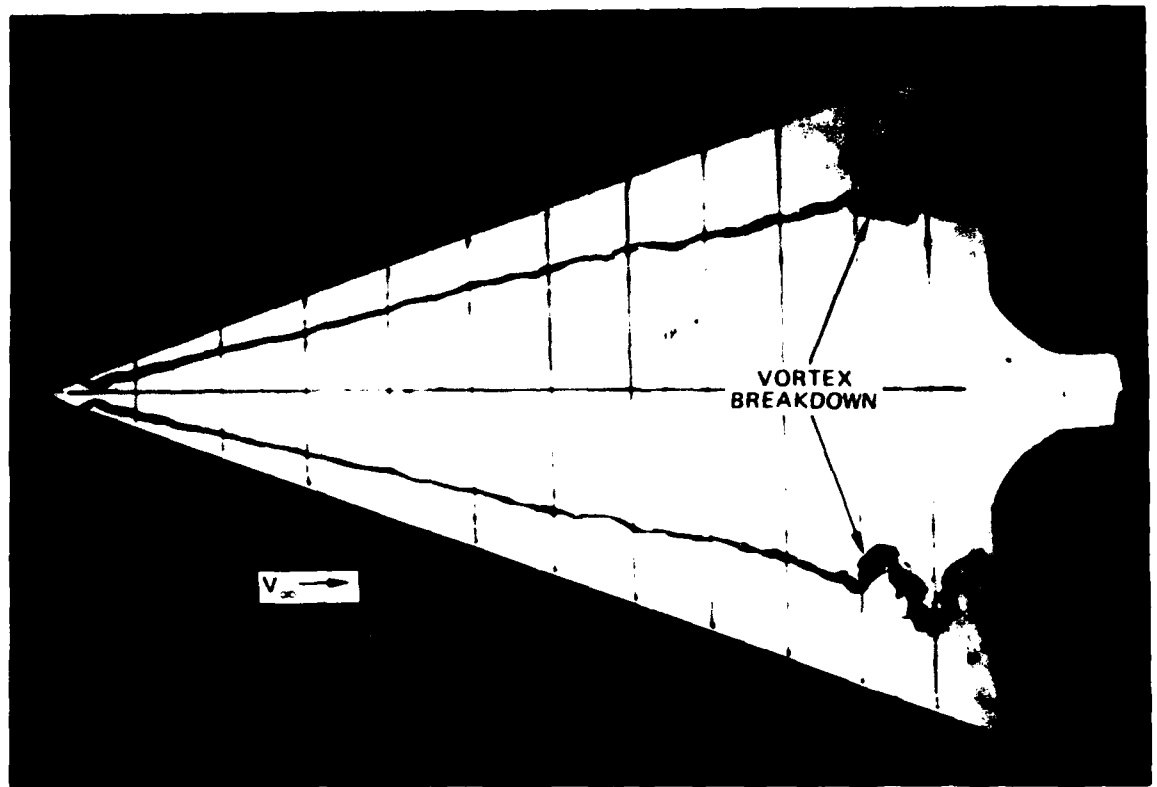
FIGURE 111. VORTEX BREAKDOWN PHENOMENON ON SLENDER DELTA WINGS (NORTHROP WATER TUNNEL)
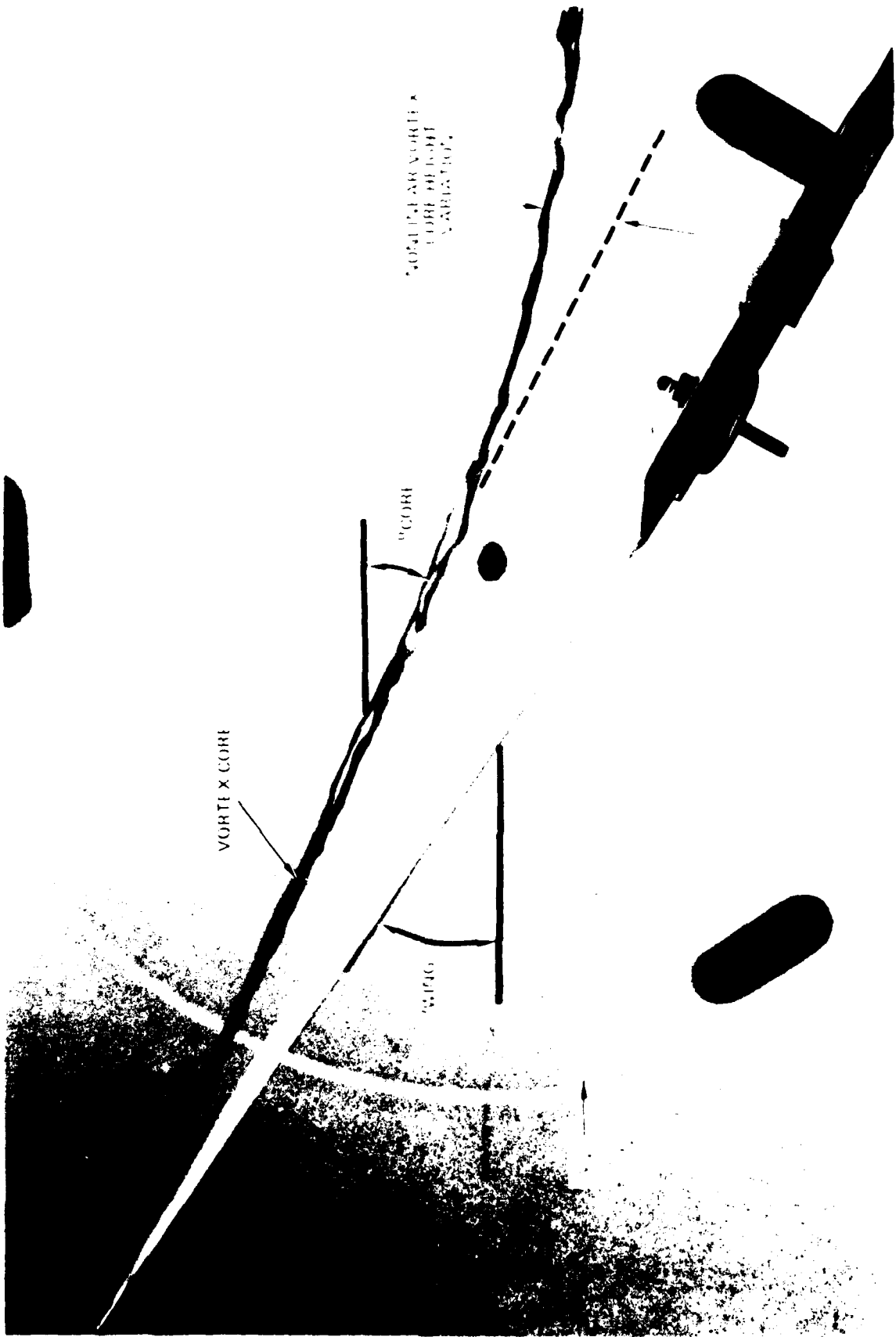
FIGURE 112 VORTEX CORE TRAJECTORY ON A SLENDER WING (NORTHROP WATER TUNNEL)
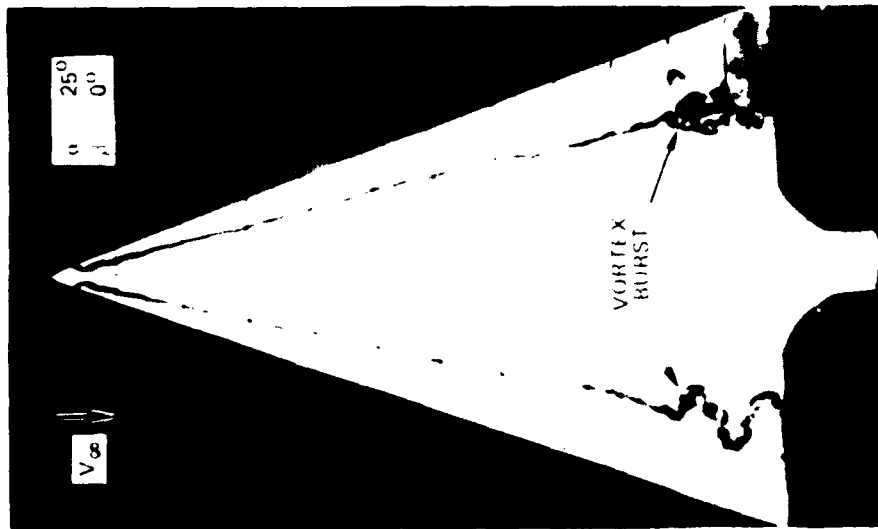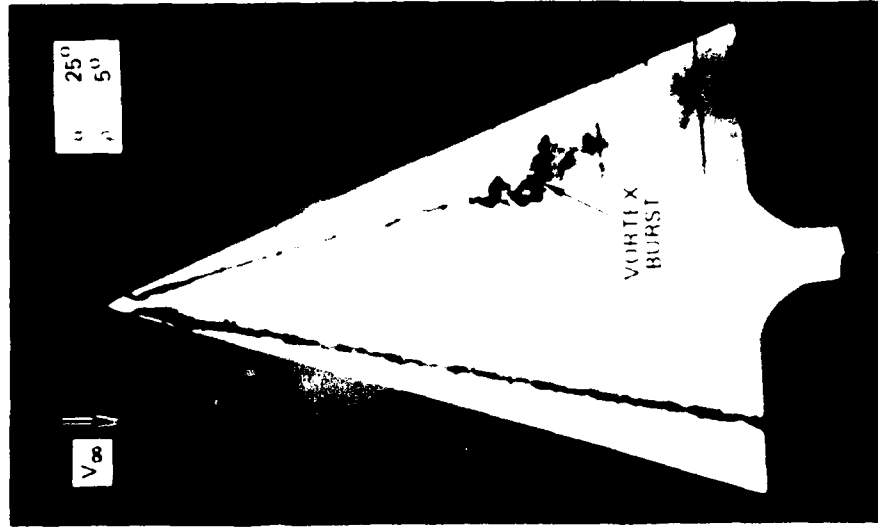
(a) 0 DEGREES AND 5 DEGREES ANGLE OF SIDESLIP

FIGURE 113 SIDESLIP EFFECT ON 70- DEGREE DELTA WING VORTEX CORE BEHAVIOR
(NORTHROP WATER TUNNEL)
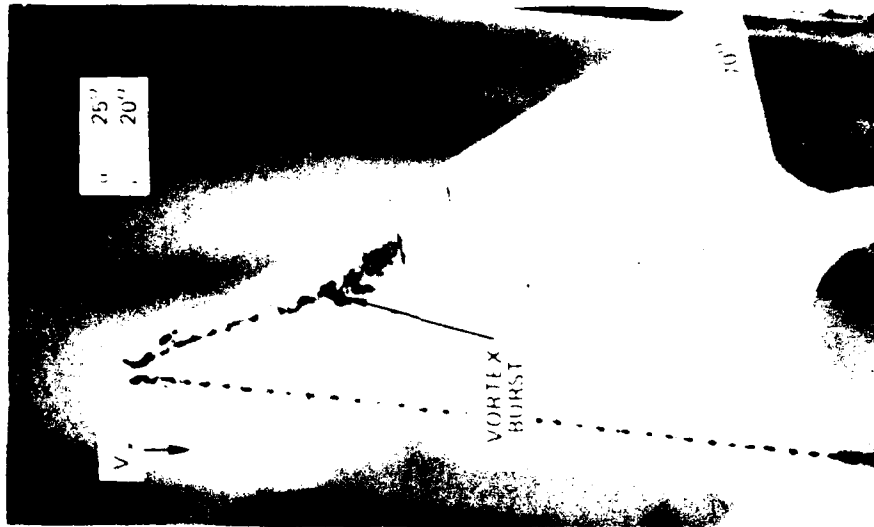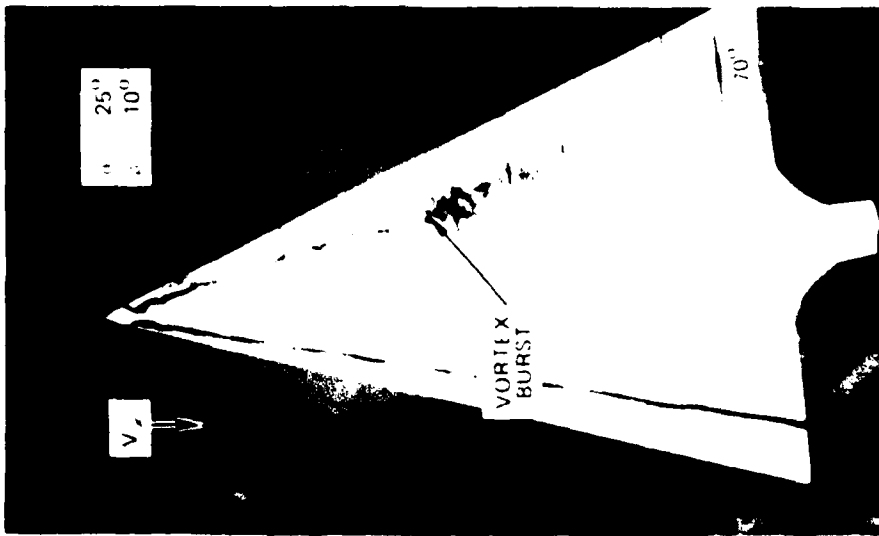
(h) 10 DEGREES AND 20 DEGREES ANGLE OF SIDESLIP

FIGURE 113. CONCLUDED
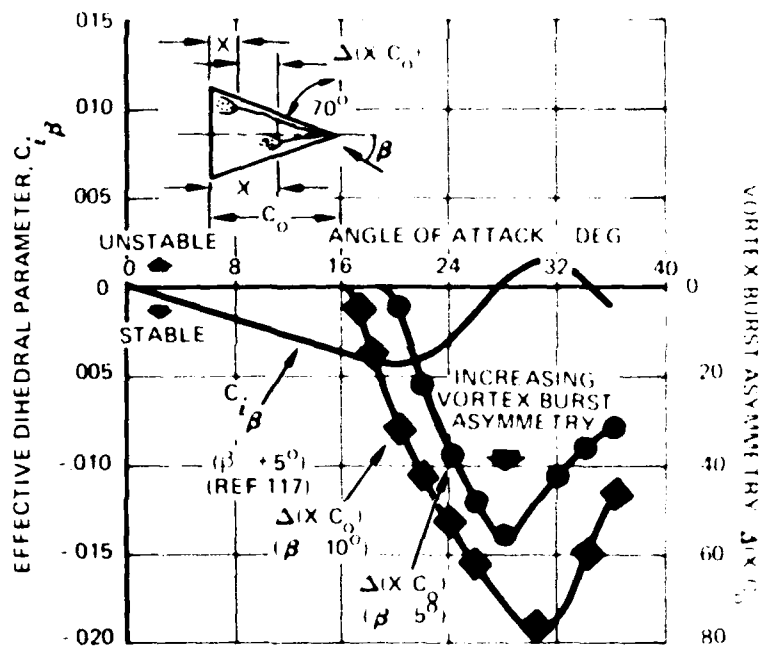
(a) DELTA WING LATERAL STABILITY AND VORTEX
BURST ASYMMETRY CHARACTERISTICS
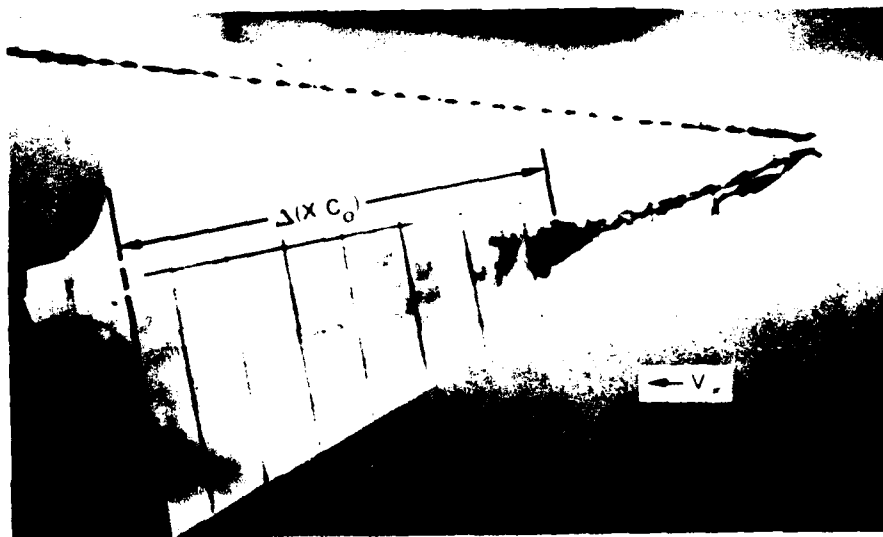
(b) DEFINITION OF VORTEX BURST ASYMMETRY.

FIGURE 114. CORRELATION OF DELTA WING LATERAL
STABILITY CHARACTERISTICS WITH
VORTEX BREAKDOWN ASYMMETRY

213

$V_8 \longrightarrow$

VORTEX BURST

NO BURST
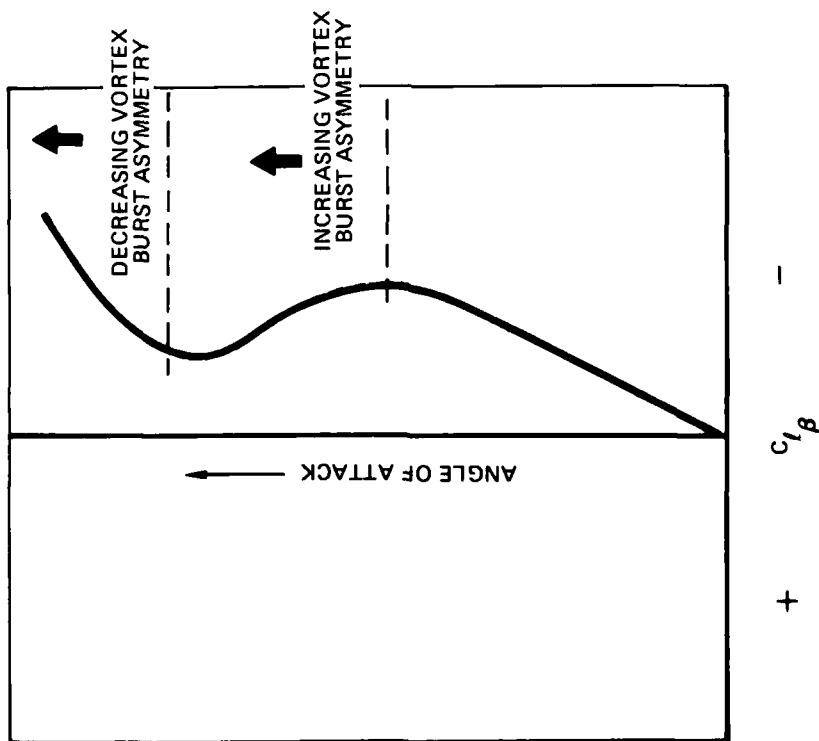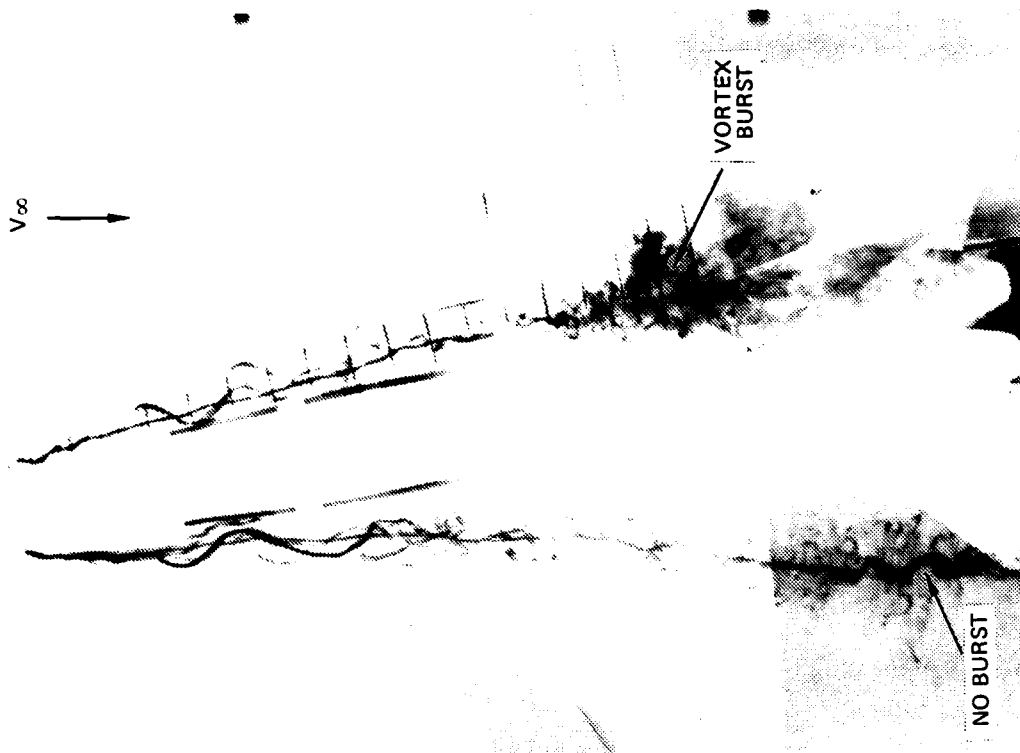
(A) TWIN TAIL FIGHTER WITH LARGE LEX

DECREASING VORTEX BURST ASYMMETRY

INCREASING VORTEX BURST ASYMMETRY

ANGLE OF ATTACK

C_{l_β}

$-$

$+$

FIGURE 115. CORRELATION OF LATERAL STABILITY AND LEX VORTEX BREAKDOWN CHARACTERISTICS

WINDWARD
VORTEX BURST

LEEWARD
VORTEX BURST

β

$(\lambda - \beta)$

$(\lambda + \beta)$

EFFECT OF
ASYMMETRIC LEX
VORTEX
BREAK
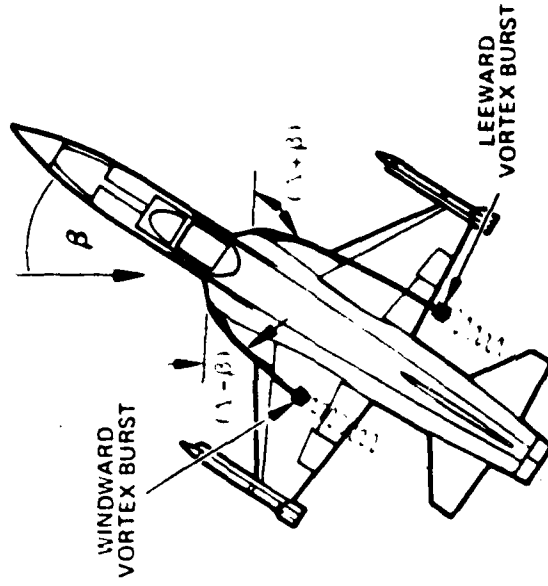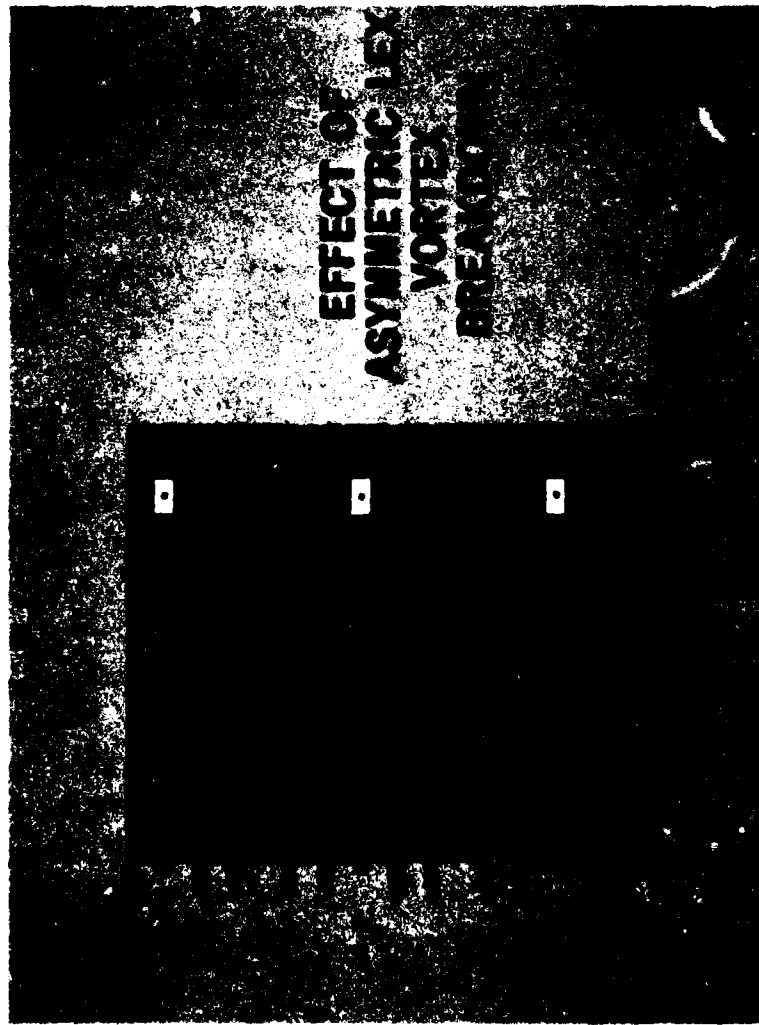
(b) TWIN-JET FIGHTER WITH SMALL LEX

FIGURE 115. CONCLUDED

edge. Maximum reduction in lateral stability level occurs at approximately the angle of attack at which the degree of vortex breakdown asymmetry is maximum, which agrees well with observations made in a wind tunnel in Reference 100. Similar effects are present on fighter aircraft with LEX-wing geometries (see Figure 115),the water tunnel observations revealing the correct trends.

Longitudinal Characteristics of Double-Delta and LEX-Wing Planforms

Lift and pitching moment characteristics obtained in Reference 141 on an 80°/65° double-delta planform are shown in Figure 116 along with Northrop water tunnel vortex burst observations. Vortex burst at the trailing edge correlates with initial reduction in lift curve slope, whereas vortex burst at the junction of the fore and aft leading edges corresponds with the development of maximum lift and abrupt pitch-up. Similar effects can be seen on advanced fighter aircraft with large leading-edge extensions, as depicted in Figures 117 and 118.

Trailing-Edge Flap Effects

Water tunnel studies have indicated that in sideslip conditions a deflected trailing-edge flap tends to reduce the degree of vortex burst asymmetry exhibited with flaps retracted. The leeward vortex strength is reduced relative to the windward vortex and, consequently, cannot as easily traverse the positive pressure gradient associated with the deflected trailing-edge flap. Examination of low-speed wind tunnel data on twin-tail and twin-jet fighter configurations reveals an increase in lateral stability at high angles of attack due to deflected plain trailing-edge flaps as shown in Figure 119. Since the primary contributor to static lateral stability is

the wing, the increase in lateral stability may be associated with a reduction in vortex burst asymmetry.

Twin Vertical Tail Effects

Several current fighter aircraft feature twin vertical tail arrangements in order to maintain directional stability in the extended angle of attack range attainable with hybrid (wing-LEX) geometries. Twin vertical tail placement can influence LEX vortex stability in a manner similar to that observed with downstream obstacles placed in the path of the vortex core. Improper placement of the vertical tails can promote premature vortex bursting and, consequently, limit the attainable C_{Lmax} and influence longitudinal and lateral-directional stability levels. A basic example of the effect of twin-tail surface location on vortex stability is presented in Figure 120 for a slender, nonplanar wing in sideslip. Tip-mounted tails have essentially no effect on vortex stability whereas the inboard-mounted tails are seen to have a large influence on vortex core behavior. On the twin-tail fighter configuration shown previously in Figure 95, removal of the tails was found to have no effect on the behavior of the LEX vortex. These results are quite surprising in light of observations made in wind tunnel tests in Reference 138 which reveal large tail effects on LEX vortex stability, particularly at lower angles of attack at which the LEX vortex core passes in the vicinity of the downstream surfaces. As was discussed in paragraph 5.2.1, however, vortex simulation in a water tunnel is subject to limitations at low angles of attack and, consequently, the wing separation characteristics appear to "mask" the effects of the twin tails.

LEX Boundary Layer Bleed Slot Effects

Investigation of the effect of LEX boundary layer bleed slots on vortex behavior was made on a current twin-tail fighter configuration. Closing the bleed slots had a dramatic
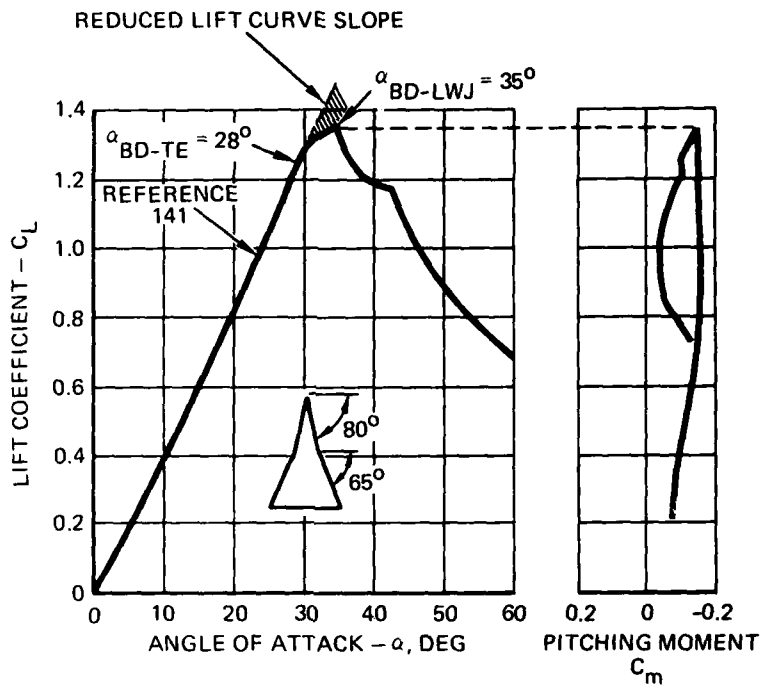
FIGURE 116. DOUBLE-DELTA WING LIFT AND PITCHING
MOMENT CHARACTERISTICS
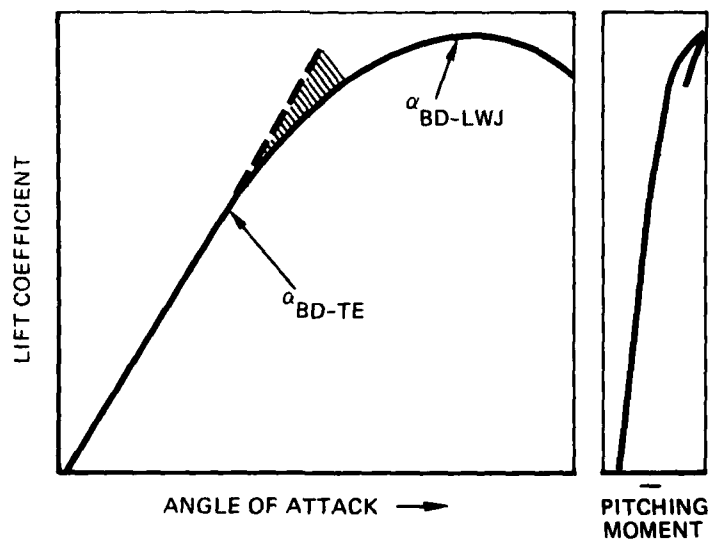
FIGURE 117. LIFT AND PITCHING MOMENT TRENDS
OF A FIGHTER AIRCRAFT

218

VORTEX BREAKDOWN

LEX VORTEX

LEX WING JUNCTION (LWJ)

V

(a) NORTHROP WATER TUNNEL MODEL OF CURRENT TWIN TAIL FIGHTER

FIGURE 118 FLOW VISUALIZATION OF LEX VORTEX BREAKDOWN AT THE LEX WING JUNCTION (BD LWJ)

LEX VORTEX

VORTEX BREAKDOWN
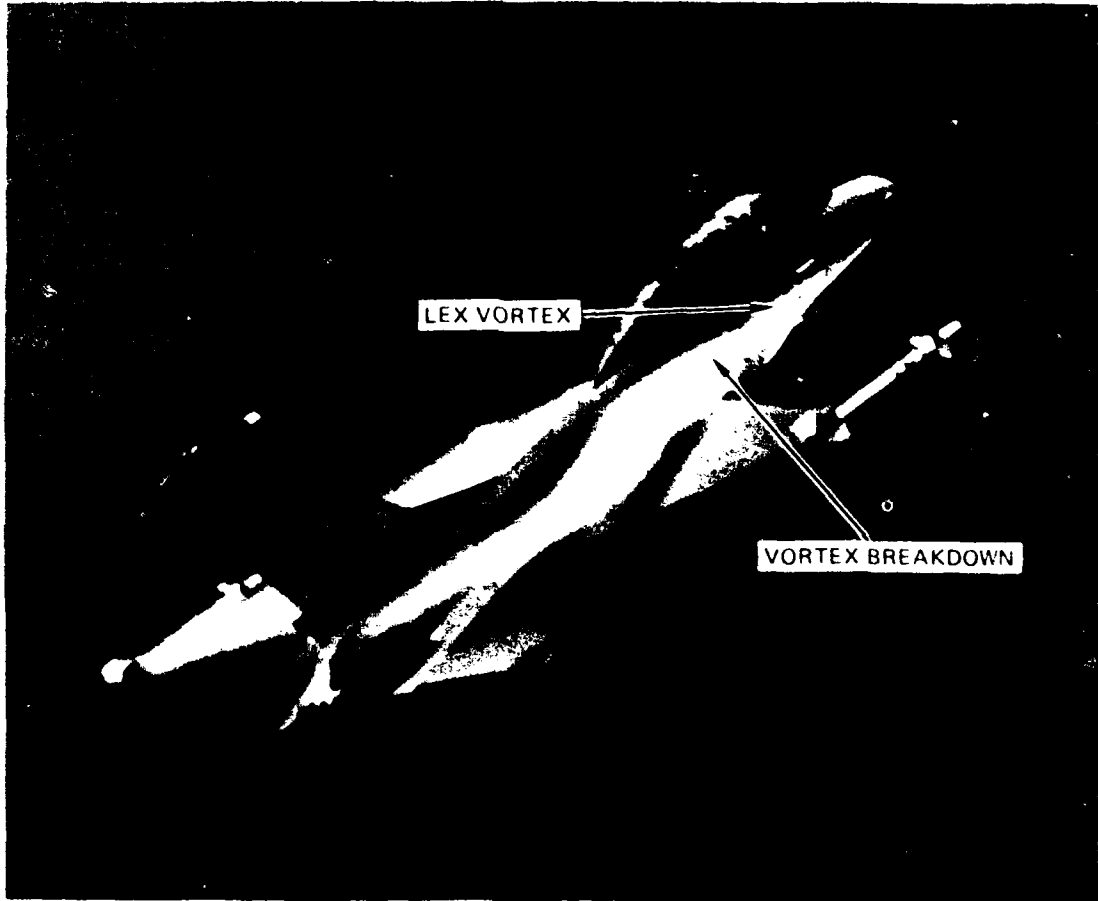
(b) FLIGHT PHOTOGRAPH OF CURRENT LIGHTWEIGHT FIGHTER (PHOTOGRAPH
COURTESY OF AVIATION WEEK AND SPACE TECHNOLOGY).

FIGURE 118. CONCLUDED
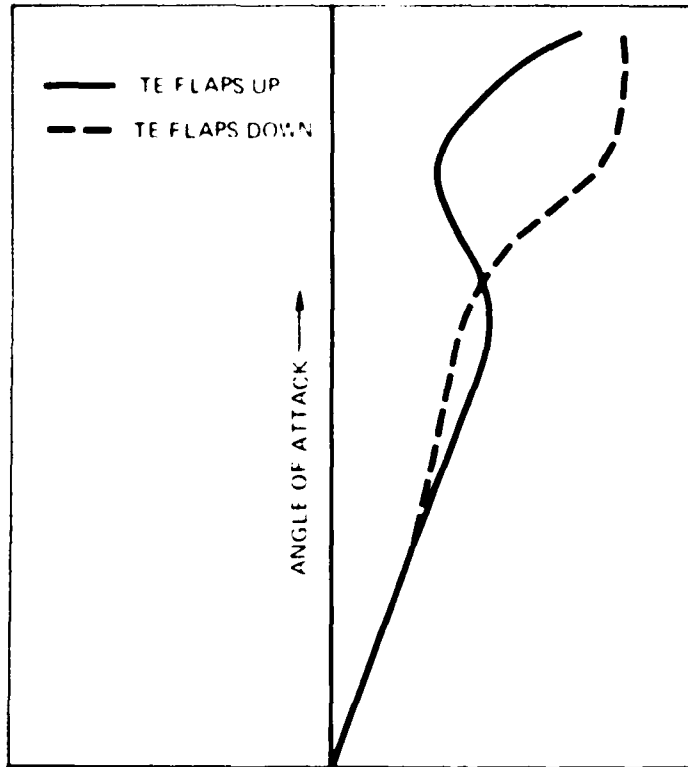
(a) TWIN-TAIL FIGHTER
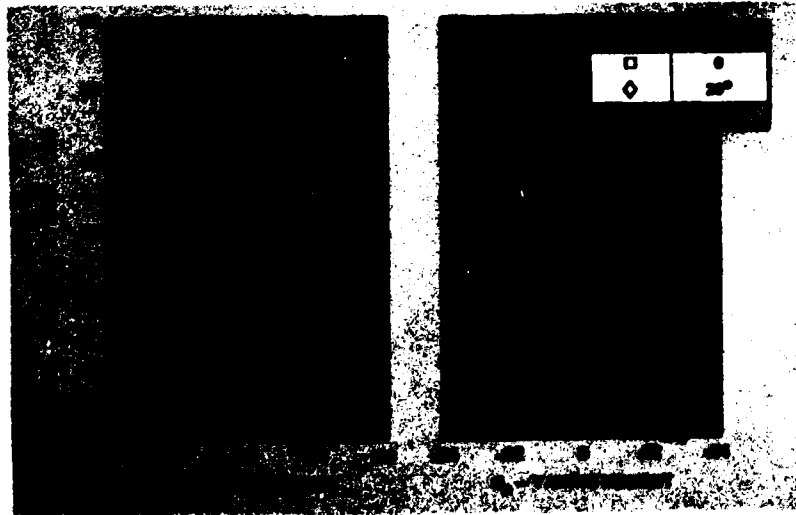
(b) CURRENT TWIN-JET FIGHTER

FIGURE 119. EFFECT OF TRAILING-EDGE FLAP DEFLECTION
ON FIGHTER AIRCRAFT STABILITY CHARACTERISTICS
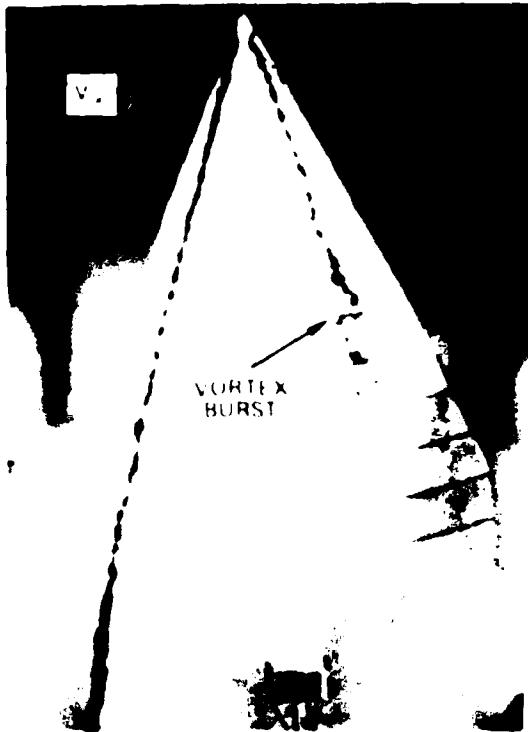
(a) TAILS OFF
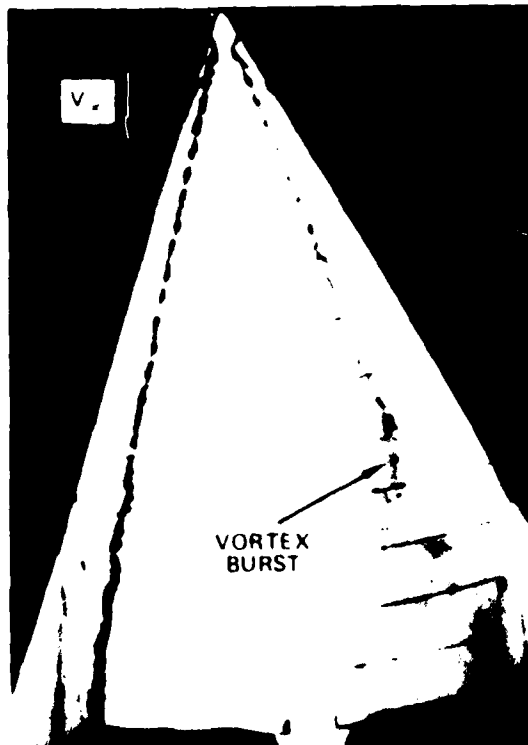
(b) TIP-MOUNTED TAILS

FIGURE 120. EFFECT OF VERTICAL TAIL LOCATION ON VORTEX STABILITY AT 20 DEGREES
ANGLE OF ATTACK AND 10 DEGREES OF SIDESLIP (NORTHROP WATER TUNNEL)
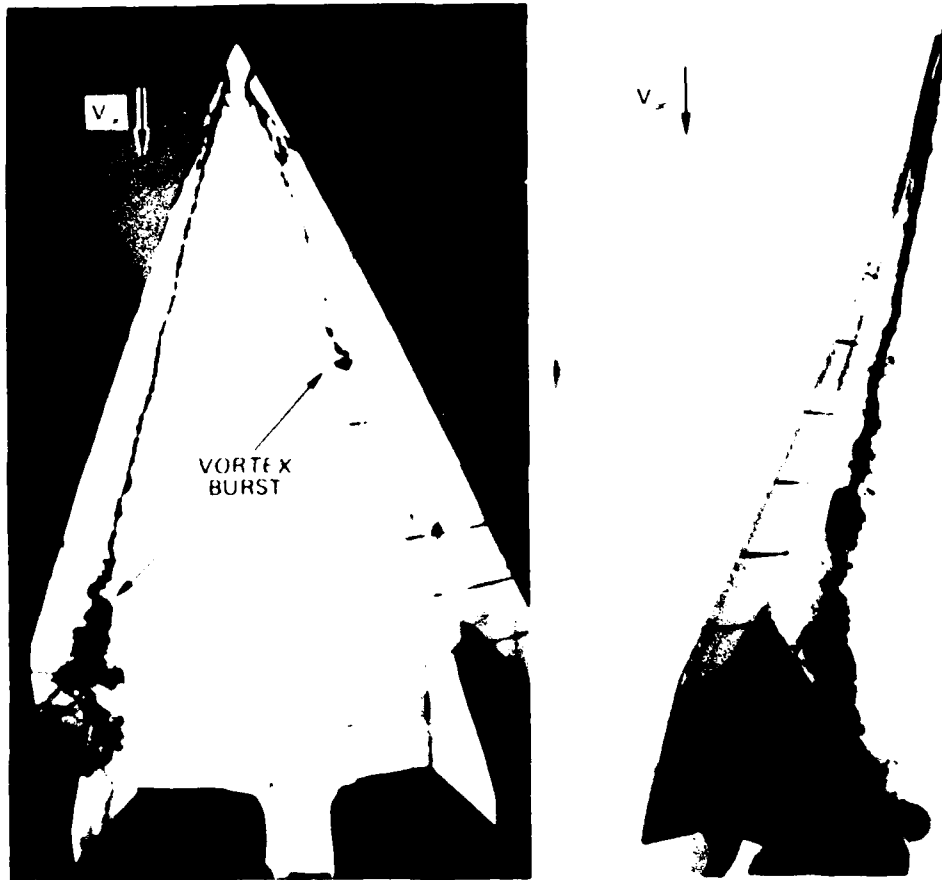
(c) INBOARD TAILS

FIGURE 120. CONCLUDED

effect on the structure of the LEX vortex such that a single, concentrated vortex core was developed, as seen in the close-up photograph in Figure 121, in contrast to the two-vortex system peculiar to this LEX planform with slots open. These visual observations are in complete agreement with wind tunnel flow visualization (using helium-filled bubbles) in Reference 148. These results suggest an increase in lift due to slot closure, as is confirmed in the low-speed wind tunnel data in Figure 122.

Lifting Surface Planform Studies

Wing and LEX planform studies have correlated well with high Reynolds number results. Vortex stability characteristics of an ogee wing obtained in water agree very well with wind tunnel measurements in Reference 141 (see Figure 123) and with limited flight test results in Reference 149 where the leading-edge vortex core was visualized by natural condensation, depicted in Figure 124. Special note is made of the outstanding correlation between water tunnel vortex core location obtained at a Reynolds number of approximately 2×10^4 and upper surface tuft patterns obtained in flight at a Reynolds number of 2×10^7 as shown in Figure 125.

The increased stability of the F-5 W_6 LEX vortex relative to the "production" or W_8 LEX geometry shown in Figure 126, as observed in the water tunnel, was found to be in quantitative agreement with wind tunnel-determined lift characteristics and directional stability at high angles of attack.

As a final example, an as yet unresolved discrepancy has been observed in the stability characteristics of a very large LEX, shown in Figure 127, in water and in air. A difference

LEX VORTEX CORE

WING LEADING EDGE FLAP

LEX APEX

V_∞
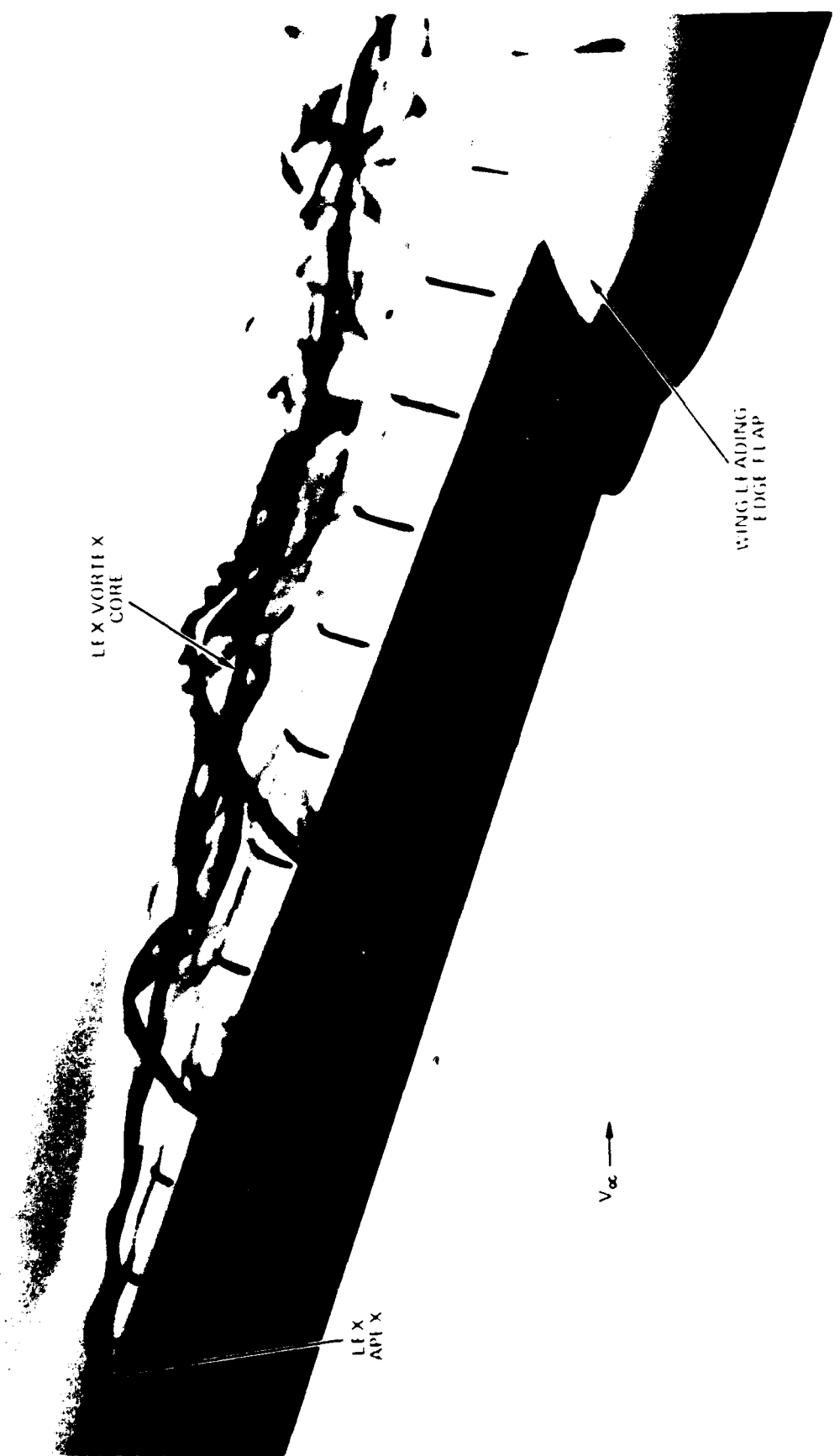
FIGURE 121. LEX VORTEX CORE WITH BOUNDARY LAYER BLEED SLOTS CLOSED (NORTHROP WATER TUNNEL)
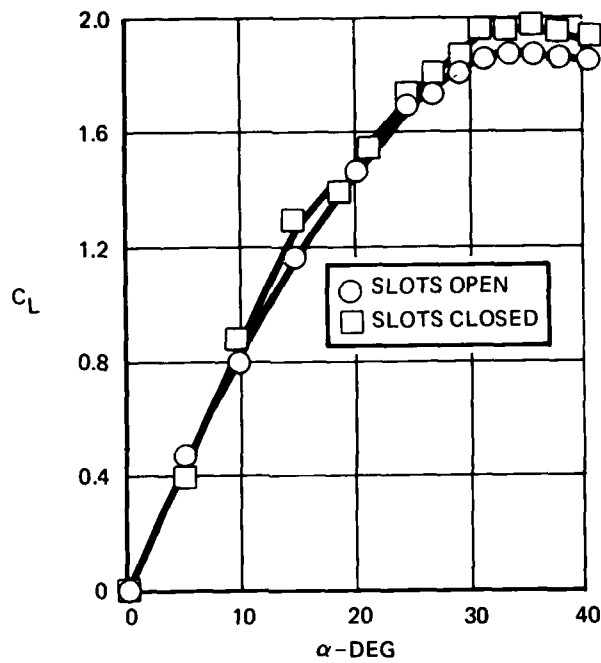
FIGURE 122. EFFECT OF LEX SLOT CLOSURE ON LIFT CHARACTERISTICS OF A TWIN-TAIL FIGHTER
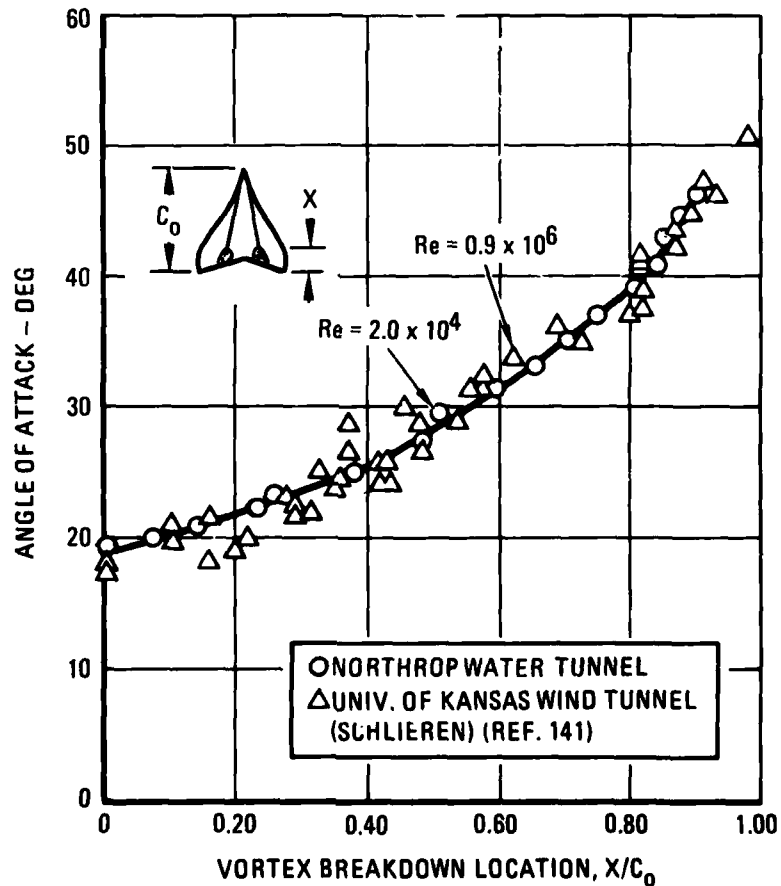
FIGURE 123. VORTEX STABILITY CHARACTERISTICS OF AN OGEE WING

FIGURE 124. FLIGHT PHOTOGRAPH OF THE DOUGLAS F-5D AIRCRAFT WITH
OGEE WING (REFERENCE 149)

(a) 7.5 DEGREES   (b) 18 DEGREES
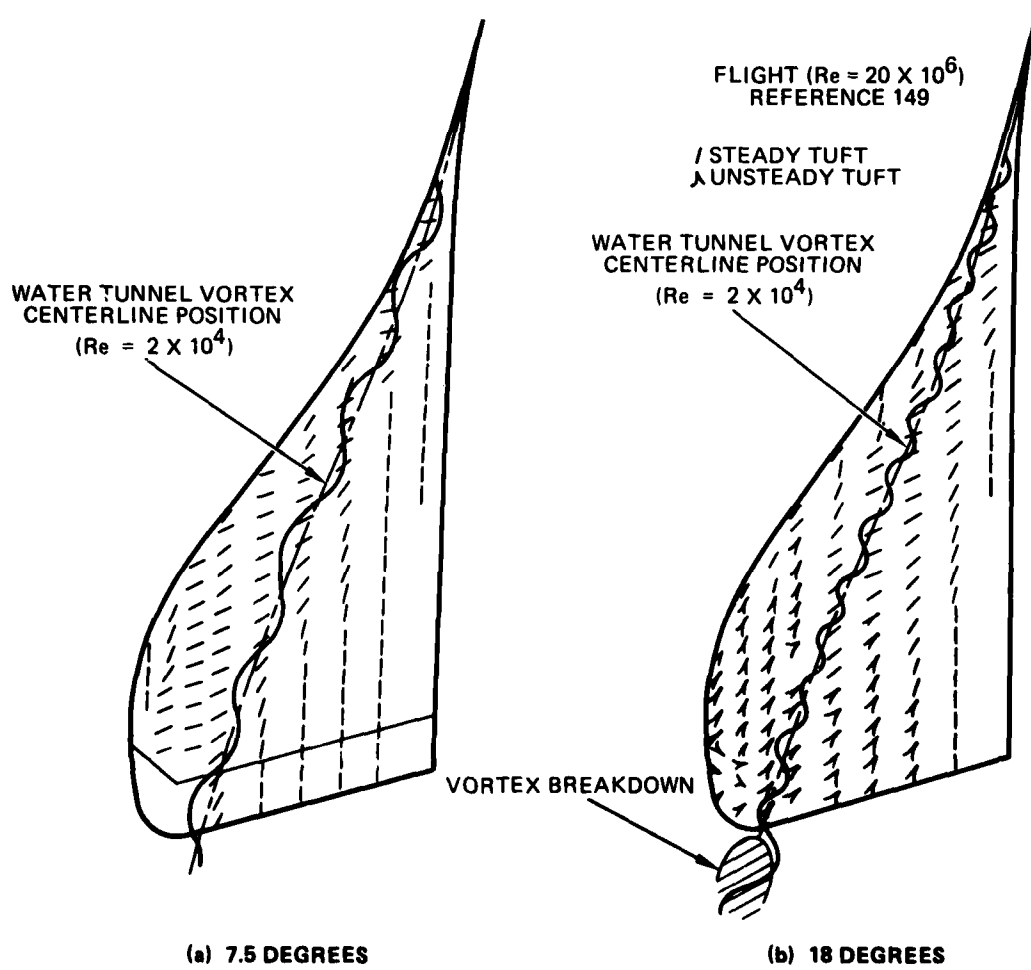
FIGURE 125. UPPER SURFACE TUFT PATTERNS IN FLIGHT AND COMPARISON
WITH WATER TUNNEL VORTEX CORE CENTERLINE POSITION

227
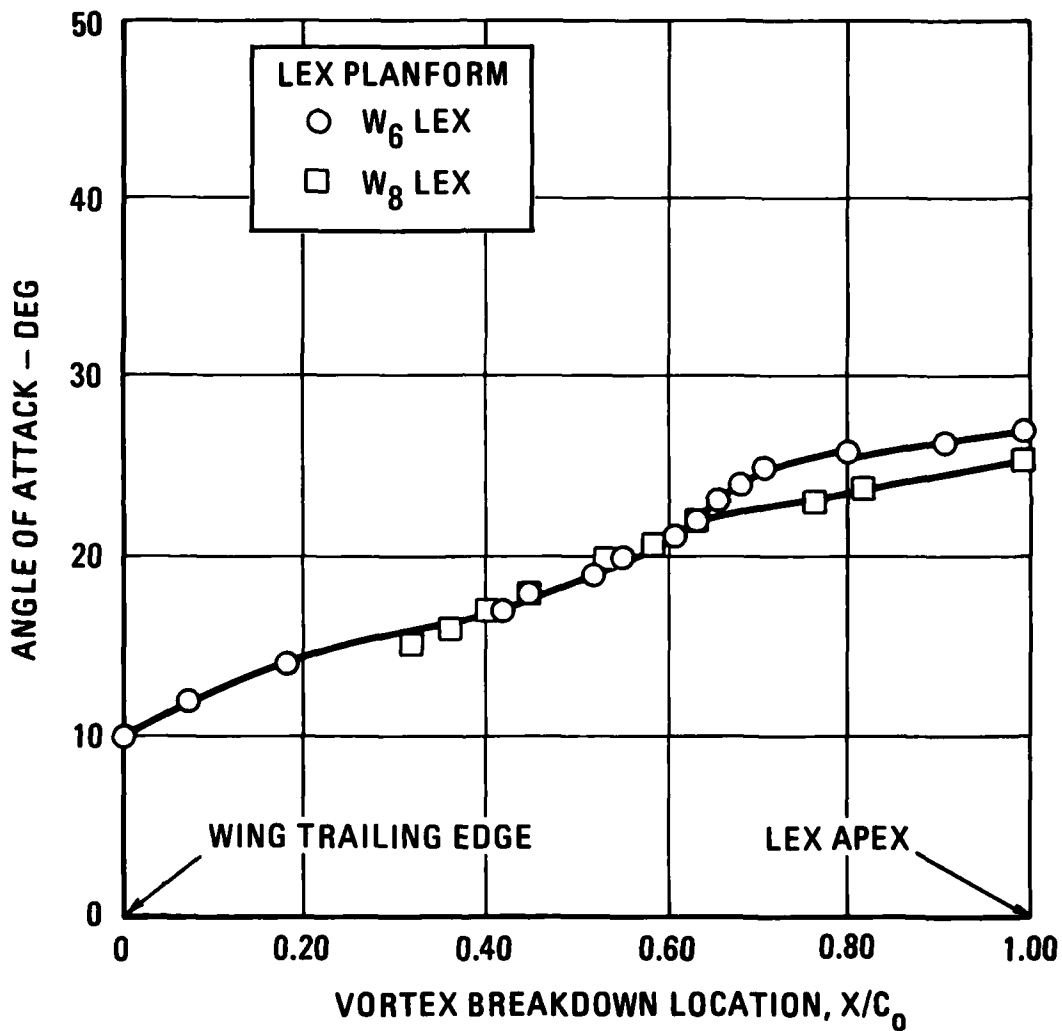
(a) F-5F W_6 AND W_8 LEX VORTEX BREAKDOWN CHARACTERISTICS.

FIGURE 126. CORRELATION OF NORTHROP WATER TUNNEL VORTEX BREAKDOWN
CHARACTERISTICS WITH SUBSONIC WIND TUNNEL DATA.
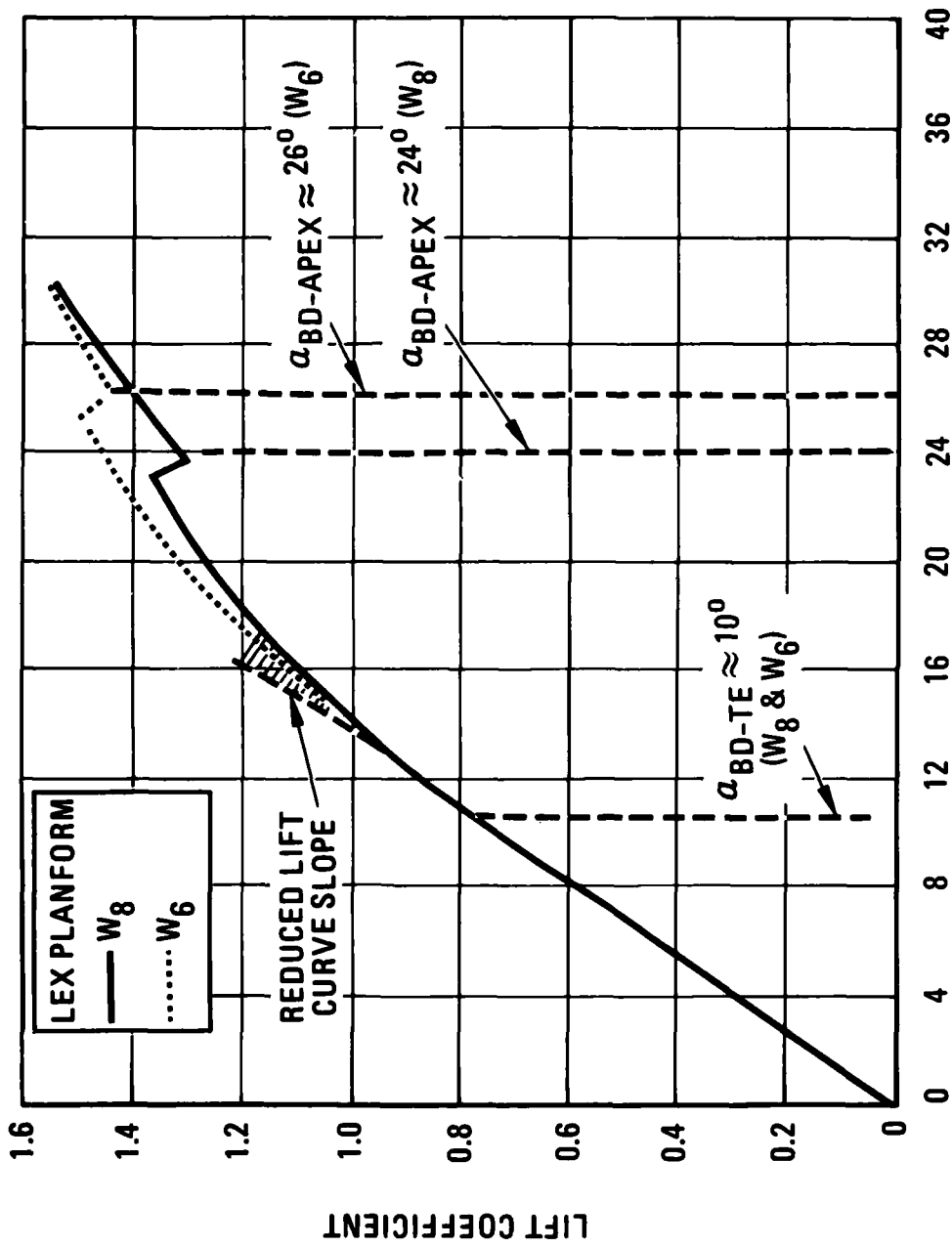
(b) F-5F LIFT CHARACTERISTICS WITH W_8 AND W_6 LEX PLANFORMS; M = 0.26.

FIGURE 126. CONTINUED.

229
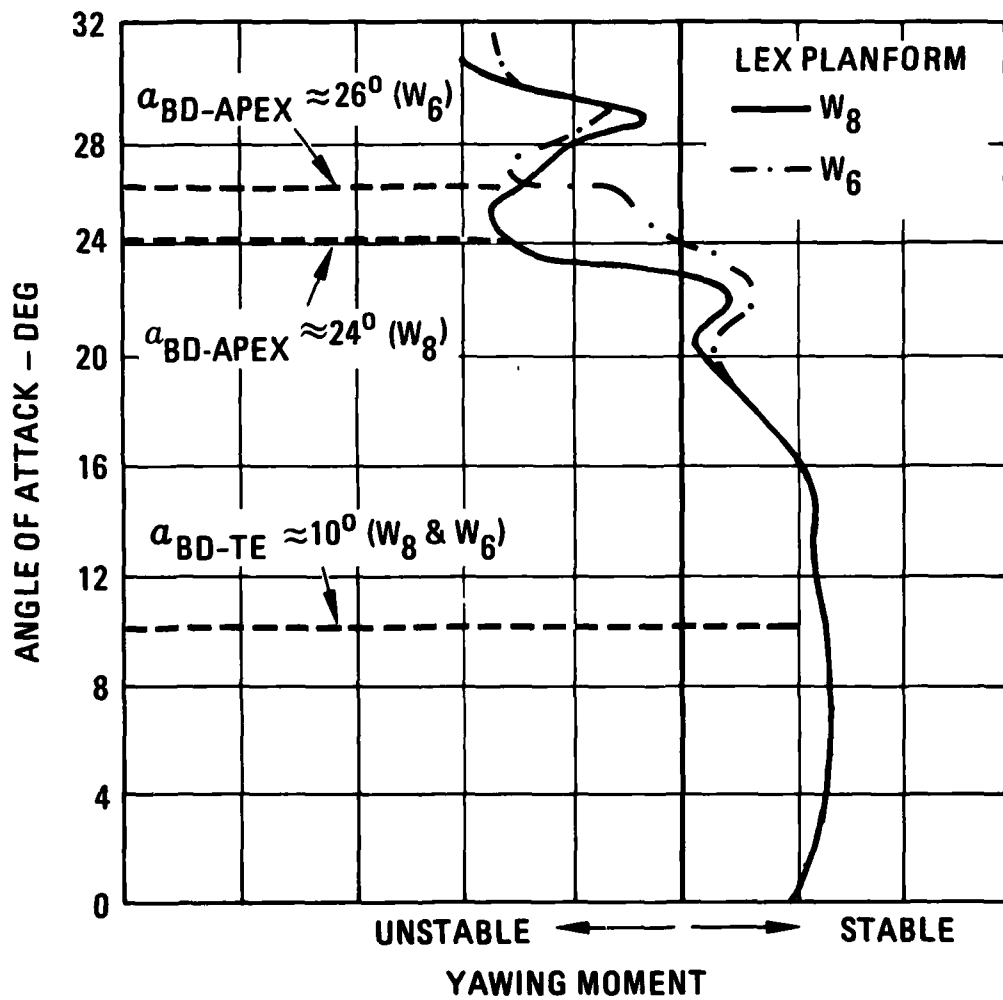
(c) F-5F YAWING MOMENT CHARACTERISTICS WITH W₈ AND W₆ LEX PLANFORMS; β= -10°; M = 0.26.

FIGURE 126. CONCLUDED.

V_∞

LEX
VORTICES
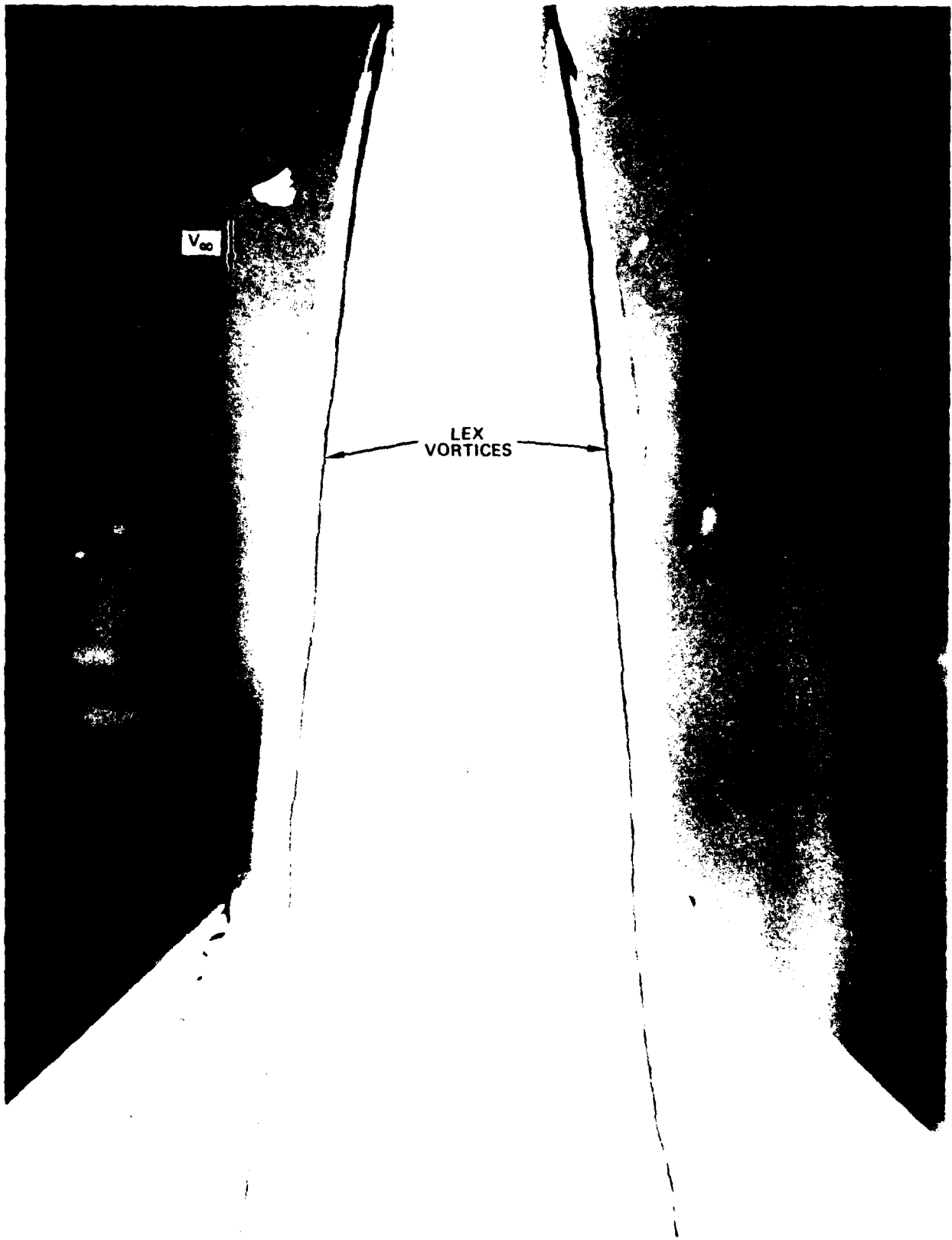
**FIGURE 127. LARGE GOTHIC LEX GEOMETRY (NORTHROP WATER TUNNEL)
AT 20 DEGREES ANGLE OF ATTACK**

231

of approximately 6 degrees was observed between the angle of attack for vortex bursting at the wing trailing edge, α_{BD-TE} being about 20 degrees in water and 26 degrees in air (determined by natural condensation in the wind tunnel in Reference 150). This LEX, which was roughly 32 percent of the wing reference area, generates a very powerful vortex which can remain quite concentrated far downstream and, consequently, the different model support arrangements may be the source of disagreement between the data. The high angles of attack would appear to preclude vortex core-boundary layer interaction as the key to this problem.

5.3 SLENDER BODY VORTICES IN STEADY FLOW

A water tunnel can provide useful information pertaining to vortex shedding from slender bodies at high angles of attack in symmetric and asymmetric flight conditions. It is the intent of the discussion in this paragraph to identify water tunnel applications to (1) bodies alone and (2) wing-body combinations where strong vortex interactions may occur.

5.3.1 Bodies Alone

The large effect of Reynolds number on the boundary layer flow about a slender body at angle of attack has been discussed in detail in Section 4. Studies in a water tunnel are typically conducted under conditions of laminar separation. For example, Reynolds numbers based on body diameter, Re_D, in the Northrop water tunnel are about 0.25×10^4. Even in higher-speed water tunnels which can achieve an order of magnitude increase in Reynolds number, the NEAR water tunnel (Reference 151) for example, flow conditions are still below the transition Reynolds number as can be seen in Figure 128. The transition Reynolds number, as defined in Figure 128, is approximately $Re_{tran} \approx 10^5$. Although the general structure of

232

the vortex flow field at <u>sub-critical conditions</u> is expected to be characteristic of high Reynolds number <u>supercritical flows</u>, it is obviously of interest to study the vortex behavior in a water tunnel on a slender body with turbulent boundary layer flow. Such studies, however, appear to be precluded in most water tunnel facilities currently in use. At the low subcritical conditions in the Northrop facility, attempts to trigger boundary layer transition to turbulence by surface roughness or trips appear to result only in separation of the laminar boundary layer without reattachment. The flow conditions in the NEAR and Cal Tech HSWT facilities would appear more suitable for such investigations. It should be noted, however, that increasing the Reynolds number by increasing the free-stream velocity poses problems with respect to quality of flow visualization. Very slow speeds are deemed necessary to derive maximum information of the detailed structure of vortical motions. At higher speeds, details of the flow field are compromised as the flow structure appears more diffuse -- a problem typically encountered in wind tunnel flow visualization (using smoke, for example).

The effects of forebody and afterbody fineness ratios on onset of vortex asymmetry have been successfully studied in the Northrop water tunnel, as was shown previously in Section 4. It is possible to assess in a qualitative manner the increase in vortex strength (identified from the more tightly-coiled vortices) and vortex asymmetry (variation in core lateral and vertical locations) due to increased angle of attack. One or more additional vortices shed farther aft on models of high fineness ratio have been observed, although these vortices are of a highly diffuse nature, which is in agreement with the high-speed water tunnel results in Reference 151. An appreciation of the complex nature of the vortex wake shed from a body at high attitudes is gained from Figure 129.
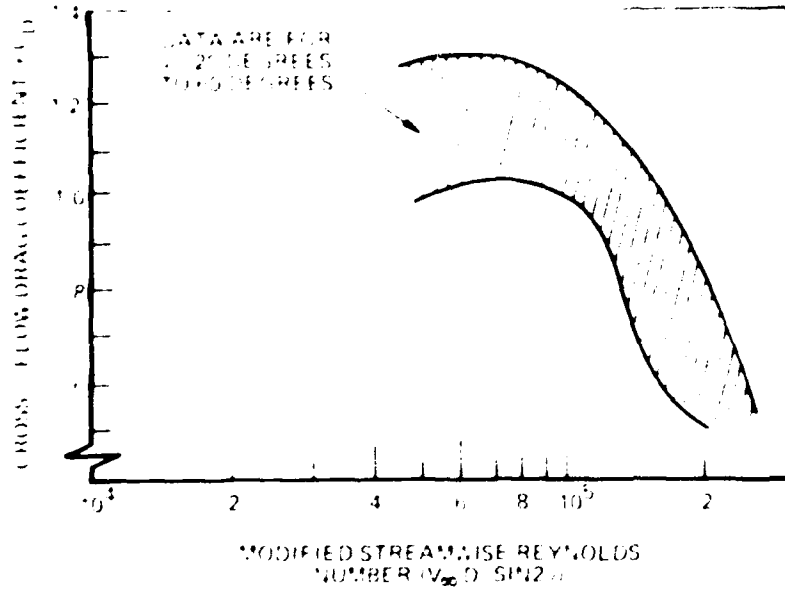
FIGURE 128. CORRELATION OF CROSS-FLOW
DRAG COEFFICIENT WITH REYNOLDS NUMBER
(FROM REFERENCE 151)
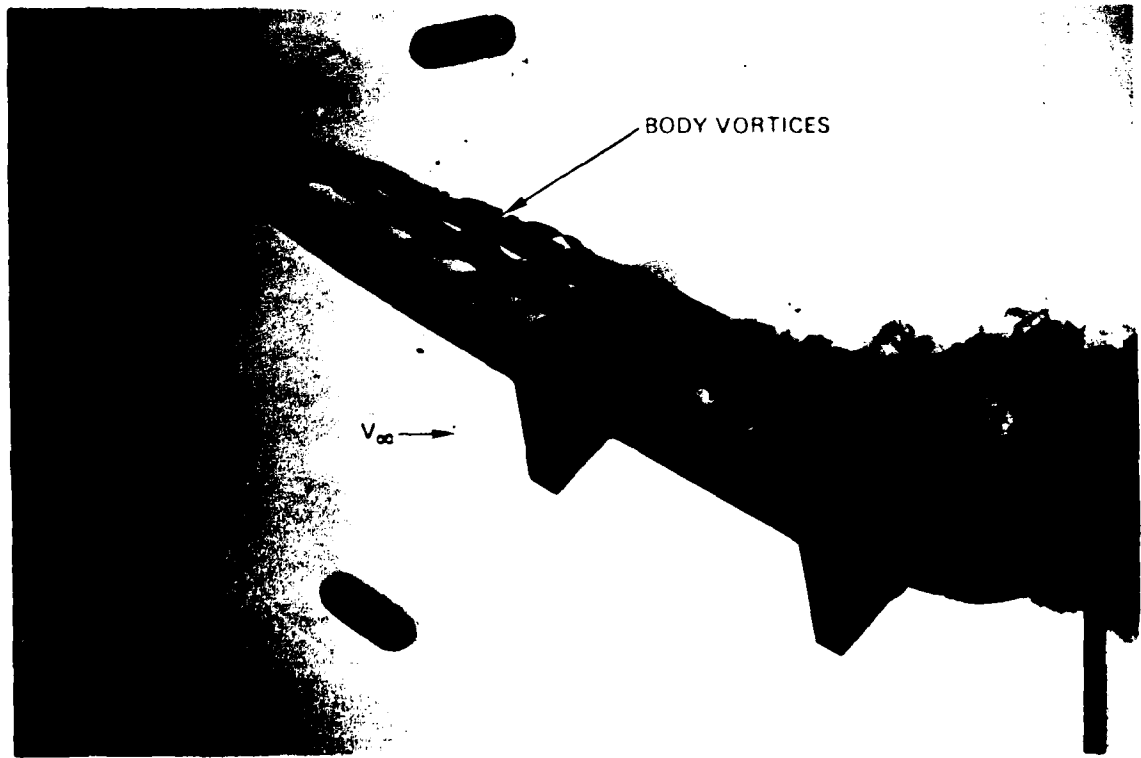
(a) 30 DEGREES ANGLE OF ATTACK.

FIGURE 129. VORTEX DEVELOPMENT ON A SLENDER
BODY AT ANGLE OF ATTACK
(NORTHROP WATER TUNNEL).

234
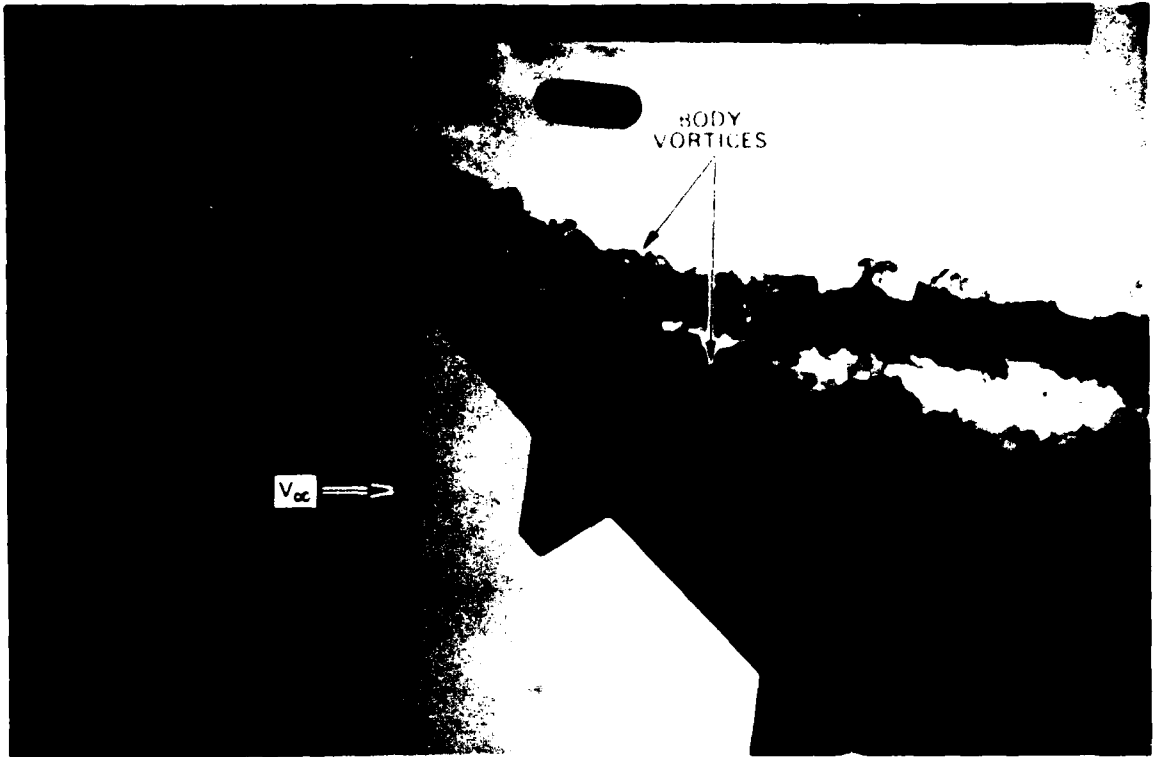
(b) 45 DEGREES ANGLE OF ATTACK
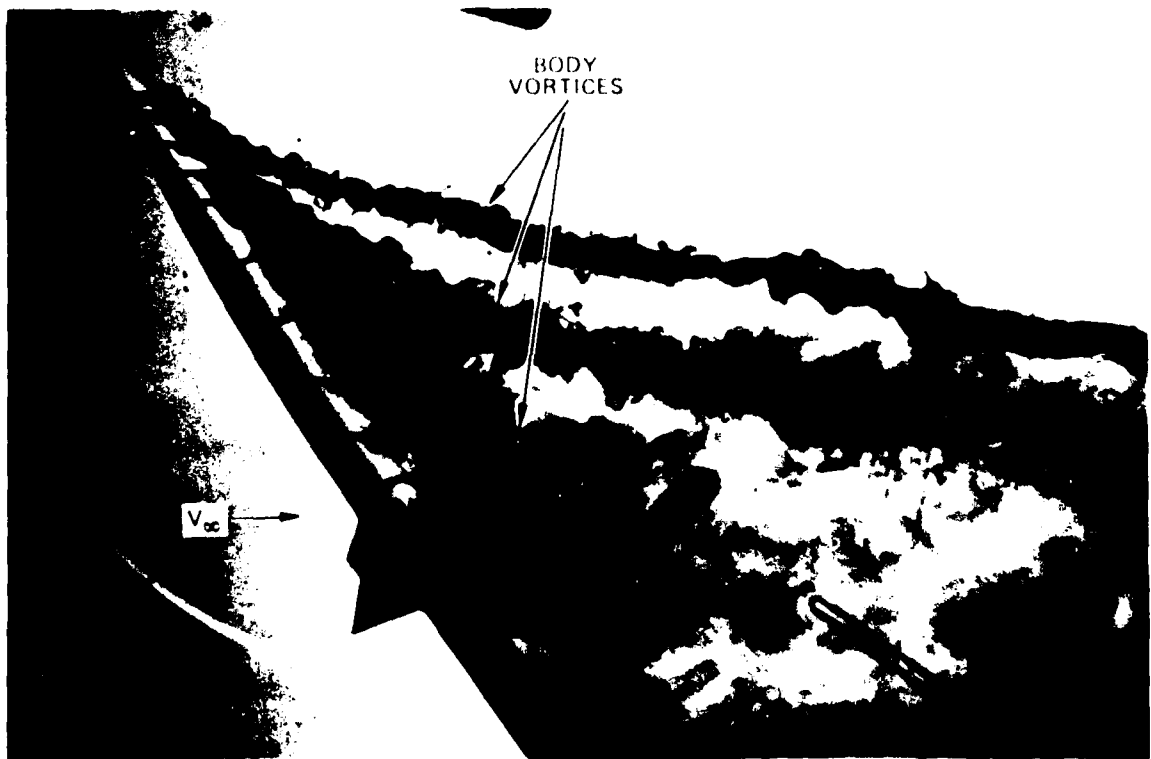
(c) 60 DEGREES ANGLE OF ATTACK

FIGURE 129. CONCLUDED

Nose boom effects on body vortex behavior are also amenable to study of a qualitative nature in a hydrodynamic test facility. A tapered nose boom was observed to increase the effective fineness ratio and, consequently, to reduce the angle of onset of vortex asymmetry, illustrated in Figure 130. In contrast, a constant-diameter nose boom with its essentially two-dimensional shed vortex wake was observed to delay onset of vortex asymmetry, which is in agreement with wind tunnel results discussed in Reference 152. A Reynolds number effect is evident, however, on a nose boom used as a side load alleviation device, since an increase in Reynolds number results in a corresponding increase in asymmetric loads (Reference 105).

Preliminary studies of the effect of forebody cross-sectional shape were made (Figure 131) which revealed large changes in vortex structure and vortex strength.

5.3.2 Wing-Body Configurations

Extensive studies have been made of forebody vortex development, location, strength, and stability on advanced fighter aircraft. The critical importance of the forebody apex region was verified in early water tunnel studies of the Northrop F-5F Production Nose and Shark Nose geometries, which complemented studies in the wind tunnel and in flight. The strong asymmetric and symmetric vortex patterns at high angle of attack and zero sideslip, characteristic of the Production and Shark Nose geometries, respectively, agreed well with high Reynolds number results (Reference 153).

Insight has been gained into the effects of forebody fineness ratio, forebody cross-sectional shape, and forebody bluntness on vortex behavior at high angles of attack. For example, comparison of the forebody vortices on the F-5F and F/A-18 fighter configurations indicates that, at a given angle

236

SLIGHT VORTEX
ASYMMETRY

$V_x \longrightarrow$

(a) NOSE BOOM OFF.

SIGNIFICANT
VORTEX ASYMMETRY

$V_x \longrightarrow$
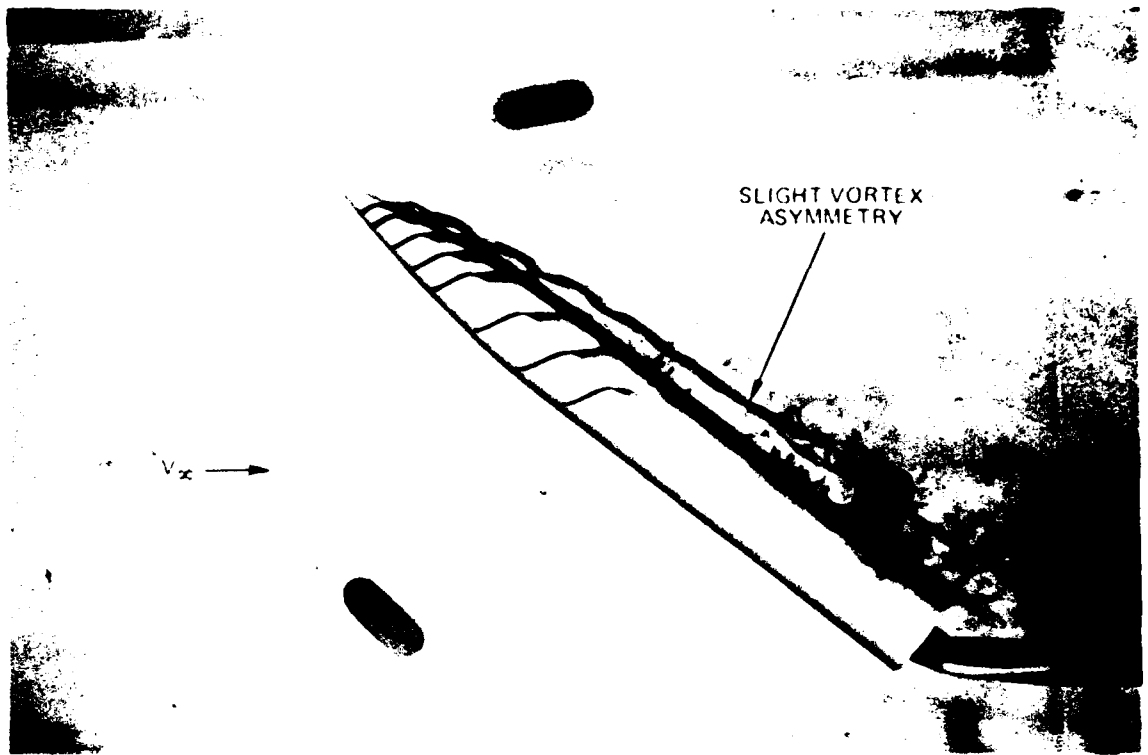
(b) NOSE BOOM ON

FIGURE 130. EFFECT OF TAPERED NOSE BOOM ON BODY VORTEX PATTERN
(NORTHROP WATER TUNNEL)

TYPICAL
CROSS SECTION

$V_\infty \longrightarrow$
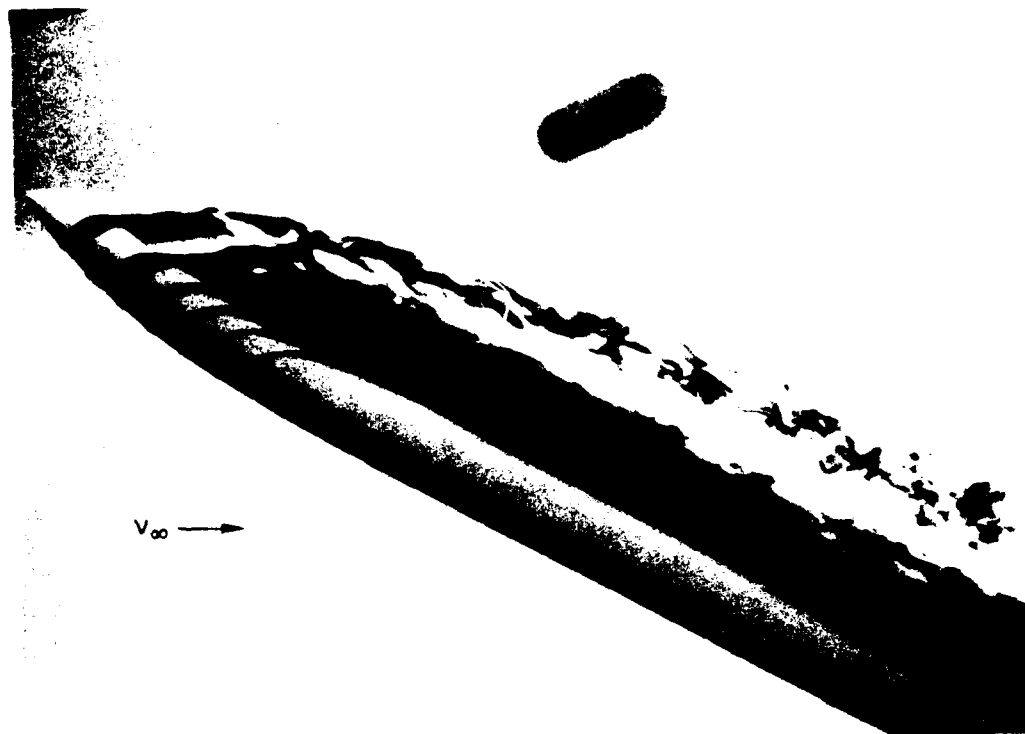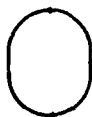
(a) WEAK VORTEX.

TYPICAL
CROSS SECTION

$V_\infty \longrightarrow$
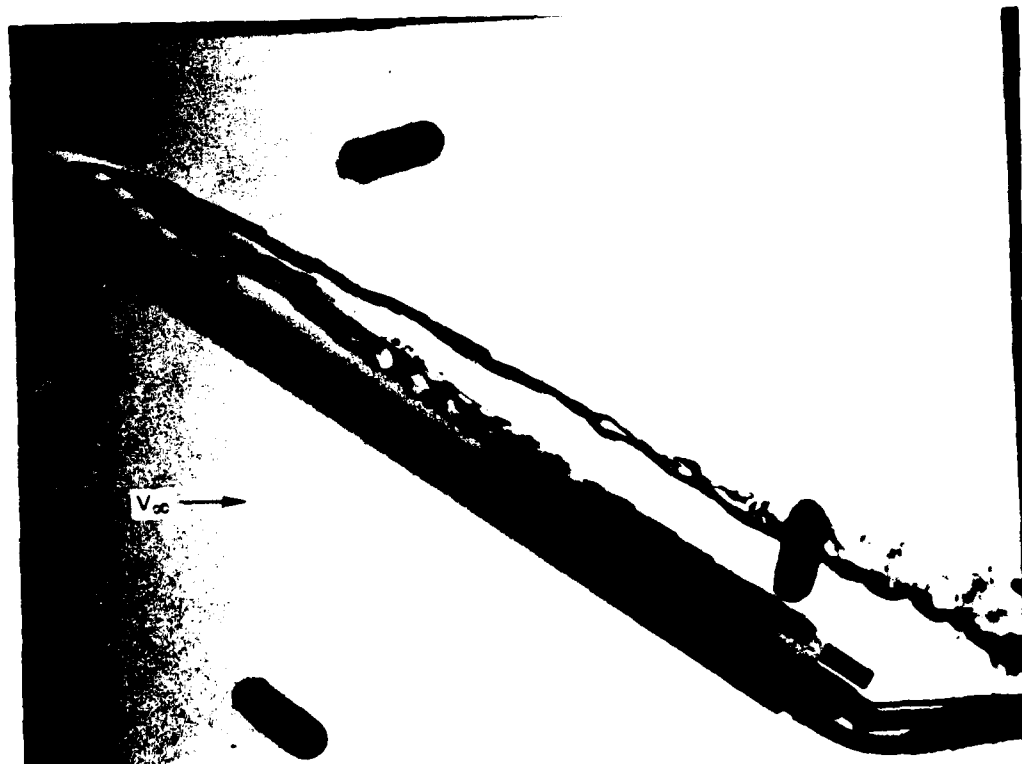
(b) STRONGER VORTEX

FIGURE 131. TYPICAL RESULTS FROM NORTHROP WATER TUNNEL STUDIES OF
FOREBODY CROSS-SECTIONAL SHAPE EFFECTS ON VORTEX BEHAVIOR

of attack, the strength of the former exceeds that of the latter, based on the more tightly-coiled vortical flows on the F-5 aircraft with its higher forebody fineness ratio and elliptical cross-section (major axis horizontal). In addition, the F-5F Production Nose develops an asymmetric vortex pattern at zero sideslip shown in Figure 132, whereas the F/A-18 does not, as can be seen in Figure 133. These results also correlate well with wind tunnel and flight test data. Water tunnel studies of the F-15 featuring several forebodies of various cross-sectional shape and fineness ratio (Reference 154) agreed quite well with the wind tunnel studies of Reference 155, typical results being shown in Figure 134.

The water tunnel has proven a valuable tool in analyzing directional stability trends obtained in wind tunnels since, at high angles of attack, the forebody can strongly affect static directional stability. An example includes the F-5F forebody which develops an unusual vortex configuration in sideslip, characterized by the windward primary vortex lying in close proximity to the forebody and the leeward primary vortex "tearing" away from the body, as shown in Figure 135. Based on these hydrodynamic studies, a flow situation can be constructed which is consistent with the large positive directional stability contribution of the forebody determined in high Reynolds number wind tunnel and flight tests. A further illustration is provided by the F/A-18, which exhibits highly nonlinear lateral-directional stability at high angles of attack (Reference 156). Water tunnel investigations have revealed a strong interaction between the forebody and LEX vortices (to be discussed subsequently) which, in sideslip, orient themselves in a very unusual manner. Consequently, a plausible explanation for the stability trends observed in wind tunnels and in flight, having a sound basis in vortex flow fluid mechanics, can be developed. As a final example, the destabilizing effect of the F-15 production forebody has been

VORTEX CORE
ASYMMETRY

(a) NORTHROP WATER TUNNEL PHOTOGRAPH OF FOREBODY VORTEX ASYMMETRY   45 DEGREES ANGLE OF ATTACK

FIGURE 132. ASYMMETRIC VORTEX SHEDDING ON A SLENDER FUSELAGE FOREBODY

ASYMMETRICAL SURFACE FLOW PATTERN
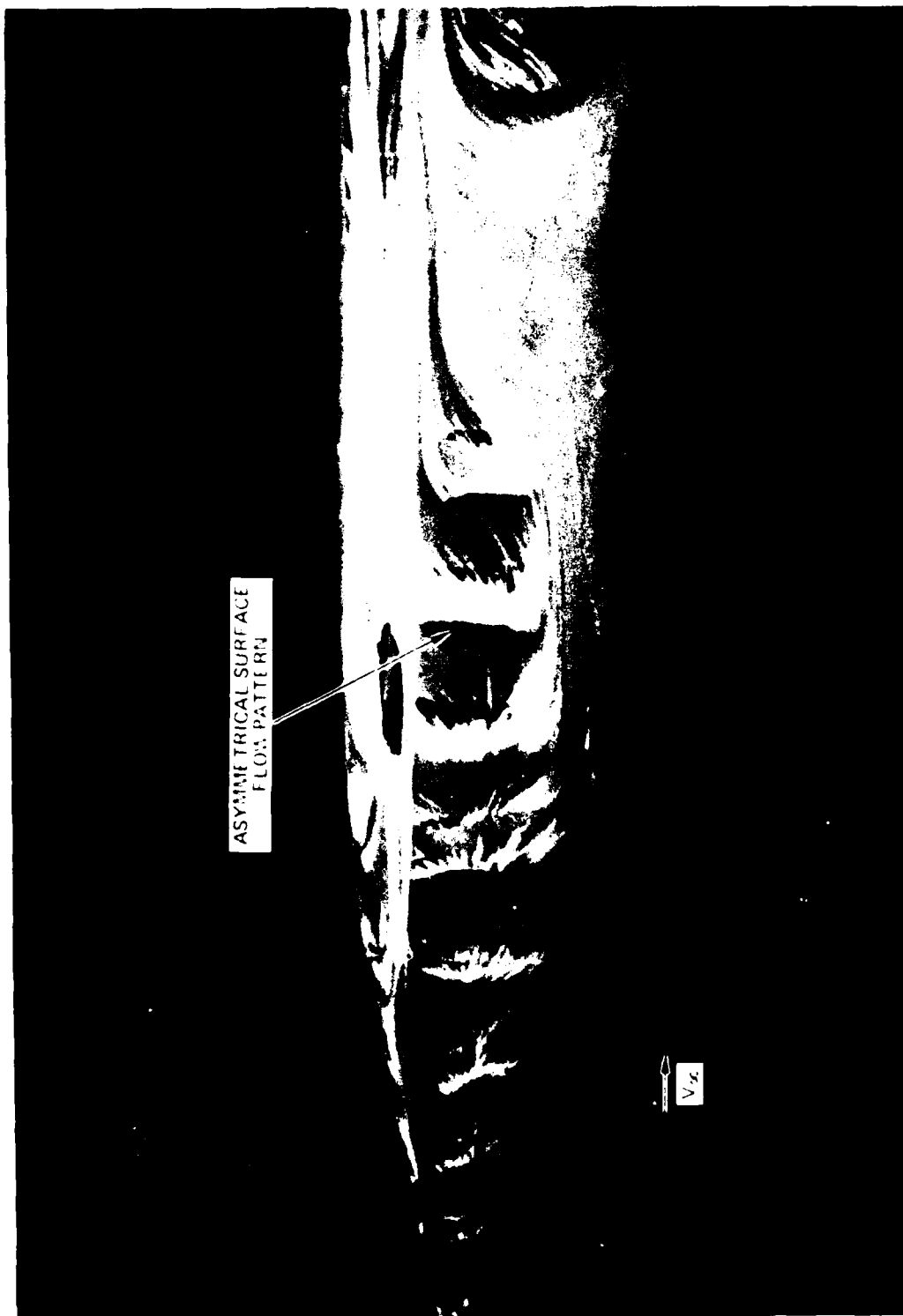
(b) NORTHROP WIND TUNNEL SURFACE OIL FLOW PATTERN 44 DEGREES ANGLE OF ATTACK

FIGURE 132. CONCLUDED

FOREBODY
VORTICES

LEX
VORTEX

V_∞
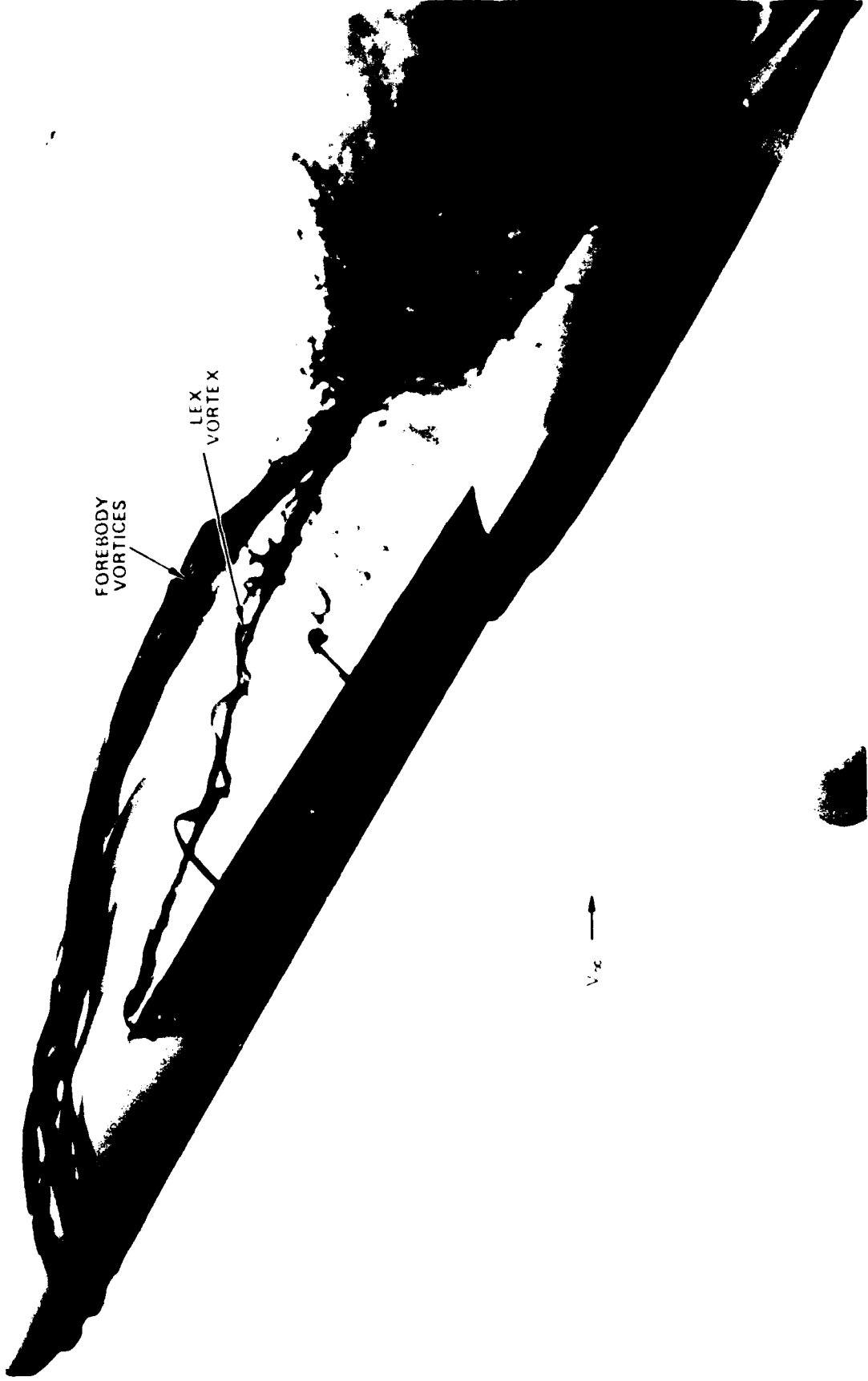
FIGURE 133. FOREBODY-WING-LEX VORTEX FLOW INTERACTION AT
HIGH ANGLE OF ATTACK (NORTHROP WATER TUNNEL)
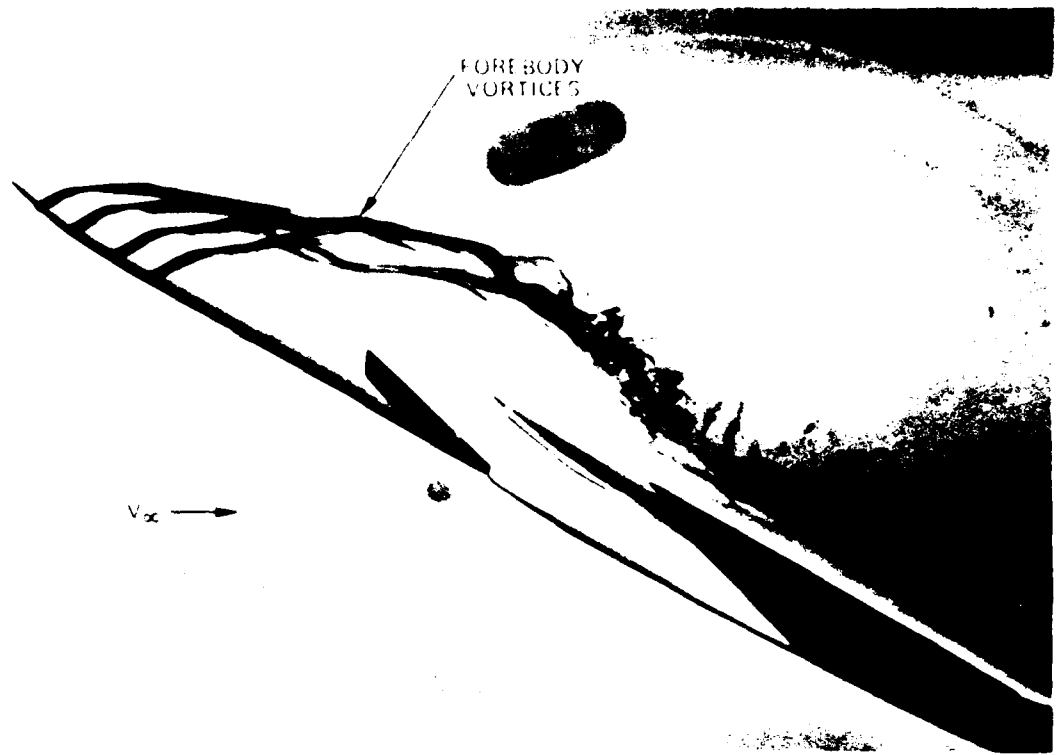
(a) PRODUCTION FOREBODY
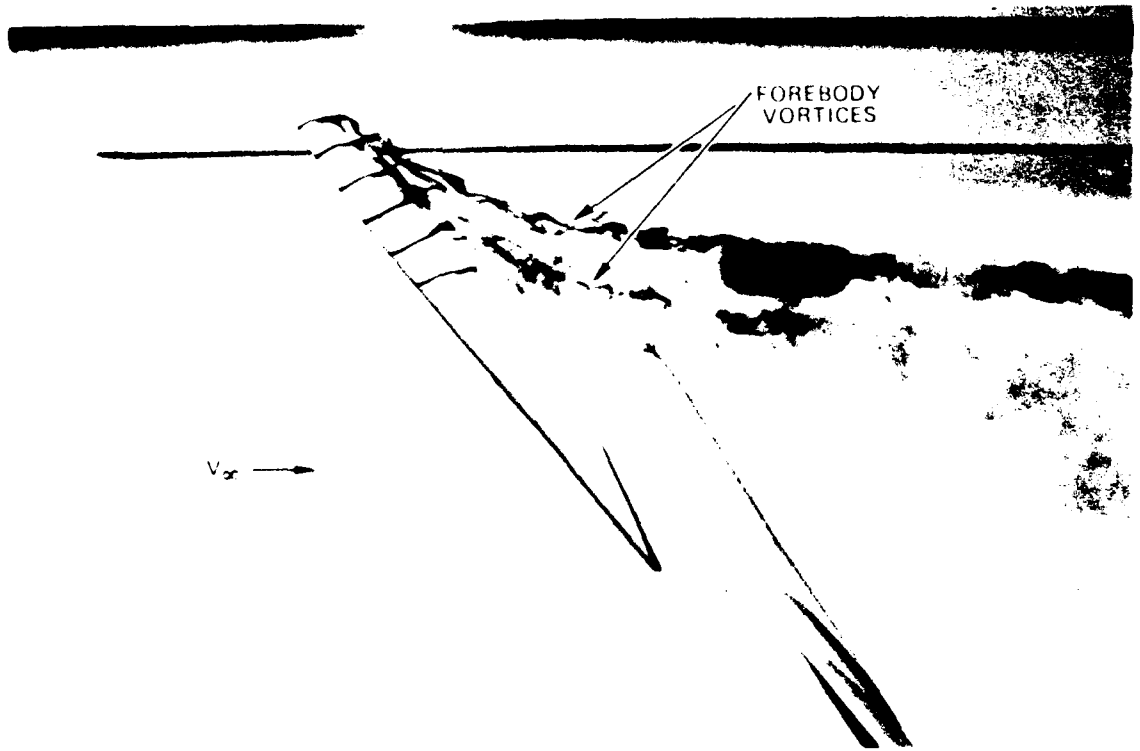
(b) MODIFIED SLENDER FOREBODY

FIGURE 134. TYPICAL RESULTS FROM NORTHROP WATER TUNNEL STUDIES OF
THE F-15 VORTEX FLOW FIELD (FROM REFERENCE 35)
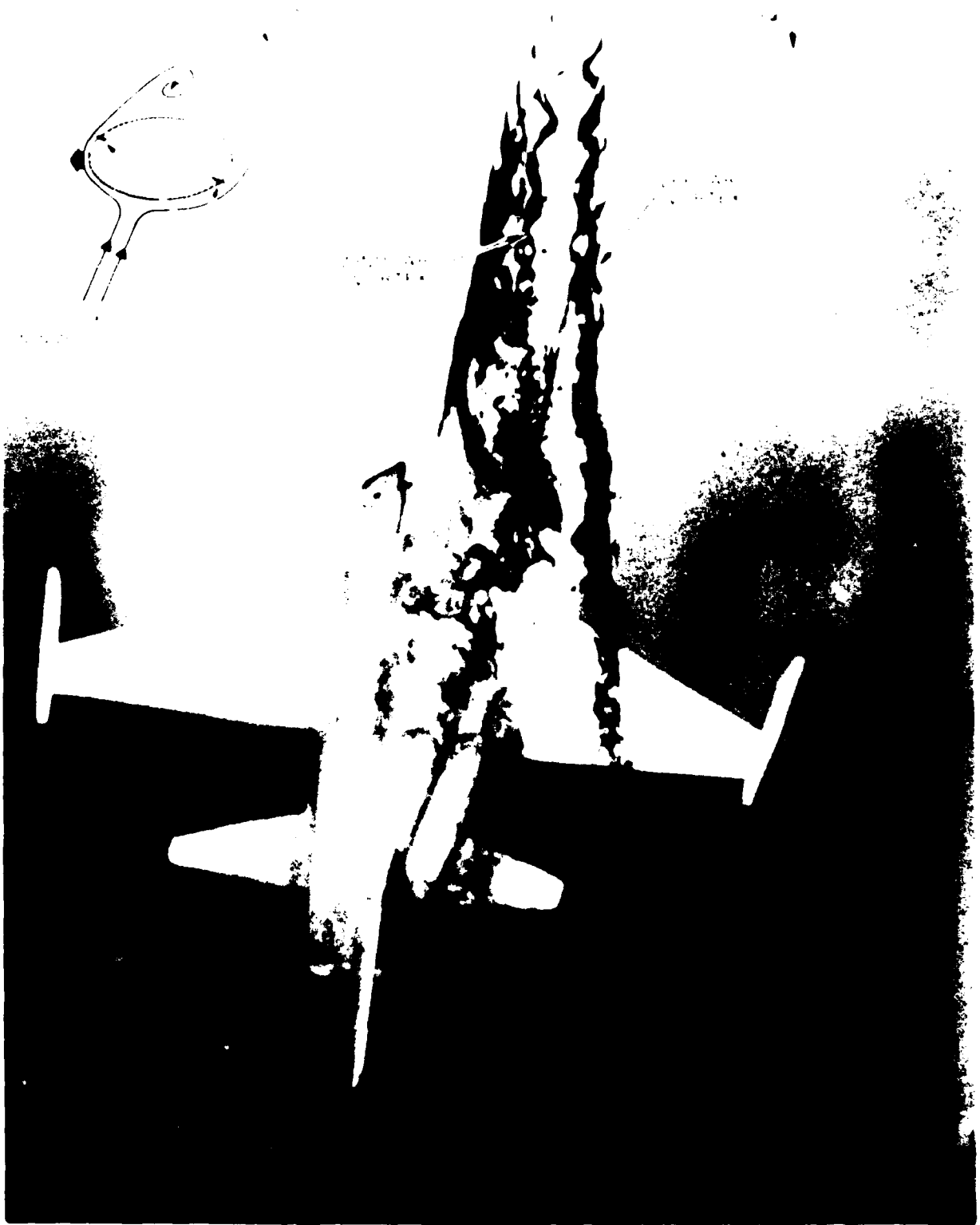
FIGURE 135 F 5F FOREBODY VORTEX ORIENTATION IN SIDE
SLIP (NORTHROP WATER TUNNEL)

attributed to the forebody vortex orientation in sideslip observed in water tunnel tests in Reference 154. The correlations of Northrop water tunnel studies of the vortex flows of the F-15 aircraft were cited as a highlight of 1979 in Reference 157.

In all of these studies, emphasis has been made on trends in forebody vortex behavior. Explanations have been developed, based on water tunnel observations of vortex core location, strength, and stability, for peculiarities in high Reynolds number test data. It should be noted that, in many cases, variations in vortex core location, strength, and stability occur at angles of attack quite comparable to the angles at which changes in longitudinal and lateral-directional characteristics are observed in wind tunnel tests.

Methods of asymmetric sideload alleviation can be investigated in the water tunnel. In addition to nose bluntness and cross-sectional shape optimization, of which the Northrop Shark Nose is one example, alternative concepts include nose strakes, helical separation trips, and normal and tangential blowing on the forebody. Nose strakes commonly employed are mounted along the maximum half-breadth of the body and, in most cases, do not extend all the way to the tip. Flow visualization studies of strakes mounted on the F-5F forebody indicate that the strakes impede the formation of asymmetric vortices since they provide a distinct discontinuity in the vorticity feeding mechanism due to the fixed separation along the sharp leading edge of the strake. Asymmetric vortices still occur, however, since there is room near the nose for the development of flow asymmetry. Results of wind tunnel tests in Reference 123 reveal trends consistent with the observed fluid flow mechanisms.

245

The helical separation trip concept (Reference 158) was studied extensively in the Northrop water tunnel and preliminary results confirmed the effectiveness of the device in alleviating asymmetric vortex shedding on the F-5F. The vortex flow patterns in sideslip at these subcritical test conditions suggested, however, an adverse effect due to the trips on static directional stability. This effect was confirmed in subsequent wind tunnel tests at low supercritical Reynolds number in Reference 158.

The water tunnel was utilized to assess in a somewhat qualitative manner the effects of asymmetric tangential blowing along the forebody to reverse the sense of asymmetry of the vortices on the F-5F (Reference 159). Results provided guidelines for a subsequent wind tunnel test in which favorable blowing locations and orientations of the blowing nozzle determined in water were found to be quite effective in air. In addition, quantitative estimates of jet momentum coefficient made from water tunnel experiments proved not only to give the correct trends but also predicted absolute levels with reasonable accuracy. (Blowing concepts will be discussed in more detail subsequently.) The fluid mechanics of forebody vortex blowing are not fully understood but one possible mechanism is that, by blowing tangentially under the "high" vortex, separation of the primary boundary layer on this side of the windward generator is delayed. This causes the "high" vortex to shift downward and inboard and forces the "low" vortex to now assume a "high" position. This mechanism suggests a coupling between the separation line degree of freedom and hydrodynamic instability phenomena discussed previously. Laminar separation of the primary boundary layers near the nose of the wind tunnel model, as indicated by surface oil flow

patterns, may result in the good agreement with the subcritical results obtained in the water tunnel.

Simulation of vortices shed from bluff bodies is, of course, subject to large Reynolds number effects since the dominating effect of a sharp pointed apex is no longer present. A flow phenomenon analogous to the flow about a blunt leading edge of an unswept wing occurs. In a water tunnel, laminar boundary layer separation results in a large region of reversed flow within a separation bubble on the leeside of the body depicted in Figure 136, and the locations of the vortex sheets and vortex cores are expected to vary considerably with changes in Reynolds number, particularly in the region of the blunt nose. Yet, the qualitative structure of the flow field appears quite comparable to higher Reynolds number tests (Reference 160).

Regarding wing and body vortex flows and subsequent flow interactions, provided flow separation occurs from a sharp leading edge of a slender wing or LEX and the forebody features a slender pointed apex, the water tunnel is expected to provide a good qualitative representation of the flow field at high angles of attack. Excellent correlation has been obtained on the F-5F which exhibits a strong LEX vortex up to angles of attack of about 26 degrees and, beyond this, the emergence of powerful forebody vortices. This overlap of the dominance of LEX and forebody vortices within their respective angle of attack ranges agrees well with the longitudinal and lateral-directional characteristics in wind tunnels and flight.

Many fighter aircaft feature relatively large LEXs in proximity to the forebody. At maneuver conditions, the LEX vortices are, in general, the dominant flows and the forebody vortices are entrained into the low pressure region associated with the wing flow field, as illustrated previously in Figure 133. Simulation of slender wing (or LEX) vortex generation,

247
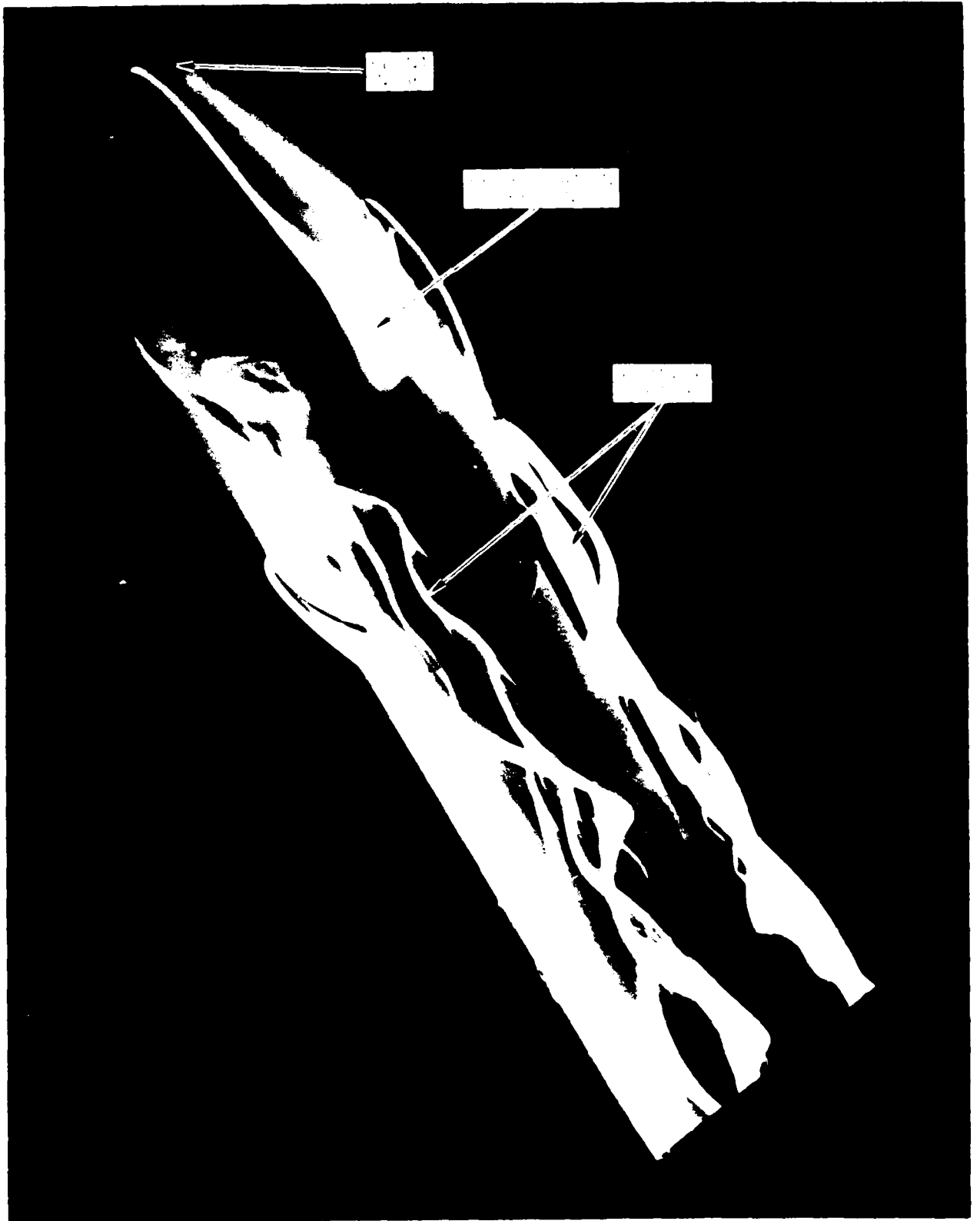
(a) CLOSE UP VIEW OF PRIMARY VORTICES AND REGIONS THAT ....

FIGURE 136 WATER TUNNEL FLOW VISUALIZATION OF VORTEX SHEDDING
FROM A BLUNT NOSED FOREBODY FROM REFERENCE 12

(b) FOREBODY VORTEX CHARACTERISTICS AT VARIOUS CROSS-SECTIONS.

FIGURE 136. CONCLUDED

location, and breakdown is quite good under these conditions and, despite the limitations in forebody vortex simulation, a good approximation of the trajectory and breakdown of the forebody vortices is achieved. The unique orientation of the forebody-LEX vortex flows on the F/A-18 in sideslip is depicted in the water tunnel photograph in Figure 137 and Reference 161 has indicated that a similar flow situation has been observed in the wind tunnel using helium-filled bubbles to visualize the vortices.

Small-scale wind tunnel tests at high Reynolds number of the Navy/McDonnell Douglas/Northrop F/A-18 yielded lateral-directional stability characteristics at high angle of attack that were totally unrepresentative of the full-scale aircraft. A comparison of wind tunnel and flight test results is shown in Figure 138. It was discovered in subsequent low-speed wind tunnel tests in the Full-Scale Tunnel at NASA Langley Research Center that the lateral stability characteristics of 0.07- and 0.16-scale models of the F/A-18 were quite different at the same Reynolds number, the former indicating a high level of stability whereas the latter indicated near-neutral or slightly unstable characteristics (which were in agreement with the full-scale flight test results!). This situation is depicted in Figure 139. In an effort to determine a "fix" to the lateral stability problem, the 0.16-scale model was used to assess the effects of modifications to the forebody and LEX geometries, typical geometric changes illustrated in Figure 140 included radome strakes, LEX lower surface fences, and increased LEX slot width and length. On closely-coupled LEX-wing-forebody arrangements such as the F/A-18, wind tunnel and flight tests indicate that a change in the LEX or forebody geometry affects the lateral and directional stability charac-teristics, as shown in Figures 141 to 143. Since at high angles of attack the wing and forebody are, respectively, the primary contributors to static lateral and directional stabi-lity, this suggests a strong coupling between the body and wing

250

WINDWARD
FOREBODY
VORTEX

LEEWARD
FOREBODY
VORTEX

LEEWARD
LEX
VORTEX
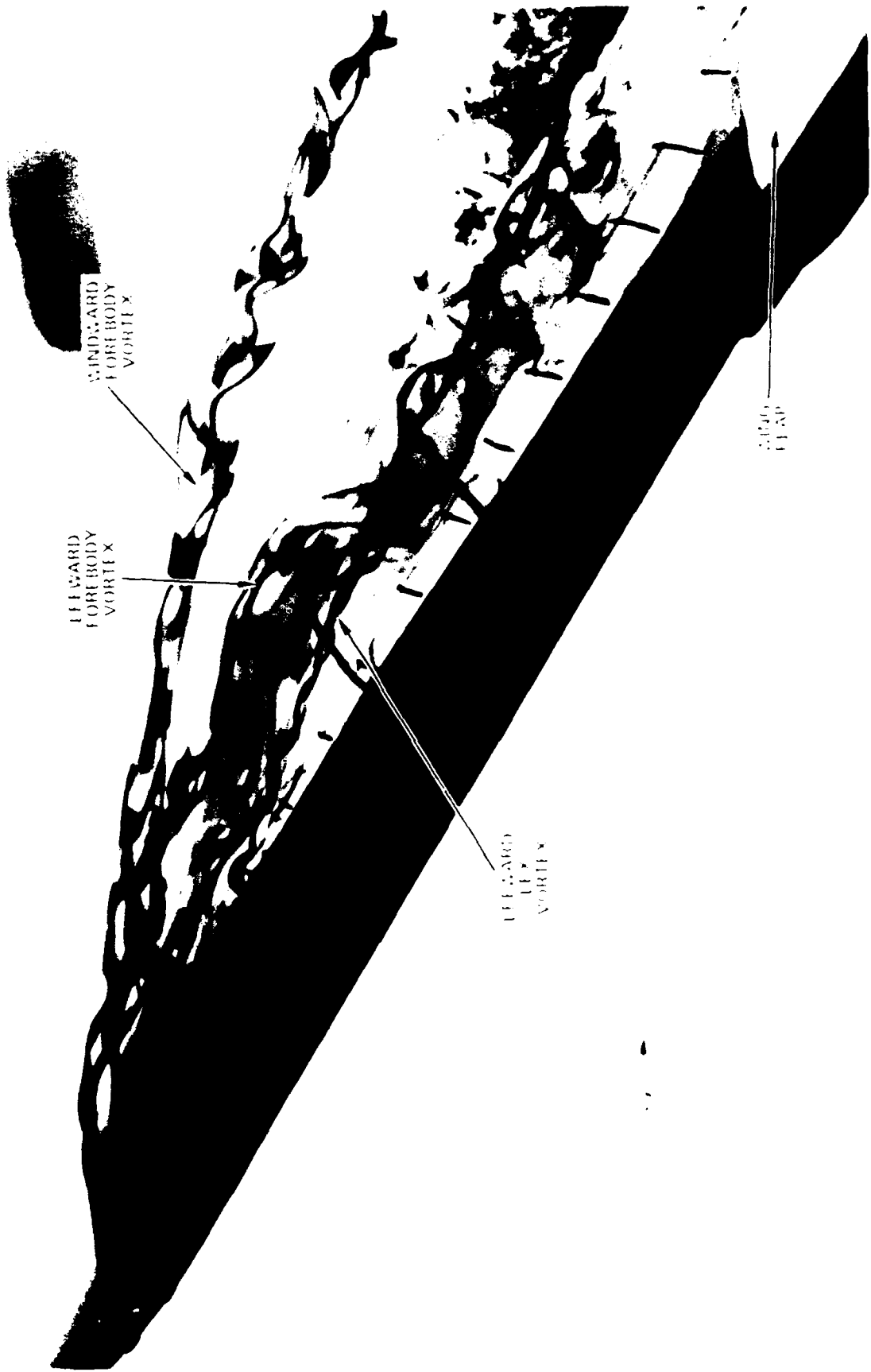
WING
FLAP

FIGURE 137 NORTHROP WATER TUNNEL FLOW VISUALIZATION OF THE STRONG COUPLING BETWEEN
THE FOREBODY AND WING LEX VORTEX FLOW FIELDS AT SMALL ANGLE OF SIDESLIP
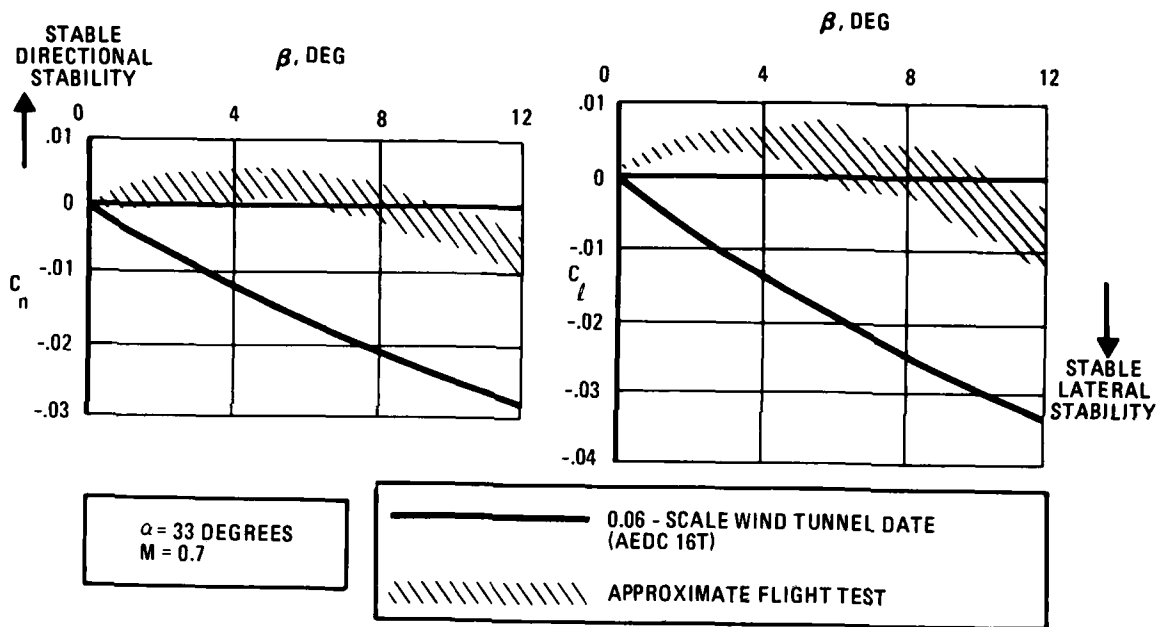
A) COMPARISON OF LATERAL – DIRECTIONAL CHARACTERISTICS
OBTAINED IN 0.06 – SCALE HIGH-REYNOLDS-NUMBER WIND
TUNNEL TESTS AND IN FULL-SCALE FLIGHT TESTS
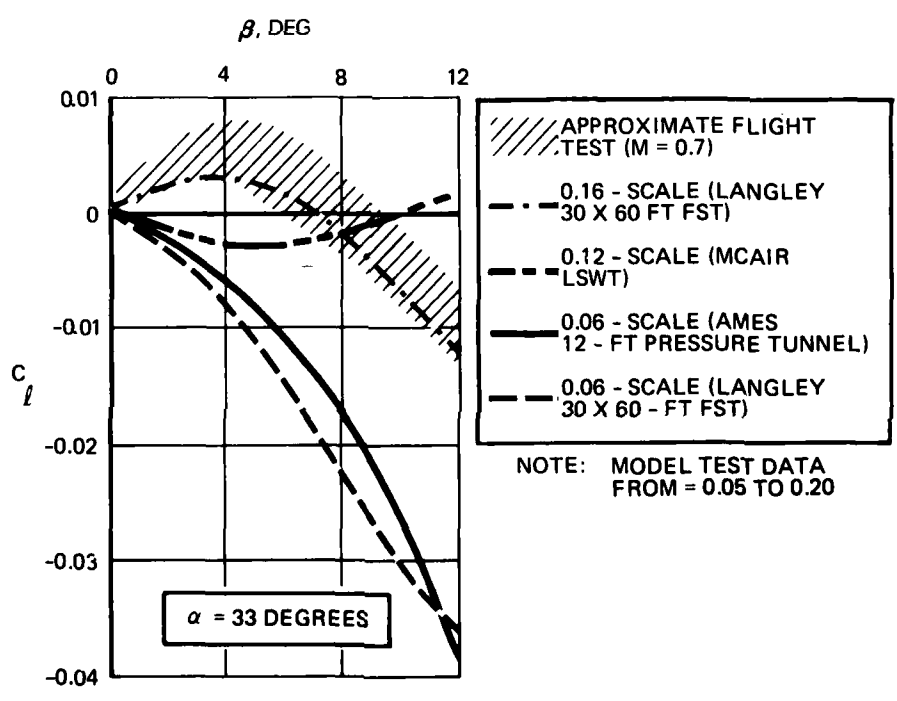
B) COMPARISON OF SUB-SCALE WIND TUNNEL MODEL AND
FULL SCALE FLIGHT TEST LATERAL STABILITY

FIGURE 138. SUB-SCALE WIND TUNNEL AND FULL-SCALE FLIGHT TEST RESULTS
ON A CURRENT TWIN-TAIL FIGHTER CONFIGURATION

252
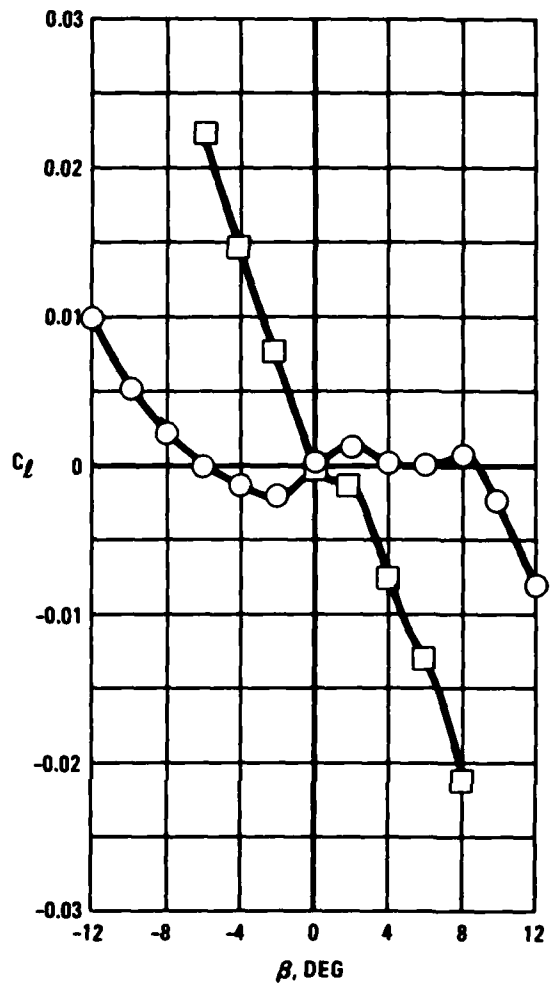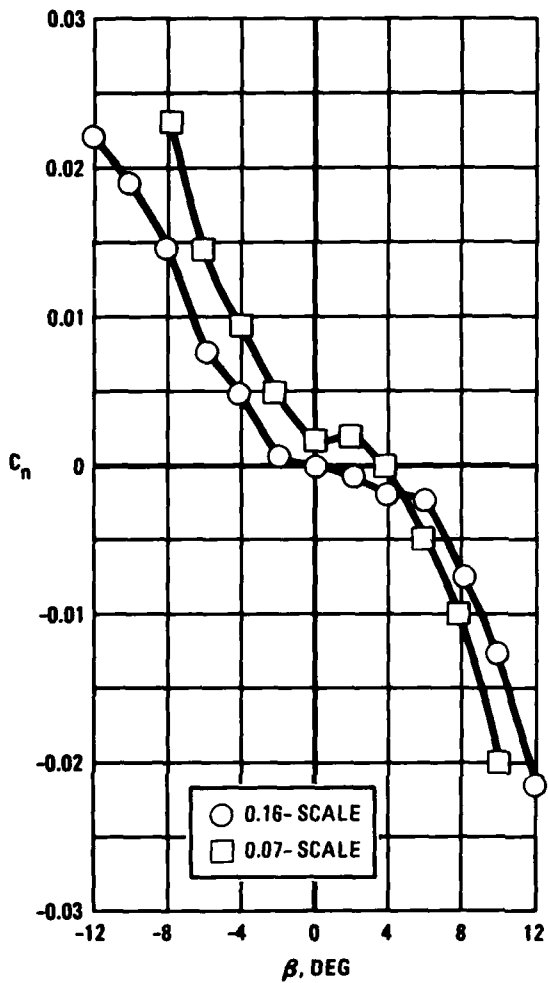
FIGURE 139. LATERAL-DIRECTIONAL CHARACTERISTICS OF
0.07-AND 0.16-SCALE F/A-18 MODELS — NASA LANGLEY
30 X 60-FT FULL-SCALE TUNNEL; $\alpha = 35^\circ$

INCREASED LEX
SLOT WIDTH

INCREASED LEX
SLOT WIDTH AND
LENGTH

LEX LOWER
SURFACE FENCE

FENCE A
FENCE B

FOREBODY
STRAKES

FAIRED STRAKE

STRAKE

ϕ

SECTION A-A

A

A
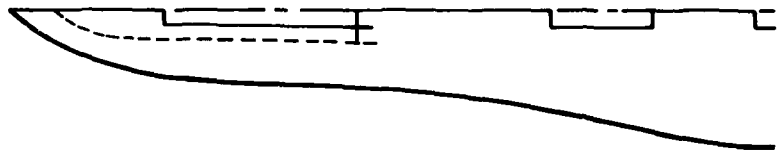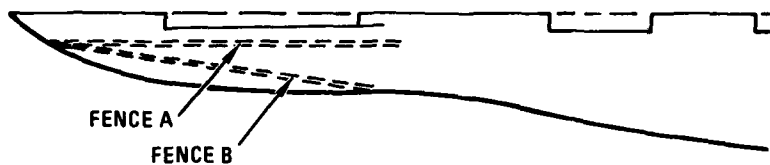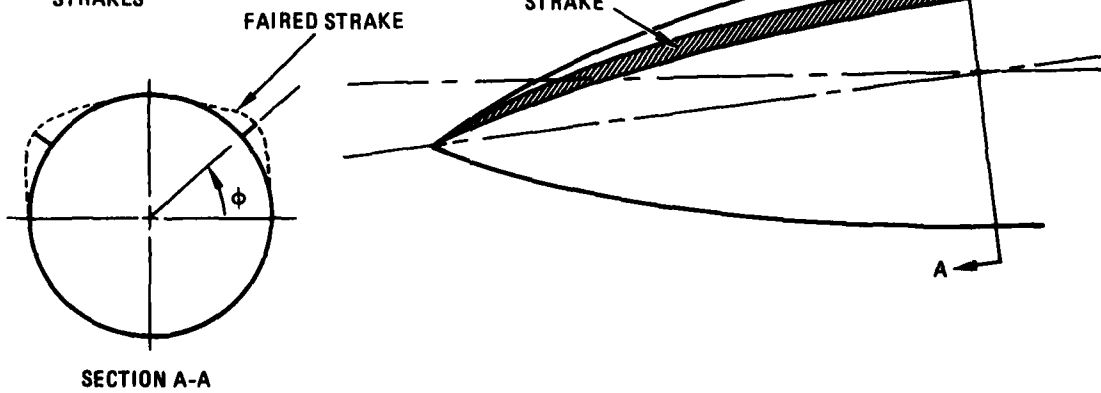
FIGURE 140. FOREBODY AND LEX GEOMETRY MODIFICATIONS (SCHEMATIC)

254
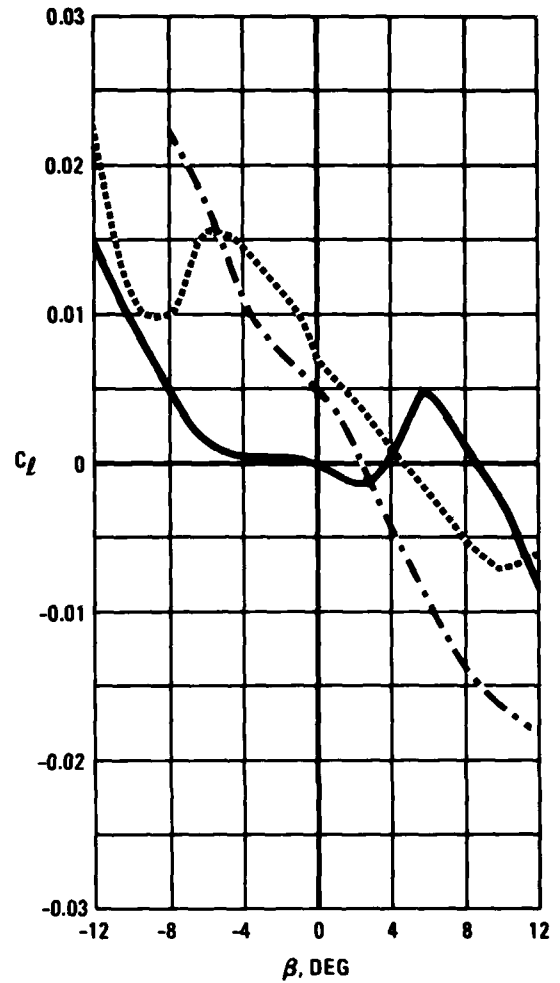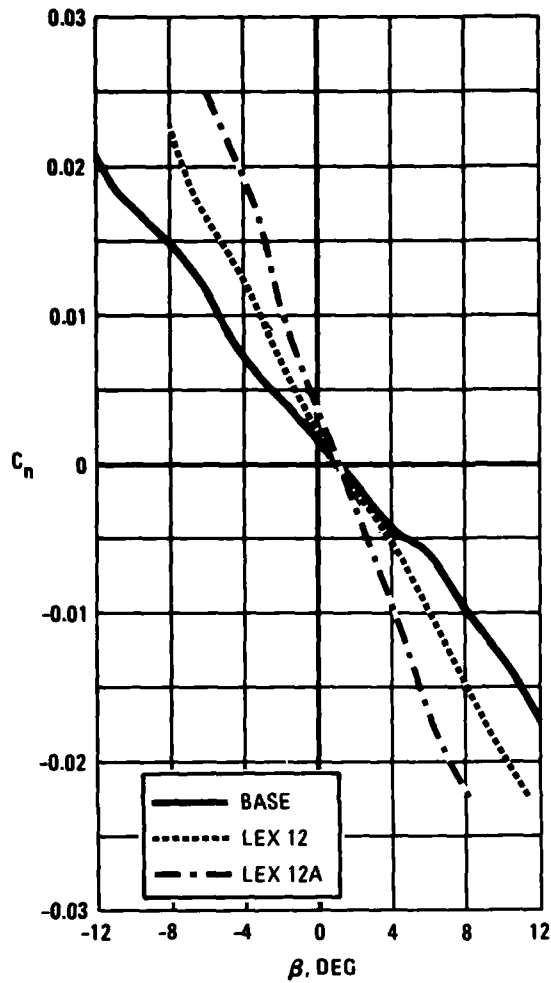
FIGURE 141. EFFECTS OF INCREASED FORWARD LEX SLOT WIDTH AND
LENGTH ON 0.16-SCALE F/A-18 LATERAL-DIRECTIONAL
CHARACTERISTICS; M = 0.05; α = 40 DEG

255
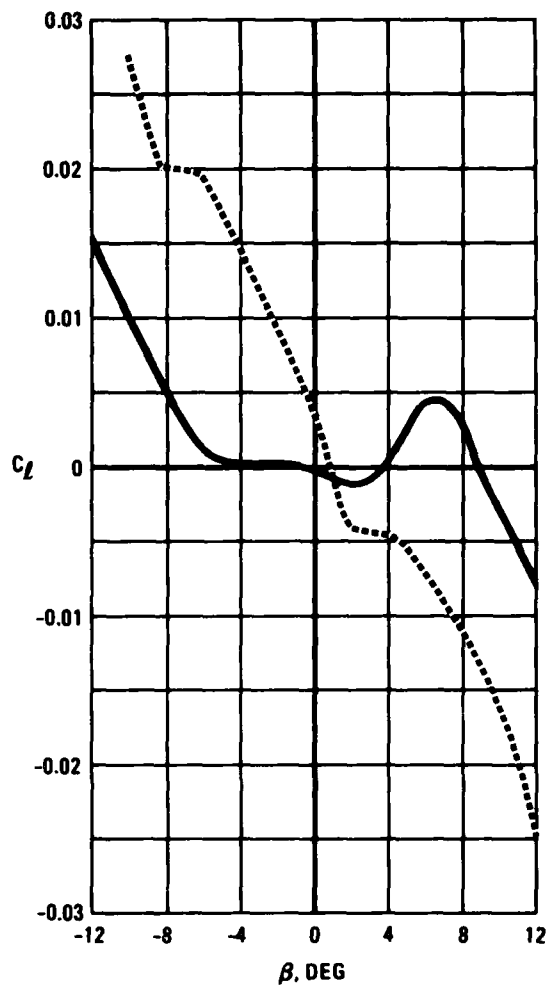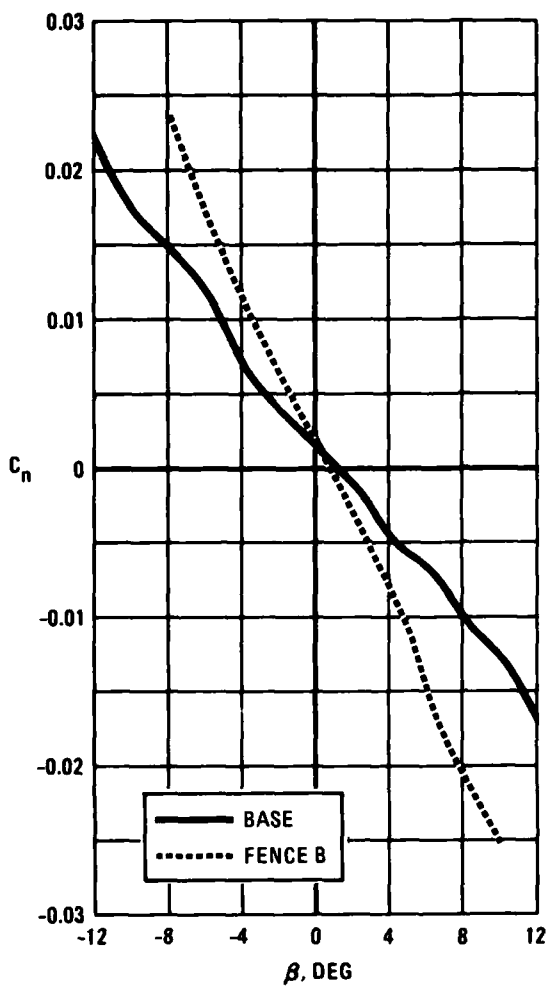
FIGURE 142. EFFECT OF LEX LOWER SURFACE FENCE ON 0.16-SCALE F/A-18
LATERAL-DIRECTIONAL CHARACTERISTICS; M = 0.05; α = 40 DEG;
δ_n = 35 DEG; δ_h = -12 DEG
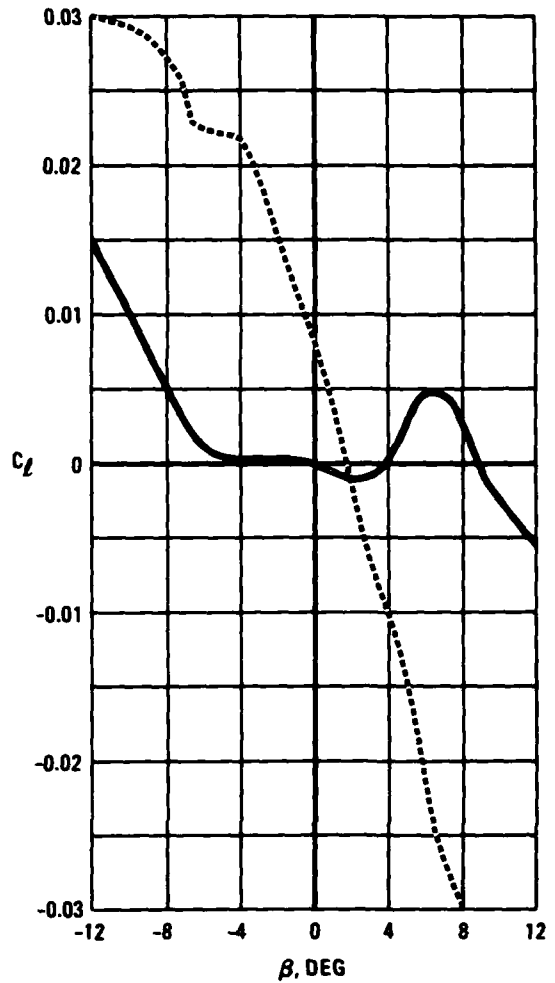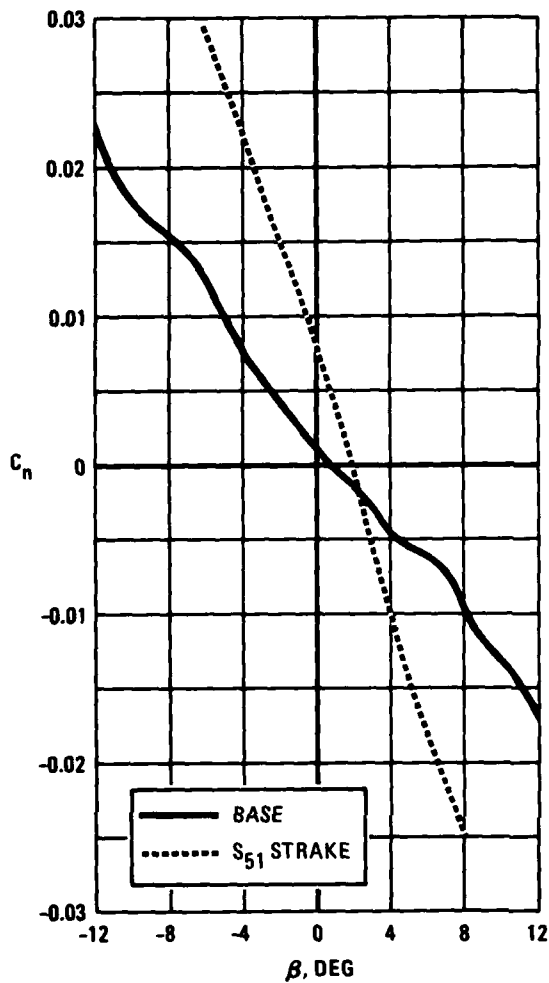
FIGURE 143. EFFECT OF RADOME STRAKES ON 0.16-SCALE F/A-18
LATERAL-DIRECTIONAL CHARACTERISTICS;
M = 0.05; α = 40 DEG; ϕ = 40 DEG
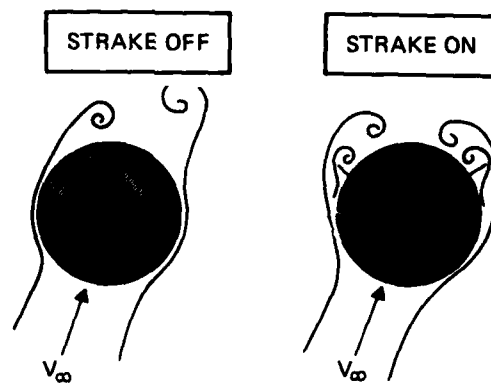
FIGURE 144. SCHEMATIC OF STRAKE EFFECT ON VORTEX PATTERNS AT
TYPICAL RADOME SECTION AT HIGH ANGLE OF ATTACK

257

vortex flows. Northrop water tunnel studies of these geometric changes confirm this. For example, the effect of small strakes mounted on the leeside of the forebody and extending to the nose apex have been examined in the water tunnel. Results indicate that at high angles of attack the vortices shed from the strakes, which are nearly coincident with the primary separation lines in this region, enhance the forebody primary vortices, as sketched in Figure 144. This, in turn, results in a stronger interaction with the wing flow field. As a result, a fluid flow mechanism based on the water tunnel studies has been developed which is consistent with lateral-directional stability trends observed in the wind tunnel.

5.4 LEADING-EDGE AND SLENDER BODY VORTEX FLOWS -- SIMULATION OF INLET AND EXHAUST EFFECTS AND PROPULSIVE LIFT CONCEPTS IN STEADY FLOW

Inlet and exhaust flow effects have been investigated quite extensively in the Northrop water tunnel. The majority of configurations tested in the Diagnostic Water Tunnel Facility now feature flow-through inlets with variable mass flow ratio capability. Depending on inlet geometry and location relative to a highly-swept LEX, measurable effects on LEX vortex stability can be ascertained due to inlet flow rate. LEX vortex stability characteristics presented in Figure 145 obtained on a 0.025-scale F-5F suggest that influx into the side-mounted inlets at moderate-to-high angles of attack induces a local upwash near the LEX apex, such that the effective angle of attack in this region is approximately 2 degrees higher than the geometric angle of attack. A top-mounted inlet configuration which has been tested in the water tunnel is illustrated in Figure 146.

Studies were made of exhaust flow effects on afterbody surface flow patterns for several 2-D nozzle geometries.
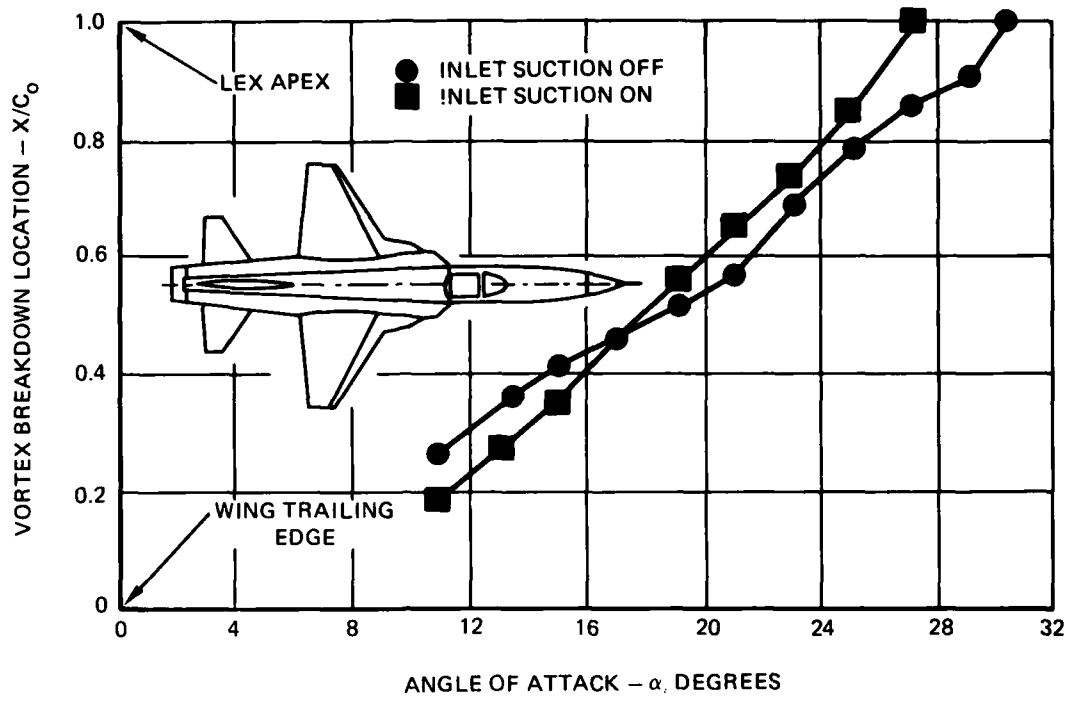
FIGURE 145. INLET FLOW EFFECTS ON LEX VORTEX STABILITY
(NORTHROP WATER TUNNEL)

259

FIGURE 146. TOPSIDE INLET MODEL MOUNTED IN NORTHROP WATER TUNNEL AT LOW ANGLE OF ATTACK

Knowledge a priori of the surface flow characteristics on the ADEN nozzle from wind tunnel oil flow studies (Reference 162) enabled a matching of the flow patterns in the water tunnel by increasing the nozzle exit velocity (V_e) relative to freestream velocity (V_∞). A qualitative assessment was then made of the effect of V_e/V_∞ variations on the boundary layer separation characteristics.

Propulsive lift enhancement concepts have also been quite amenable to study in a water medium. Upper surface spanwise blowing (SWB) concepts have been investigated on models of current fighter aircraft as a means of vortex-induced lift enhancement and/or boundary layer control. Studies made of the F-5E with SWB (see Figure 147) provided fascinating results on the time-dependent effect of blowing on LEX vortex stability. At high angles of attack where the LEX vortex is essentially a large, diffuse, rotating mass without blowing, initiation of blowing from a single circular water-jet nozzle near the LEX-wing junction was observed to cause a gradual rolling up of the vortical flow until, in the steady-state condition, a thin, concentrated vortex core was evident. Core breakdown then occurred at about mid-chord (see Reference 163). More recent studies made on a model of the F-4 aircraft in Reference 164 revealed similar beneficial effects on the wing stall characteristics due to SWB.

Blowing in a spanwise direction on a deflected trailing-edge flap of a slender wing at high angle of attack produced some intriguing results, as seen in Figure 148. Flow entrainment effects due to the blowing jet were observed to enhance the leading-edge vortex and to cause the vortex-core to follow more closely the curvature of the wing surface.

It was shown previously that the water tunnel studies of a forebody vortex control concept featuring asymmetric tangential blowing along the leeside of the F-5F forebody provide

261
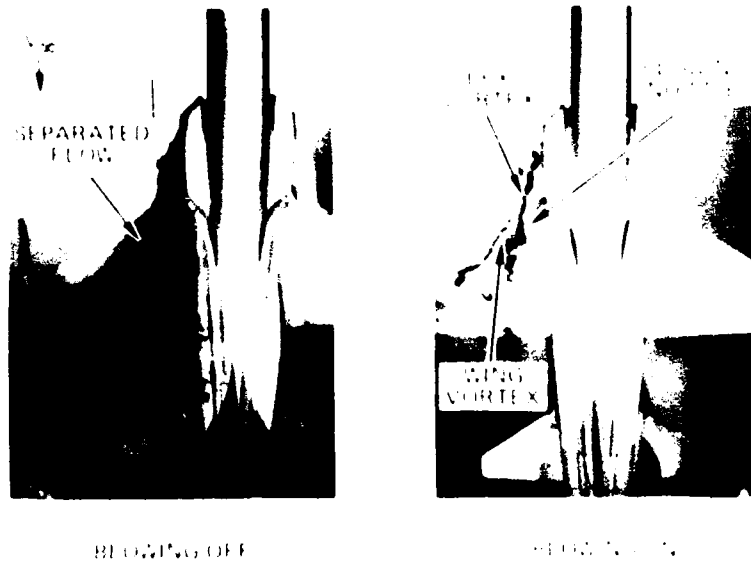
FIGURE 147. SPANWISE BLOWING EFFECTS ON THE VORTEX FLOW FIELD OF THE
NORTHROP F 5F AT 26 DEGREES ANGLE OF ATTACK (NORTHROP WATER TUNNEL)
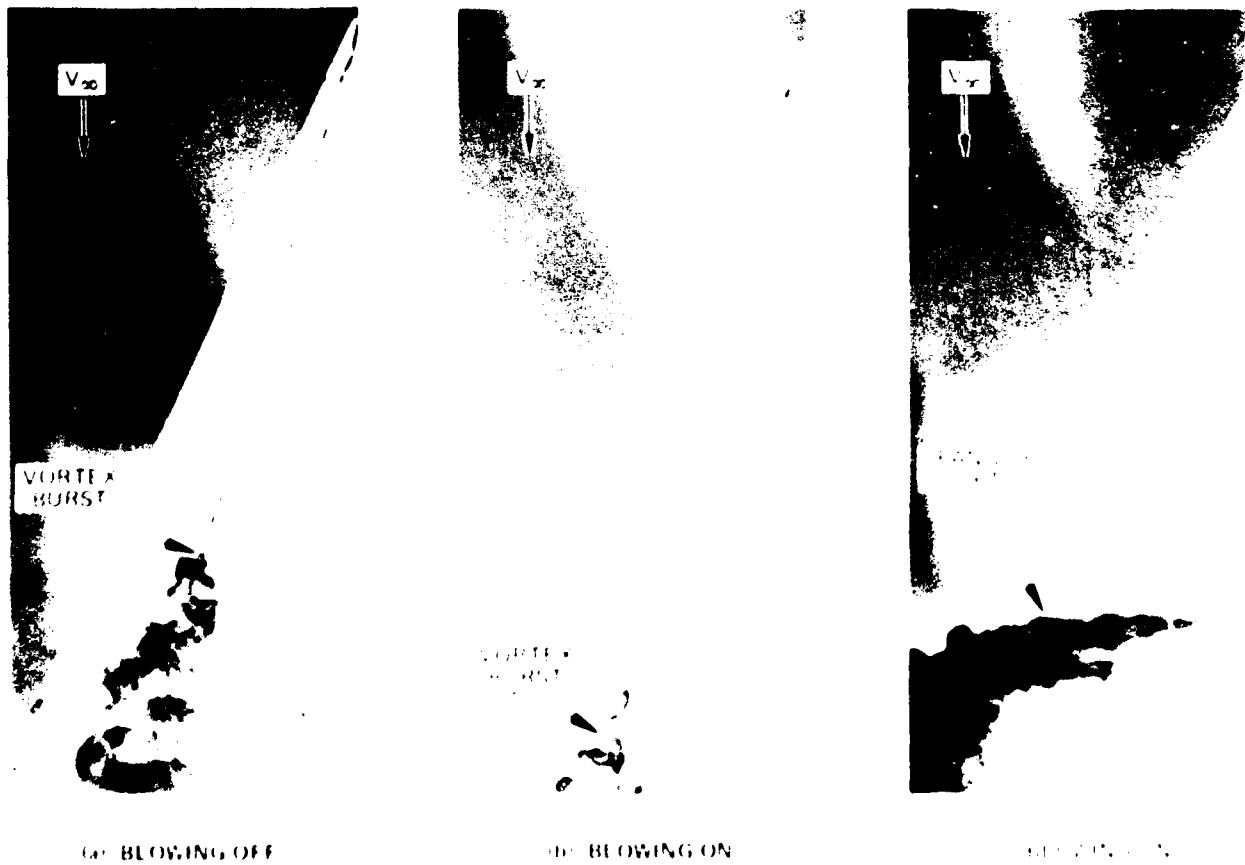
FIGURE 148 TRAILING EDGE FLAP SPANWISE BLOWING EFFECT ON SLENDER WING VORTEX
STABILITY AT 23 DEGREES ANGLE OF ATTACK AND 25 DEGREES TRAILING EDGE FLAP
DEFLECTION ANGLE (NORTHROP WATER TUNNEL)

excellent quantitative estimates of the blowing rates required
in air to affect a particular change in the orientation of the
body apex vortex pair.   In incompressible flow about slender
wings or wing-LEX geometries where flow separation occurs at a
salient edge, it is conjectured that the blowing rates required
in water and in air to affect a particular change in leading-
edge vortex stability should be in reasonable agreement.
Consider the following argument.   A general trend has emerged
from Northrop water tunnel studies of the past several years,
namely, that water tunnel onset angles for the occurrence of
significant changes in the vortex flow field about slender
wings and bodies are generally somewhat higher than those
attained in air.   Onset angles of attack for wing rock on a
slender wing, for example, and for vortex asymmetry on slender
bodies are consistently higher (by a few degrees) than the
values determined in wind tunnels.   (These discrepancies may
be due to apparent mass effects in the case of a slender wing
and, for bodies, due to a Reynolds number effect.)   In keeping
with this trend, the blowing rates required for reversal of
body vortex asymmetry were somewhat higher than those required
in the wind tunnel.   It seems reasonable, then, that in order
to energize the laminar boundary layer on the upper surface of
wings by SWB in a water tunnel, slightly higher blowing rates
would seem necessary relative to the values required to achieve
the same effect of turbulent boundary layer energization
in air.   In other words, water tunnel blowing rates appear to
provide an upper bound to the amounts of blowing needed in
air.   Verification of this hypothesis requires comparison of
surface flow patterns and vortex core behavior in water and in
air at comparable blowing rates, data which are generally not
available at this time.

263

5.5   VORTICAL MOTIONS IN UNSTEADY FLOW

Relatively few studies have been made in a water tunnel
of the dynamic behavior of vortex flows in unsteady or oscilla-
tory conditions.   The following discussion describes represen-
tative theoretical and experimental investigations of unsteady
flow and will point out the need for detailed studies in a
hydrodynamic test facility of these complex flow phenomena.

5.5.1   Unsteady Vortex Core Behavior in Steady Flight --
Slender Wings

Oscillatory behavior is frequently observed in leading-
edges vortices shed from slender wings at angles of attack
where core breakdown occurs, either downstream of the wing
trailing edge or over the wing panel.   This unsteady behavior
is evidenced by the familiar fore and aft traversal of the
breakdown point at constant incidence, being more dramatic when
bursting occurs downstream of the wing where the positive
pressure gradient varies slowly with distance and, as a result,
enables a greater travel of the burst position.   This pheno-
menon has been observed in water tunnels (see Reference 27) and
in wind tunnels (see Reference 141) using dye and smoke,
respectively, to visualize the vortex core and is also in
evidence by velocity measurements within the burst vortex and
wing surface pressure measurements made in wind tunnels
(Reference 86, for example) where large velocity and pressure
fluctuations are observed.   In flight, upper surface tufts
oscillate violently in the presence of vortex burst (see Figure
149 from Reference 149) and the fluctuating pressures asso-
ciated with a burst vortex system are experienced on many
fighter aircraft which generate powerful vortex flows (see
Reference 153, for example).

It is evident that the water tunnel flow phenomena
represent quite well the actual flow experienced in air at high
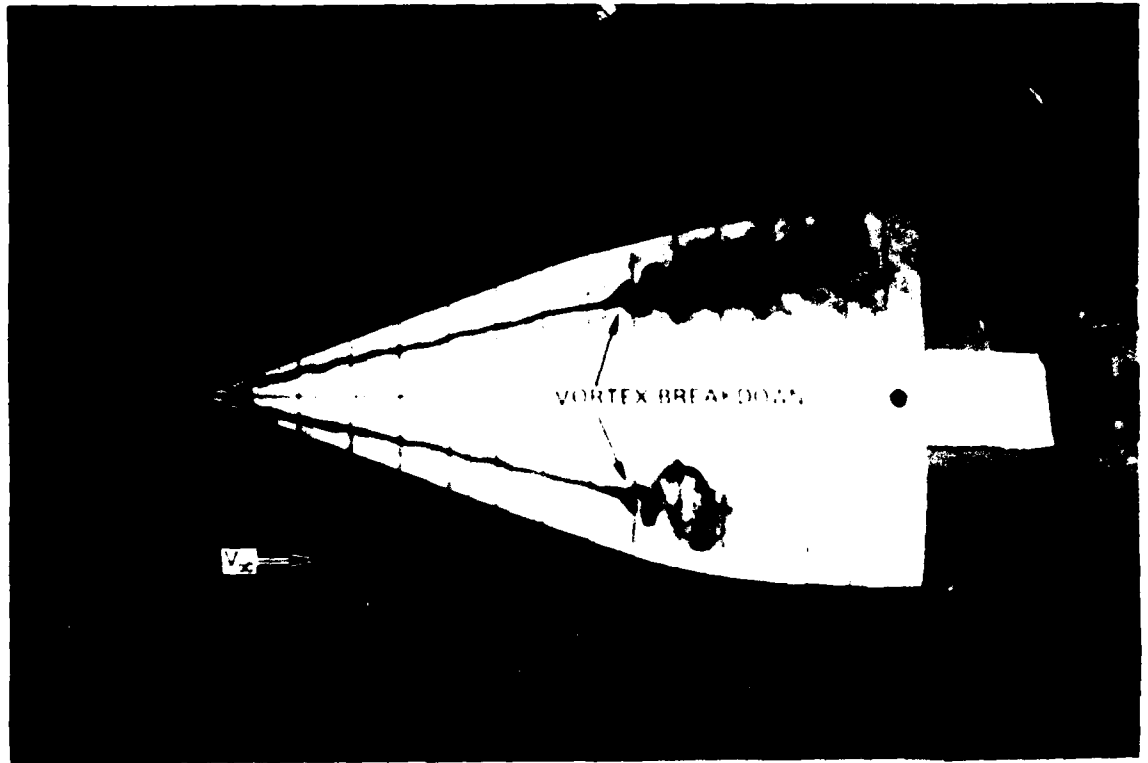
(a) NORTHROP WATER TUNNEL PHOTOGRAPH OF UNSTEADY VORTEX BURST
PHENOMENON ON A SLENDER WING (UPPER VORTEX EXHIBITS MOMENTARY
AXISYMMETRIC BREAKDOWN TYPE, LOWER VORTEX EXHIBITS SPIRAL TYPE
BREAKDOWN), RE = 2×10^4
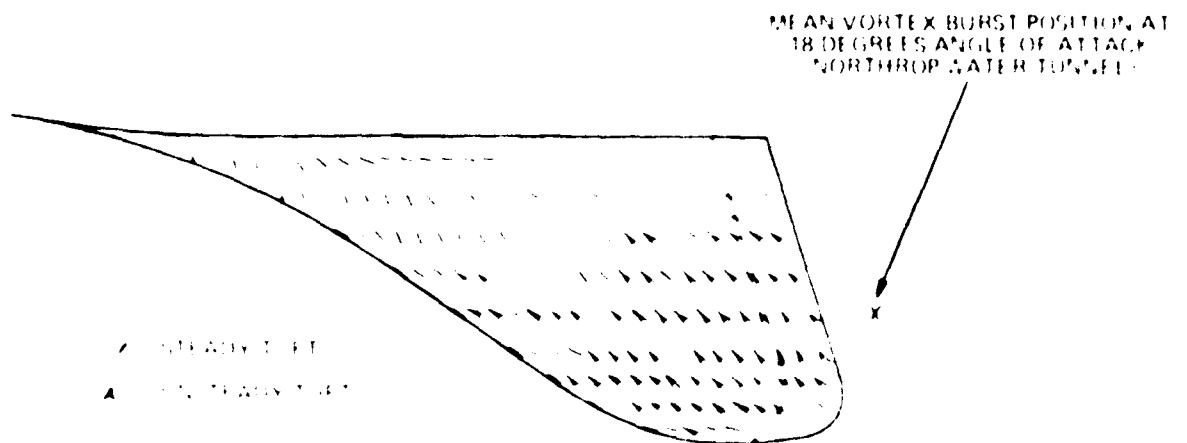
(b) OSCILLATORY UPPER SURFACE TUFT PATTERNS IN
FLIGHT IN THE PRESENCE OF VORTEX BURST
RE 20×10^6 (FROM REFERENCE 149

FIGURE 149 UNSTEADY FLOW PHENOMENA IN STEADY
FLIGHT CONDITIONS

Reynolds numbers. Note should be made, however, of the large viscous effects that may be present in the large, decelerated, rotating mass associated with a burst vortex system. For example, comparison of a burst LEX vortex in water and in air, illustrated in Figure 150, suggests that viscous effects are more significant within the expanded core in a water tunnel and, hence, the slowly-spinning burst vortex appears much larger in radial extent than that observed in a wind tunnel.

An additional unsteady phenomenon occurs on very slender wings (sweep angles of approximately 80 degrees or more) in which an unsteady, asymmetric leading-edge vortex core pattern is developed. Since flow separation is fixed at the sharp leading-edges, this unsteady phenomenon (and the steady, asymmetric pattern) appears due to a basic inviscid hydrodynamic instability mechanism. The oscillatory core breakdown pattern may also contribute to this flow behavior, as well as free-stream turbulence and model support oscillation.

Unsteadiness can occur in the vortex core itself. Related to a stationary, closed core breakdown bubble discussed in Reference 165 are unsteady core instabilities which have been observed in wing vortices at moderate-to-high angles of attack. Slight perturbations in angle of attack trigger the development of a continuous series of local core expansions, one of which is illustrated in Figure 151, which propagate downstream along the core axis. A sinusoidal oscillation of the entire vortex core may be initiated and, depending on the angle of attack, these instabilities can promote total breakdown of the vortex flow. The vortex core is transformed by an adverse pressure gradient, such that an originally stable core becomes unstable. After onset of instability, the disturbance waves may be amplified such that the vortex becomes asymmetric, leading to breakdown. Instability in a vortex core has also been detected on slender wing planforms featuring abrupt changes in local sweep angle which result in a discontinuity in

266
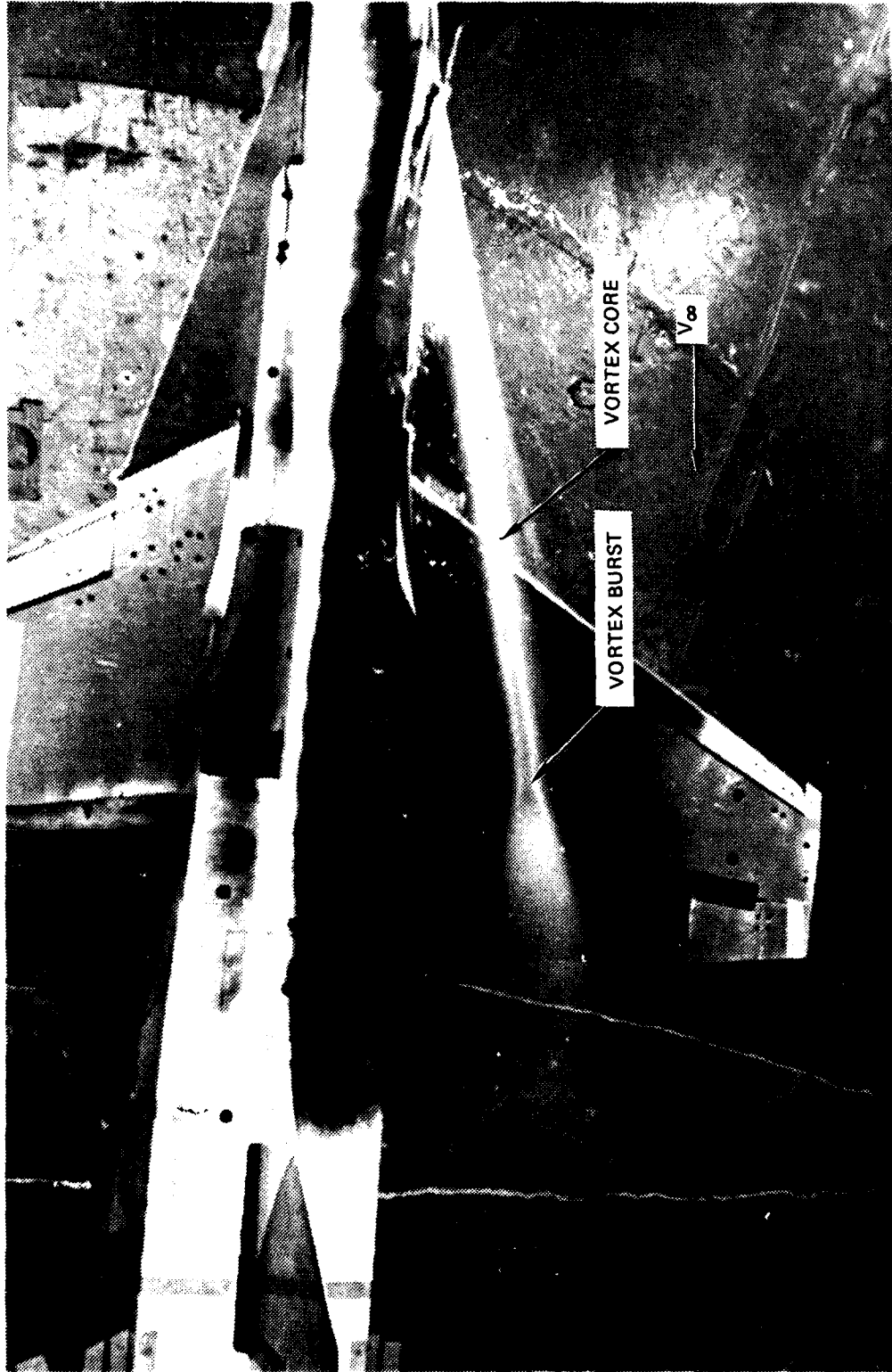
(a) WIND TUNNEL — 14 DEGREES ANGLE OF ATTACK

FIGURE 150. VORTEX CORE BURSTING IN NORTHROP WIND TUNNEL AND WATER TUNNEL TESTS

VORTEX CORE

VORTEX BURST

V_∞
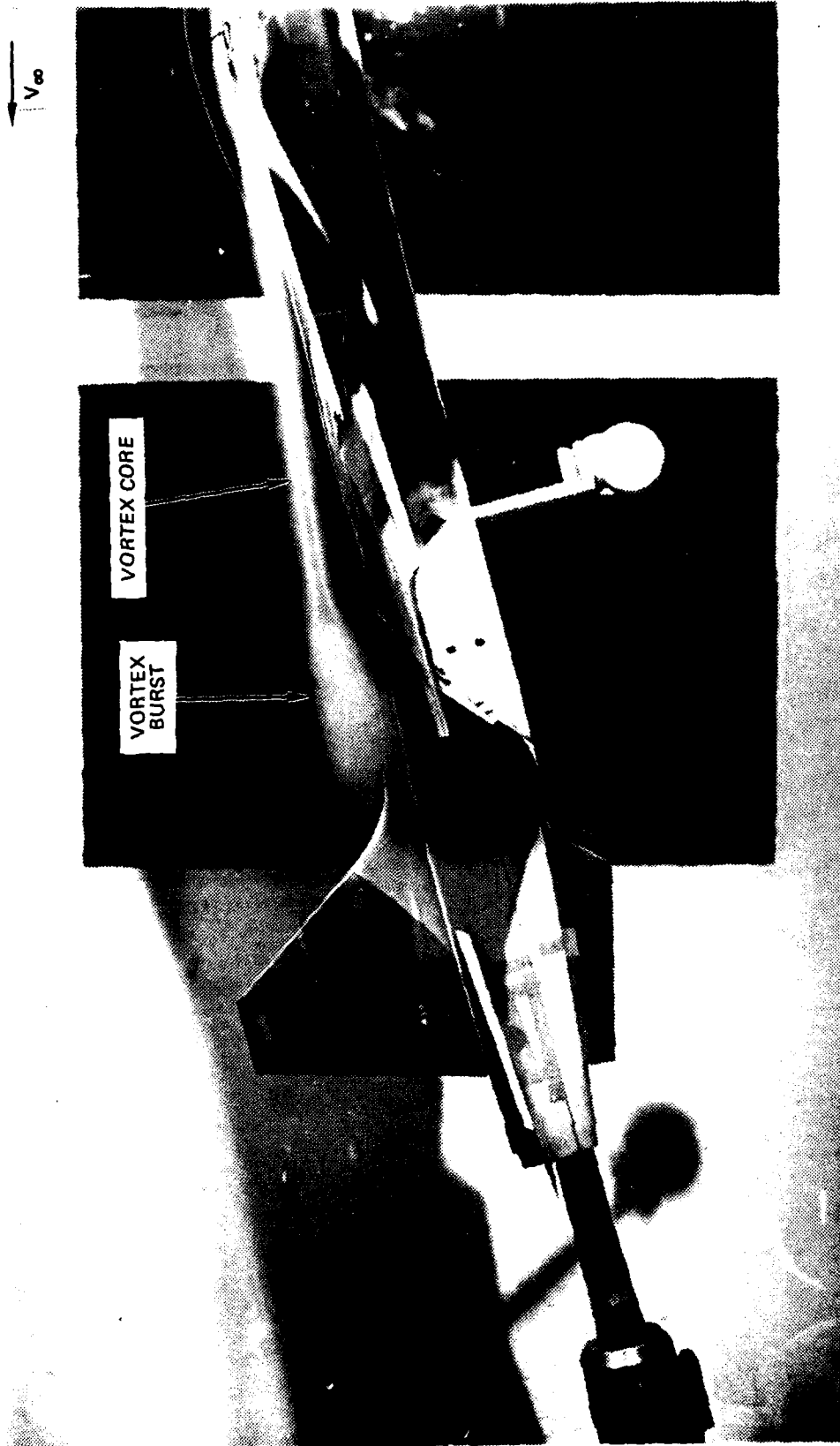
(b) WIND TUNNEL — 14 DEGREES ANGLE OF ATTACK

FIGURE 150. CONTINUED

VORTEX BREAKDOWN

LEX VORTEX

V_∞
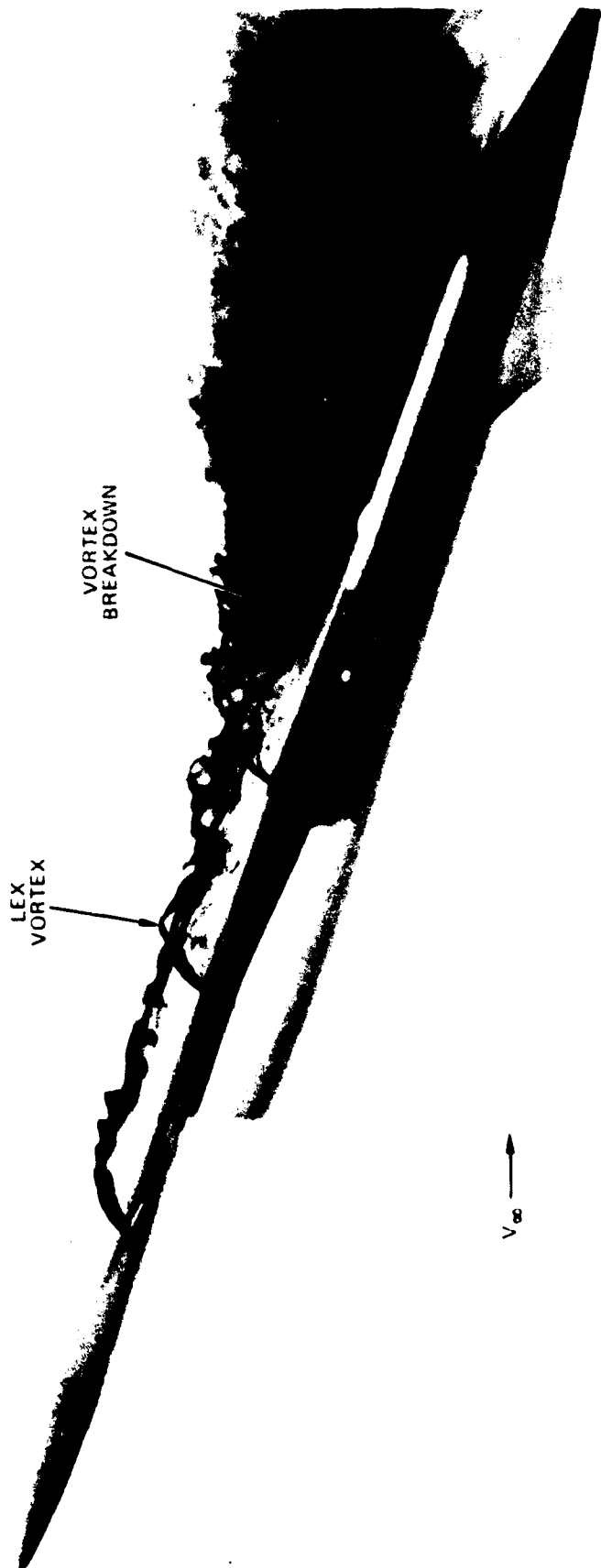
(c) WATER TUNNEL — 20 DEGREES ANGLE OF ATTACK

FIGURE 150. CONCLUDED
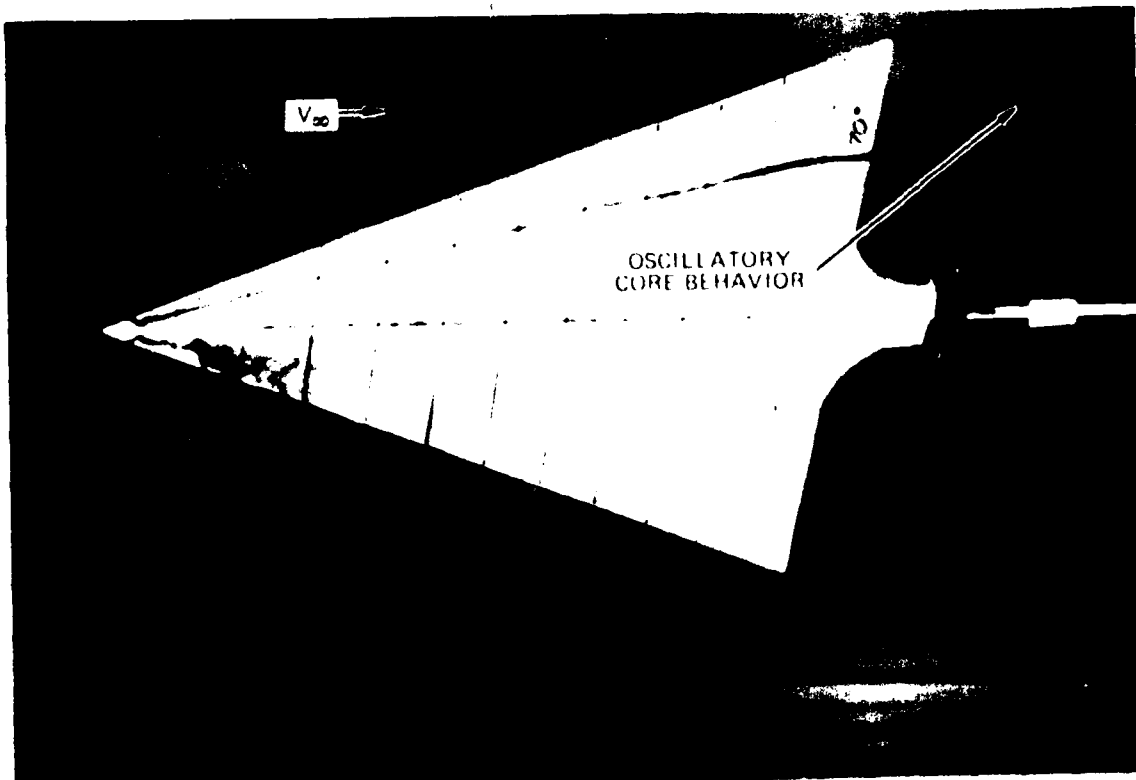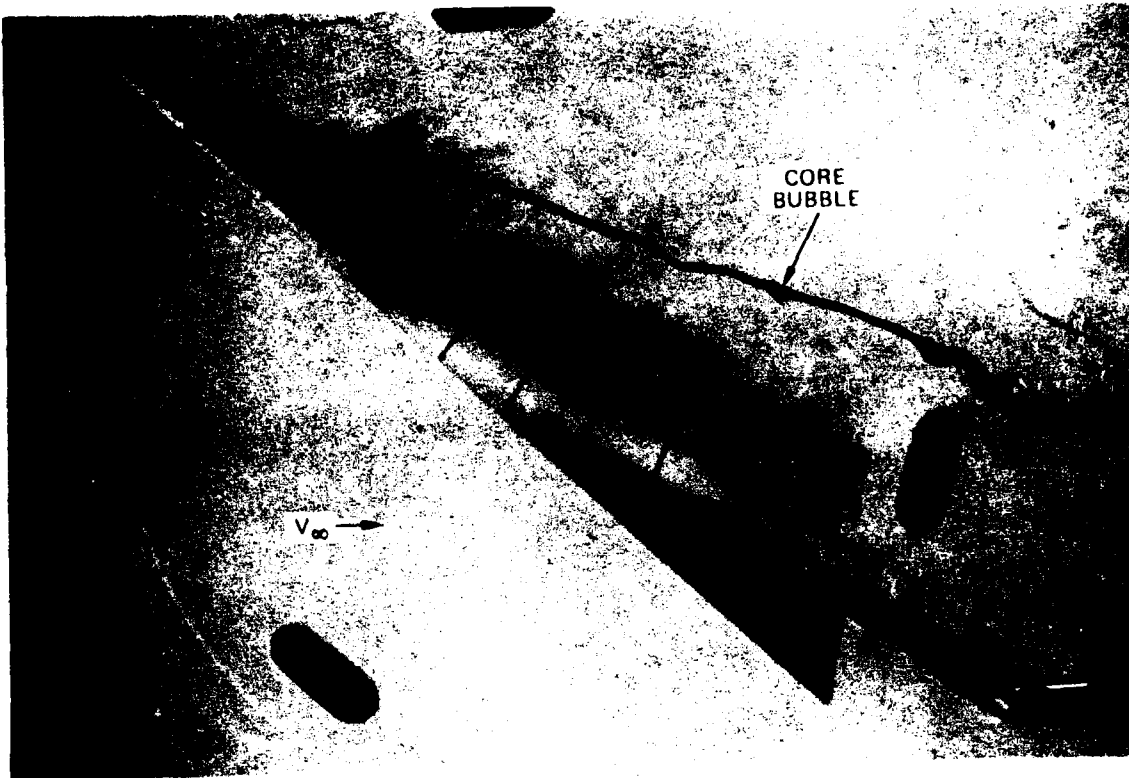
(a) LEEWARD VORTEX CORE OSCILLATION ON A 70-DEGREE DELTA WING

FIGURE 151. OSCILLATORY VORTEX CORE BEHAVIOR
IN STEADY FLOW (NORTHROP WATER TUNNEL)

DIFFUSED CORE
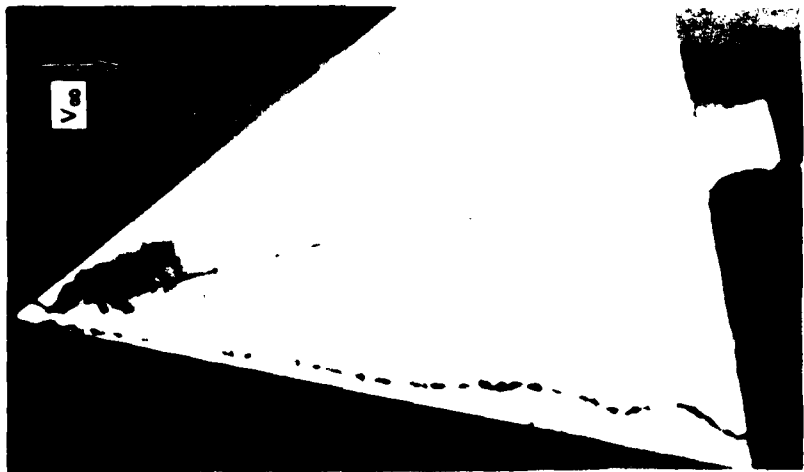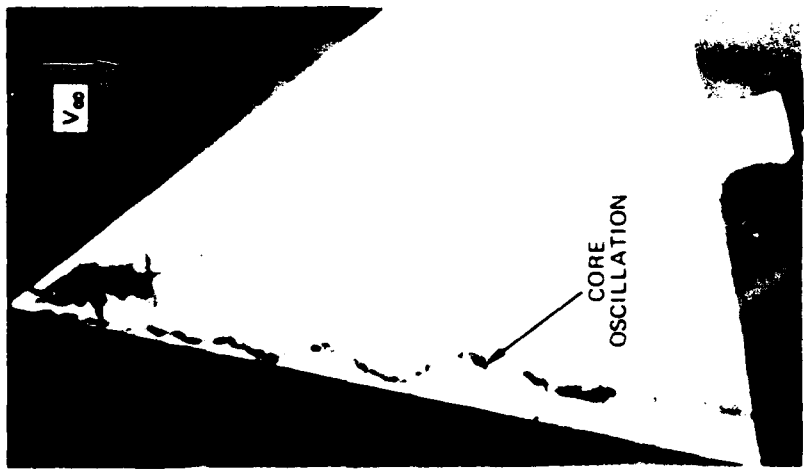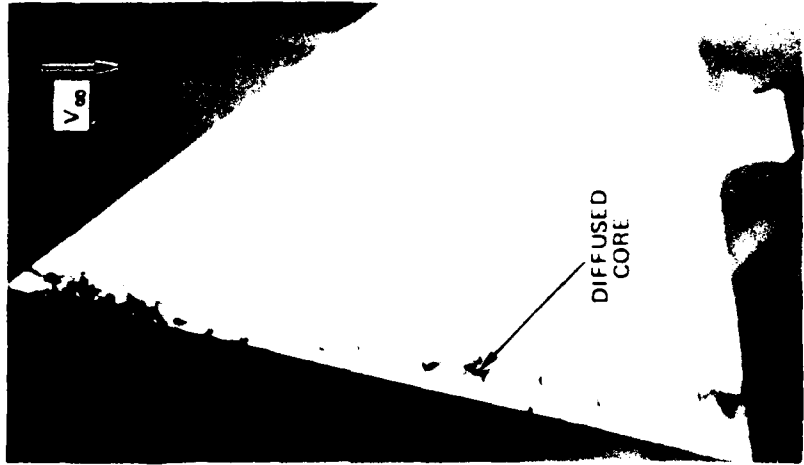
CORE OSCILLATION

(b) LEEWARD VORTEX CORE OSCILLATION AT CONSTANT ANGLE OF ATTACK ON A 65-DEGREE DELTA WING.

FIGURE 151. CONCLUDED

the vorticity feeding mechanism. The core expansions in this case are, however, stationary and are located near the position at which the local leading-edge sweep abruptly changes.

5.5.2 Unsteady Vortex Core Behavior in Steady Flight -- Slender Bodies

On aircraft and missile forebodies at high angles of attack, up to 90 degrees, where the influence of the axial flow component steadily diminishes, the vortex system can assume an alternating, unsteady pattern (one instant of time in such a periodic flow is depicted in Figure 152) or an unsteady, nonlinear wake (see Figure 153 and Reference 107). Water tunnel simulation of unsteady vortex flows on slender bodies has received little attention in the past, as was demonstrated in the literature survey of water tunnel applications in this contract. Oscillatory vortex shedding was observed in Northrop water tunnel tests of bodies of revolution and non-circular bodies at high angles of attack (see Figure 154). Flow studies also revealed a periodic reversal of the asymmetric vortex pattern on a forebody with a long, tapered nose boom which is in qualitative agreement with the oscillatory side-forces that have been observed on the F-5F with flight test boom. Such phenomena may be promoted by free-stream turbulence or non-rigidity of the model support system in a water or wind tunnel (see Reference 166).

The unsteadiness of the flow patterns at these high attitudes requires the introduction of an additional flow parameter which permits an assessment of the applicability of the water tunnel results to wind tunnel and flight data. A parameter which is related to the frequency of vortex shedding is the Strouhal number defined as:

$$S_{vo} = \frac{nd}{U_\infty} \qquad \text{Equation 7}$$

272
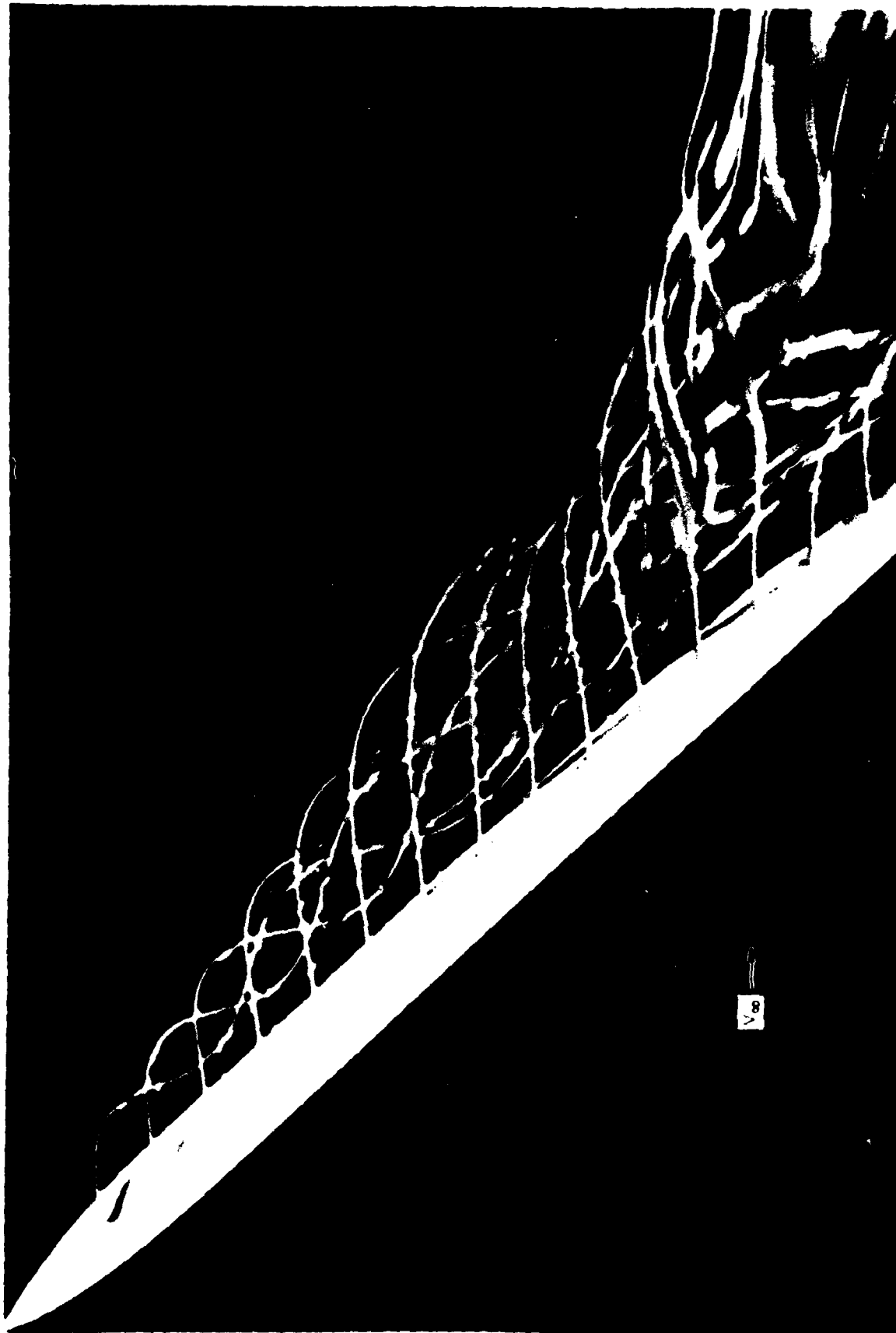
FIGURE 152. WATER TUNNEL FLOW VISUALIZATION OF STEADY, ASYMMETRIC VORTEX SHEDDING ON A SLENDER BODY (FROM REFERENCE 108)
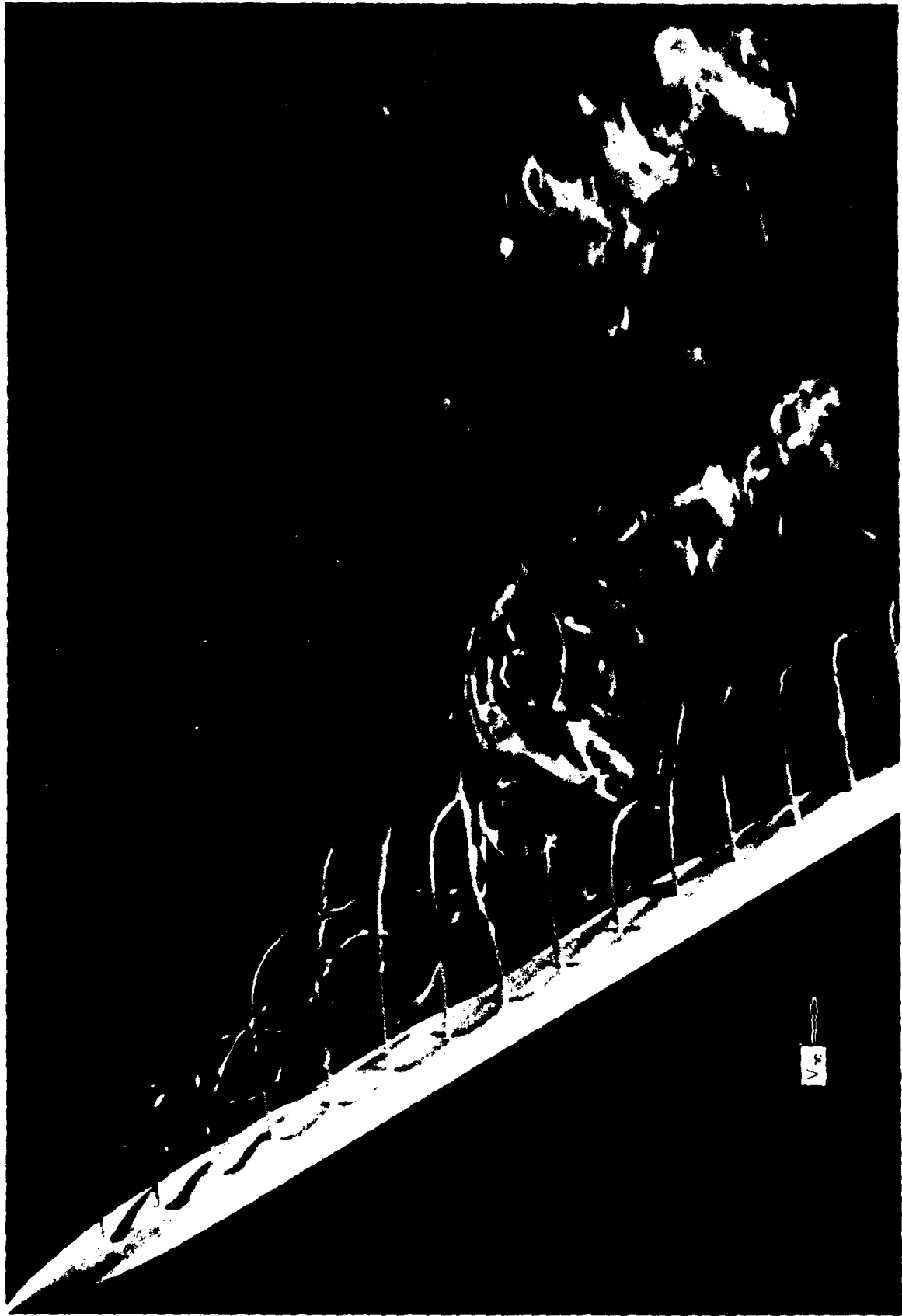
FIGURE 153. WATER TUNNEL FLOW VISUALIZATION OF UNSTEADY, ASYMMETRIC VORTEX SHEDDING ON A SLENDER BODY (FROM REFERENCE 108)
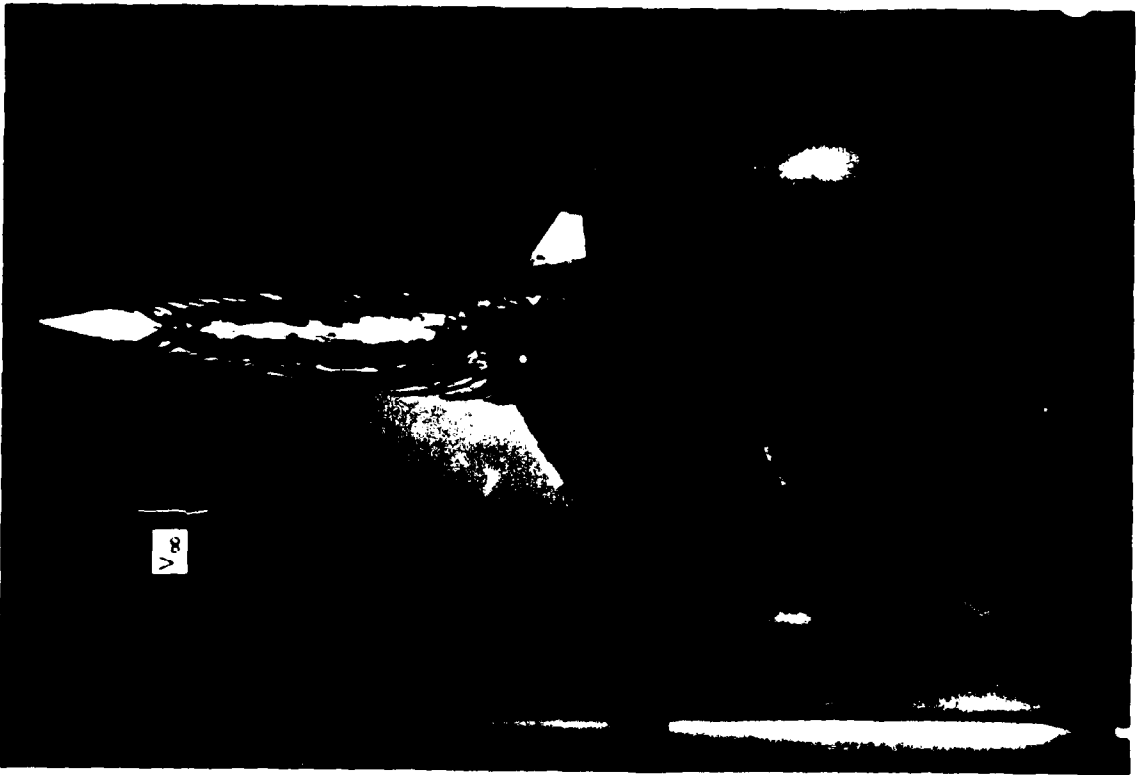
FIGURE 15.4. OSCILLATORY BODY VORTEX CORE BEHAVIOR AT CONSTANT ANGLE OF ATTACK ON A CRUCIFORM MISSILE CONFIGURATION (40 DEGREES ANGLE OF ATTACK. NORTHROP WATER TUNNEL)

where n and d are the frequency and body diameter, respectively. The Strouhal number is a function of the Reynolds number, as shown in Figure 155 (from Reference 105) for two-dimensional cylinders. At subcritical Reynolds numbers, typical of the water tunnel operating range and many low-speed wind tunnel tests, the Strouhal number is essentially a constant at approximately 0.21 which is quite valid for slender bodies at low speed. At high, or supercritical, Reynolds numbers, however, S_{vo} is a strong function of Reynolds number. When the laminar boundary layer separates near the top of the cylinder, discrete vortex cores are formed in the free shear layer at a low frequency. Turbulent boundary layer separation, however, occurs downstream of the top of the cylinder and the shed vortex frequency is high and irregular. Tnis effect may be magnified when considering non-circular cross-sections, typical of the Northrop F-5F forebody, for example. Thus, flow-separation geometries can vary widely in the supercritical Reynolds number range.

5.5.3 Vortex Behavior in Oscillatory Flight -- Theoretical Methods

Unsteady flow problems involving the concentration and subsequent decay of vorticity in vortex cores are also present on aircraft and missiles undergoing oscillatory motions. In unsteady flow, both the position and strength of the primary vortices shed from wings and bodies may vary because of the changes in shedding rate of vorticity. The flow situation is further complicated when interactions occur between vortices shed from multiple lifting-surface (canard-wing), slender forebody-wing-LEX and advanced missile configurations.

Slender Wings -- Theoretical Methods. -- Several theoretical methods for unsteady flow about slender, sharp-edged wings have been developed. A model from Reference 67 was the basis for an approach developed in Reference 167 in which a
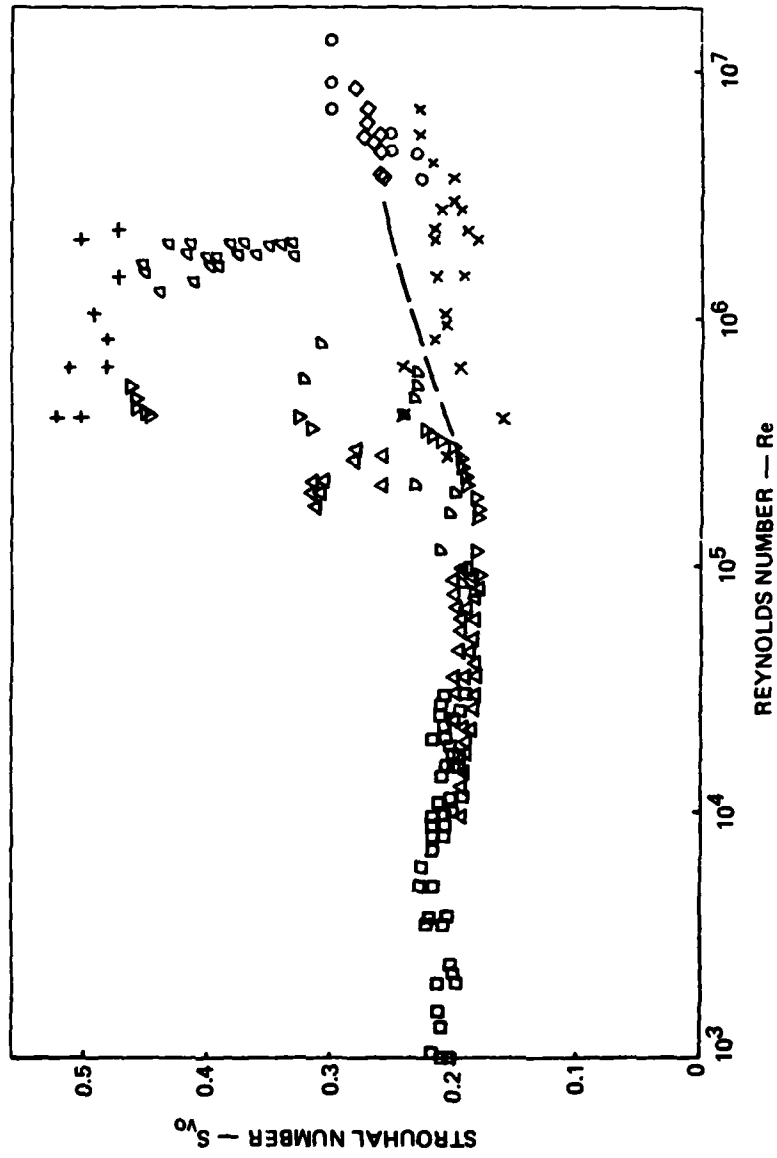
FIGURE 155. STROUHAL NUMBER VERSUS REYNOLDS NUMBER FOR CIRCULAR CYLINDERS (FROM REFERENCE 105).

solution was obtained for a thin, slender delta wing undergoing sinusoidal oscillations in a steady stream. The resulting motion was reduced to a linear perturbation of a steady motion due to the assumption of small oscillation amplitude relative to the mean angle of attack. Reference 168 obtained solutions for a delta planform undergoing both pitching and heaving motions without the assumption of linear perturbations. A solution was obtained in terms of the passage of an effective camberline through a section of air. These theoretical approaches emphasized the motion of the vortex cores. For example, theory predicts that if the angle of attack becomes zero at some point in the cycle, the vortex moves rapidly inboard and collapses.

5.5.4 Water Tunnel Utility in Dynamic Flow Simulations

Hydrodynamic test facilities have proven useful in the study of dynamic motions. For example, dynamic stall of a modified NACA 0012 airfoil oscillating in pitch has been investigated in the AVRADCOM water tunnel facility (see Figure 156 from Reference 169). Trajectories of air bubbles over an airfoil undergoing pitch oscillations in ONERA water tunnel experiments (Reference 170) are in qualitative agreement with streamlines computed from the Navier-Stokes equations in terms of vorticity and stream function for laminar flow (Reference 171).

It has been noted in Reference 172 that theoretical investigations of unsteady stall have been relatively unsuccessful due to inherent difficulties of modeling unsteady separation and unsteady vortices. An interesting point made in Reference 172 is that given the correct rate of vortex shedding, even inviscid flow models predict quite accurately the flow phenomenon. The role of a water tunnel in the study of dynamic stall has long been established (see Reference 173, for example) since such flow visualization provides vivid
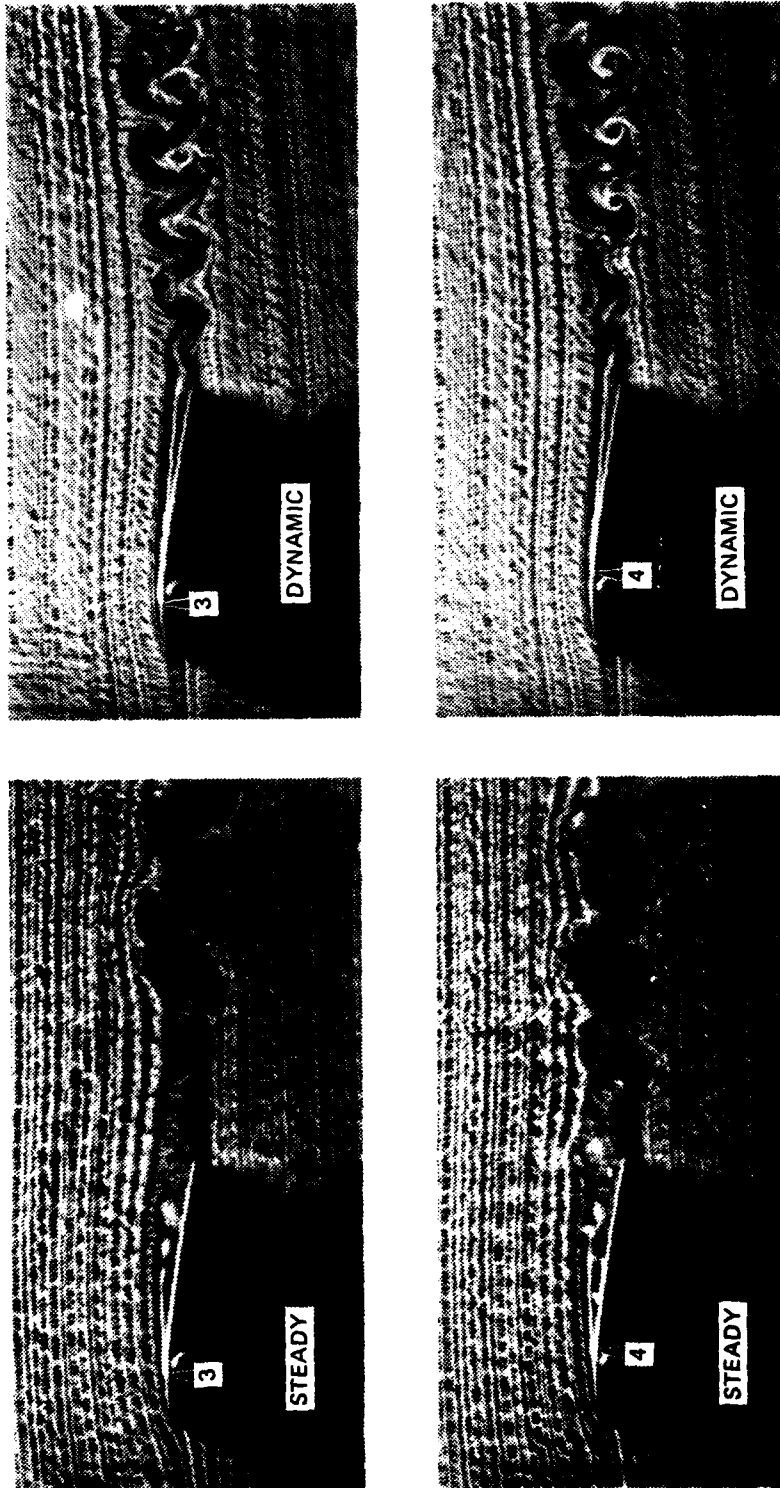
FIGURE 156. WATER TUNNEL STUDY OF THE FLOW FIELD ABOUT AN OSCILLATING AIRFOIL
(FROM REFERENCE 169)

279

information regarding vortex generation, growth, and breakdown. Although proper simulation of dynamic stall in water is questionable, such techniques have been adopted "to provide qualitative information and guide the researcher to make intelligent choices of the areas to be investigated more thoroughly" (see Reference 172). This was the approach taken in the water tunnel studies of Reference 172 in the Virginia Polytechnic Institute and State University (VPI-SU) facility.

Of greater relevance to the "Vortex Flow Correlation" study is that the water tunnel is a potentially powerful diagnostic tool in the simulation of slender wing and body vortex flows in unsteady conditions. For example, most of the measurements of vortex positions have, up to the present time, been obtained in water tunnel facilities. Reference 27 has conducted experiments in the Southampton University (England) water tunnel of an 80-degree delta wing oscillating in heave with an amplitude of 9 degrees, mean angle of attack 18 degrees, and frequency parameter 1. In the steady case, the angle of attack could be gradually increased up to 41 degrees before breakdown occurred on the wing, although a hysteresis effect was evident in that the incidence could be reduced to 34 degrees before breakdown left the wing again (similar hysteresis effects have been observed on slender wings in the Northrop water tunnel). In the dynamic case, the maximum instantaneous angle of attack was only 27 degrees, yet vortex breakdown occurred on the wing near the trailing edge. Breakdown position eventually shifted off the wing with a decrease in incidence, although bursting was still in evidence near the trailing edge when the instantaneous angle of attack had reached 20 degrees. That hysteresis is more pronounced in the dynamic case is not altogether surprising since this phenomenon has been observed in past studies (Reference 174) and aerodynamic phenomena are, in general, accentuated under dynamic flow conditions.

280

References 168 and 175 tested an 80-degree delta wing performing pitch oscillations identical to those theoretically analyzed in References 167 and 168. Discrepancies in the vortex core locations between theory and experiment are evident in Figure 157, the experimental results lying well inboard of the theoretical curves (which is due, perhaps, to the inherent limitations of the theoretical models). The theory of Reference 168, however, provides a good qualitative prediction of the vortex core motion and the predicted collapse of the vortex at $\alpha = 0$ degrees is confirmed by experiment.

Water tunnel studies provide a relatively simple picture of the unsteady leading-edge separation and the formation of the leading-edge vortex. For example, water tunnel observations of slender wings in plunging motion (Reference 176) indicate that the steady-state vortex position is established after a certain time interval. The vortex is initially convected downstream from the apex with free-stream speed, this transient vortex being parallel to the leading edge since the local shedding of vorticity takes place at the same rate along the leading edge. As the vortex strength increases, the core moves inboard and upwards, which is completely analogous to the static case. The results reveal the vortex to assume its steady-state height position somewhat before the time at which the steady-state spanwise position is reached, as illustrated in Figure 158 (from Reference 177).

Reference 178 has investigated in a wind tunnel the effect of oscillatory bending deformation of the forward half of a delta wing by studying the pressure fluctuations over the rigid aft half of the wing. The effects on the vortex-induced loads due to upward or downward deflection can be assessed with the aid of water tunnel studies made at Northrop in which steady flow results were obtained on a similar configuration (see Figure 159 and Reference 179). The water tunnel steady
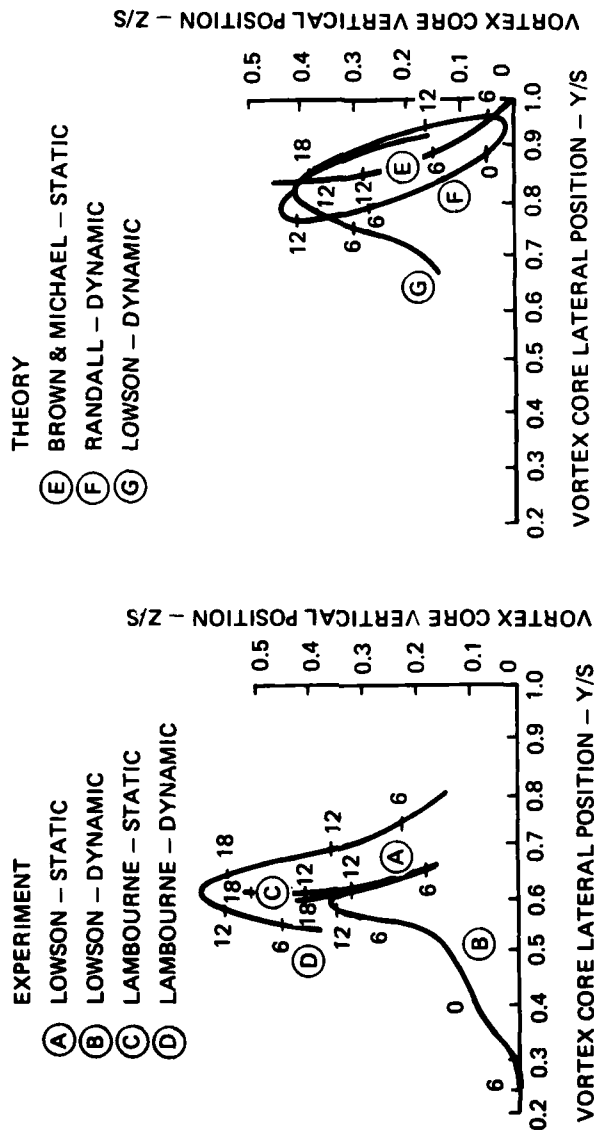
FIGURE 157. VORTEX CORE POSITIONS — PITCHING OSCILLATIONS
(FROM REFERENCE 55)

TIME t_1

TIME $t_2 > t_1$ VORTEX AXIS

- - - - - PREVIOUS PATH
OF VORTEX CENTER
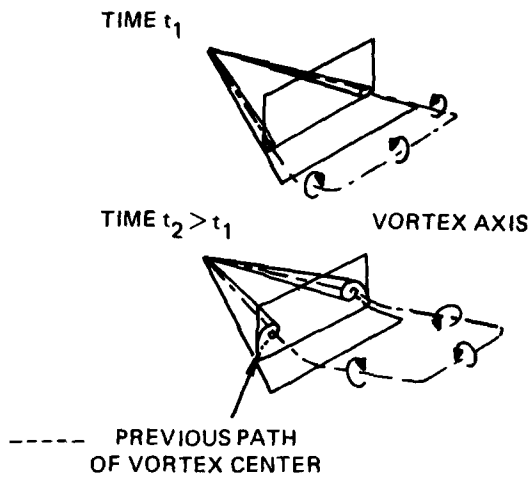
A) SCHEMATIC REPRESENTATION OF FLOW
DURING PLUNGE FROM ZERO TO
POSITIVE INCIDENCE

$X/C_o = 0.67$
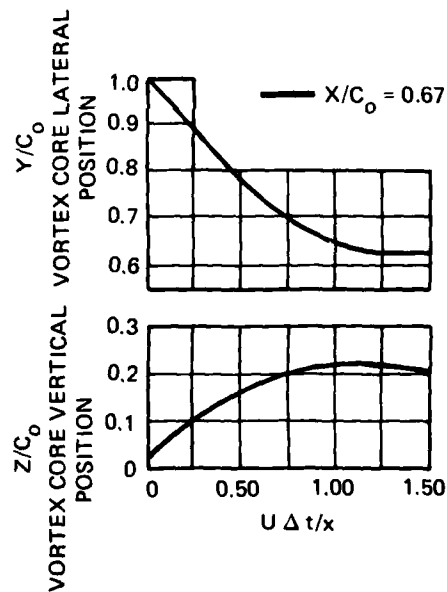
(B) LATERAL AND VERTICAL POSITIONS OF VORTEX
CORE VERSUS TIME; 12.4 DEGREES ANGLE OF ATTACK

FIGURE 158. LEADING-EDGE VORTEX FORMATION DURING PLUNGE FROM ZERO
TO POSITIVE ANGLE OF ATTACK (FROM REFERENCE 177)

283
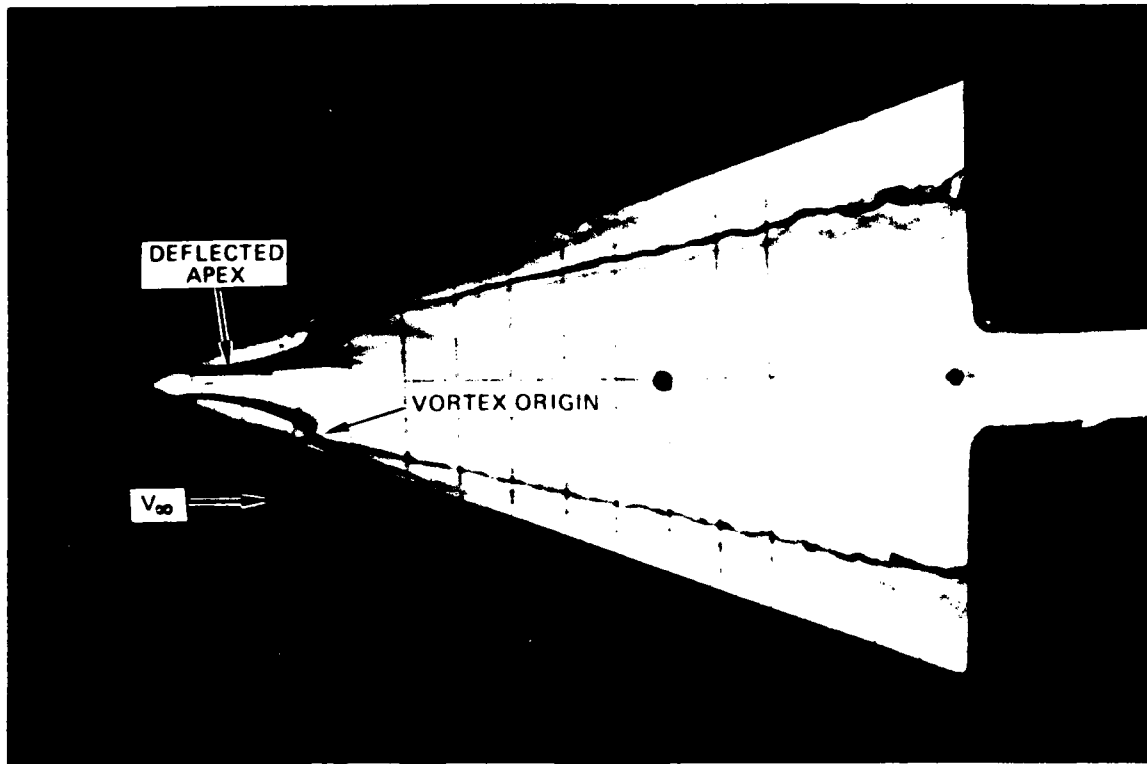
(a) NORTHROP WATER TUNNEL PHOTOGRAPH OF SLENDER WING WITH
DEFLECTED APEX (APEX DOWN).
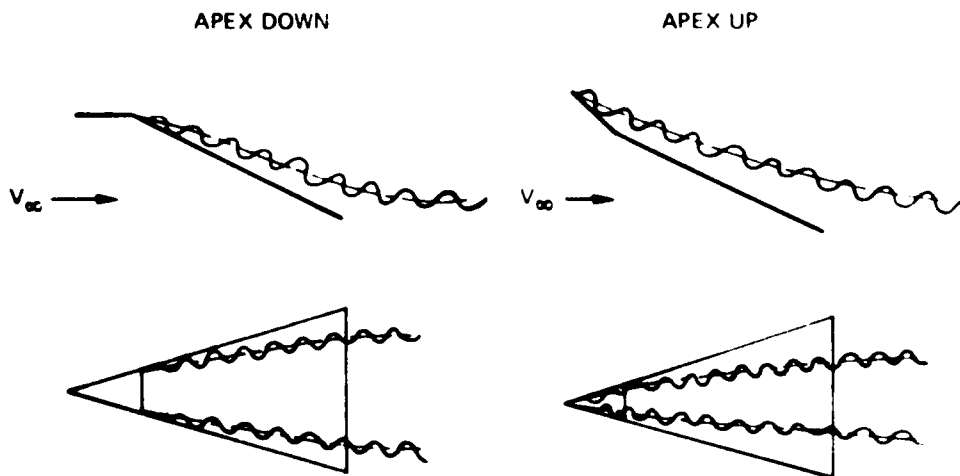
(b) SCHEMATIC OF VORTEX CORE POSITIONS OVER A SLENDER
WING WITH DEFLECTED APEX.

FIGURE 159. LEADING-EDGE VORTEX BEHAVIOR ON A
70-DEGREE DELTA WING WITH DEFLECTED APEX REGION

flow phenomena provide a fluid flow mechanism which is consistent with the wind tunnel surface pressure measurements in Figure 160 and the physical reasoning discussed in Reference 177. With upward deflection, the vortex core movement upward and away from the surface dominates over the effect of increased vortex strength, causing a loss in aft wing peak suction. The wing geometry with upward deflection is such that the shedding sheet from the leading edge weakens earlier since the ratio of local angle of attack to local wing sweep decreases along the chord and, thus, decelerates the vortex shedding process. The opposite is true for the case of downward deflection.

5.5.5 Recent Applications of Water Tunnels to Dynamic Vortex Motions

It can be seen, then, that a water tunnel can be used to visualize the dynamic behavior of vortex flows and to assist in the analysis of wind tunnel and flight test results. Yet, surprisingly, few detailed studies have been made with regards to unsteady effects on separation-induced wing and body vortices.

After the pioneering efforts of the British in the late 1950's and early 1960's, which were stimulated by the development of the Anglo-French supersonic transport "Concorde," ONERA emerged at the forefront of water tunnel simulation of wings and bodies in unsteady flow (see Reference 120). Extensive research conducted at NAE (Ottawa, Canada) on the effects of high angles of attack on dynamic stability parameters (see Reference 180, for example) has been complimented by dynamic flow studies of an aircraft-like configuration in the NAE water tunnel (see Figure 161). Special note of the latter research will be made subsequently since it illustrates the extent to which a water tunnel may, at the present time, be applied to the understanding of dynamic vortex flows.

285
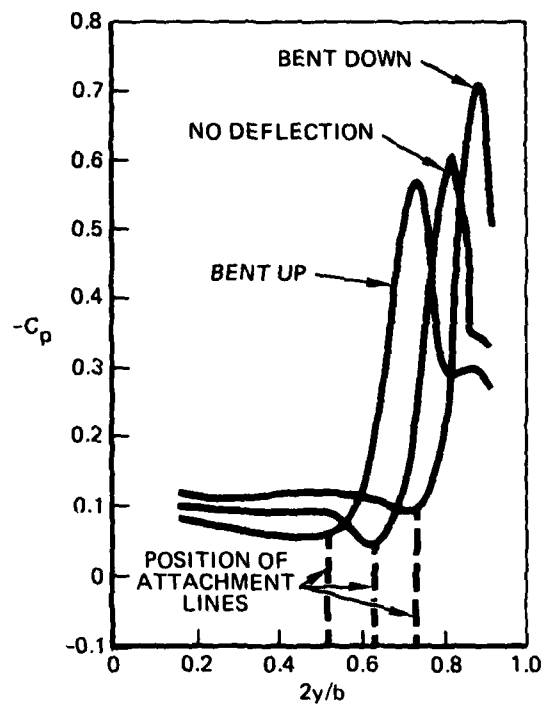
FIGURE 160. SPANWISE PRESSURE DISTRIBUTION FOR STEADY
DEFORMATION (FROM REFERENCE 177)

$\alpha = 25^{\circ}, \beta = 10^{\circ}$ $\alpha = 30^{\circ}, \beta = 10^{\circ}$
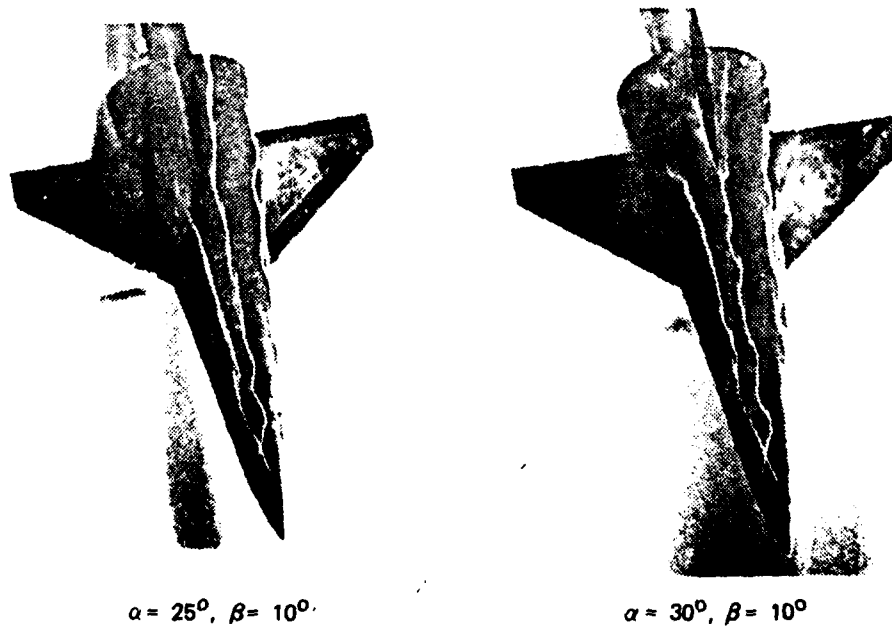
FIGURE 161. FLOW VISUALIZATION PHOTOGRAPHS IN A WATER
TUNNEL AT 10 DEGREES ANGLE OF SIDESLIP AND AT A
REYNOLDS NUMBER OF 4.5 X 10^4 BASED ON MODEL LENGTH
(FROM REFERENCE 180)

286

High angle-of-attack aerodynamics is likely to have a more pronounced impact on dynamic or unsteady parameters than on their steady flow counterparts. Figure 162, taken from Reference 181, illustrates several aerodynamic flow phenomena associated with oscillatory flight at high angles of attack. Several of these flow phenomena have been discussed for the steady case in previous sections of this report and their amenability to study in a water tunnel has been described in detail. Dynamic simulation in a hydrodynamic test facility of vortex shedding, vortex interaction, and vortex breakdown on advanced fighter aircraft and missile configurations at high angles of attack is essentially unexplored due to the lack of adequate water tunnel facilities, the relatively recent emergence of vehicles operating in the extended α-range, and the complexity of these aerodynamic problems. Intuitively, however, the water tunnel should, at the very least, provide a reasonable first-order approximation to the unsteady vortex flow field, the simulation of leading-edge and body vortices still being subject to the general guidelines developed for the steady-flow case.

For example, the oscillatory phenomena listed in Figure 162 have been observed in water tunnel studies at ONERA, NAE, and Northrop. The oscillatory motion of the vortex cores and core breakdown points relative to the generating surfaces and to other aircraft components have been observed and the convective time lags of the vortex motions are strongly in evidence. Consequently, an understanding of the aerodynamic reactions that are both in-phase and out-of-phase with the aircraft motion that may occur in a sophisticated wind tunnel test or in flight may be gained from a relatively simple study made in a water tunnel.

By way of illustration, the aerodynamic cross-coupling described in Reference 181 was dramatically confirmed in a movie of an aircraft-like configuration, installed in the NAE

287

- SEPARATED FLOWS OVER WINGS AND TAIL SURFACES
- SEPARATED FLOW OVER FOREBODY
- CROSS-FLOW EFFECTS
- FORMATION AND SHEDDING OF FOREBODY VORTICES
- ASYMMETRIC VORTEX SHEDDING
- INTERACTION OF FOREBODY VORTICES WITH SEPARATED WING FLOW
- LEADING EDGE VORTICES AND VORTEX BURSTS

OSCILLATORY PHENOMENA

- OSCILLATORY MOTION OF VORTICES
- LONGITUDINAL OSCILLATION OF VORTEX BURST LOCATION
- RELATIVE OSCILLATORY MOTION OF A C COMPONENTS AND EMBEDDED FLOW REGIONS
- CONVECTIVE TIME LAGS

FIGURE 162. SOME AERODYNAMIC PHENOMENA ASSOCIATED WITH OSCILLATORY FLIGHT AT HIGH ANGLES OF ATTACK (FROM REFERENCE 181)
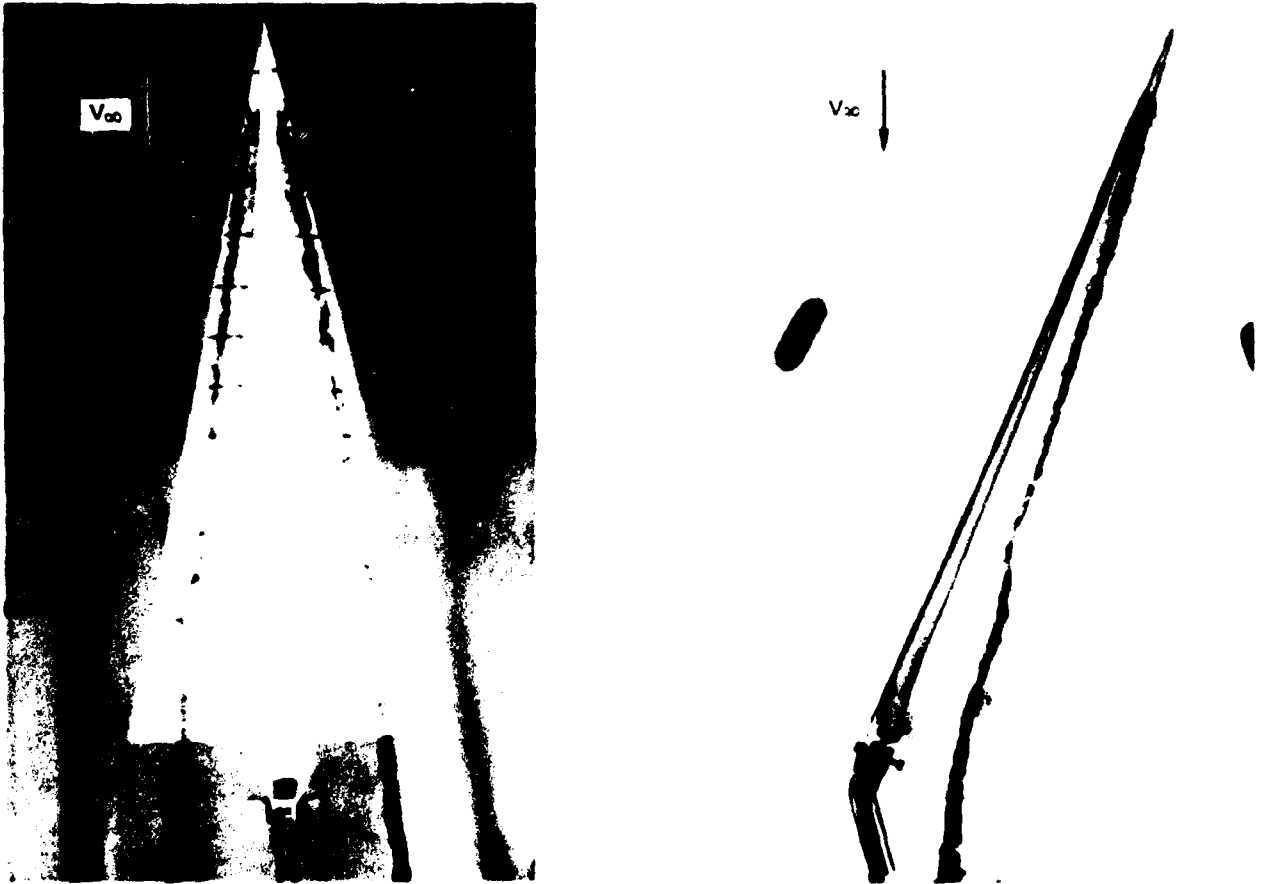
(a) MODEL INSTALLED IN TUNNEL

FIGURE 163. ULTRA-LIGHTWEIGHT 78-DEGREE DELTA WING-BODY MODEL FOR NORTHOP WATER TUNNEL WING ROCK STUDIES

VORTEX FLOW

POTENTIAL FLOW
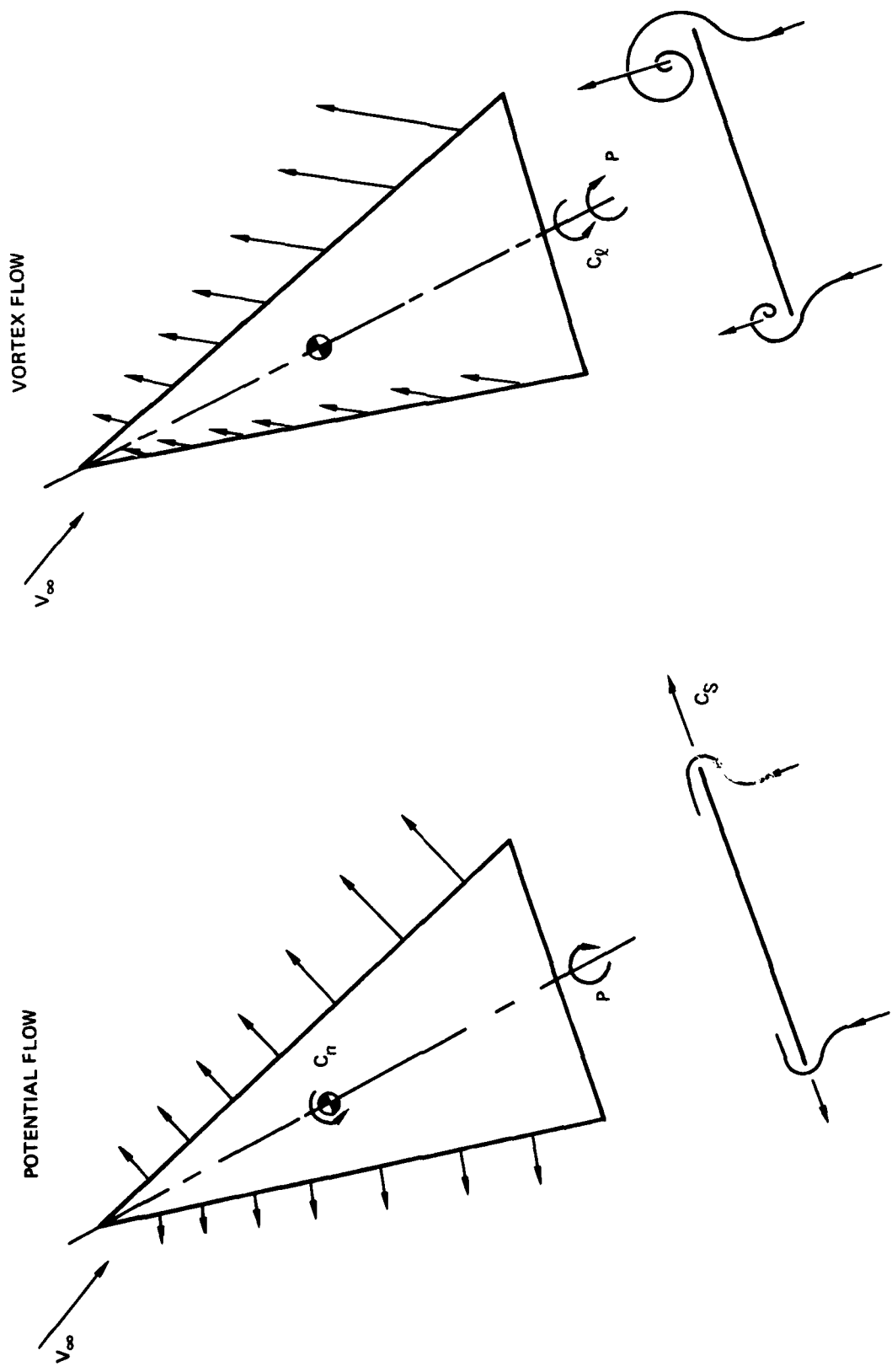
(B) SKETCH OF ROLL-DAMPING EFFECTS ON SLENDER DELTA WING USING THE LEADING-EDGE SUCTION ANALOGY (FROM REFERENCE 182)

FIGURE 163. CONCLUDED

289

water tunnel, which underwent forced oscillations in pitch (Reference 41). At high angles of attack and in symmetric and asymmetric flight conditions, it is expected that secondary lateral aerodynamic forces and moments will be incurred in response to a primary pitching maneuver and, conversely, secondary longitudinal reactions in response to a primary lateral maneuver. The water tunnel simulation revealed a lateral oscillation of the forebody vortices due to an oscillation in pitch and, as a result, the vortices were observed to shift from one side to the other of a top-mounted vertical fin. Lateral aerodynamic reactions as functions of angle of attack could clearly be envisioned. Acceleration of the flow over the body geometry can be seen and, despite the Reynolds number effect on the primary boundary layer separation lines along the body sides, the water tunnel results reveal a realistic vortex flow phenomenon including the convective times lags involved in which the lateral motions are both in-phase and out-of-phase with the model motion. Determination of cross-coupling derivatives requires access to sophisticated equipment which is generally not available. Consequently, preliminary studies of a qualitative nature in a hydrodynamic test facility of the complex vortex flow interactions which lead to cross-coupling of the longitudinal and lateral aircraft motions are desirable.

The occurrence of wing rock is common to most fighter aircraft when operating in a tactical environment. Simulation of the low-speed, high angle-of-attack mode when vortex flows are present represents a potentially far-reaching application of water tunnels. Recent Northrop studies of a slender hypersonic research configuration unconstrained in roll revealed a bounded wing rock behavior (and oscillatory vortex core motions) similar to that observed on a geometrically-similar model at a NASA-Langley wind tunnel. The water tunnel studies of this ultra-light-weight scale model, illustrated in Figure 163, provide a plausible vortex flow mechanism leading to a bounded wing rock behavior. The relatively good agreement

290

between onset angles of attack determined in water ($\alpha \approx 35$ degrees) and in air ($\alpha \approx 30$ degrees (Reference 183)) may be fortuitous, however, since the water tunnel model was not dynamically-scaled and the period of the wing rock motion and onset angle in the water tunnel are quite sensitive to small changes in dynamic pressure, as shown in Figure 164. The water tunnel vortex patterns do provide a key, however, to understanding why the model exhibited a bounded, not divergent, motion. A free-stream disturbance or, perhaps, a slight model asymmetry triggered the initial wing rock motion. A leading-edge vortex pattern is established in which the upward-moving wing develops a vortex of increasing stability relative to the down-going wing due to the increased effective sweep resulting from the rolling motion. As the effective sideslip increases, however, the inherent lateral stability of the wing predominates. As a result, the wing attains a maximum roll angle, the motion is reversed, and the opposite wing (now the upward-moving panel) develops a vortex of increasing stability. In this manner, a self-sustaining cycle is established. This flow situation may correlate with the F-5E and F-5F low-speed wing rock, both aircraft exhibit essentially single degree-of-freedom behavior rolling oscillations. The roll oscillations are bounded at a moderate amplitude, as shown in the wind tunnel data (Reference 184) in Figure 165. The damping in roll derivative in the angle of attack range where wing rock occurs exhibits a strong effect of oscillation amplitude, being undamped at small amplitudes and highly-damped at higher amplitudes. Attempts at studying a self-induced wing rock oscillation at $\alpha \approx 35$ degrees using a light-weight scale model of the F-5E in the Northrop water tunnel were unsuccessful. It was found, however, that forced oscillations above a certain amplitude and frequency resulted in the development of an oscillatory LEX vortex pattern similar to that observed on the slender hypersonic research model.

291
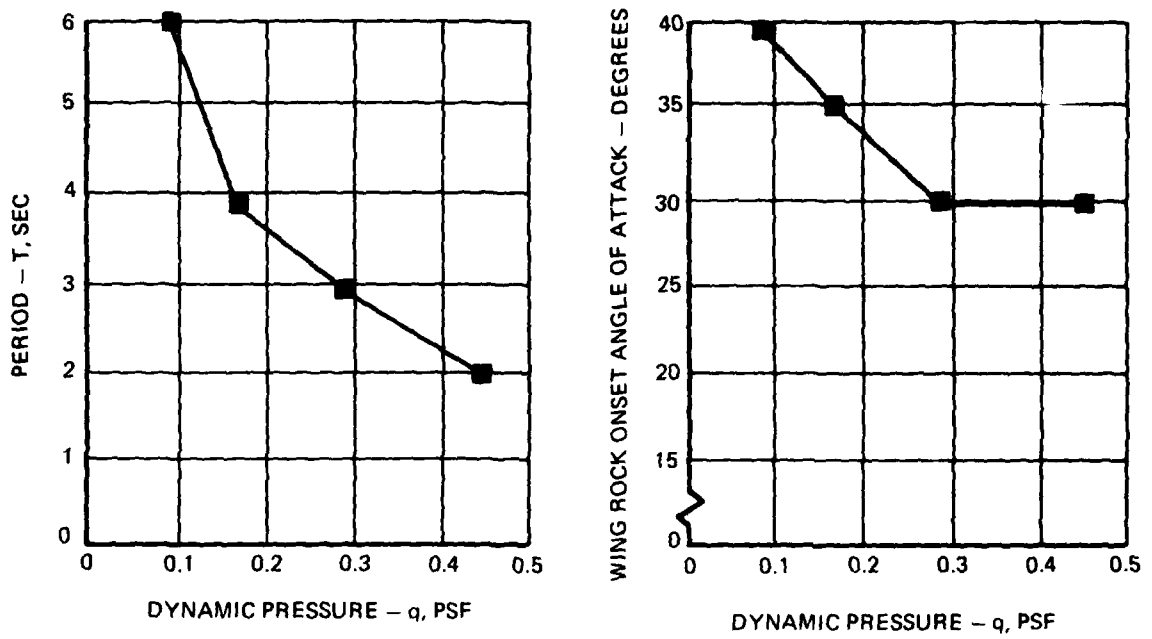
FIGURE 164. WATER TUNNEL WING ROCK RESULTS
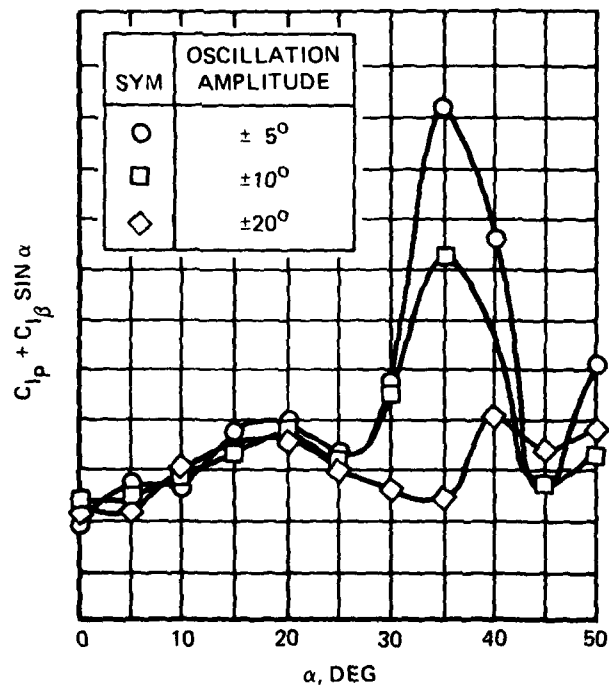
FIGURE 165. DAMPING-IN-ROLL CHARACTERISTICS

292

Rolling divergence is observed on the F-4 and F-16, for example, which exhibit lateral instability in the wing stall angle of attack range.

The leading-edge suction analogy (Reference 56) can be used to predict the effects of the leading-edge vortex flow on the roll-damping of sharp-edged highly-swept wings. The potential flow leading-edge suction forces on a rolling delta wing at angle of attack are depicted in the sketch in Figure 163 which is taken from Reference 182. As a result of the combined angle of attack and rolling pressure distributions, an asymmetrical suction-force distribution is developed and a negative yawing moment is generated resulting in the yawing moment due to roll rate. The leading-edge suction analogy assumes that for thin, sharp-edged wings featuring vortex flows with induced reattachment on the upper surface, the suction forces are rotated normal to the leading edge. Consequently, the asymmetrical normal force loading contributes an effective rolling moment due to roll rate or an effective roll damping from the leading edge vortex flow.

Preliminary analysis of the requirements for proper water tunnel simulation using a frequency parameter, $f = \omega c/U$ where ω is the oscillation frequency and c the wing chord, indicate unrealistically-high oscillation frequencies required for water tunnel simulation. In addition, the large disparity in apparent mass between models in air and in water poses a problem in dynamic flow simulation. The weight of an aircraft in air far exceeds that of the surrounding fluid, whereas in water the opposite generally holds true since the density of water is approximately 800 times that of air and, in general, very light models are tested. Testing a very heavy model in water creates another unique problem in that at the very slow speeds characteristic of a water tunnel the loads are so small as to be incapable of overcoming support friction. In this case, it may be necessary to provide an initial disturbance and observe the resultant motion.

The most important parameter, however, may be the roll-induced angle of attack (Reference 185). Damping-in-roll, a significant parameter in wing-rock phenomena, varies at high angle of attack largely as a function of the induced local normal velocity, regardless of the combination of oscillation amplitude and frequency used to obtain that velocity. Since the angle of attack at which various flow asymmetries occur in a water tunnel often appears to be a little higher than in air, it may be appropriate to make this induced angle of attack somewhat larger than what is experienced in full-scale wing rock behavior. Further analysis and test using a recently-developed automated pitch, roll, and yaw mechanism in the Northrop water tunnel will provide additional insight into this class of vortex flows.

As a final note, it has been observed at Northrop and NAE (Reference 41) that very abrupt changes in the model attitude cause the shed vortices to momentarily dissipate, which suggests that any change in model motion by an automated pitch, roll, or yaw mechanism should be made in a smooth fashion.

In summary, utilization of a water tunnel in the study of unsteady flows requires careful consideration of various parameters such as Reynolds number and Strouhal number for bodies which exhibit unsteady vortex shedding and bodies undergoing oscillatory flight at high angles of attack. Consideration must be given to free-stream turbulence effects and the rigidity of the model support arrangement (as well as interference effects). For slender wings undergoing roll oscillations, simulation of the roll-induced angle of attack may enable a reasonable representation of wing rock phenomena experienced at high Reynolds numbers on fighter aircraft which generate strong vortical flows. The differences in apparent mass between a model in air and a model in water require analysis in order to assess the viability of proper simulation

of separation-induced vortex flows from slender wings and bodies and their subsequent interactions. The water tunnel has been shown, however, to provide excellent qualitative data on vortices in unsteady flow conditions. Consequently, when a water tunnel is used judiciously, an understanding can be gained of complex fluid mechanics phenomena and general trends that are likely to be developed at high Reynolds numbers in wind tunnels and in flight.

5.6   SPECIFIC VORTEX FLOW PROBLEM

The advent of advanced composite materials has provided a promising solution to the aeroelastic divergence problem associated with wings of forward sweep (Reference 188). The potential benefits associated with a forward swept wing (FSW) with proper aeroelastic tailoring are numerous (see Reference 189) and, consequently, research activity in this area has increased considerably in recent years. A water tunnel was used by the British many years ago (1958) in Reference 190 to investigate the effects of wing sweep on the vortex flow patterns of thin wings at high angles of attack. FSW planforms were tested and the phenomena of low angle of attack wing root stall, "never-stalling" wing tip, and leading-edge separation-induced vortex flow originating from the wing tip, peculiar to wings of forward sweep, were identified. Recent studies of thin, sharp-edged wings at Northrop (Reference 179) have duplicated these results as shown in Figures 166 and 167. Good correlation has been obtained between Northrop water tunnel results obtained on a FSW with leading-edge extension (LEX) and low-speed wind tunnel data in Reference 191 on a thin, sharp-edged FSW-LEX geometry as shown in Figure 168. These results indicate that a conventional LEX is quite ineffective in combination with a FSW since the largest streamwise pressure gradients are in the wing root region, thereby tending to promote LEX vortex breakdown, and the spanwise flow induced

295
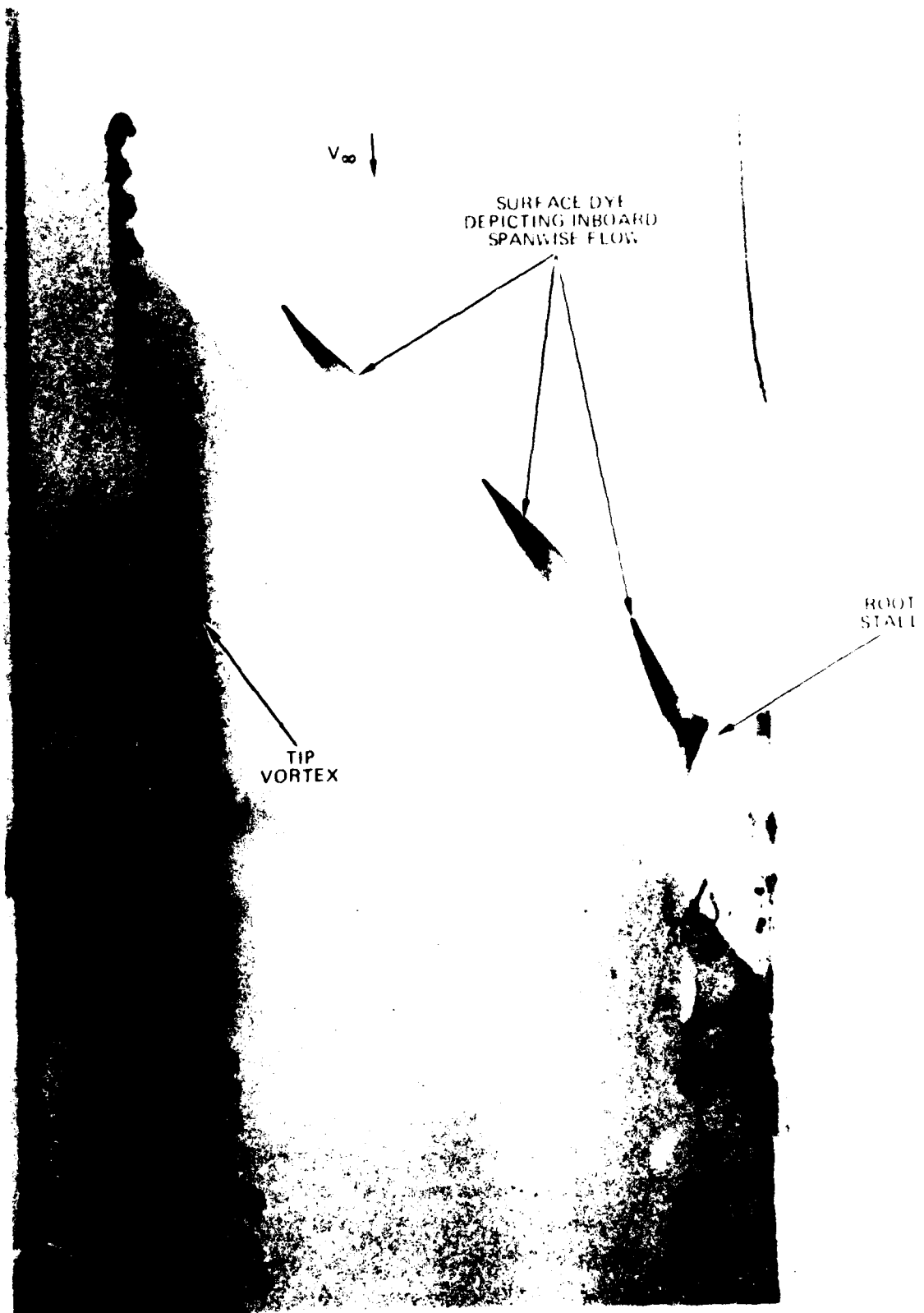
FIGURE 166. FLOW CHARACTERISTICS ON A FORWARD SWEPT WING
(NORTHROP WATER TUNNEL)
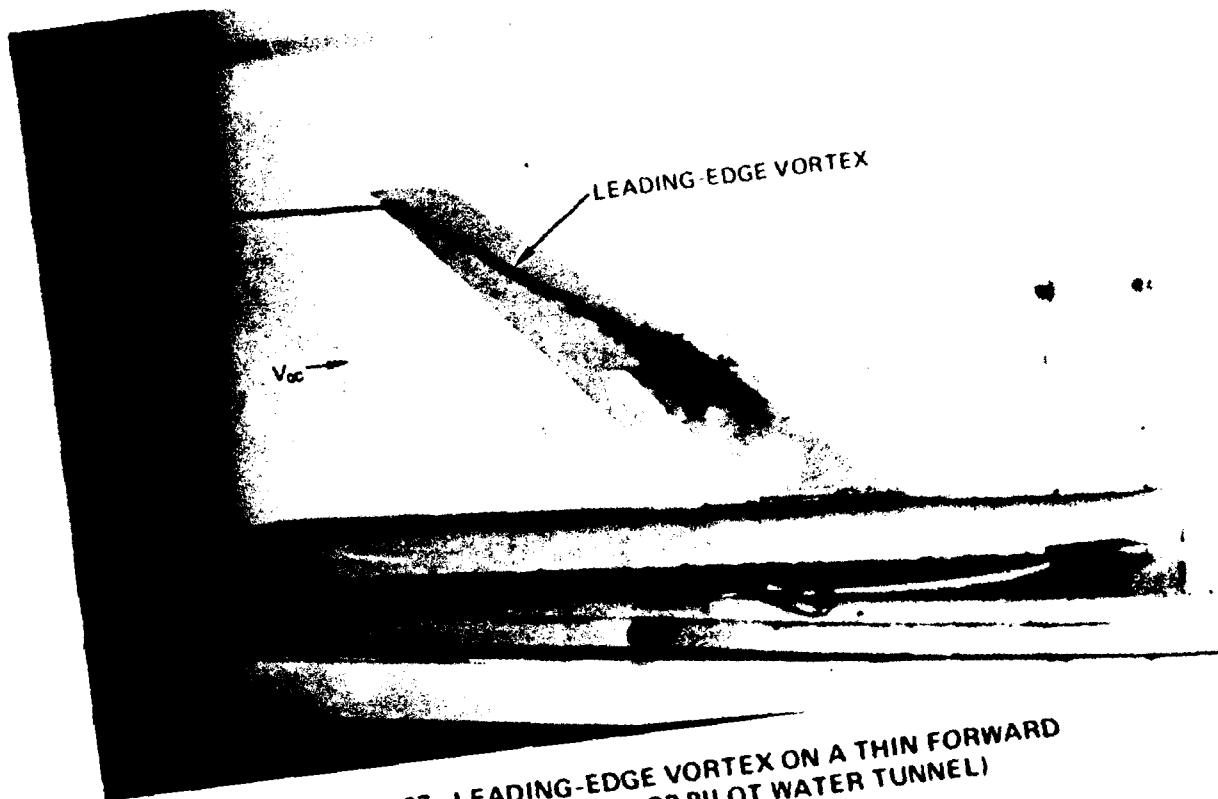
FIGURE 167. LEADING-EDGE VORTEX ON A THIN FORWARD
SWEPT WING (NORTHROP PILOT WATER TUNNEL)
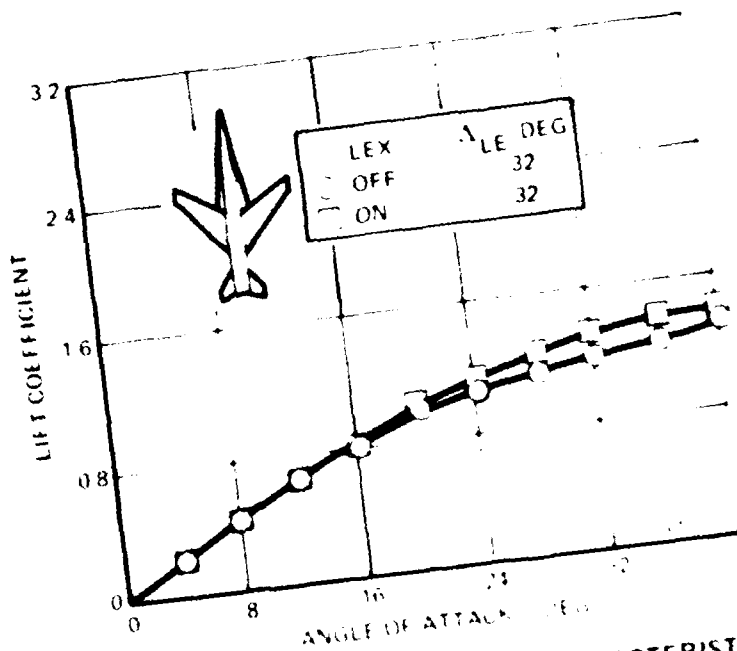
FIGURE 168. EFFECT OF LEX ON LIFT CHARACTERISTICS OF
SWEPT-FORWARD WING CONFIGURATION (REFERENCE 191)

by the LEX vortex is in opposition to the inboard spanwise flow
on the main wing panel. The shed trailing-edge vorticity rolls
up into a concentrated core, as seen in Figure 169. This water
tunnel result also correlates with wind tunnel oil flow studies
in Reference 191 which reveal a strong sweeping action on the
wing upper surface near the trailing edge.

A water tunnel facility can be utilized to investigate
the 3-D separated flow about a FSW fighter configuration (as
illustrated in the artist's conception in Figure 170) up to
high angles of attack. Preliminary studies made at Northrop of
a low aspect ratio (2.12) FSW planform, depicted in Figure
171, have suggested that a conventional wing root leading-edge
extension may prove quite effective in conjunction with this
planform. The envisioned flow pattern on this configuration is
analogous to the "stall-cell" concept in Reference 192 and is
sketched in Figure 172. The wing tip and root regions remain
attached to high angles of attack with a region of controlled
flow separation at mid-span. The downwash field from a conven-
tional close-coupled canard may produce similar effects on the
wing stall characteristics.

Interactions of the vortex system shed from a slender
fuselage forebody at high angle of attack with the lifting
surface flow field introduce an additional element of com-
plexity to the three-dimensional flow patterns. Water tunnel
results indicate that premature instability of the forebody
vortex pair is promoted due to entrainment of turbulent fluid
into the vortex cores near the stalled wing root region, as
depicted in Figure 173, on a modified F-5 model with FSW.
This phenomenon is in contrast to the flow situation exhibited
by a conventional aft-swept wing configuration, shown also in
Figure 173, which reveals no comparable instability at the
same angle of attack.

TRAILING EDGE VORTEX

PRESSURE TAP ON OPPOSITE WALL

$V_\infty \longrightarrow$
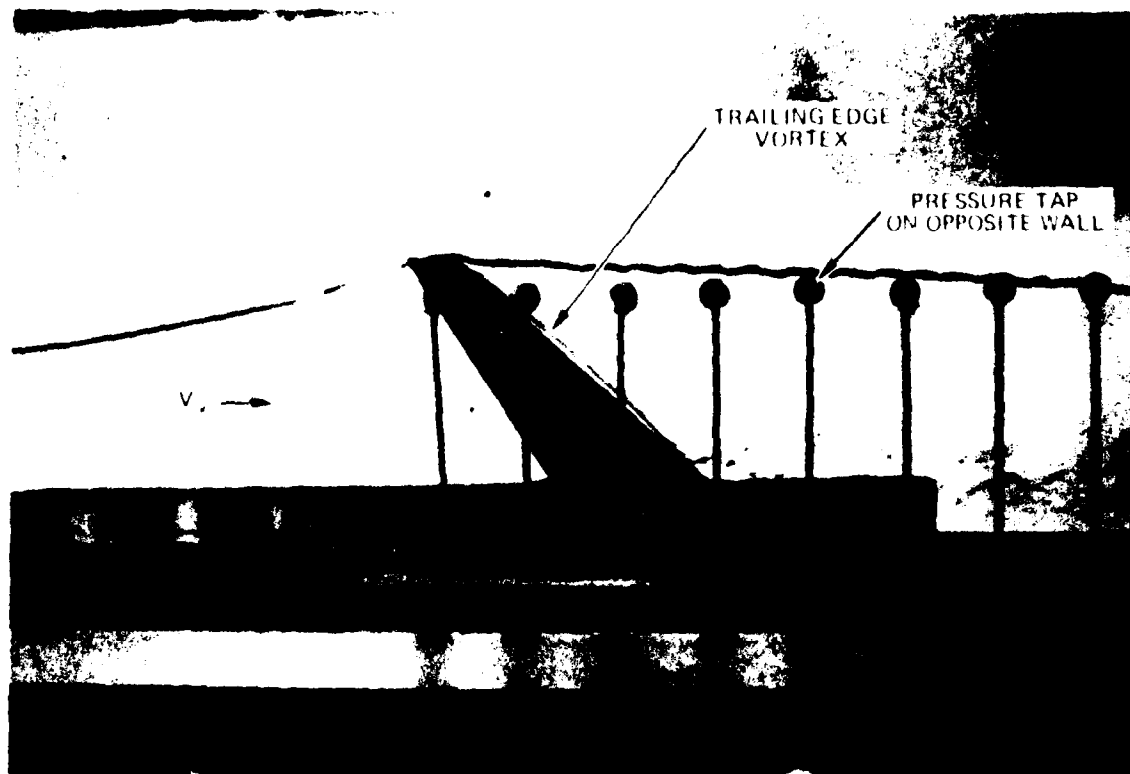
FIGURE 169. CONCENTRATED TRAILING EDGE VORTEX ON AN FSW
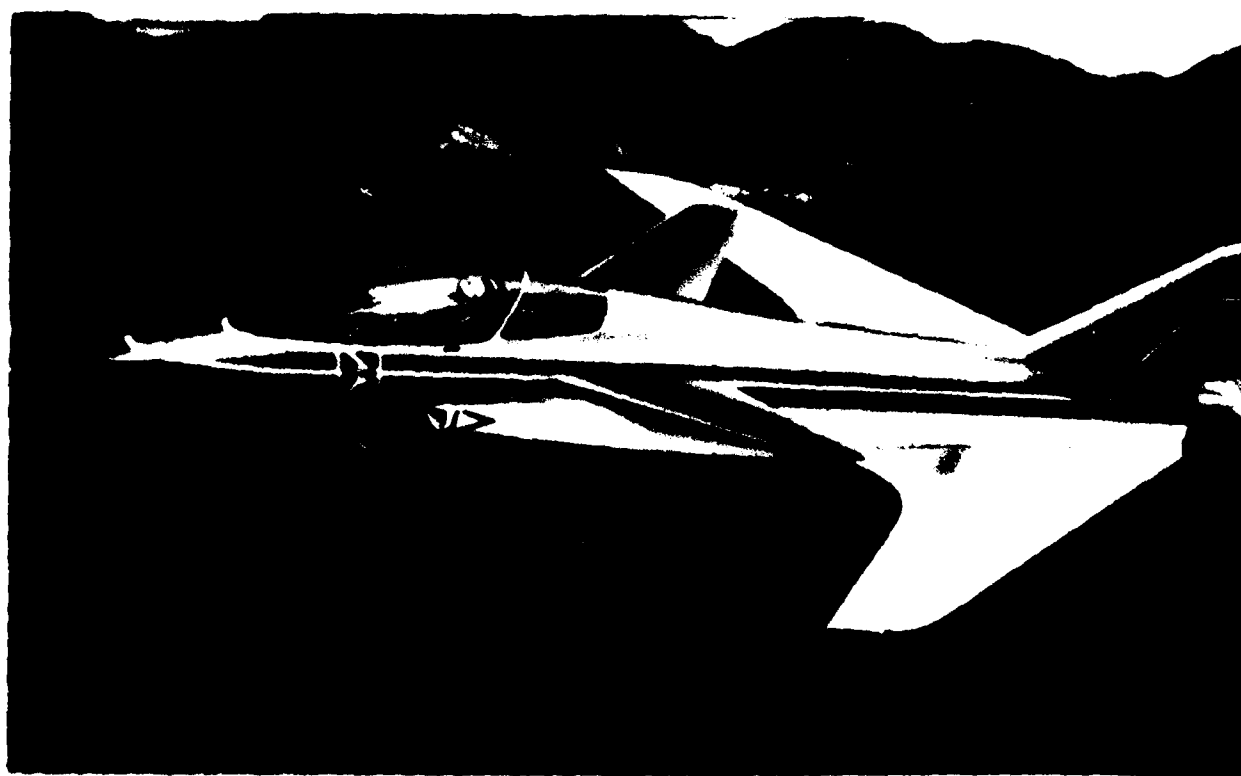
FIGURE 170 SKETCH OF A FORWARD SWEPT WING FIGHTER

LEX VORTEX

$V_\infty \longrightarrow$
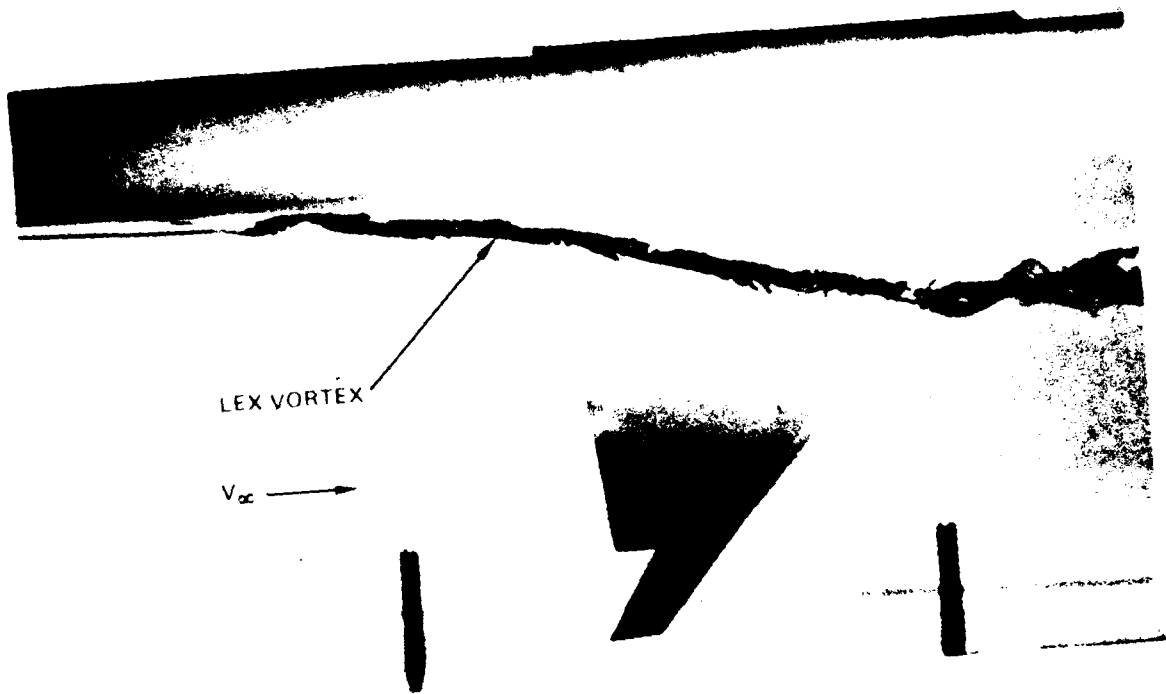
FIGURE 171. FLOW VISUALIZATION PHOTOGRAPH OF A LOW
ASPECT RATIO FSW WITH LEX (NORTHROP WATER TUNNEL)

$V_\infty \longrightarrow$

ATTACHED FLOW

SEPARATED
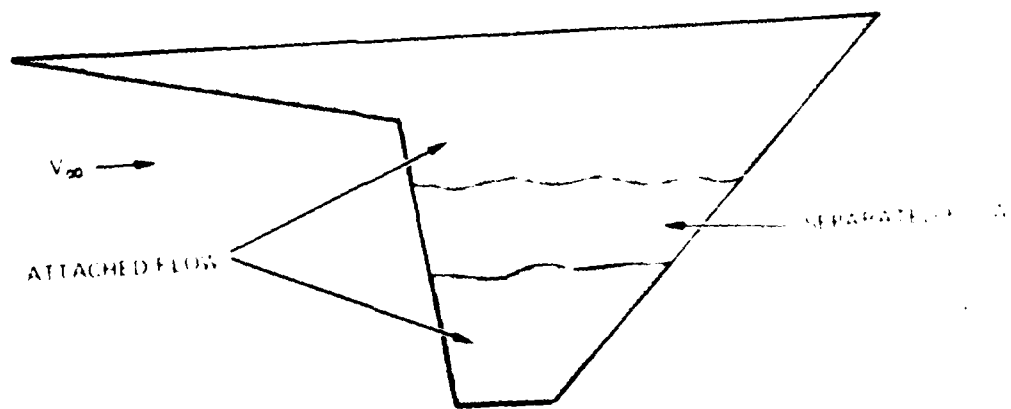
FIGURE 172. SKETCH OF "STALL-CELL" FLOW PHENOMENON
ENVISIONED ON LOW ASPECT RATIO FSW LEX
GEOMETRY IN FIGURE 171

FOREBODY
VORTICES

VORTEX
BREAKDOWN

V_∞ →

(a) FORWARD SWEPT WING

FOREBODY
VORTICES

NO
BREAKDOWN

V_∞ →
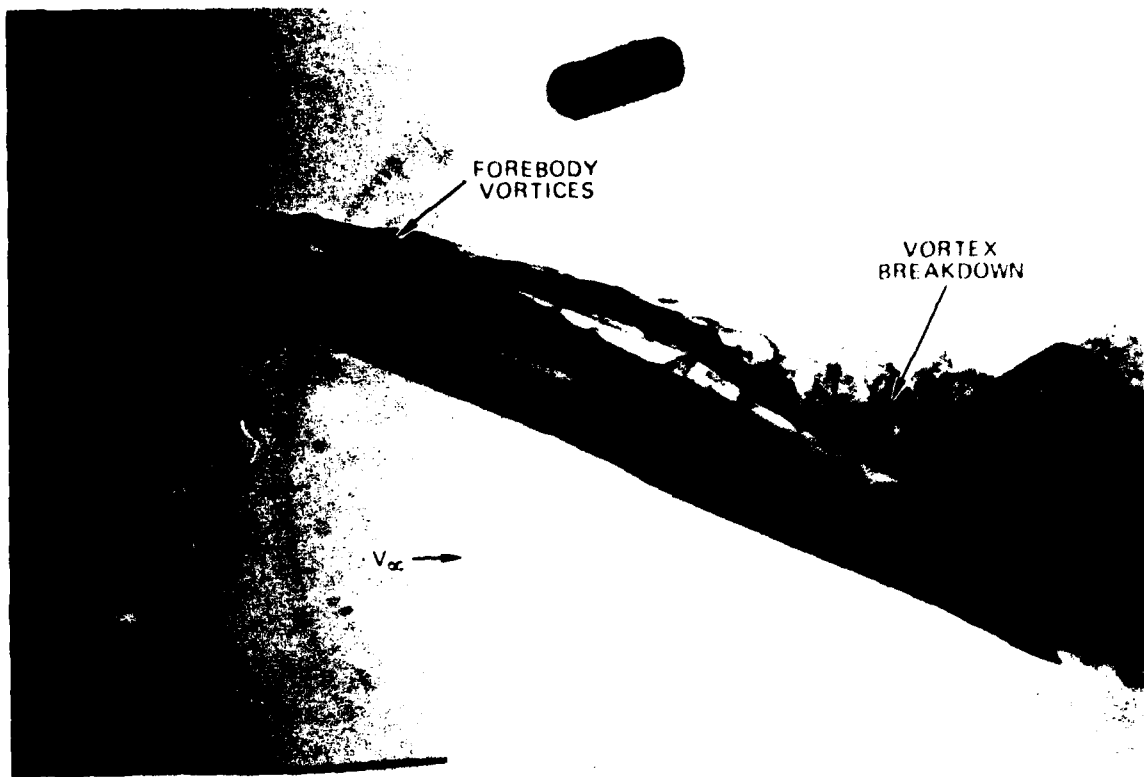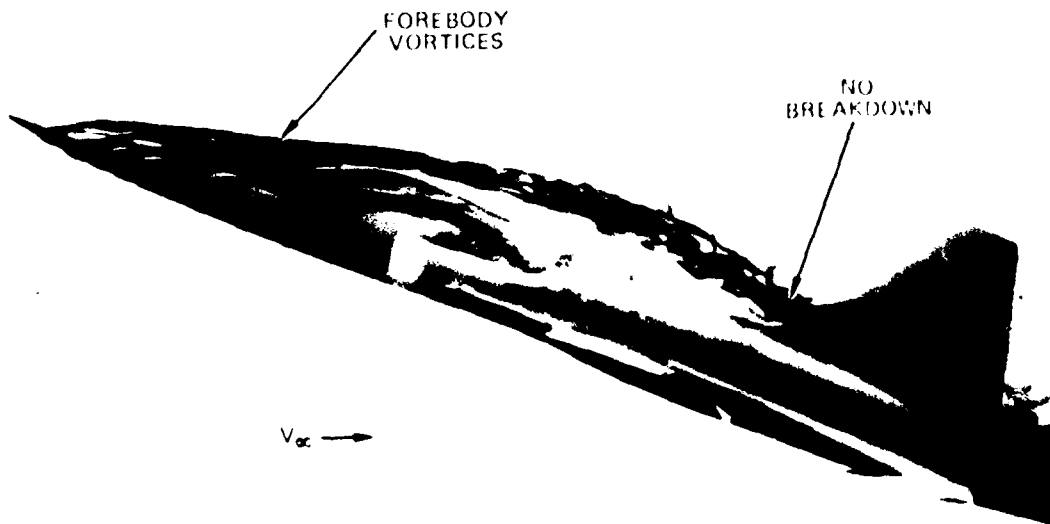
(b) AFT SWEPT WING

FIGURE 173. FOREBODY VORTEX PATTERNS ON A FIGHTER CONFIGURATION
(NORTHROP WATER TUNNEL)

Development of flow-control devices which generate vortices rotating in the proper sense so as to induce favorable *spanwise flow gradients* warrants investigation. The water tunnel photograph in Figure 174 shows the viability of such a concept as a means of delaying wing stall. The vortex shed from the notch created by deflection of an inboard leading-edge flap induces strong spanwise flow components, as can be seen by the surface dye in the photograph. The surface dye pattern at the outboard wing station reveals attached flow.

Forced model oscillations about the pitch, roll, and yaw axes would provide valuable information on the 3-D flow field behavior in unsteady flow conditions. Intuitively, a FSW fighter should not undergo severe wing rock oscillations at subsonic speeds (indeed, wing rock behavior may not be in evidence at all (Reference 193)) that are experienced on most "conventional" fighters in the wing stall angle of attack region and, consequently, flow visualization studies may provide a fluid mechanism to substantiate this conjecture.

Clearly, a model featuring all of the aforementioned concepts represents an intriguing research study in a water tunnel. Consideration must be given to the greater region of separated flow at inboard wing stations which is evident in water tunnel studies as a result of the subcritical separation characteristics. Consequently, an approximation to the FSW surface flow pattern at high Reynolds number may be gained by applying small amounts of suction from ports distributed in the wing root region. This increases the complexity of the model but is deemed necessary in order to provide representative simulation of the wing flow field at high Reynolds number. Dye ports mounted flush with the wing upper surface and distributed across the wing span would provide an excellent assessment of the effects of a LEX, canard, and leading-edge vortex generators on the wing stall pattern. A remotely-controlled external dye port or a dye probe rake would enable a survey of

302
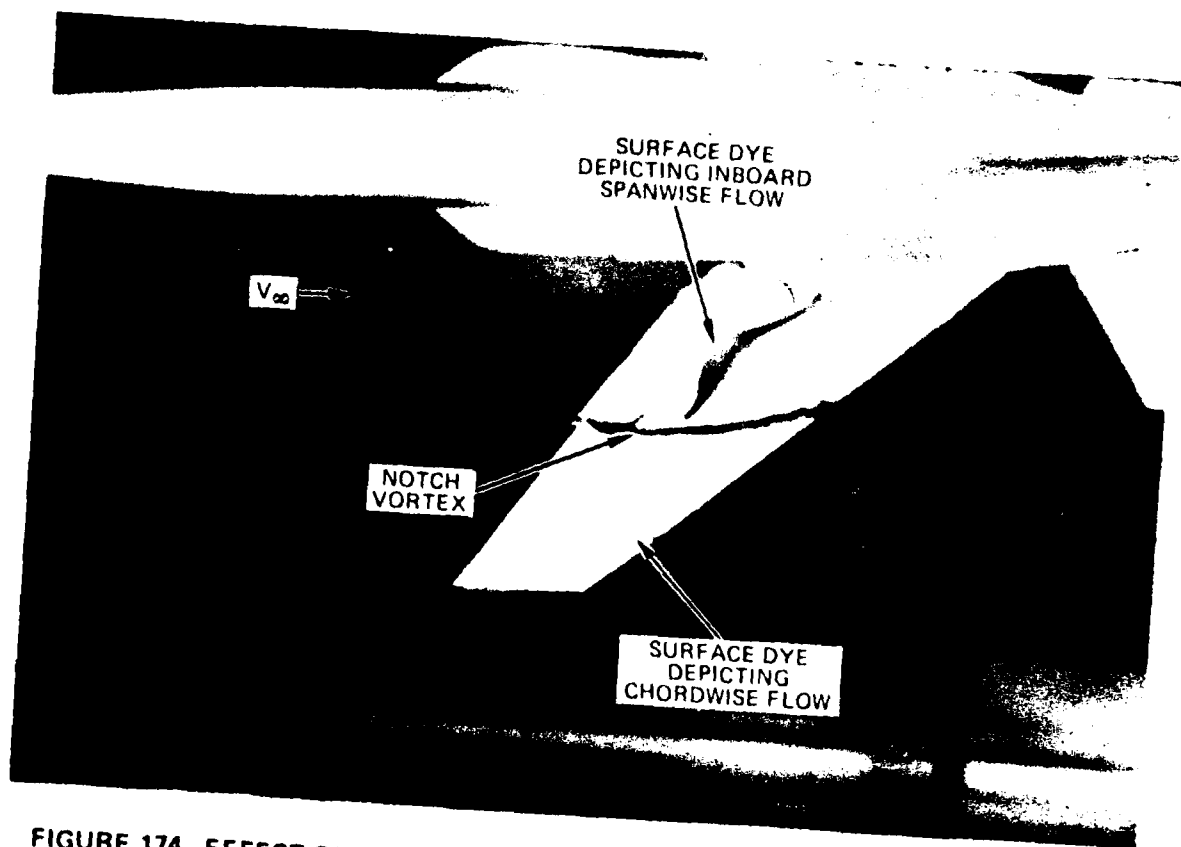
FIGURE 174. EFFECT OF LEADING-EDGE NOTCH VORTEX ON FSW SURFACE FLOW (NORTHROP WATER TUNNEL)

the external flow field, for example, in the vicinity of the wing tip and leading-edge extension where powerful vortical motions are present and to qualitatively define the downwash field associated with a canard surface. The flow field variations due to a variable-incidence canard and deflected wing leading- and trailing-edge flaps can also be determined in this manner, bearing in mind the Reynolds number effects associated with flap deflections discussed in the body of this report. One of the purported benefits of forward sweep - roll-control capability up to high angles of attack - can be assessed by visualization of the flow over deflected ailerons.

Shedding of forebody vortices at high angles of attack can be visualized by injecting dye from a series of flush dye ports located slightly off-center from the windward meridian. The vortex trajectories can be tracked back to the wing where the effect of inboard wing stall on forebody vortex stability can be determined. To assist in determining vortex-induced effects on a vertical tail component, flush surface dye ports on the latter are desirable.

Boundary layer suction and dye ports internal to the model, interchangeable model components, and model oscillations surely require a relatively sophisticated model and experimental test rig. However, this program is well within the capabilities of a water tunnel and the data derived from such a study would be timely and quite relevant to the extensive research efforts currently underway in the ongoing joint DARPA/AFWAL FSW Technology Program. This vortex flow study would provide the researcher with an understanding of complex vortical motions and the opportunity to correlate in a qualitative manner the water tunnel results with the wealth of experimental data being gathered in the FSW Technology Program.

SECTION 6

CONCLUSIONS

An extensive literature survey of water tunnel facilities and applications has been conducted and results reveal a significant number of facilities in current use throughout the world for a multiplicity of fluid flow applications. Relatively few hydrodynamic test facilities have been utilized, however, for detailed studies of steady and unsteady vortex flow phenomena on advanced fighter aircraft and missile configurations at high angles of attack.

The National Physical Laboratory (NPL) in Teddington, England and the Office National d'Etudes et de Recherches Aerospatiales (ONERA) in Chatillon, France were the pioneers in the study of separation-induced leading-edge and body vortical motions in a water tunnel, beginning in the late 1950's and early 1960's. The National Aeronautical Establishment (NAE) in Ottawa, Canada has also made important contributions to vortex-flow research, particularly with regard to unsteady flow pheonomena. Northrop Corporation in Hawthorne, California, beginning in the late 1970's has made extensive use of the water tunnel to study fighter aircraft which generate powerful vortex systems in the extended angle-of-attack regime.

From a review of the literature it is clear that the water tunnel, operating at <u>low speeds</u>, is capable of providing high-quality, detailed flow visualization of complex fluid flows. Water tunnels are capable of operating at higher Reynolds numbers by increasing the test section velocity, for example. However, a corresponding decrease in quality of vortex flow visualization occurs. This situation is analogous

to the difficulty in visualizing the details of vortical motions in wind tunnels using smoke, water vapor, or helium-filled bubbles, for example. A low-Reynolds-number water tunnel is particularly suitable for studying vortex flows from sharp-edged strakes, LEXs, and highly-swept wings. Visualization tests have been a valuable means of obtaining an understanding of vortex generation, interactions between multiple vortices and aerodynamic surfaces, and vortex burst.

The flow phenomena which must be simulated in a water tunnel to ensure correlation of vortex flow results are (1) vortex generation, (2) vortex sheet and core location, and (3) vortex breakdown. For thin, sharp-edged slender wings vortex generation, vortex sheet and core location, and vortex strength are accurately represented in a water tunnel due to the insensitivity of the separation point location to changes in Reynolds number. The fact that theoretical methods which ignore viscous effects can reasonably predict vortex flow aerodynamics is one indication of the Reynolds number insensitivity of these flow phenomena.

This is not the case for cambered or blunt-nosed wings and slender bodies, where the boundary layer separation point location and, hence, vortex sheet and core locations and vortex strength vary with the Reynolds number. The fundamental structure of the vortex at high angles of attack is similar, however, regardless of Reynolds number since, once a vortex is shed from the generating surface the vortex core is embedded in an essentially potential flow field.

The behavior of a vortex core is governed by flow parameters such as swirl angle, core stream tube divergence, and core Reynolds number. The Reynolds number of the vortex core is the more important of the three parameters. In the absence of an external pressure gradient, core breakdown is strongly dependent on the Reynolds number. External pressure

306

gradient has been shown to be an important parameter affecting the location of vortex breakdown and, although as yet there has been no theoretical verification that this parameter is the dominant one, vortex burst location has been observed to occur at comparable positions in the water tunnel as in the wind tunnel and flight. At high angles of attack, provided flow separation occurs from a salient edge, the water tunnel provides a realistic representation of the size and structure of the wake and, hence, the positive pressure gradient through which the vortex core must traverse. When the primary separation point varies with Reynolds number, the wake region is less representative in a water tunnel and, as a result, the vortex core behavior must be viewed in a qualitative sense.

A water tunnel is useful in gaining an understanding of the phenomenological aspects of vortex flows shed from flat-plate, cambered, and blunt-nosed wings and slender bodies at high angles of attack. Under these conditions, the scale of the vortex flow is much greater than the undisturbed boundary layer thickness, in other words, the flow field is vortex-dominated. Quantititative comparisons of vortex position, strength, and stability are possible only for thin, flat-plate, sharp-edged wing, wing-LEX, and wing-canard geometries. Care must be exercised, however, on nonplanar wings, wings with large leading-edge radius, and slender bodies. This is due to the laminar boundary layer separation characteristics at low Reynolds number in water relative to turbulent boundary layer separation at high Reynolds number in air which results in different vortex sheet and core locations, vortex strength, and stability characteristics. For example, studies made in a water tunnel of (1) deflected wing flap effects on vortex stability and (2) body fineness ratio effects on vortex asymmetry onset angle reveal the correct trends but, in general, do not predict the quantitative effects. As a rule, however, improved agreement is obtained as wing or body slenderness is

307

increased. In general, any geometric modification which alters the rate of vorticity shedding from a wing or body at high angles of attack such as radome strakes, wing leading-edge discontinuities, planform geometry variations, body cross-sectional shape, boundary layer trips, etc. can be studied in a qualitative manner in a water tunnel.

A general guideline, then, at high angles of attack where large regions of separated flow exist, that is, when the flow field is vortex-dominated, is that the fundamental structure of the vortex flow field about wings and bodies is similar regardless of Reynolds number. Since wings and bodies are topologically equivalent objects, the fluid behavior of slender wing vortices should find a counterpart in the behavior of vortices shed from slender bodies. At high angles of attack, vortex strength increases and the vortex core is higher above the generating surface, thereby alleviating vortex core-boundary layer interactions. Under these conditions, once the vortex is shed from a wing or body, the vortex core is subject to the external potential flow field and, consequently, the vortex core trajectories, including vortex system interactions on advanced fighter aircraft and missile configurations can be assessed in a water tunnel. The dominance of the positive pressure gradient in the external flow field at high angles of attack makes the improper simulation of the surface flow characteristics irrelevant and, as a result, wing, wing-LEX, wing-canard, and forebody vortex stability characteristics can be visualized to a degree of accuracy sufficient for correlation of a qualitative nature with wind tunnel and flight test data.

At low angles of attack (of the order of 10 degrees or less), water tunnel simulation of leading-edge vortex behavior on wing, wing-LEX, and wing-canard geometries is not representative due to interaction of the vortex core with the wake resulting from separation of the laminar boundary layer. The

308

vortex exhibits premature instability and subsequent "break-down" due to entrainment of turbulent fluid from the separated boundary layer and, consequently, the strong vortex interactions with other airframe components that have been observed at high Reynolds numbers in wind tunnel tests are not in evidence at low Reynolds numbers in a water tunnel. Improved simulation of the surface flow characteristics can be achieved by boundary layer suction or small vortex generators to energize the laminar boundary layer. For cambered wings, wings with large leading-edge radius, and slender bodies, an additional source of error is introduced due to premature formation of separation-induced vortex flows. A second general guideline may be stated as follows: At low angles of attack where the flow field is not yet vortex-dominated, water tunnel simulation of vortical motions at low Reynolds numbers is inadequate unless means are taken to properly simulate the surface flow characteristics.

In summary, the philosophy that a water tunnel is a powerful diagnostic tool has been justified by the detailed discussions in this report. Strong viscous effects are present near the surfaces of wings and bodies which preclude, in most cases, quantitative comparisons of results obtained in a water tunnel with high Reynolds number data obtained in wind tunnels and in flight. This is not surprising since difficulties have often been encountered when attempting to correlate wind tunnel results on fighter and missile configurations to flight conditions. The strength of a water tunnel facility lies in the detailed information which can be gained of the general structure of complex vortical motions. Once the vortex has been displaced away from the generating surface, the overall behavior of vortex flows, including vortex system interactions and interactions with other airframe components, is dominated by potential flow effects. Consequently, results obtained in water at low Reynolds number can be extrapolated in a qualitative manner to high Reynolds number flows in air.

REFERENCES

1. Crimi, P.; "Experimental study of the Effects of Sweep on Hydrofoil Loading and Cavitation." Report No. AD-845151, RASA-68-14, Rochester Applied Science Associates, Inc., 1968.

2. Lehman, A. F.; Romandetto, R.; "An Experimental Study of the Unsteady Forces Induced on a Rudder Due to a Propeller Acting in a Wake," Report No. AD-848435 Rept-68-58, Oceanics, Inc., Plainview, N.Y., 1968.

3. Oey, K. T.; "On the Leading-Edge Flutter of Supercavitating Hydrofoils." Cavitation and Polyphase Flow Forum, Fort Collins, Colo., 12-14 June 1978.

4. Karlikov, V. P.; Khomiakov, A. N.; Sholomovich, G. I.; "A New Organization Method for Fully-Developed Cavitating Flows." Izdatel'stvo Moskovskogo Universiteta, 1978, p. 34-47.

5. Kamijo, K.; Shimura, T.; "An Experimental Investigation of Cavitating Inducer Instability." 12th International Symposium on Space Technology and Science, Tokyo, Japan, 16-20 May 1977.

6. Reed, R. L.; "The Influence of Surface Characteristics and Pressure History on the Inception of Cavitation." CR-10552, NASA, 1969.

7. Werle, H.: "Hydrodynamic Flow Visualization." Annual Review of Fluid Mechanics, Vol. 5, 1973, pp. 361-382.

310

8.   Dobrodzicki, G. A.; "Flow Visualization in the National Aeronautical Establishment's Water Tunnel," Aeronautical Report LR-557, Ottawa, February 1972.

9.   Taylor, W. E.; "Research Program to Extend Cascade Data to Liquids and Higher Inlet Angles." NASA-CR-91652, 1967.

10. Telionis, D.P.; Koromilas, C. P.; "Flow Visualization of Transient and Oscillatory Separating Laminar Flows." Proceedings of the ASME Winter Meeting, 1978, pp. 21-32.

11. Sarpakaya, T.; "Fluid Forces on Oscillating Cylinders." American Society of Civil Engineers, Journal, Vol. 104, p. 275-290, August 1978.

12. Tanaka, H.; Shinohara, K.; Hanamura, Y.; "Comparison Between Theoretical and Experimental Results of Torsional Stall Flutter of an Airfoil." Revue Francaise de Mecanique, Special Issue, p. 81-88, 1976.

13. Neppert, H.: Sanderson, R.; "Effect of Gusts on High-Speed Trains" Zeitschrift fuer Flugwissenshaften, Vol. 24, p. 151-161, May-June 1976.

14. Werle, H.; "Aerospace, Industrial, and Maritime Applications of Flow Visualization in Hydraulic Tunnels." ONERA TP No. 1975-58, 1975.

15. Marchenko, A. G.; "Experimental Study of the Structure of Turbulent Boundary Layers in Incompressible Fluids in the Presence of a Longitudinal Pressure Gradient." Fluid Mechanics - Soviet Research, Vol. 1, p. 166-172, July-Aug. 1972.

16. Schutzenhofer, L.; Morrow, D.; Shih, C.; "Development of an Unsteady Water Tunnel." AIAA Paper No. 72-999, 1972.

17. Fanaki, F. H.; "Some Laboratory Observations on Convective Plumes." Journal of Applied Meteorology, Vol. 12, p. 728-731, June 1973.

18. Werle, H.; Gallon, M.; "Flow Control by Cross Jet." L'Aeronautique et l'Astronautique, No. 34, p. 21-23, 1972.

19. Bellhouse, B.; Bellhouse, F.; "Fluid Mechanics of Model Normal and Stenosed Aortic Valves." Circulation Research, Vol. 25, p. 693-704, 1969.

20. Chen, C. C.; Gibson, C. H.; Liu, S. C.; "Measurements of Turbulent Velocity and Temperature Fluctuations in the Wake of a Sphere." AIAA Journal, Vol. 6, p. 642-649, 1967.

21. Sies-Oosterveld, N. B.; Vanrenesse, R. L.; "Holographic Investigation of Boundary Layer and Cavitation Phenomena." Technische Physische Dieust TNO-TH, Delft, 1975.

22. Schloemer, H. H.; "Installation of a Rectangular Test Section for Acoustic Water Tunnel Studies of Flow-Induced Noise." NUSC-TR-4763, 1974.

23. Landgrebe, A. J.; Bellinger, E. D.; "An Investigation of the Quantitative Applicability of Model Helicopter Rotor Wake Patterns Obtained from a Water Tunnel." USAAMRDL-TR-71-69, 1971.

24. Grosskneutz, R.; "Interaction Between Turbulent Boundary Layers and Compliant Walls." Max-Planck-Institut fuer Stroemungsforschung Rep. 53, 1971.

25. Lehman, A. F.; "Model Studies of Helicopter Tail Rotor Flow Patterns in and out of Ground Effect." Oceanics, Inc. Rept-70-79, 1971.

26. Lambourne, N. C.; and Bryer, D. W.; "The Bursting of Leading-Edge Vortices - Some Observations and Discussion of the Phenomenon," Aeronautical Research Council Technical Report RM 3282, London, 1961.

27. Lowson, M. V.; "Some Experiments with Vortex Breakdown." Journal of The Royal Aeronautical Society, Vol. 68, p. 343, 1964.

28. Sarpkaya, T.; "On Stationary and Travelling Vortex Breakdowns." Journal of Fluid Mechanics, Vol. 45, Part 3, 1971, pp. 545-559.

29. Treiber, G. E.; "An Experimental Investigation of the Effect of Adverse Pressure Gradient on Vortex Breakdown." Master's Thesis, Naval Postgraduate School, June 1973.

30. Poisson-Quinton, P.; Werle, H.; "Water Tunnel Visualization of Vortex Flow." Astronautics and Aeronautics, June 1967.

31. Bower, R. E.; "Wake Vortex Minimization." Unpublished data (NASA Langley Research Center).

32. Moore, W. A.; Erickson, G. E.; Lorincz, D. J.; and Skow, A. M.; "Effects of Forebody, Wing and Wing-Body-LEX Flow-fields on High Angle of Attack Aerodynamics." SAE Paper No. 791082, December 1979.

33. Skow, A. M.; Moore, W. A.; and Lorincz, D. J.; "Forebody Vortex Blowing - A Novel Control Concept to Enhance Departure/Spin Recovery Characteristics of Fighter and Trainer Aircraft,' Presented 14-17 May, 1979 at the AGARD Fluid Dynamics Panel Symposium on Aerodynamic Characteristics of Controls, Naples,Italy.

34. Erickson, G. E.; "Flow Studies of Slender Wing Vortices." AIAA Paper No. 80-1423; Presented at the 13th Fluid & Plasma Dynamics Conference, Snowmass, Colo, 1980.

35. Lorincz, D. J.; "Water Tunnel Flow Visualization Study of the F-15," CR-144878, NASA, 1978.

36. Werle, H.; "Investigations of Blowing in a Water Tunnel by Flow Visualization." NASA-TT-F-13742, 1971.

37. Erickson, G. E.; "Effects of Spanwise Blowing on the Aerodynamic Characteristics of the F-5E." AIAA Paper No. 79-0118, January 1979.

38. Lorincz, D. J.; Unpublished Data (Northrop Corp.).

39. Journal of Fluid Mechanics, Vol. 68, part 4.

40. Demotakis, P.; Unpublished Cal Tech Data, 1979.

41. Orlik-Ruckemann, K. J.; Presentation given in the Aircraft Aerodynamics Session, AIAA 7th Atmospheric Flight Mechanics Conference, 11-13 August 1980, Danvers, Massachusetts.

42. Moore, W. A.; and Lorincz, D. J.; Unpublished Northrop Data, 1979. (Northrop movie is available upon request.)

314

/

43. Mattingly, G. E.; "The Hydrogen-Bubble, Flow-Visualization Technique," David Taylor Model Basin, Research and Development Report 2146, February 1966.

44. Clark, W. C.; and Nelson, R. C.; "Body Vortex Formation on Missiles at High Angles of Attack," AIAA Paper No. 76-65, January 1976.

45. Plesset, M.S.; "Cavitating Flows," ONR Report NO. 85-46, April 1969.

46. Knapp, R. T. et al.; "The Hydrodynamics Laboratory of the California Institute of Technology," Transactions of the ASME, July 1948.

47. Ward, T.M.; "The Hydrodynamics Laboratory at the California Institute of Technology - 1976," Transactions of the ASME, December 1976.

48. Prandtl, L.; and Tietjens, O.G.; Applied Hydro- and Aeromechanics, Dover Publications, Inc., New York, 1934.

49. Mangler, K.W.; and Smith, J.H.B.; "Behavior of the Vortex Sheet at the Trailing Edge of a Lifting Wing," Aeronautical Journal, Vol. 74, No. 719, 1970, pp. 906-8.

50. Elle, B.J., and Jones, J.P.; "A Note on the Vorticity Distribution on the Surface of Slender Delta Wings with Leading-Edge Separation," J. Roy. Aeron. Soc., Vol. 65, 1961, pp. 195-198.

51. Hummel, D.; and Redeker, G., "Experimentelle Bestimmung der gebundenen Wirbellinien sowie des Stromungsverlaufs in der Umgebung der Hinterkante eines schlanken Delta -

flugels," Abhandlg d. Braunschw. Wiss. Ges. 22 (1972), 273-290.

52. Kuchemann, D.; The Aerodynamic Design of Aircraft. Permagon Press, 1978.

53. Mirande, J.; Schmitt, V.; and Werle, H. ; "Vortex Pattern Developing on the Upper Surface of a Swept Wing at High Angle of Attack," NASA TM-75377, March 1979.

54. Peake, D.J.; and Tobak, M., "Three-Dimensional Interactions and Vortical Flows with Emphasis on High Speeds," NASA TM-81169, March 1980.

55. Parker, A.G.; "Aerodynamic Characteristics of Slender Wings," J. of Aircraft, Vol.13, March 1976.

56. Polhamus, Edward C.; "A Concept of the Vortex Lift of Sharp-Edge Delta Wings Based on a Leading-Edge Suction Analogy," NASA TN D-3767, 1966.

57. Mehrotra, S.C.; and Lan, C.E.; "A Theoretical Investigation of the Aerodynamics of Low Aspect-Ratio Wings with Partial Leading-Edge Separation," NASA CR-145304, 1978.

58. Johnson, F.T.; Lu, P.; Brune, G.W.; Weber, J.A.; and Rubbert, P.E.; "An Improved Method for the Prediction of Completely Three-Dimensional Aerodynamic Load Distributions on Configurations with Leading-Edge Separation," AIAA Paper No. 76-417, 1976.

59. Shen, G.; Unpublished Data. Northrop Corporation Aircraft Division, 1979.

60. Lamar, J.E.; and Luckring, J.M.; "Recent Theoretical Developments and Experimental Studies Pertinent to Vortex Flow Aerodynamics - with a View Towards Design," AGARD-CP-247, October 1978.

61. Lan, C.E.; "A Quasi-Vortex-Lattice Method in Thin Wing Theory," J. of Aircraft, Vol. 11, No. 9, Sept. 1974, pp. 518-527.

62. Mook, D.T.; and Maddox, S.A.; "Extension of a Vortex-Lattice Method to Include the Effects of Leading-Edge Separation," J. of Aircraft, Vol. 11, No. 2, Feb. 1974, pp. 127-128.

63. Hummel, D.; "On the Vortex Formation Over a Slender Wing at Large Angles of Incidence," AGARD-CP-247, October 1978.

64. L.P.; "Low-Speed Static Stability and Damping-in-Roll Characteristics of Some Swept and Unswept Low-Aspect-Ratio Wings," NACA TN 1468, 1947.

65. Demotakis, P., Private Communication, 1980.

66. Kandil, O.A.; "State of the Art of Nonlinear, Discrete-Vortex Methods for Steady and Unsteady High Angle of Attack Aerodynamics," AGARD-CP-247, October 1978.

67. Brown, Clinton E.; and Michael, William H., Jr.; "On Slender Delta Wings with Leading-Edge Separation," NACA TN 3430, 1955.

68. Smith, J.H.B; "Improved Calculations of Leading-Edge Separation From Slender, Thin, Delta Wings," Proceedings of the Royal Aeronautical Society A. 306, 1968, p. 67-90.

69. Kuhlman, J.M.; "Analytical Studies of Separated Vortex Flow on Highly Swept Wings," NASA CR-3022, 1979.

70. Northrop Unpublished Data.

71. Wentz, W.H., Jr.; "Effects of Leading-Edge Camber on Low-Speed Characteristics of Slender Delta Wings, "NASA CR-2002, October 1972.

72. Tinoco, E.N.; and Yoshihara, H.; "Subcritical Drag Minimization for Highly Swept Wings with Leading Edge Vortices," AGARD-CP-247, October 1978.

73. Hummel, D.; "Untersuchungen uber das Aufplatzen der Wirbel an Schlanken Deltaflugeln," Z. Flugwiss. 13 (1965), Heft 5.

74. Szodruch, J.; and Ganzer, U., "On the Lee-Side Flow Over Delta Wings at High Angle of Attack." AGARD-CP-247, October 1978.

75. Elle, B.J.; "On the Breakdown at High Incidences of the Leading Edge Vortices on Delta Wings," J. of Roy. Aeronaut. Soc. 64: 491-493, 1960.

76. Polhamus, Edward C.; "Predictions of Vortex-Lift Characteristics by a Leading-Edge Suction Analogy." J. Aircraft., Vol. 8. No. 4, Apr. 1971, pp. 193-199.

77. Monnerie, B.; Discussion of Paper 23, AGARD-CP-30, May 1968.

78. Lee, G.H.; "Note on the Flow Around Delta Wings with Sharp Leading Edges," ARC R&M 3070, 1955.

79. Elle, B.J.; "An Investigation at Low Speed of the Flow Near the Apex of Thin Delta Wings with Sharp Leading Edges," R. & M. No. 3176, A.R.C. Technical Report, 1961.

80. Fidler, J.E.; "Leading-Edge Separation," Martin Marietta Aerospace, Orlando, Florida.

81. Hummel, D.; "Study of the Flow Around Sharp-Edged Slender Delta Wings with Large Angles of Attack," NASA TT F-15, 107, 1973.

82. Maskell, E.C.; "Some Recent Developments in the Study of Edge Vortices," Proceedings 3rd Congress ICAS, 1962, Spartan Books.

83. Hoeijmakers, H.W.M.; and Bennekers, B.; "A Computational Model for the Calculation of the Flow About Wings with Leading-Edge Vortices," AGARD-CP-247, October 1978.

84. Werle, H.; "On Vortex Bursting," ONERA-NT 175, 1971.

85. Chigier, N.A.; "Measurement of Vortex Breakdown Over a Deta Wing Using a Laser Anemometer," NEAR TR 62, June 1974.

86. Hayashi, Y., and Hakaya, T.; "Flow Field in a Vortex with Breakdown Above Sharp-Edged Delta Wings," Report NAL-TR-423, August 1975.

87. Lambourne, N.C.; and Bryer, D.W.; "Some Measurements in the Vortex Flow Generated by a Sharp Leading Edge Having 65° Sweep," A.R.C., C.P. 477.

88. Earnshaw, P.B.; "An Experimental Investigation of the Structure of a Leading-Edge Vortex," R&M No. 3281, 1961.

89. Kao, H.C.; Unpublished Data, Northrop Corp., 1977.

90. Raat, J.; "Vortex Development and Breakdown," AFFDL-TR-75-69, August 1975.

91. Hall, M.G.; "Vortex Breakdown," Annual Review of Fluid Mechanics, Vol. 4,pp. 195-218, 1972.

92. Leibovich, S.; "The Structure of Vortex Breakdown," Annual Review of Fluid Mechanics, Vol. 10, pp. 221-246, 1978.

93. Grabowski, W.J.; "Solutions of the Navier-Stokes Equations for Vortex Breakdown," NASA CR-138901, May 1974.

94. Mager, A., "Dissipation and Breakdown of a Wing-Tip Vortex," Journal of Fluid Mechanics, Vol. 55, 1972, p. 609.

95. Gartshore, I.S., "Some Numerical Solutions for the Viscous Core of an Irrotational Vortex," NRC (Canada) Aero Report LR-378.

96. Bossel, H.H.; "Inviscid and Viscous Models of the Vortex Breakdown Phenomenon," PhD Thesis, Univ. of Calif., Berkeley, 1967.

97. Bossel, H.H., "Vortex Equations: Singularities, Numerical Solution, and Axisymmetric Vortex Breakdown," NASA CR-2090, July 1972.

98.   Batchelor, G.K.; "Axial Flow in Trailing Line Vortices,"
        Journal of Fluid Mechanics, Vol. 20, pp. 645-658, 1964.

99.   Garg, A.K.; "Oscillatory Behavior in Vortex Breakdown
        Flows: An Experimental Study Using a Laser Dappler Anemo-
        meter," M.S. Thesis, Cornell University, 1977.

100.   Johnson, J.L.; Grafton, S.B.; and Yip, L.P.; "Exploratory
        Investigation of the Effects of Vortex Bursting on the
        High Angle-Of-Attack Lateral Directional Stability
        Characteristics of Highly-Swept Wings," AIAA Paper No.
        80-0463, 1980.

101.   Allen, H.J., and Perkins, E.W.; "A Study of the Effects
        of Viscosity on Flow Over Slender Inclined Bodies of
        Revolution," NACA Report 1048, 1951.

102.   Thomson, K.D.; and Morrison, D.F.;" The Spacing, Posi-
        tion, and Strength of Vortices in the Wake of Cylindri-
        cal Bodies at Large Incidence," Report HSA 25, June
        1969.

103.   Deffenbaugh, F.D.; and Koerner, W.G., "Asymmetric Vortex
        Wake Development on Missiles at High Angles of Attack,"
        J. Of Spacecraft and Rockets, Vol. 14, No. 3, March 1977,
        pp. 155-162.

104.   Spangler, S.B., and Perkins, S.C.; "Prediction of Lateral
        Aerodynamic Loads on Fighter Aircraft at High Angles of
        Attack," Report ONR-CR212-225-4F, July 1978.

105.   Ericsson, L.E.; and Reding, J.P.; "Vortex-Induced Asy-
        metric Loads on Slender Vehicles," Lockheed Missiles and
        Space Company, LMSC-D630807, January 1979.

321

106. Peake, D.J.; and Owen, F.K.; "Control of Forebody Three-Dimensional Flow Separations," AGARD-CP-262, May 1979.

107. Nielsen, J.N.; "Nonlinearities in Missile Aerodynamics," AIAA Paper No. 78-20, January 1978.

108. Fiechter, M.; "Uber Wirbelsysteme an schlanken Rotation-Skorpern und ihren Einfluss auf die aerodynamic chen Beiwerte," Deutsch-Franzosisches Forshungs-Institut Saint-Louis, Report 10/66, 1966.

109. Lamont, P.J.; "Pressure Measuremer.ts on an Ogive-Cylinder at High Angles of Attack with Laminar, Transition, or Turbulent Separation," AIAA Paper No. 80-1556, August 1980.

110. Keener, E.R. and Chapman, G.T.; "Similarity in the Vortex Asymmetries Over Slender Bodies and Wings," AIAA Journal, Vol. 15, No. 9, September 1976.

111. Smith, L.H. and Nunn, R.H.; "Aerodynamic Characteristics of an Axisymmetric Body Undergoing a Uniform Pitching Motion," J. Spacecraft and Rockets, Vol. 13, No. 1, Jan. 1976, pp. 8-14.

112. Crabbe, R.S.; "Flow Separation About Elliptic Cones at Incidence," Nat. Res. Coun. of Canada Aero Report LR-436, August 1965.

113. Rainbird, W.J.; Crabbe, R.S.; and Jurewicz, L.S.; "A Water Tunnel Investigation of the Flow Separation About Circular Cones At Incidence," Nat. Res. Coun. of Canada Aero. Report LR-385, Sept. 1963.

114. Werle, H.; "Separation on Axisymmetrical Bodies at Low Speed," Rech. Aeron. No. 90, Sept.-Oct. 1962, pp. 3-14.

115. Peake, D.J., "Phenomenological Aspects of Quasi-Stationary Controlled and Uncontrolled Three-Dimensional Flow Separations." AGARD LS 94, Feb. 1978.

116. Deane, J.R.; "Visualization of the Vortex Dominated Flow About a Missile-Type Wing-Body Combination Using a Water Tunnel: Preliminary Report," British Aerospace, Dynamics Group, Report No. St. 21299, December 1978.

117. Shanks, R.E., "Low Subsonic Measurements of Static and Dynamic Stability Derivatives of Six Flat-Plate Wings Having Leading Edge Sweep Angles of 70° to 84°," NASA TN D-1827, July 1963.

118. Gowen, F.E. and Perkins, E.W.; "A Study of the Effects of Body Shape on the Vortex Wakes of Inclined Bodies at a Mach Number of 2," NASA RM A53I17, December 1953.

119. Lamont, P.J. and Hunt, B.L., "Pressure and Force Distributions on a Sharp-Nosed Circular Cylinder at Large Angles of Inclination to a Uniform Subsonic Stream," Journal of Fluid Mechanics, Vol. 76, 1976.

120. Werle, H., "Vortices on Slender Bodies at High Angles of Attack," L'Aeronautique et L'Astronautique, No. 79-1979-6-3.

121. Peake, D.J.; Private Communication, 1980.

122. Grosche, F.R.; "Wind Tunnel Investigation of the Vortex System Near an Inclined Body of Revolution With and Without Wings," AGARD-CP-71, Sept. 1970.

123. Headley, J.W.; "Analysis of Wind Tunnel Data Pertaining to High Angle of Attack Aerodynamics," AFFDL-TR-78.

124. Oberkampf, W.L. and Bartel, T.J.; "Symmetric Body Vortex Wake Characteristics in Supersonic Flow," AIAA Paper 78-1337, 1978.

125. Hall, I.M.; Rogers, E.W.E.; and Davies, B.M.; "Experiments with Inclined Blunt-Nosed Bodies at M = 2.45," ARC R&M 3128, 1957.

126. Thomson, K.D. and Morrison, D.F., "The Spacing, Position, and Strength of Vortices in the Wake of Slender Cylindrical Bodies at Large Incidence," J. Fluid Mech., Vol. 50, 1971, pp. 751-783.

127. Keener, E.R.; Chapman, G.T.; and Kruse, R.L.; "Effects of Mach Number and Afterbody Length on Onset of Asymmetric Forces on Bodies at Zero Sideslip and High Angles of Attack," AIAA Paper 76-66, 1976.

128. Jorgensen, L.H.; and Nelson, E.R.; "Experimental Aerodynamic Characteristics for a Cylindrical Body of Revolution with Various Noses at Angles of Attack from 0° to 58° and Mach Numbers from 0.6 to 2.0," NASA TM X-3128, 1974.

129. Hefner, J.N., "Lee-Surface Heating and Flow Phenomena on Space Shuttle Orbiters at Large Angles of Attack and Hypersonic Speeds," NASA TN D-7088, 1972.

130. Reding, J.P. and Ericsson, L.E., "Review of Delta Wing Space Shuttle Vehicle Dynamics," Space Shuttle Aerothermodynamics Technology Conference, Vol. III, NASA TM X-2508, 1972, pp. 861-931.

131. Lorincz, D.J.; "Space Shuttle Orbiter Flow Visualization Study," NASA CR-163092, Feb. 1980.

132. Akcay, M.; Richards, B.E.; Stahl, W.; and Zarghami, A.; "Aerodynamic Characteristics of a Missile Featuring Wing with Strakes at High Angles of Attack," AGARD-CP-247, October 1978.

133. Cahn, M.S.; Private Communication, Northrop Corp., 1980.

134. Thomson, D.H.; "A Water Tunnel Study of Vortex Breakdown Over Wings with Highly Swept Leading Edges," ARL/A-Note-356, May 1975.

135. Poisson-Quinton, P.; "Slender Wings for Civil and Military Aircraft," Israel Journal of Technology, Volume 16, 1978, pp. 97-131.

136. Hummel, D.; and Srinivasan, P.S.; "Vortex Breakdown Effects on the Low-Speed Aerodynamic Characteristics of Slender Wings in Symmetrical Flow," J. Roy. Aeron. Soc. 71, 1967, pp. 319-322.

137. Earnshaw, P.B.; and Lawford, J.A.; "Low-Speed Wind Tunnel Experiments on a Series of Sharp-Edged Delta Wings," R.A.E., Tech. Note Aero. No. 2750, 1961.

138. Gerhardt, H.A.; "The Aerodynamic Development of the Wing Root Leading Edge Extension of the P530 Airplane Configuration," Northrop Corporation, Aircraft Division, NOR 73-71, 1972.

139. Bartlett, G.E.; and Vidal, R.J.; "Experimental Investigation of Influence of Edge Shape on the Aerodynamic Characteristics of Low Aspect Ratio Wings at Low Speeds," J. Aeronaut. Sci., Vol. 22, No. 8, Aug. 1955, pp. 517-533, 588.

140. Lovell, J.C., and Wilson, H.A., Jr.; "Langley Full-Scale-Tunnel Investigation of Maximum Lift and Stability Characteristics of an Airplane Having Approximately Triangular Planform (DM-1 Glider)," NACA RM L7F16, August 1947.

141. Wentz, William H., Jr.; and Kohlman, David L.; "Wind Tunnel Investigations of Vortex Breakdown on Slender Sharp-Edged Wings," NASA CR-98737, 1968.

142. Campbell, J.F.; and Erickson, G.E.; "Effects of Spanwise Blowing on the Surface Pressure Distributions and Vortex-Lift Characteristics of a Trapezoidal Wing-Strake Configuration," NASA TP-1290, Feb. 1979.

143. Campbell, J.F.; Gloss, B.B.; and Lamar, J.E.; "Vortex Maneuver Lift for Super-Cruise Configurations," NASA TM X-72836, 1976.

144. White, R.P.; "Prediction and Measurement of the Aerodynamic Forces and Pressure Distributions of Wing-Tail Configurations at Very High Angles of Attack," AGARD-CP-247, October 1978.

145. Agnew, J.W.; Lyerla, G.W.; and Grafton, S.B.; "The Linear and Non-Linear Aerodynamics of Three-Surface Aircraft Concepts," AIAA Paper No. 80-181, 1980.

146. Poisson-Quinton, P.; and Werle, H.; "Water Tunnel Visualization of Vortex Flow," AIAA Astronautics and Aeronautics, June 1967.

147. Lorincz, D.J.; "Flow Visualization Study of the HiMAt RPRV," NASA CR-163094, August 1980.

148. Gilbert, W.P.; Unpublished NASA Data, 1979.

149. Rolls, S., Koenig, D.G. and Drinkwater, F.J., "Flight Investigation of the Aerodynamic Properties of an Ogee Wing," NASA TN D-3071, December 1965.

150. Frink, N.T.; and Lamar, J.E.; "Water-Tunnel and Analytical Investigation of the Effect of Strake Design Variables on Strake Vortex Breakdown Characteristics," TP-1676, NASA, 1980.

151. Clark, W.H.; "Body Vortex Formation in Incompressible Flows," AIAA Paper No. 77-1154, August 1977.

152. Moore, W.A.; Erickson, G.E.; Lorincz, D.J.; and Skow, Al.M.; "Effects of Forebody, Wing, and Wing-Body-LEX Flow-fields on High Angle of Attack Aerodynamics,"SAE Paper No. 792082, December 1979.

153. Skow, A.M.; Titiriga, A., Jr.; and Moore, W.A.; "Forebody/Wing Vortex Interactions and Their Influence on Departure and Spin Resistance," AGARD-CP-247, October 1978.

154. Lorincz, D.J.; and Friend, E.L.; "Water Tunnel Visualization of the Vortex Flows of the F-15,"AIAA Paper No. 79-1649, August 1979.

155. Carr, P.C.; and Gilbert, W.P.; "Effects of Fuselage Forebody Geometry on Low-Speed Lateral-Directional Characteristics of a Twin-Tail Fighter Model at High Angles of Attack," NASA TP-1592, 1979.

156. Gilbert, W.P.; Unpublished Data, NASA, 1979.

157. <u>Astronautics and Aeronautics</u>, December 1979, pg. 39.

158. Erickson, G.E. and Lorincz, D.J.; "Water Tunnel and Wind Tunnel Studies of Asymmetric Load Alleviation on a Fighter Aircraft at High Angles of Attack,"AIAA Paper No. 80-1618, August 1980.

159. Skow, A.M.; Moore, W.A.; and Lorincz, D.J.; "Forebody Vortex Blowing -- A Novel Control Concept to Enhance Departure/Spin Recovery Characteristics of Fighter and Trainer Aircraft," presented at AGARD Fluid Dynamics Panel Symposium on Aerodynamics of Controls, Naples, Italy, 14-17 May 1979.

160. Han, T.; and Patel, V.C.; "Flow Separation on a Spheroid at Incidence," J. of Fluid Mech.; Vol. 92, Part 4, 1979.

161. Gilbert, W.P.; Private Communication, NASA, 1980.

162. Gowadia, N.S.; Northrop Unpublished Data, 1978.

163. Erickson, G.E.; "Effects of Spanwise Blowing on the Aerodynamic Characteristics of the F-5E," AIAA Paper No. 79-0118, January 1979.

164. Lorincz, D.J. ; "Flow Visualization Study of Spanwise Blowing Applied to the F-4 Fighter Aircraft Configuration," NASA CR-169096, August 1980.

165. Sarpkaya, T.; "On Stationary and Travelling Vortex Breakdowns," Journal of Fluid Mechanics, Vol. 45, Part 3, pp. 545-559, 1971.

166. Hunt, B.L.; and Dexter, P.C.; "Pressures on a Slender Body at High Angle of Attack in a Very Low Turbulence Level Air Stream," AGARD-CP-247, October 1978.

167. Randall, D.G.; "A Theoretical Determination of the Flow Past and the Air Forces on an Oscillating Slender Delta Wing with Leading-Edge Separation," Royal Aeronautical Establishment, Farnborough, England, Structures Rept. 286, 1963.

168. Lowson, M.V.; "The Separated Flows on Slender Wings in Unsteady Motion," Communicated by J.P. Jones, Aeronautical Research Council, London, Rep. 24, 118, 1963.

169. McAlister, K.W., and Carr, L.W.; "Water Tunnel Experiments on an Oscillating Airfoil at Re = 21,000," NASA TM-78446, March 1978.

170. Werle, H.; ONERA NT 180 and film ONERA No. 666, 1971.

171. Mehta, U.B.; "Dynamic Stall of an Oscillating Airfoil," AGARD-CP-227, September 1977.

172. Maresca, C.; Favier, D.; Rebont, J.; Jones, G.; and Telionis, D.; "Measurement and Visualization of a Stalling Airfoil in Translational Oscillation," AIAA Paper No. 79-1519, July 1979.

173. Folan, J.J.; "Dynamic Stall of Airfoils in Oscillating Flow," MS Thesis, Dept. Mechanics and Mechanical and Aerospace Engineering, Illinois Institute of Technology, May 1976.

174. Ericsson, L.E., Private Communication, August 1980.

175. Lambourne, N.C.; and Bryer, D.W.; "Some Measurements of the Positions of the Vortices for Sharp Edged Delta and Swept Back Wings," Aeronautical Research Council, London, Rept. 19,953, 1958.

176. Lambourne, N.C.; Bryer, D.W.; and Maybrey, J.F.M.; "The Behavior of Leading Edge Vortices Over a Delta Wing Following a Sudden Change of Incidence," Aeronautical Research Council, London, R&M 3645, March 1964.

177. Ericsson, L.E.; and Reding, J.P.; "Unsteady Aerodynamics of Slender Delta Wings at Large Angles of Attack," J. of Aircraft, Vol. 12, No. 9, September 1975.

178. Lambourne, N.C.; Bryer, D.W.; and Maybrey, J.F.M.; "Pressure Measurements on a Model Delta Wing Undergoing Oscillatory Deformation," NPL Aero Report 1314, March 1970, Aeronautical Research Council, London.

179. Erickson, G.E.; "Water Tunnel Flow Visualization: Insight Into Complex Three-Dimensional Flow Fields," AIAA Paper No. 9-1530, July 1979.

180. Orlik-Ruckemann, K.J.; "Recent Advances in Techniques for Dynamic Stability Testing at NAE," Proceedings of the Symposium on Unsteady Aerodynamics, Vol. 1, March 1975, ed. by R.B. Kinney.

181. Orlik-Ruckemann, K.J.; "Effect of High Angles of Attack on Dynamic Directional Stability Parameters," AGARD-CP-247, October 1978.

182. Boyden, R.P.; "Effects of Leading-Edge Vortex Flow on the Roll Damping of Slender Wings," J. of Aircraft, Vol. 8, No. 7, July 1971, pp. 543-547.

183. Chambers, J., Jr, Private Communication, NASA, 1979.

184. Chambers, J., Jr.; Gilbert, W.; and Grafton, S.; "Results of Recent NASA Studies on Spin Resistance," AGARD-CP-199, June 1976.

185. Orlik-Ruckemann, K. J.; Private Communication, August 1979.

186. Marsden, D. J.; Simpson, R. W.; and Rainbird, B. E.; "An Investigation into the Flow Over Delta Wings at Low Speeds with Leading-Edge Separation," The College of Aeronautics, Cranfield, England, Report No. 114, Feb. 1958.

187. Harvey, J. K.; "Some Measurements on a Yawed Slender Delta Wing with Leading Edge Separation," ARC Report 20451, 1958.

188. Krone, N. J., Jr.; "Divergence Elimination with Advanced Composites," AIAA Paper No. 75-1009, August 1975.

189. Robinson, M. R.; and Silverman, S. M.; "From HiMAT to Future Fighters," AIAA Paper No. 79-1816, August 1979.

190. Lambourne, N. C.; and Pusey, P. S.; "Some Visual Observations of the Effects of Sweep on the Low-Speed Flow Over a Sharp-Edged Plate at Incidence," NPL R.&M. No. 3106, January 1958.

191. Huffman, J. K.; and Fox, C. H.; "Subsonic Longitudinal and Lateral-Directional Aerodynamic Characteristics for a Model with Swept-Back and Swept-Forward Wings," TM-74093, NASA February 1978.

192. Meznarsic, V. F.; and Gross, L. W.; "An Experimental Investigation of a Wing with Controlled Mid-Span Flow Separation," McAir 80-025, August 1980.

193. Campbell, J. F.; Private Communication, 1979.

194. Stahl, W.; "Zum nichtlinearen Verhalten des Auftriebes schlanker, ebener Deltaflugel in Ueberschallstromung. Bericht 67 A 44, 1968.

195. Von Karman Institute, Unpublished Data, 1979.

196. Mendenhall, M.R.; Nielsen, J.N.; "Effect of Symmetrical Vortex Shedding on the Longitudinal Aerodynamic Characteristics of Wing-Body-Tail Combinations," NASA C - 1473, 1975.

197. Rainbird, W.J.; "Turbulent Boundary-Layer Growth and Separation on a Yawed 12-1/2° Cone at Mach Numbers of 1.8 and 4.25," AIAA Journal, Vol. 6, No. 12, Dec. 1968, pp. 2410-2416.